

**284**

# **Topics in Current Chemistry**

**Editorial Board:**

**V. Balzani · A. de Meijere · K. N. Houk · H. Kessler · J.-M. Lehn  
S. V. Ley · S. L. Schreiber · J. Thiem · B. M. Trost · F. Vögtle  
H. Yamamoto**

# Topics in Current Chemistry

## Recently Published and Forthcoming Volumes

### **STM and AFM Studies on (Bio)molecular Systems: Unravelling the Nanoworld**

Volume Editor: Samorì, P.  
Vol. 285, 2008

### **Amplification of Chirality**

Volume Editor: Soai, K.  
Vol. 284, 2008

### **Anthracycline Chemistry and Biology II**

Mode of Action, Clinical Aspects and New Drugs  
Volume Editor: Krohn, K.  
Vol. 283, 2008

### **Anthracycline Chemistry and Biology I**

Biological Occurrence and Biosynthesis,  
Synthesis and Chemistry  
Volume Editor: Krohn, K.  
Vol. 282, 2008

### **Photochemistry and Photophysics of Coordination Compounds II**

Volume Editors: Balzani, V., Campagna, S.  
Vol. 281, 2007

### **Photochemistry and Photophysics of Coordination Compounds I**

Volume Editors: Balzani, V., Campagna, S.  
Vol. 280, 2007

### **Metal Catalyzed Reductive C–C Bond Formation**

A Departure from Preformed Organometallic Reagents  
Volume Editor: Krische, M. J.  
Vol. 279, 2007

### **Combinatorial Chemistry on Solid Supports**

Volume Editor: Bräse, S.  
Vol. 278, 2007

### **Creative Chemical Sensor Systems**

Volume Editor: Schrader, T.  
Vol. 277, 2007

### **In situ NMR Methods in Catalysis**

Volume Editors: Bargon, J., Kuhn, L. T.  
Vol. 276, 2007

### **Sulfur-Mediated Rearrangements II**

Volume Editor: Schaumann, E.  
Vol. 275, 2007

### **Sulfur-Mediated Rearrangements I**

Volume Editor: Schaumann, E.  
Vol. 274, 2007

### **Bioactive Conformation II**

Volume Editor: Peters, T.  
Vol. 273, 2007

### **Bioactive Conformation I**

Volume Editor: Peters, T.  
Vol. 272, 2007

### **Biominingalization II**

Mineralization Using Synthetic Polymers and Templates  
Volume Editor: Naka, K.  
Vol. 271, 2007

### **Biominingalization I**

Crystallization and Self-Organization Process  
Volume Editor: Naka, K.  
Vol. 270, 2007

# Amplification of Chirality

Volume Editor: Kenso Soai

With contributions by

J. M. Brown · T. Buhse · M. Fujiki · I. Gridnev · H. Hyuga

J. R. Islas · T. Kawasaki · J. Klankermayer · D. Lavabre

J.-C. Micheau · Y. Saito · K. Soai

The series *Topics in Current Chemistry* presents critical reviews of the present and future trends in modern chemical research. The scope of coverage includes all areas of chemical science including the interfaces with related disciplines such as biology, medicine and materials science. The goal of each thematic volume is to give the nonspecialist reader, whether at the university or in industry, a comprehensive overview of an area where new insights are emerging that are of interest to a larger scientific audience.

As a rule, contributions are specially commissioned. The editors and publishers will, however, always be pleased to receive suggestions and supplementary information. Papers are accepted for *Topics in Current Chemistry* in English.

In references *Topics in Current Chemistry* is abbreviated *Top Curr Chem* and is cited as a journal.

Visit the TCC content at [springerlink.com](http://springerlink.com)

ISBN 978-3-540-77868-4

e-ISBN 978-3-540-77869-1

DOI 10.1007/978-3-540-77869-1

Topics in Current Chemistry ISSN 0340-1022

© 2008 Springer-Verlag Berlin Heidelberg

This work is subject to copyright. All rights are reserved, whether the whole or part of the material is concerned, specifically the rights of translation, reprinting, reuse of illustrations, recitation, broadcasting, reproduction on microfilm or in any other way, and storage in data banks. Duplication of this publication or parts thereof is permitted only under the provisions of the German Copyright Law of September 9, 1965, in its current version, and permission for use must always be obtained from Springer. Violations are liable to prosecution under the German Copyright Law.

The use of general descriptive names, registered names, trademarks, etc. in this publication does not imply, even in the absence of a specific statement, that such names are exempt from the relevant protective laws and regulations and therefore free for general use.

Cover design: WMXDesign GmbH, Heidelberg

Typesetting and Production: le-tex publishing services oHG, Leipzig

Printed on acid-free paper

9 8 7 6 5 4 3 2 1 0

[springer.com](http://springer.com)

---

## Volume Editor

Prof. Dr. Kenso Soai

Department of Applied Chemistry  
Tokyo University of Science  
Kagurazaka, Shinjuku-ku  
Tokyo 162-8601 Japan  
*soai@rs.kagu.tus.ac.jp*

## Editorial Board

Prof. Vincenzo Balzani

Dipartimento di Chimica „G. Ciamician“  
University of Bologna  
via Selmi 2  
40126 Bologna, Italy  
*vincenzo.balzani@unibo.it*

Prof. Dr. Armin de Meijere

Institut für Organische Chemie  
der Georg-August-Universität  
Tammanstr. 2  
37077 Göttingen, Germany  
*ameijer1@uni-goettingen.de*

Prof. Dr. Kendall N. Houk

University of California  
Department of Chemistry and  
Biochemistry  
405 Hilgard Avenue  
Los Angeles, CA 90024-1589  
USA  
*houk@chem.ucla.edu*

Prof. Dr. Horst Kessler

Institut für Organische Chemie  
TU München  
Lichtenbergstraße 4  
86747 Garching, Germany  
*kessler@ch.tum.de*

Prof. Jean-Marie Lehn

ISIS  
8, allée Gaspard Monge  
BP 70028  
67083 Strasbourg Cedex, France  
*lehn@isis.u-strasbg.fr*

Prof. Steven V. Ley

University Chemical Laboratory  
Lensfield Road  
Cambridge CB2 1EW  
Great Britain  
*Svl1000@cus.cam.ac.uk*

Prof. Stuart L. Schreiber

Chemical Laboratories  
Harvard University  
12 Oxford Street  
Cambridge, MA 02138-2902  
USA  
*sls@slsiris.harvard.edu*

Prof. Dr. Joachim Thiem

Institut für Organische Chemie  
Universität Hamburg  
Martin-Luther-King-Platz 6  
20146 Hamburg, Germany  
*thiem@chemie.uni-hamburg.de*

**Prof. Barry M. Trost**

Department of Chemistry  
Stanford University  
Stanford, CA 94305-5080  
USA  
*bmtrost@leland.stanford.edu*

**Prof. Dr. Hisashi Yamamoto**

Department of Chemistry  
The University of Chicago  
5735 South Ellis Avenue  
Chicago, IL 60637  
USA  
*yamamoto@uchicago.edu*

**Prof. Dr. F. Vögtle**

Kekulé-Institut für Organische Chemie  
und Biochemie  
der Universität Bonn  
Gerhard-Domagk-Str. 1  
53121 Bonn, Germany  
*voegtle@uni-bonn.de*

---

## Topics in Current Chemistry Also Available Electronically

For all customers who have a standing order to Topics in Current Chemistry, we offer the electronic version via SpringerLink free of charge. Please contact your librarian who can receive a password or free access to the full articles by registering at:

[springerlink.com](http://springerlink.com)

If you do not have a subscription, you can still view the tables of contents of the volumes and the abstract of each article by going to the SpringerLink Homepage, clicking on "Browse by Online Libraries", then "Chemical Sciences", and finally choose Topics in Current Chemistry.

You will find information about the

- Editorial Board
- Aims and Scope
- Instructions for Authors
- Sample Contribution

at [springer.com](http://springer.com) using the search function.

*Color figures* are published in full color within the electronic version on SpringerLink.

---

## Preface

Biomolecules in nature exhibit overwhelming one-handedness, often called homochirality, such as L-amino acids and D-sugars. Since the discovery of molecular chirality by Pasteur, the origins of chirality and the process leading to enantiopure biomolecules have attracted broad attention from many researchers. Several theories have been proposed for the origin of chirality in organic compounds, for example, left and right-circularly polarized light, spontaneous absolute asymmetric synthesis, and chiral inorganic crystals such as quartz. However, the enantioenrichments induced by these mechanisms have been very low or even below detection levels. Thus, the process of amplification of enantioenrichment is inevitable to reach enantiopure compounds. In 1953, Frank proposed a mechanism of asymmetric autocatalysis without mentioning any chemical structure. However, it then took over 40 years for us to discover asymmetric autocatalysis with amplification of chirality in 1995.

This book illustrates the recent aspects of amplification of chirality by asymmetric autocatalysis and by forming helical structures. The first four chapters summarize experimental asymmetric autocatalysis with amplification of enantiopurity, the mechanism of asymmetric autocatalysis examined by NMR and calculation, the computer simulation models of the reaction mechanism of asymmetric autocatalysis, and the theoretical models of amplification of chirality. The last chapter deals with the amplification of chirality by the formation of helical structures. However, the amplification of enantiopurity in non-autocatalytic asymmetric reaction and the amplification by enantiomer separation involving crystallization or sublimation are beyond the scope of this book.

One of the main features of asymmetric autocatalysis and the formation of the helix is that the initial extremely low enantioenrichment is amplified significantly to near enantiopure. These processes of amplification of chirality have become powerful tools to elucidate the origin of chirality of organic compounds. For example, by using asymmetric autocatalysis, spontaneous absolute asymmetric synthesis without the intervention of any chiral factor has been realized.



---

## Contents

<b>Asymmetric Autocatalysis with Amplification of Chirality</b> K. Soai · T. Kawasaki . . . . .	1
<b>Asymmetric Autocatalysis with Organozinc Complexes; Elucidation of the Reaction Pathway</b> J. M. Brown · I. Gridnev · J. Klankermayer . . . . .	35
<b>Kinetic Insight into Specific Features of the Autocatalytic Soai Reaction</b> D. Lavabre · J.-C. Micheau · J. R. Islas · T. Buhse . . . . .	67
<b>Rate Equation Approaches to Amplification of Enantiomeric Excess and Chiral Symmetry Breaking</b> Y. Saito · H. Hyuga . . . . .	97
<b>Helix Generation, Amplification, Switching, and Memory of Chromophoric Polymers</b> M. Fujiki . . . . .	119
<b>Author Index Volumes 251–284 . . . . .</b>	187
<b>Subject Index . . . . .</b>	203

# Asymmetric Autocatalysis with Amplification of Chirality

Kenso Soai (✉) · Tsuneomi Kawasaki

Department of Applied Chemistry, Tokyo University of Science, Kagurazaka,  
 Shinjuku-ku, 162-8601 Tokyo, Japan  
 soai@rs.kagu.tus.ac.jp

<b>1</b>	<b>Introduction</b>	<b>2</b>
<b>2</b>	<b>Asymmetric Autocatalysis</b>	<b>3</b>
2.1	Discovery of Asymmetric Autocatalysis with Amplification of Chirality	3
2.2	Practically Perfect Asymmetric Autocatalysis with Amplification of Chirality	6
2.3	Kinetic Analysis of Asymmetric Autocatalysis	10
2.4	Asymmetric Autocatalysis Triggered by Chiral Organic Compounds	11
<b>3</b>	<b>Experimental Approaches to the Understanding of the Origins of Biological Homochirality Using Asymmetric Autocatalysis</b>	<b>12</b>
3.1	Enantioselective Synthesis of an Enantiomerically Pure Organic Compound by Asymmetric Autocatalysis Triggered by CPL	12
3.2	Asymmetric Autocatalysis Utilizing Enantiomorphous Inorganic Crystals as an Initial Source of Chirality	15
3.3	Enantioselective Synthesis Mediated by Chiral Crystals of an Achiral Organic Compound in Conjunction with Asymmetric Autocatalysis	17
3.4	Chiral Sensing of Amino Acids with Small Enantiomeric Excess Using Asymmetric Autocatalysis	19
3.5	Direct Examination of Extraterrestrial Chirality in Meteorites Using Asymmetric Autocatalysis	21
3.6	Spontaneous Absolute Asymmetric Synthesis in Conjunction with Asymmetric Autocatalysis	21
<b>4</b>	<b>Highly Sensitive Chiral Discrimination by Using Asymmetric Autocatalysis with Amplification of Chirality</b>	<b>24</b>
4.1	Discrimination of Cryptochirality in a Saturated Quaternary Hydrocarbon by Asymmetric Autocatalysis	24
4.2	Asymmetric Autocatalysis Initiated by Isotopically Chiral Primary Alcohols	26
4.3	Asymmetric Autocatalysis Initiated by Heterogeneous Chiral Substances	27
<b>5</b>	<b>Summary</b>	<b>28</b>
	<b>References</b>	<b>30</b>

**Abstract** We found that chiral 5-pyrimidyl alkanols are highly enantioselective asymmetric autocatalysts for the addition of *i*-Pr<sub>2</sub>Zn to the corresponding aldehyde. Asymmetric autocatalysis with amplification of ee from extremely low (0.00005%) ee to > 99.5% ee was realized for the first time by consecutive asymmetric autocatalysis. The chirality of CPL was directly correlated with the chirality of the pyrimidyl alkanol with high

ee by asymmetric photodegradation of the racemic pyrimidyl alkanol in combination with asymmetric autocatalysis. Chiral inorganic crystals such as quartz act as chiral triggers and regulate the sense of the asymmetric autocatalysis. Chiral organic crystals composed of an achiral compound such as hippuric acid act as the initial source of chirality for asymmetric autocatalysis to produce the nearly enantiomerically pure product. Highly sensitive chiral discrimination of amino acids with low ee is described. Direct examination of extraterrestrial chirality was performed on meteorites by applying asymmetric autocatalysis as the chiral sensor. Spontaneous absolute asymmetric synthesis is described in the formation of enantiomerically enriched pyrimidyl alkanol from the reaction of pyrimidine-5-carbaldehyde and *i*-Pr<sub>2</sub>Zn without adding any chiral substance in combination with asymmetric autocatalysis. Asymmetric autocatalysis of a chiral pyrimidyl alkanol is the only possible method to discriminate a cryptochiral quaternary saturated hydrocarbon, whose chirality is not capable of determination by any current method. The discrimination of chirality due to deuterium substitution is also accessible by the highly sensitive asymmetric autocatalysis.

**Keywords** Asymmetric autocatalysis · Amplification of chirality · Pyrimidyl alkanol · Automultiplication · Origin of homochirality

## 1

### Introduction

Most biomolecules, including amino acids and sugars, are chiral. Although they have left- and right-handed mirror image forms, biology only uses one enantiomer, with only a few exceptions. One of the greatest puzzles in science is the question of biological homochirality, i.e., why life on Earth is based on L-amino acids and D-sugars, and not based on the mirror molecules [1]. This homochirality of biomolecules might have been established before the origin of life, and the chiral homogeneity of biomolecules is considered to closely relate to the origin and evolution of life. How and when biomolecules achieved high enantioenrichment is an attractive issue requiring significant analysis. To date, several mechanisms have been proposed for elucidating the origins of the chirality of organic compounds, including circularly polarized light (CPL) [2–6], chiral inorganic crystals [7] such as quartz [8], chiral organic crystals composed of achiral organic molecules [9–13], spontaneous symmetry breaking [14, 15], parity-violating energy difference (PVED) [16], etc. Although the initial enantiomeric imbalance from an achiral condition can be introduced via these proposed mechanisms, a suitable amplification process for chirality is required to reach single-handedness of biological organic compounds.

Frank proposed a mechanism for the autocatalytic self-replicating process in which a chemical substance catalyzes its own production and acts as an anticatalyst for the production of the enantiomer without mentioning any actual compound or actual reaction [17]. In this kinetic model, it is possible to obtain an enantiomerically enriched compound from an ex-

tremely small enantiomeric excess, such as a small random fluctuation in the initially formed racemic mixture. We recently discovered asymmetric autocatalysis with amplification of chirality as a real chemical reaction, and this reaction provided the first experimental demonstration of the theoretical kinetic scheme.

We describe here our pioneering work on asymmetric autocatalysis [18–44] with amplification of chirality in the dialkylzinc addition system. Asymmetric autocatalysis with amplification of chirality gives a strong correlation between the origin of chirality and the homochirality of organic compounds, so an experiment on the effect of proposed chiral factors as the origin or trigger of biological homochirality was performed using this reaction. We also describe enantioselective synthesis, in combination with asymmetric autocatalysis, triggered by CPL, quartz, chiral organic crystals, amino acids, etc., including a spontaneous absolute asymmetric synthesis. We have also developed the application of asymmetric autocatalysis as a highly sensitive chiral sensor of many kinds of chiral factors and materials, using it as the chiral seed of asymmetric autocatalysis.

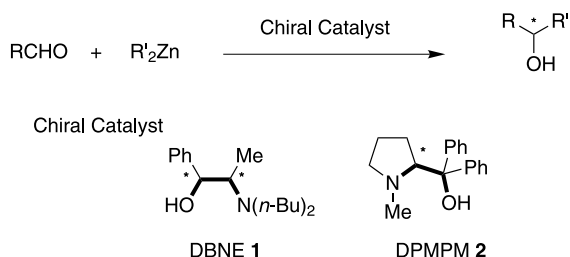
## 2

### Asymmetric Autocatalysis

#### 2.1

##### Discovery of Asymmetric Autocatalysis with Amplification of Chirality

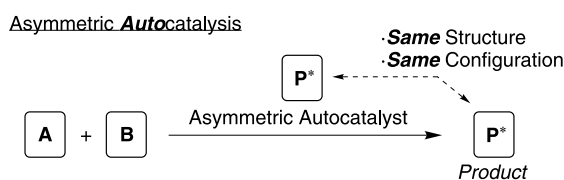
Significant progress has been made in asymmetric catalysis [45–47]. Independently, we developed the addition of dialkylzincs to aldehydes using  $\beta$ -amino alcohols as the chiral ligand to produce *sec*-alcohols (Scheme 1) [48–50]. The coordination of nitrogen and oxygen atoms to the zinc atom activates dialkylzincs to accelerate the nucleophilic attack of the alkyl group on a suitable nucleophile. The formation of the complex between dialkylzinc and amino alcohol enables the C–C bond-forming reaction [51]. Using appropriate chiral amino alcohols as the chiral ligand, asymmetric catalysis



**Scheme 1** Chiral amino alcohol catalyzed asymmetric dialkylzinc addition to aldehydes

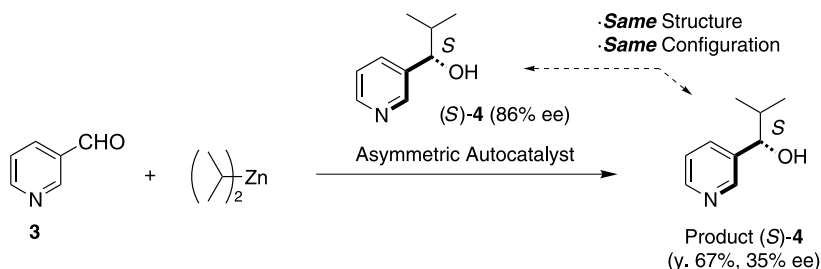
is available, in particular, *N,N*-dibutylnorephedrine (DBNE **1**) [52–54] and diphenyl-(1-methylpyrrolidin-2-yl)-methanol (DPMPM **2**) [55, 56] are well-established chiral catalysts for producing chiral products in high yield and high enantiomeric excess.

In conventional asymmetric catalysis, the asymmetric catalyst provides the enantioenriched product, whose structures are generally different from those of the asymmetric catalysts. In contrast, asymmetric autocatalysis is an auto-multiplication of a chiral compound  $P^*$ , in which the chiral product  $P^*$  acts as a chiral catalyst  $P^*$  for its own production (Scheme 2). We considered that, if the reaction product has the amino alcohol functionality as the result of alkylzinc addition, it should work as the catalyst for the next reaction, i.e., the autocatalytic reaction might proceed.



**Scheme 2** The concept of asymmetric autocatalysis

During our continuing study on the enantioselective addition of dialkylzincs to nitrogen-containing aldehydes, we found, for the first time, that chiral 3-pyridyl alkanol **4** acts as an asymmetric autocatalyst in the addition of diisopropylzinc (*i*-Pr<sub>2</sub>Zn) to pyridine-3-carbaldehyde **3** (Scheme 3) [57]. In the enantioselective addition of *i*-Pr<sub>2</sub>Zn to 3-pyridinecarbaldehyde **3**, (*S*)-3-pyridyl alkanol **4** with 86% ee acts as an asymmetric autocatalyst to produce the same compound **4** with 35% ee. In this reaction, the resulting product **4** forms the amino alcohol moiety that acts as the chiral catalyst for the next *i*-Pr<sub>2</sub>Zn addition, i.e., it catalyzes its own production. This is the first experimental observation that achieves asymmetric autocatalysis.



**Scheme 3** Asymmetric autocatalysis of a chiral pyridyl alcohol

After studying various nitrogen-containing compounds, we found that the zinc alkoxide of 2-methyl-1-(3-quinolyl)propan-1-ol **5** (Fig. 1) catalyzes the enantioselective formation of itself with the same configuration in the reaction between quinoline-3-carbaldehyde and *i*-Pr<sub>2</sub>Zn to produce the product **5** in high ee (up to 94% ee) [58]. In addition, the 5-carbamoyl-3-pyridyl alkanol **6** (Fig. 1) can act as an efficient autocatalyst to catalyze its own production in a highly enantioselective manner (up to 86% ee) [59].

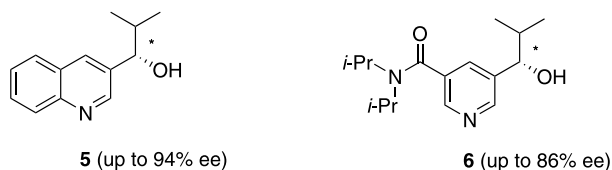
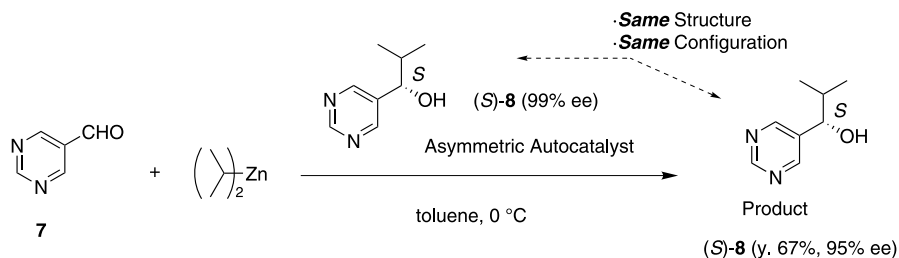


**Fig. 1** Asymmetric autocatalysts of alkanols containing quinoline and carbamoylpyridine rings in the reaction of *i*-Pr<sub>2</sub>Zn and the corresponding aldehydes

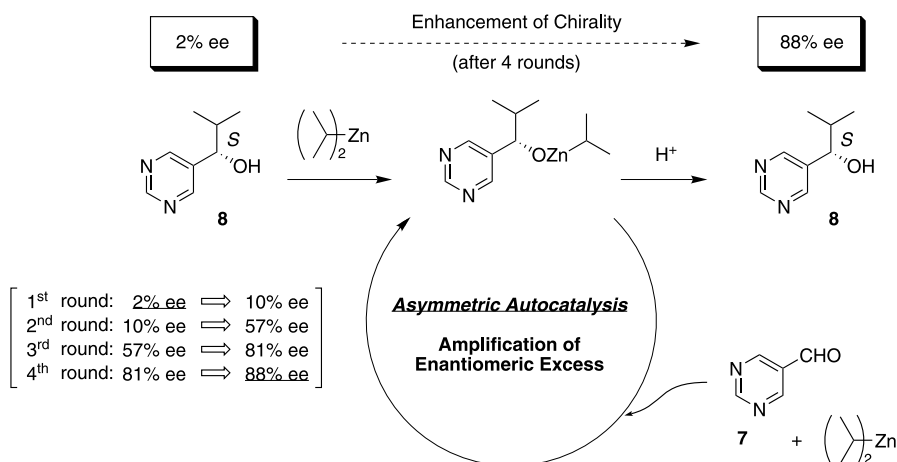
Then, we discovered that chiral 2-methyl-1-(5-pyrimidyl)propan-1-ol **8** serves as a highly enantioselective asymmetric autocatalyst for the addition of *i*-Pr<sub>2</sub>Zn to pyrimidine-5-carbaldehyde **7** (Scheme 4) [60]. In this compound, the formyl group is connected to the symmetric pyrimidine ring instead of the pyridine ring. When highly enantioenriched (*S*)-pyrimidyl alkanol **8** with 99% ee was employed as an asymmetric autocatalyst, (*S*)-**8** with 95% ee composed of both the newly formed and the initially used **8** was obtained. The yield of the newly formed **8** was calculated to be 67% and the enantiomeric excess was 93% ee.

The results of such a high enantioselectivity in the autocatalytic reaction encouraged us to investigate the enantioselective alkylation utilizing an autocatalyst with a small enantiomeric imbalance of 2% ee. In an earlier study on asymmetric autocatalysis using other compounds as the autocatalyst, the enantiomeric excess of chiral product has always been lower than that of the chiral catalyst. However, in this pyrimidine system, we found for the first time



**Scheme 4** Highly enantioselective asymmetric autocatalysis of pyrimidyl alkanol in enantioselective *i*-Pr<sub>2</sub>Zn addition

asymmetric autocatalysis with amplification of enantiomeric excess, i.e., the initial small enantioenrichment (2% ee) was significantly enhanced to a high enantioenrichment (88% ee) (Scheme 5) [61]. When the (*S*)-pyrimidyl alcohol **8** (20 mol %, 2% ee) was employed as an asymmetric autocatalyst, (*S*)-**8** with 10% ee was obtained in 46% yield as a mixture of newly formed product and initial catalyst. Surprisingly, the enantiomeric excess of newly formed product **8** was increased to 16% ee, a higher value than that of the initially employed autocatalyst **8** [61]. The reaction was performed successively by using the chiral product of one reaction as the autocatalyst of the next round of reactions, observing a further enhancement of enantiomeric excess to reach 88% ee after four rounds of reactions. The overall process was the asymmetric autocatalysis of (*S*)-**8** starting from a low ee of 2% with significant amplification of chirality to 88% ee, with the increase in the amount not needing any other chiral auxiliary. This chemical process is the first example of realization of asymmetric autocatalysis with amplification of chirality [61].



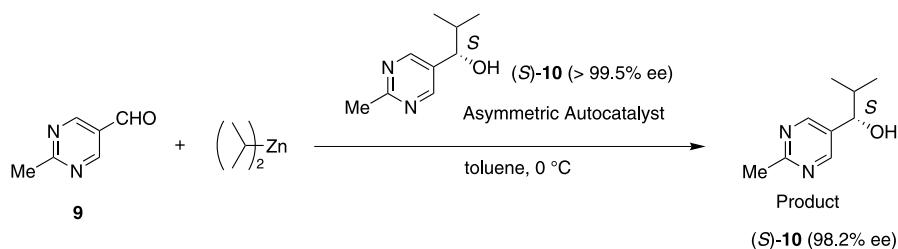
**Scheme 5** Asymmetric autocatalysis with significant amplification of chirality from low (2%) to high (88%) ee

## 2.2

### Practically Perfect Asymmetric Autocatalysis with Amplification of Chirality

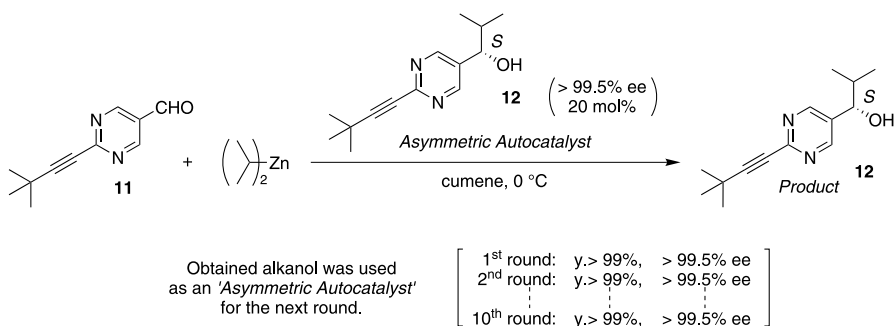
The next investigation focused on the substituent effect at the pyrimidine ring, especially at the 2-position. The asymmetric autocatalysis in the addition reaction of *i*-Pr<sub>2</sub>Zn to pyrimidine-5-carbaldehyde was examined using enantiomerically enriched (*S*)-2-methyl-1-(5-pyrimidyl)-propan-1-ol **10**. The treatment of the corresponding 2-methylpyrimidine-5-carbaldehyde **9** with *i*-Pr<sub>2</sub>Zn in the presence of autocatalyst **10** with > 99.5% ee resulted in highly

efficient asymmetric automultiplication to produce the product (*S*)-**10** with 98.2% ee [60]. In addition, the result of the experiment using (*S*)-**10** with 0.28% ee as autocatalyst demonstrated the potential ability of asymmetric autoamplification in this pyrimidine autocatalytic system. That is, the enhancement of the enantiomeric ratio from 0.28% ee to 87% ee was achieved by the asymmetric autocatalysis (Scheme 6) [62].



**Scheme 6** Highly enantioselective catalytic asymmetric automultiplication of a chiral pyrimidyl alkanol

Further studies on the influence of the substituent at the 2-position showed that substrates having the ethynyl group instead of methyl substituent possessed a greater ability as an asymmetric autocatalyst. When (*S*)-2-(*tert*-butylethynyl)-5-pyrimidyl alkanol **12** with > 99.5% ee was employed as an asymmetric autocatalyst, (*S*)-**12** with > 99.5% ee composed of both the newly formed **12** and the initially used **12** was obtained (Scheme 7) [63]. In addition, the yield of the newly formed **12** was > 99%. To take advantage of asymmetric autocatalysis—that the structures of the asymmetric autocatalyst and the product are the same—**12** obtained in the first round was used as an asymmetric autocatalyst for the following round. Again, the product (*S*)-**12** and the initial autocatalyst had an ee of > 99.5%, and the yield of the newly formed (*S*)-**12** was > 99%. The product **12** was therefore used as an asymmetric autocatalyst for the following round. Even after the tenth round, the yield of



**Scheme 7** Near-perfect consecutive asymmetric autocatalysis of a chiral pyrimidyl alkanol

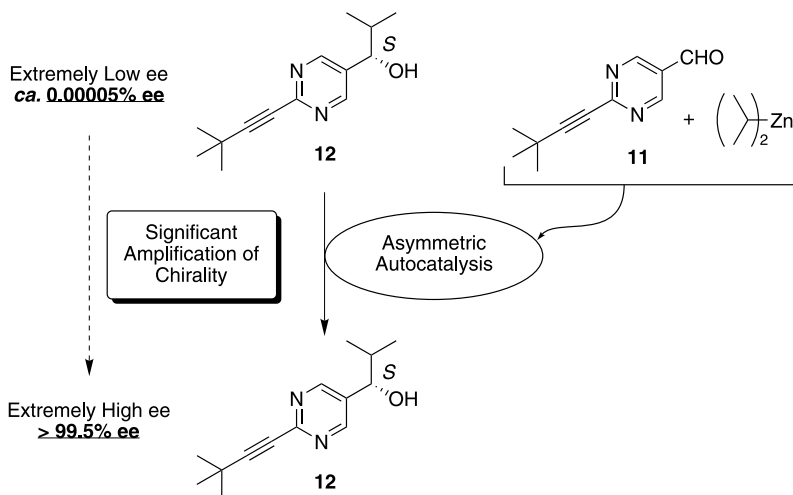


**12** was > 99% and the ee was > 99.5%. Thus, 2-alkynylpyrimidyl alkanol **12** served as a near perfect asymmetric autocatalyst [63]. During these ten consecutive asymmetric autocatalyses, (*S*)-**12** has automultiplied by a factor of ca. 60 000 000, without any decrease in enantioenrichment.

Moreover, we found efficient amplification of chirality by using (*S*)-2-(*tert*-butylethynyl)-5-pyrimidyl alkanol **12** from as low as ca. 0.00005% ee to an almost enantiomerically pure (> 99.5% ee) product **12** in only three consecutive asymmetric autocatalyses (Scheme 8) [64]. The first round of asymmetric autocatalysis using (*S*)-**12** with ca. 0.00005% ee gave (*S*)-**12** in 96% yield with an enhanced ee of 57%. The second round of asymmetric autocatalysis with the autocatalyst of 57% ee produced (*S*)-**12** with 99% ee, and the ee of (*S*)-**12** finally reached > 99.5% ee following the third round of asymmetric autocatalysis.

During these three consecutive asymmetric autocatalyses, the initial major (*S*)-enantiomer of **12** automultiplied by a factor of ca. 630 000 whereas the initially minor (*R*)-enantiomer of **12** automultiplied by less than 1,000 (Fig. 2). The tiny enantiomeric imbalance of ca. 0.00005% ee corresponds to only a few molecules of difference in the number of enantiomeric **12** in an almost racemic mixture of ca. 5 000 000 molecules of (*S*)-**12** and ca. 5 000 000 molecules of (*R*)-**12**.

Derivatization of 2-substituted 5-pyrimidyl alkanol **12** expanded the applicable compounds for asymmetric autocatalysis with amplification of chirality. The capabilities of chiral amplification were clarified by the use of an autocatalyst with low ee value. The *n*-butylethynyl derivative **13** (Fig. 3), including initial catalyst, with 21% ee was formed by one round of reaction using **13**



**Scheme 8** Amplification of chirality from ca. 0.00005% ee to near enantiomerically pure compound via asymmetric autocatalysis

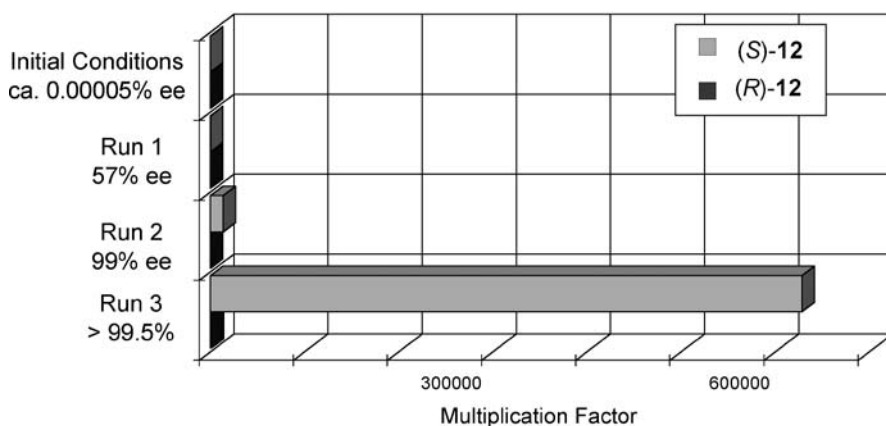


**Fig. 2** The increase in the amount of *S* and *R* isomers during consecutive asymmetric autocatalyses with significant amplification of ee

with 5.8% ee. Alkanols **12** (*t*-Bu) and **14** (trimethylsilyl, TMS) with 5.5 and 8.4% ee were efficiently enhanced to 70 and 74% ee by the enantioselective addition of *i*-Pr<sub>2</sub>Zn to the corresponding aldehyde, respectively. The phenyl group was also effective, although the efficiency of amplification was lower than for the *t*-Bu and TMS groups [63]. Recently, we have reported that a chiral ferrocene-containing pyrimidyl alkanol can be efficiently synthesized via asymmetric autocatalysis as an enantiomerically pure product. The initially employed chiral autocatalyst with 8% ee was automultiplied to reach 67% ee by a single round of addition reaction. After consecutive cycles of reaction, the enantioenrichment was amplified to over 99% ee [65]. Interestingly, a pyrimidyl alkanol possessing an alkenyl group instead of the ethynyl group at the 2-position also displays significant amplification of enantiomeric excess in the addition of *i*-Pr<sub>2</sub>Zn [66]. The consecutive reaction starting from autocatalyst **17** with 7% ee increased the ee of the product alkanol **17** to 99% ee.

These asymmetric autocatalytic processes are a very powerful method for amplifying the tiny imbalance of enantiomer to high enantioenrichment. When a pyrimidyl alkanol with low ee was used as an asymmetric auto-

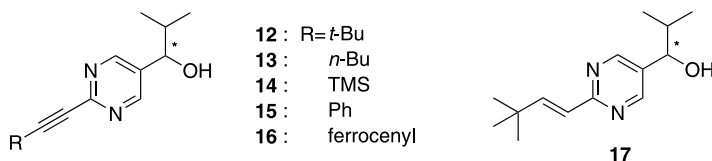


**Fig. 3** Asymmetric autocatalysts with various substituents at the 2-position of the pyrimidine ring

catalyst, the ee of the product was higher than that of the original catalyst. One of the advantages of asymmetric autocatalysis with amplification of ee over nonautocatalytic amplification of ee is that the product of one round is used as the asymmetric autocatalyst for the following round. Thus, extremely low enantioenrichment of pyrimidyl alkanol could be amplified to very high enantioenrichment by the consecutive process.

## 2.3

### Kinetic Analysis of Asymmetric Autocatalysis

Kinetic analysis of asymmetric autocatalysis was performed to study the reaction mechanism of asymmetric autocatalysis. The relationship between the reaction time and the yields of the product was investigated [67]. The *i*-Pr<sub>2</sub>Zn addition to pyrimidine-5-carbaldehyde **11** was performed in the presence of enantiomerically pure autocatalyst, the reaction being monitored by HPLC using naphthalene as an internal standard. The plots shown in Fig. 4(a) constitute S-shaped curves that are characteristic of an autocatalytic reaction. The relationship between time, yield and enantiomeric excess was also measured in the asymmetric autocatalysis with amplification of ee using high to low ee of pyrimidyl alkanol as the catalyst (Fig. 4b) [68]. Portions of the reaction mixture were quenched periodically and analyzed by chiral HPLC. When pyrimidyl alkanols with high to good ee are used as the asymmetric autocatalyst, the observed values of yield and ee were well matched to our simulated

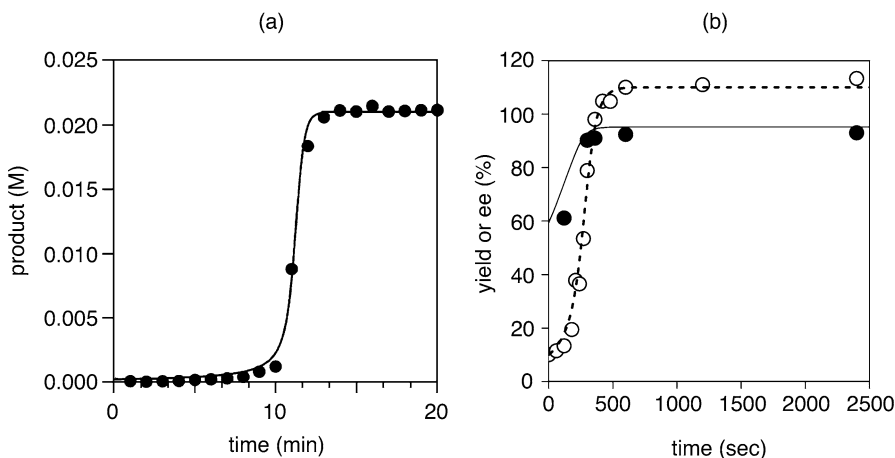


**Fig. 4** Relationship between time, concentration, yield and ee in asymmetric autocatalysis of alkanol **12**. **a** Enantiopure (> 99.5% ee) asymmetric autocatalyst was used. Experimental concentration of alkanol (filled circle), simulation (solid line). **b** Asymmetric autocatalyst with 59% ee was used. Experimental yield (open circle), experimental ee (filled circle)

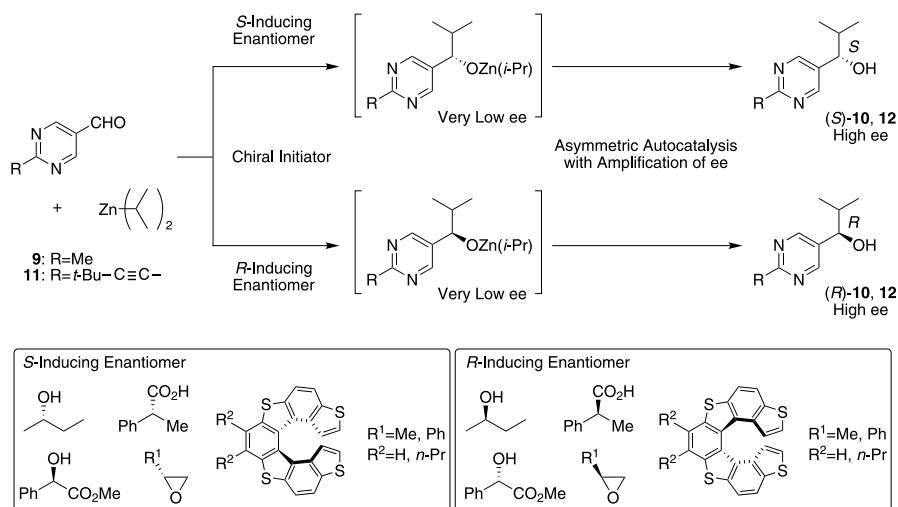
kinetic model, i.e., first order in *i*-Pr<sub>2</sub>Zn and pyrimidine-5-carbaldehyde and second order in pyrimidyl alkanol. However, the analysis using a pyrimidyl alkanol with low (20%) ee exhibited higher ee than the calculated value of ee based on the above model. Therefore, we considered the possibility of the presence of an inhibition process other than our simulated kinetic model. The inhibition process, i.e., the major enantiomer inhibits the production of the minor enantiomer, might enable the high magnitude of amplification of ee in asymmetric autocatalysis. The models and mechanism of the reaction have also been studied by other groups and indicate second-order kinetics for pyrimidyl alkanol [15, 67–73].

## 2.4

### Asymmetric Autocatalysis Triggered by Chiral Organic Compounds

We mentioned that asymmetric autocatalysis could amplify the initially added asymmetric autocatalyst, pyrimidyl alkanol, with slight enantiomeric excess (ca. 0.00005% ee) to almost enantiomerically pure product (> 99.5% ee) during consecutive reactions [64]. Not only the asymmetric autocatalyst itself, but also other chiral organic compounds can act as a chiral trigger for asymmetric autocatalysis, i.e., a slight asymmetry induced by the chiral organic compound is amplified by asymmetric autocatalysis to reach high enantioenrichment [74]. When pyrimidine-5-carbaldehyde is alkylated by *i*-Pr<sub>2</sub>Zn in the presence of a chiral organic compound, a tiny enantiomeric excess is induced in the alkylated product. The subsequent addition of *i*-Pr<sub>2</sub>Zn and pyrimidine-5-carbaldehyde to the reaction mixture leads to an asymmetric autocatalysis, and a highly enantiomerically enriched pyrimidyl alkanol is obtained. Therefore, the absolute configuration of the product alkanol with high ee is correlated to that of the chiral initiator that was originally used.

As shown in Scheme 9, various organic compounds can act as a chiral initiator of asymmetric autocatalysis. 2-Methylpyrimidine-5-carbaldehyde **9** was subjected to the addition of *i*-Pr<sub>2</sub>Zn in the presence of chiral butan-2-ol, methyl mandelate and a carboxylic acid [74]. When the chiral alcohol, (S)-butan-2-ol with ca. 0.1% ee was used as a chiral initiator of asymmetric autocatalysis, (S)-pyrimidyl alkanol **10** with 73% ee was obtained. In contrast, (R)-butan-2-ol with 0.1% ee induced the production of (R)-**10** with 76% ee. In the same manner, methyl mandelate (ca. 0.05% ee) and a chiral carboxylic acid (ca. 0.1% ee) can act as a chiral initiator of asymmetric autocatalysis, therefore the S- and R-enantiomers of methyl mandelate and carboxylic acid induce the formation of (R)- and (S)-alkanol **10**, respectively. Chiral propylene oxide (2% ee) and styrene oxide (2% ee) also induce the imbalance of ee in initially forming the zinc alkoxide of the pyrimidyl alkanol in the addition reaction of *i*-Pr<sub>2</sub>Zn to pyrimidine-5-carbaldehyde **11** [75]. Further consecutive reactions enable the amplification of ee to produce the highly enantiomerically enriched alkanol **12** (up to 96% ee) with the corresponding



**Scheme 9** Asymmetric autocatalysis initiated with chiral organic compounds

absolute configuration to that of the chiral epoxide. *P*- and *M*-thiahelicene with helical chirality can serve as chiral initiators of asymmetric autocatalysis to produce the enantiomerically enhanced chiral alkanol **12** with a good correlation between the absolute configurations [76].

The chirality in the organic compound (even though with small ee) can be converted into almost enantiomerically pure pyrimidyl alkanol by asymmetric autocatalysis with amplification of chirality.

### 3

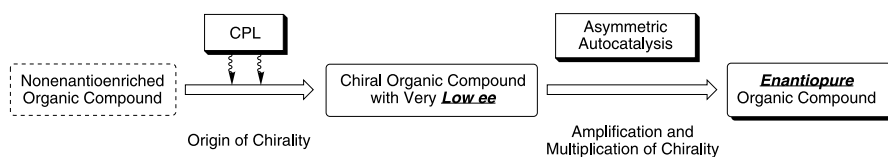
## Experimental Approaches to the Understanding of the Origins of Biological Homochirality Using Asymmetric Autocatalysis

### 3.1

#### Enantioselective Synthesis of an Enantiomerically Pure Organic Compound by Asymmetric Autocatalysis Triggered by CPL

Right- and left-handed CPL have long been proposed as one of the origins of chirality of organic compounds [2–6]. The occurrence of strong left (*l*)- or right (*r*)-handed CPL in nature has been observed in a star formation region of the Orion constellation [77]. However, because of the very small anisotropy (*g*) factors of organic compounds, only very low enantioenrichments of organic compounds have been induced, particularly in the initial stages of asymmetric photoreaction [3, 78–80] by irradiation with CPL. Asymmetric photodegradation of racemic leucine by right-handed CPL (*r*-CPL, 213 nm)

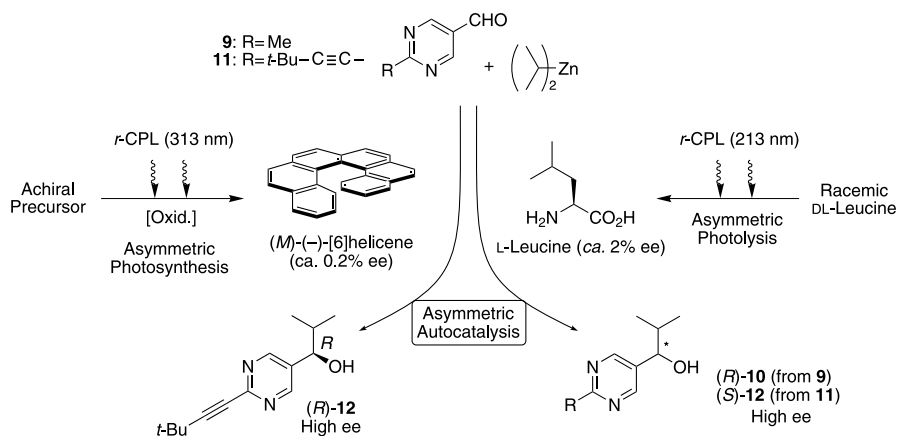
produces L-leucine with only 2% ee [78]. Hexahelicene with low ee is formed by asymmetric photosynthesis using CPL [80]. These low enantiomeric enrichments induced by CPL have not been correlated with the homochirality of organic compounds (Scheme 10).



**Scheme 10** The correlation between CPL and highly enantiomerically enriched organic compound in conjunction with asymmetric autocatalysis

We reasoned that chiral organic compounds with low ee induced by CPL can act as a chiral trigger in the enantioselective addition of *i*-Pr<sub>2</sub>Zn to pyrimidine-5-carbaldehyde, and that the subsequent asymmetric autocatalysis of pyrimidyl alkanol, formed in situ, amplifies its ee to produce highly enantioenriched pyrimidyl alkanol with an absolute configuration corresponding to that of the handedness of the CPL.

Indeed, in the presence of L-leucine with only 2% ee as a chiral initiator, the reaction of 2-methylpyrimidine-5-carbaldehyde **9** with *i*-Pr<sub>2</sub>Zn produced (*R*)-pyrimidyl alkanol **10** with an enhanced ee of 21% (Scheme 11) [74, 81]. In contrast, when D-leucine with 2% ee was used as a chiral initiator, (*S*)-**10** with an increased ee of 26% was obtained. As described in the preceding section, the ee of the obtained pyrimidyl alkanol can be amplified significantly by consecutive asymmetric autocatalysis to achieve homochirality.



**Scheme 11** Asymmetric autocatalysis with amplification of chirality triggered by CPL-induced organic compound with small ee

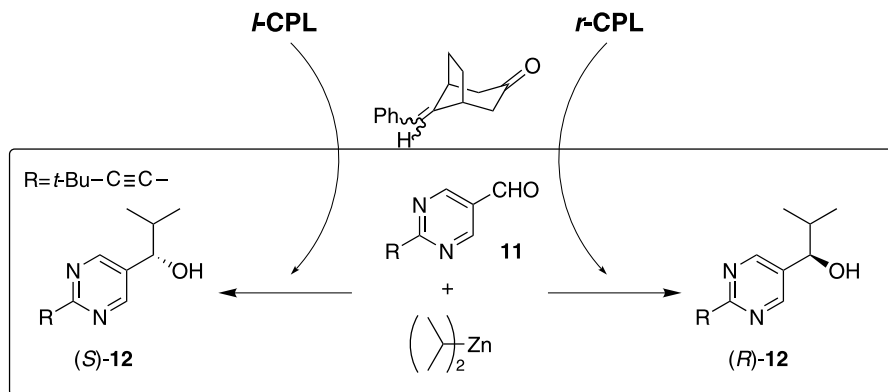
When 2-(*tert*-butylethynyl)pyrimidine-5-carbaldehyde **11**, instead of the 2-methyl derivative **9**, was subjected to reaction with *i*-Pr<sub>2</sub>Zn in the presence of chiral leucine, highly enantioenriched pyrimidyl alkanol **12** with the absolute configuration corresponding to that of chiral leucine was also obtained. But it should be noted that the resulting alkanol **12** showed the opposite enantioselectivity to that of alkanol **10**, i.e., L-leucine induces the production of (*S*)-alkanol **12** and D-leucine induces (*R*)-**12**, respectively [82]. The asymmetric amplification of **12** with an alkynyl substituent is more significant than that of the 2-methyl derivative **10** to increase to 96% ee (Scheme 11).

Hexahelicene is a chiral hydrocarbon with a helical structure. We found that (*P*)-hexahelicene with 0.13% ee, a lower ee than that induced by CPL [3, 80], acts as a chiral initiator for asymmetric autocatalysis (Scheme 11). The reaction between pyrimidine-5-carbaldehyde **11** and *i*-Pr<sub>2</sub>Zn gave (*S*)-pyrimidyl alkanol **12** with 56% ee [83]. On the other hand, when (*M*)-hexahelicene with 0.54% ee was used instead of (*P*)-hexahelicene, (*R*)-**12** with 62% ee was formed. As already described, these ee can be enhanced by further asymmetric autocatalysis. Thus, the chirality of CPL has been correlated with that of alkanol **12** with high ee by using hexahelicene as the chiral source of asymmetric autocatalysis.

Irradiation of racemic alkylidenecyclohexanone with CPL induces a small enantiomeric imbalance [79]. We found that chiral alkylidenecyclohexanones with low enantioenrichments trigger asymmetric autocatalysis to produce the highly enantioenriched pyrimidyl alkanol **12** with the absolute configuration corresponding to the handedness of the CPL (Scheme 12) [84].

Thus, low enantioenrichments in compounds induced by CPL have been correlated for the first time to an organic compound with very high enantioenrichments by asymmetric autocatalysis with amplification of chirality.

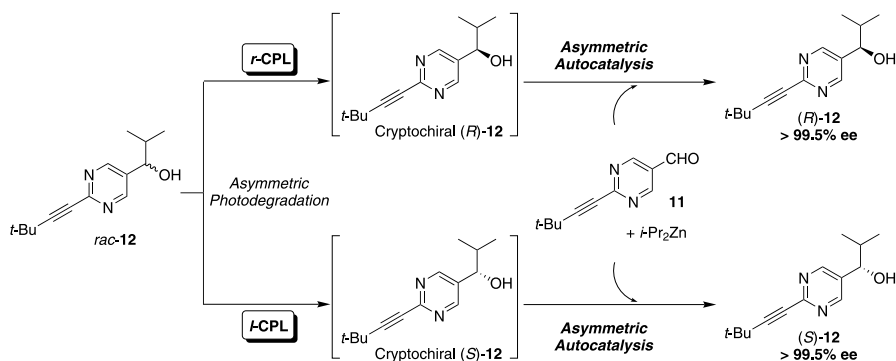
(*R*)- and (*S*)-pyrimidyl alkanols **12** exhibit positive and negative Cotton effects in circular dichroism (CD) spectra at 313 nm, respectively [85]. We



**Scheme 12** Asymmetric synthesis by CPL mediated with a chiral ketoolefin

thought that the direct irradiation of racemic alkanol **12** by left-handed (*l*) CPL would induce the asymmetric photodegradation of (*R*)-pyrimidyl alkanol **12** and leave the slightly enantioenriched (*S*)-**12**. Even when the enantioenrichment of the remaining (*S*)-pyrimidyl alkanol **12** is extremely low, as described in the preceding section, the compound serves as an asymmetric autocatalyst in the subsequent asymmetric autocatalysis with amplification of chirality to produce itself with high enantioenrichment.

Indeed, direct irradiation of racemic autocatalyst **12** by left-handed CPL and the subsequent asymmetric autocatalysis produces highly enantioenriched (*S*)-alkanol **12** with > 99.5% ee (Scheme 13). On the other hand, irradiation with right-handed (*r*) CPL instead of *l*-CPL, formed (*R*)-**12** with > 99.5% ee. The process provides direct correlation of the handedness of CPL with that of the organic compound with high enantiomeric excess [84].



**Scheme 13** Short pathway to obtain a near enantiopure compound by CPL irradiation followed by asymmetric autocatalysis

### 3.2

#### Asymmetric Autocatalysis Utilizing Enantiomorphous Inorganic Crystals as an Initial Source of Chirality

Chiral crystals provide an effective environment for discrimination of chiral molecules, so their possible roles in the origin of biological homochirality have been discussed for a long time [86]. In the Earth's crust, there is a wide variety of chiral minerals, such as chiral oxides and silicates, that serve as accessible chiral surfaces in the prebiotic evolution of chiral organic molecules. Although theoretical studies have shown the potential for significantly different adsorption between D- and L-organic molecules, no apparent asymmetric induction using chiral minerals has been observed. Only a very small asymmetric induction has been reported in an asymmetric adsorption of chiral compounds on quartz [87]. Quartz is one of the common silicate minerals

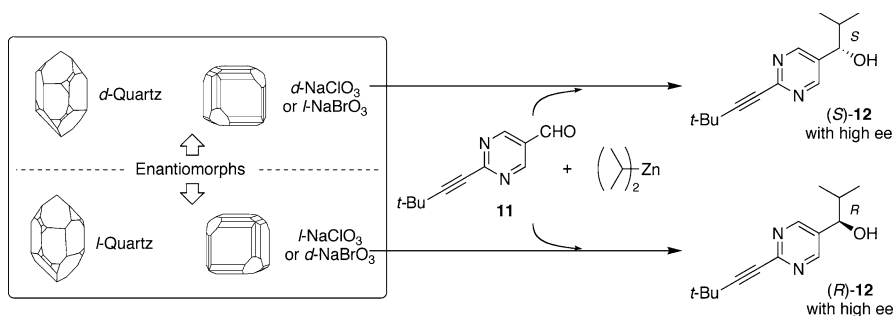


on Earth and occurs in both dextrorotatory (*d*) and levorotatory (*l*) enantiomorphs (space group  $P3_121$  or  $P3_221$ ) in approximately equal proportions in nature.

The possible response between the chiral surface of minerals and the organic molecules remains obscure, so we performed an asymmetric autocatalysis triggered by quartz. When pyrimidine-5-carbaldehyde **11** was treated with *i*-Pr<sub>2</sub>Zn in the presence of *d*-quartz powder, (*S*)-pyrimidyl alkanol **12** with 97% ee was obtained in a yield of 95% (Scheme 14) [88]. In contrast, in the presence of *l*-quartz, (*R*)-**12** with 97% ee was obtained in a yield of 97%. These reproducible results clearly show that the absolute configurations of the pyrimidyl alkanol formed were regulated by the chirality of quartz. A small enantiomeric imbalance of the initially formed pyrimidyl alkanol zinc alkoxide induced by quartz was amplified significantly by the subsequent consecutive asymmetric autocatalysis to produce pyrimidyl alkanol with very high ee. A chiral organic compound with high ee has therefore been formed for the first time, using a chiral inorganic crystal as the chiral trigger in conjunction with asymmetric autocatalysis with amplification of chirality.

The achiral inorganic ionic sodium chlorate (NaClO<sub>3</sub>) and sodium bromate (NaBrO<sub>3</sub>) crystallize in enantiomeric forms belonging to the  $P2_13$  space group for which the same crystal structures exhibit opposite optical rotation [89]. The levo-(*l*) and dextrorotatory (*d*) crystals can be obtained in equal proportions [90]. The chiral ionic crystals of NaClO<sub>3</sub> and NaBrO<sub>3</sub> were subjected to asymmetric autocatalysis as the initial seed of chirality to study the correlation between the organic compound with high ee and the chiral inorganic crystal composed of achiral ionic components.

As a result, sodium chlorate (NaClO<sub>3</sub>) crystals were found to act as a chiral trigger. In the presence of *d*-NaClO<sub>3</sub> crystals, (*S*)-**12** with 98% ee was formed in > 90% yield (Scheme 14) [91]. On the other hand, in the presence of *l*-NaClO<sub>3</sub> crystals, (*R*)-**12** with 98% ee was formed. In contrast to *d*-NaClO<sub>3</sub> crystals, *d*-NaBrO<sub>3</sub> crystals produced (*R*)-**12** and *l*-NaBrO<sub>3</sub> crystals



**Scheme 14** Asymmetric autocatalysis utilizing inorganic crystals as an initial source of chirality

(*S*)-12 [92]. The opposite configurations of 12 from *d*-NaClO<sub>3</sub> and *d*-NaBrO<sub>3</sub> are reasonable because the senses of the optical rotations are opposite between *d*-NaClO<sub>3</sub> and *d*-NaBrO<sub>3</sub> crystals, i.e., the shapes of the enantiomorphs are opposite. Thus, the above results show that the asymmetric autocatalysis does recognize the chirality of the enantiomorph of *d*-NaClO<sub>3</sub> and *d*-NaBrO<sub>3</sub> crystals to produce (*S*)- and (*R*)-12, respectively.

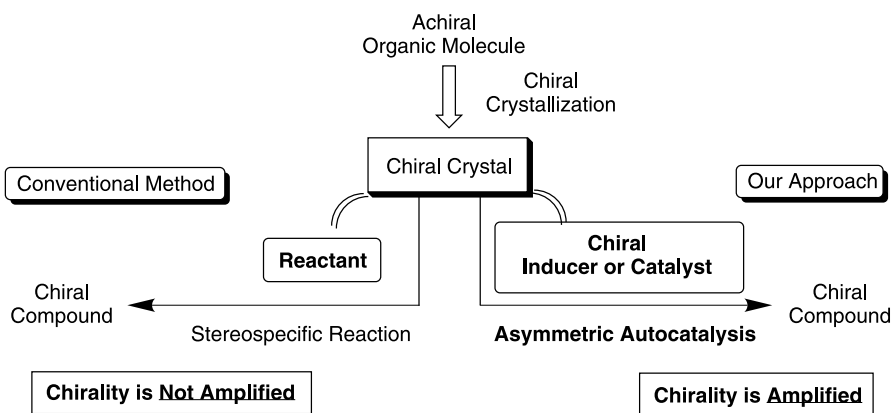
### 3.3

#### Enantioselective Synthesis Mediated by Chiral Crystals of an Achiral Organic Compound in Conjunction with Asymmetric Autocatalysis

Some achiral organic compounds form chiral crystals, with each crystal exhibiting one of two possible enantiomorphs [9–13]. These chiral crystals composed of an achiral organic compound may serve as an efficient chiral seed in a prebiotic world, therefore, a study of asymmetric autocatalysis using these chiral organic crystals is an interesting subject.

Although examples of highly stereospecific reactions using chiral crystals of achiral compounds have been reported [9–13, 93], they are limited to using themselves as reactants, i.e., the quantity of chirality does not increase. In order to provide a significant quantity of chiral compounds, amplification of the quantity of chirality is required. Thus, we investigated the highly enantioselective asymmetric autocatalysis mediated by chiral crystals formed from achiral organic molecules that significantly increases the amplification of the amount of chirality (Scheme 15).

Hippuric acid, i.e., *N*-benzoylglycine, is an achiral naturally occurring compound derived from glycine. It has been reported that hippuric acid forms enantiomorphous P2<sub>1</sub>2<sub>1</sub>2<sub>1</sub> crystals [94], which belong to a chiral space



**Scheme 15** A comparison of the concept of utilizing chiral crystals composed of achiral organic molecules in asymmetric autocatalysis and conventional stereospecific reactions

group. Investigation of the enantioselective reaction utilizing the crystal chirality of achiral biomolecules is an important experimental approach to understanding the origin of biological homochirality.

It is possible to discriminate the enantiomorphs of single crystals of hippuric acid by solid state CD spectroscopic analysis with nujol mulls. These crystals exhibit the Cotton effect at 260 nm (Fig. 5) [95].

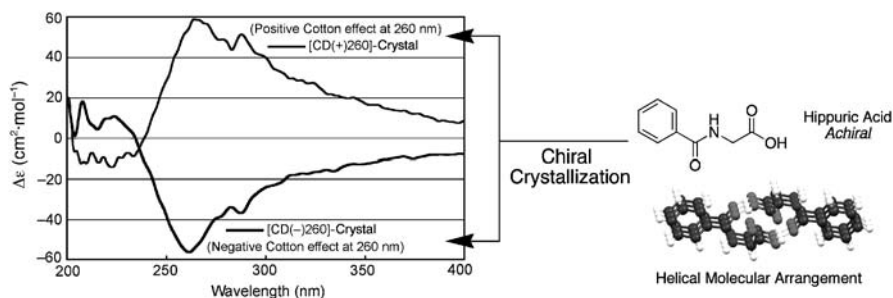
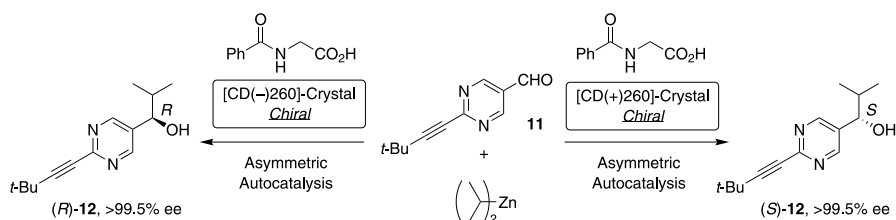


**Fig. 5** Solid-state CD spectroscopic analysis of two enantiomorphous crystals of hippuric acid

When pyrimidine-5-carbaldehyde **11** was treated with *i*-Pr<sub>2</sub>Zn in the presence of powdered [CD(+)-260]-crystal, (*S*)-pyrimidyl alkanol with 73% ee was obtained in 88% yield (Scheme 16). On the other hand, in the presence of [CD(-)-260]-crystal, the opposite enantiomer (*R*)-**12** with 89% ee was isolated in 89% yield. When the crystals, grown from the stirred methanol solution of hippuric acid using each enantiomorph of hippuric acid as the seed crystal, were used in asymmetric autocatalysis, the same correlation between the chirality of crystal and the product **12** was observed with excellent reproducibility. It should be noted that nearly enantiopure (*S*)- and (*R*)-pyrimidyl alkanols **12** with > 99.5% ee were obtained by consecutive asymmetric autocatalysis [64]. In this system, after the enantiomorphs of the crystal induced the chirality of an external organic compound, the subsequent asymmetric autocatalysis gave a greater amount of enantiomerically amplified product.

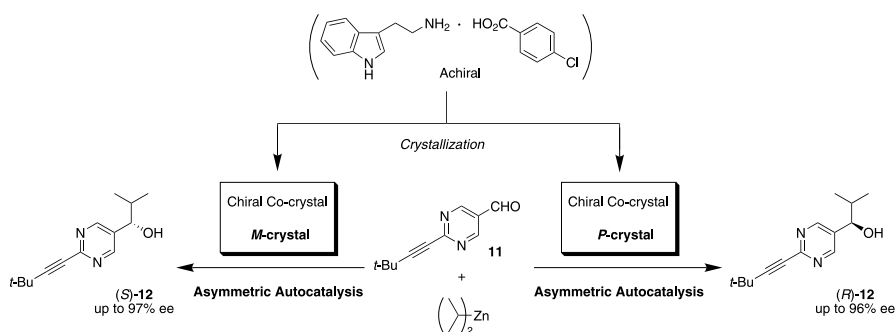


**Scheme 16** Asymmetric autocatalysis induced by a chiral crystal of hippuric acid

Moreover, it is reported that the chiral co-crystals of a quaternary ammonium salt were formed from an equimolar solution of achiral carboxylic acid and amine components [96, 97]. These crystals belong to a chiral space group, and have both clockwise (*P*) and counterclockwise (*M*) helicities.

When the reaction was performed in the presence of the *P*-crystal of tryptamine and *p*-chlorobenzoic acid, the (*R*)-pyrimidyl alkanol was obtained in 90% yield with an ee of 89% (Scheme 17) [98]. In contrast, in the presence of the *M*-crystal instead of the *P*-crystal, the reaction between aldehyde **11** and *i*-Pr<sub>2</sub>Zn always gave (*S*)-**12** with an ee of 95% in good yield. These results clearly exhibit the correlation between the chirality of the co-crystal and the absolute configuration of the resulting alkanol **12**.

A mechanistic consideration is as follows: the initial reaction of aldehyde **11** and *i*-Pr<sub>2</sub>Zn proceeded on the chiral surface of the crystal so that a small enantiomeric excess was induced. Then, subsequent asymmetric autocatalysis with an amplification of chirality produced alkanol **12** in high enantiomeric excess and with the corresponding absolute configuration. Further mechanistic details are now under investigation.



**Scheme 17** Highly enantioselective asymmetric autocatalysis using chiral co-crystals

### 3.4

#### Chiral Sensing of Amino Acids with Small Enantiomeric Excess Using Asymmetric Autocatalysis

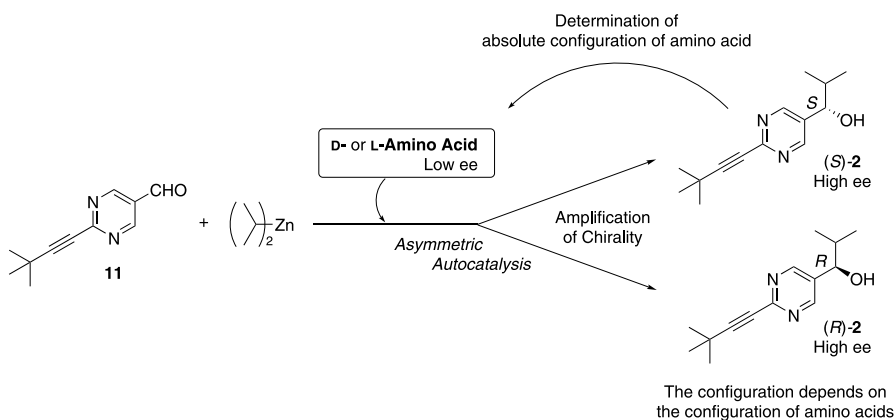
Amino acids exist not only on Earth but also in extraterrestrial substances such as meteorites. Proposals of the extraterrestrial origin of chirality have become credible in recent years by the analysis of organic compounds in meteorites [99]. Interestingly, some amino acids found in meteorites exhibit enantioenrichments. L-Amino acids with small ee were found in the Murchison meteorite. Although the degree of chirality is very low, these observations would support the extraterrestrial origin of chirality of amino acids. So, it is necessary to develop a highly sensitive method for detecting the absolute

configuration of amino acids to know which L- or D-enriched form exists in space.

Thus, we have developed a method for the detection of the absolute configuration of amino acids with low enantioenrichment. We thought that the absolute configuration of amino acids can be determined by detecting the absolute configuration of the produced pyrimidyl alkanol with high enantiomeric excess by asymmetric autocatalysis using amino acids as chiral initiators (Scheme 18).

Initially, we examined the reaction of aldehyde **11** and *i*-Pr<sub>2</sub>Zn in the presence of the 20 naturally occurring enantiopure amino acids [82]. L-Alanine induced the production of (*S*)-5-pyrimidyl alkanol **12** with 90% yield and 92% ee. In contrast, D-alanine gave (*R*)-**12** with 90% ee. These reproducible results clearly show that the configuration of alanine determined the configuration of the produced 5-pyrimidyl alkanol. In the case of all 20 amino acids, their chirality is recognized and highly enantiomerically enriched pyrimidyl alkanol **12** was obtained.

Next, asymmetric autocatalysis initiated by amino acids with low ee was examined. When L-alanine with ca. 10% ee was used as the chiral initiator, the obtained alkanol **12** with 94% ee possessed the *S*-configuration [99]. Even when the ee was as low as ca. 1% and ca. 0.1% ee, the configuration of the formed **12** was the *S*-configuration. On the other hand, asymmetric autocatalysis in the presence of D-alanine with low ee gave (*R*)-**12**. Similarly, the chirality of methionine, histidine and valine with low ee was also recognized and turned into the amplified ee of the 5-pyrimidyl alkanol.



**Scheme 18** Asymmetric autocatalysis initiated with enantiomerically imbalanced amino acid

### 3.5

#### **Direct Examination of Extraterrestrial Chirality in Meteorites Using Asymmetric Autocatalysis**

We analyzed several organic and inorganic phases identified from the Murchison and Murray meteorites [100] in order to determine whether they contain any possible chirality besides the enantiomeric amino acids [98]. Asymmetric autocatalysis is a method capable of revealing chiral imbalances in various media, therefore, we employed this method as a possible chiral sensor for the meteorites.

We performed the addition reaction of *i*-Pr<sub>2</sub>Zn to pyrimidine-5-carbaldehyde **11** in the presence of a constituent phase of the meteorite by appropriate treatments. Asymmetric autocatalysis with amplification of chirality gave pyrimidyl alkanol **12** with ee of detectable level.

Initially, the Murchison powder after water and solvent extraction was examined. After nine repetitions, the resulting pyrimidyl alkanol gave *R*-chirality in all nine experiments [100]. This statistically valid one-enantiomer selection suggests the presence of some chirality in the Murchison meteorite other than the water and solvent extractable compounds. Allende powder after water and solvent extraction also shows the same *R*-chirality of resulting alkanol **12**. Next, the insoluble organic material (IOM) obtained after demineralization of Murray powder was subjected to the asymmetric autocatalytic test. Asymmetric autocatalysis was performed in the presence of Murray IOM to give reproducible results of *R*-chirality. If these substances originated from the Murray meteorite, the possibility of the presence of chirality is suggested.

On the other hand, the IOM samples from which several percent amounts of organic compounds had been removed by hydrothermolytic treatment (IOM-H) gave results that are in sharp contrast to the above-mentioned meteoritic sample. Here, both (*R*)- and (*S*)-pyrimidyl alkanol **12** were obtained equally and indicate the absence of chiral factors in the IOM-H sample, i.e., the results are stochastic. Similar stochastic results were obtained on conducting the asymmetric autocatalysis in the presence of Murchison powders from which all the organic material had been removed by exposure to oxygen plasma.

The above results are interpreted as indicating the presence of diverse chirality in unknown meteorite organics.

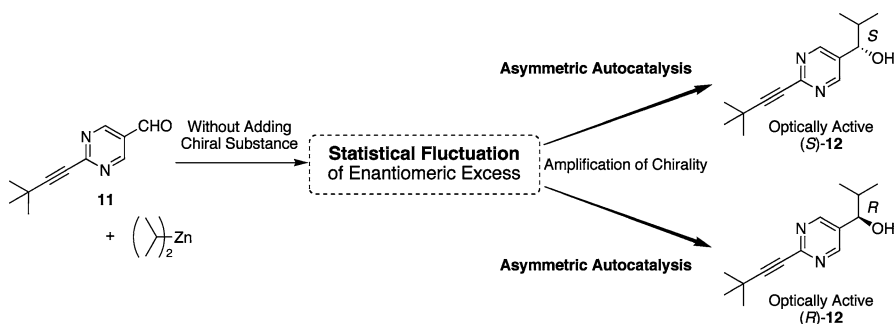
### 3.6

#### **Spontaneous Absolute Asymmetric Synthesis in Conjunction with Asymmetric Autocatalysis**

Spontaneous absolute asymmetric synthesis, i.e., the formation of an optically active compound without the use of chiral materials, has been proposed as one of the origins of biological homochirality in nature [14, 15]. Spontaneous

absolute asymmetric synthesis without the use of a chiral substance, which differs from crystallization, enables an increase in the amount of a chiral compound to occur, and can be responsible for the origin of homochirality.

Small fluctuations in the ratio of the two enantiomers are considered to be present in racemic mixtures of chiral molecules [14, 101]. We thought that, when a reaction system involves asymmetric autocatalysis with amplification of ee, the initial small fluctuation of ee in racemic mixtures that arises from the reaction of achiral reactants can produce an enantiomerically enriched product. We anticipated that when  $i\text{-Pr}_2\text{Zn}$  was treated with pyrimidine-5-carbaldehydes without adding any chiral substance, extremely slight enantioenrichment would be induced statistically in the initially formed zinc alkoxide of the alkanol, and that the subsequent amplification of chirality by asymmetric autocatalysis would produce the pyrimidyl alkanol with detectable enantioenrichment (Scheme 19).



**Scheme 19** Spontaneous absolute asymmetric synthesis of pyrimidyl alkanol without the addition of a chiral substance

The reaction of pyrimidine-5-carbaldehyde 7 and 2-methylpyrimidine-5-carbaldehyde 9 with  $i\text{-Pr}_2\text{Zn}$  without adding a chiral substance produced enantioenriched (S)- or (R)-pyrimidyl alkanol 8 and 2-methylpyrimidyl alkanol 10, respectively [102].

Indeed, when 2-alkynylpyrimidine-5-carbaldehyde was reacted with  $i\text{-Pr}_2\text{Zn}$  in a mixed solvent of ether and toluene, the subsequent one-pot asymmetric autocatalysis with amplification of ee gave enantiomerically enriched pyrimidyl alkanol 12 well above the detection level [103]. The absolute configurations of the pyrimidyl alkanol exhibit an approximate stochastic distribution of S and R enantiomers (formation of S 19 times and R 18 times) (Fig. 6).

In addition, we performed the asymmetric autocatalysis in the presence of an achiral silica gel under achiral conditions, the enantioenriched pyrimidyl alkanol 12 is generated from the reaction between 2-alkynylpyrimidine-5-carbaldehyde 11 and  $i\text{-Pr}_2\text{Zn}$  in conjunction with the subsequent asymmetric autocatalysis [104]. The reaction of pyrimidine-5-carbaldehyde 11 with

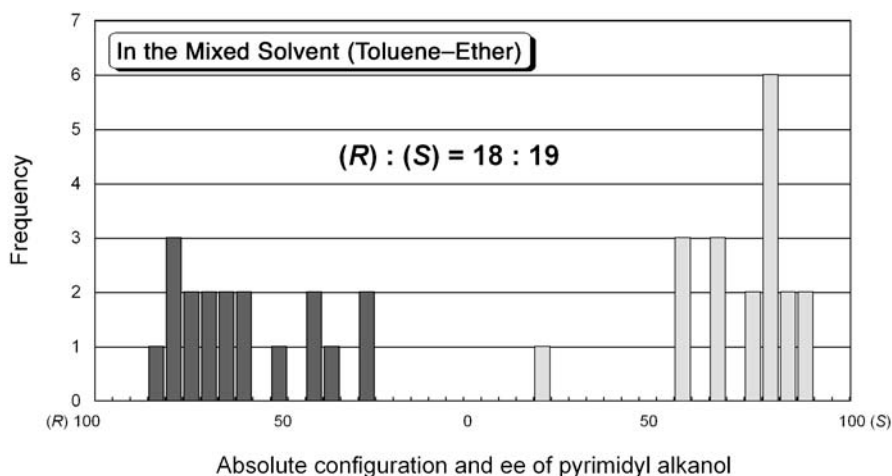


**Fig. 6** Histogram of the absolute configuration and the enantiomeric excess of pyrimidyl alkanol 12 in the mixed solvent

*i*-Pr<sub>2</sub>Zn in the presence of achiral silica gel in toluene, followed by a one-pot asymmetric autocatalysis with amplification of ee gave the enantioenriched (*S*)- and (*R*)-5-pyrimidyl alkanol 12 with ee above the detection level. To examine the distribution of the absolute configuration of the predominantly formed enantiomers in each experiment, 84 experiments were run under the same reaction conditions. In all cases, enantioenriched 5-pyrimidyl alkanols with either *S* or *R* configurations were formed. The absolute configurations of the resulting 12 exhibited an approximate stochastic distribution, i.e., the formation of the *S* form occurred 45 times and the formation of the *R* form occurred 39 times (Fig. 7).

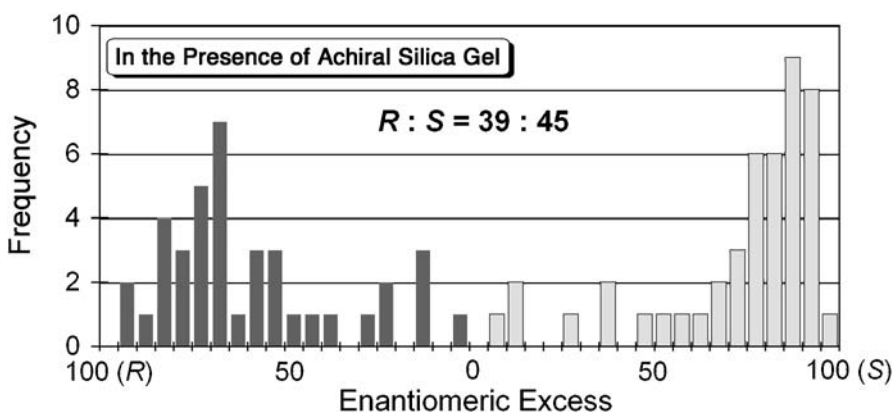


**Fig. 7** Histogram of the absolute configuration and the enantiomeric excess of pyrimidyl alkanol 12 in the presence of achiral silica gel



We have demonstrated the stochastic formation of (*S*)- and (*R*)-5-pyrimidyl alkanol **12** from pyrimidine-5-carbaldehyde **11** and *i*-Pr<sub>2</sub>Zn without the intervention of a chiral auxiliary. Even in the reactions performed in toluene alone, stochastic behavior of the formation of (*S*)- and (*R*)-**12** was observed in the presence of achiral silica gel. We believe that the approximate stochastic behavior in the formation of alkanols fulfils one of the conditions necessary for chiral symmetry breaking by spontaneous absolute asymmetric synthesis.

## 4

### Highly Sensitive Chiral Discrimination by Using Asymmetric Autocatalysis with Amplification of Chirality

#### 4.1

#### Discrimination of Cryptochirality in a Saturated Quaternary Hydrocarbon by Asymmetric Autocatalysis

Significant progress in chiral discrimination has been achieved in recent decades, however, there remains a class of compounds whose chiral discrimination has been very difficult to establish, or has not been possible at all. Chiral saturated hydrocarbons form a class of compounds whose chiral discrimination has often been very difficult [105]. Unlike other functionalized compounds, chiral saturated hydrocarbons do not bear heteroatom(s),  $\pi$ -electrons, or chromophores, and therefore, the difference between the four substituents on the asymmetric carbon atom is very small.

An example of a compound whose chiral discrimination poses the utmost difficulty is a saturated quaternary hydrocarbon bearing similar substituents on the asymmetric carbon atom, with a representative example being 5-ethyl-5-propylundecane, i.e., (*n*-butyl)ethyl(*n*-hexyl)(*n*-propyl)methane (Fig. 8) [106]. The enantiomer of this hydrocarbon exhibits practically no optical rotation ( $|\alpha| < 0.001$ ) between 280 and 580 nm. The compound is a chiral, but to all intents an optically inactive, compound. To the best of our knowledge, the chirality of this compound has not been discriminated using any current method. Mislow called such hidden chirality “cryptochirality” [14, 107].

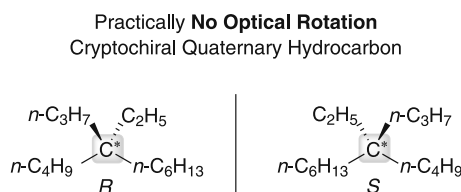
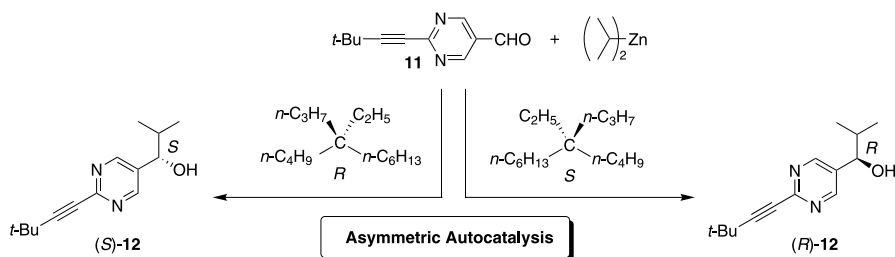


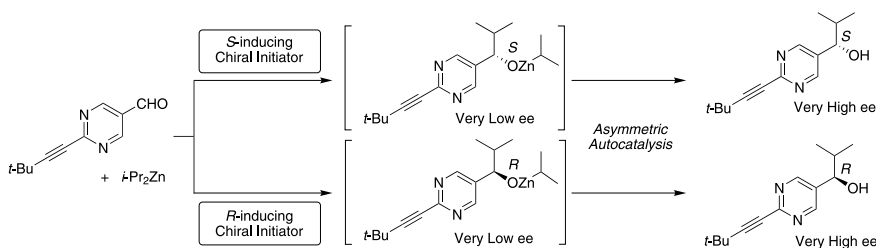
**Fig. 8** The structure of enantiomers of 5-ethyl-5-propylundecane [(*n*-butyl)ethyl(*n*-hexyl)(*n*-propyl)methane]

We found that the chirality of the saturated quaternary hydrocarbon was successfully discriminated using asymmetric autocatalysis [108]. The asymmetric autocatalysis initiated by the chiral (*R*)-quaternary hydrocarbon using pyrimidine-5-carbaldehyde **11** and *i*-Pr<sub>2</sub>Zn produced (*S*)-pyrimidyl alkanol **12** with 97% ee and 93% yield. In contrast, asymmetric autocatalysis in the presence of the (*S*)-quaternary hydrocarbon produced (*R*)-alkanol **12** with 94% ee in 91% yield. These stereochemical correlations were found to be reproducible (Scheme 20).

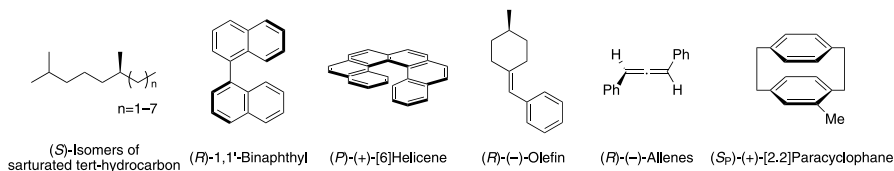


**Scheme 20** Chiral discrimination of cryptochiral quaternary hydrocarbon

Chiral quaternary alkanes do not have any  $\pi$ -electrons or a heteroatom. Thus, the present chiral discrimination may involve the CH- $\pi$  interactions between the CH group of the chiral hydrocarbon and the  $\pi$ -electrons of the pyrimidine-5-carbaldehyde **11**. This CH- $\pi$  interaction [109] may be used to discriminate between the *Re* and *Si* enantiofaces of aldehyde **11**, because the



Chiral Hydrocarbons Act as Chiral Initiators (*S*-inducing Enantiomer)



**Scheme 21** Discrimination of chirality in hydrocarbons by asymmetric autocatalysis with amplification of enantiomeric excess

quaternary alkane is chiral, and the subsequent attack of *i*-Pr<sub>2</sub>Zn on aldehyde **11** from one of the enantiofaces of the aldehyde preferentially forms the isopropyl zinc alkoxide of the pyrimidyl alkanol with an absolute configuration corresponding to that of the chiral hydrocarbon. Once the isopropyl zinc alkoxide of the pyrimidyl alkanol with a tiny enantioenrichment is formed, then the chirality amplifies during the asymmetric autocatalysis.

In addition, saturated tertiary hydrocarbons [108] also act as a chiral source of asymmetric autocatalysis to give the pyrimidyl alkanol, with the absolute configurations corresponding to that of the chiral alkanes (Scheme 21). The correlation between the absolute configuration of the hydrocarbon and that of the obtained alkanol is reproducible. Therefore, the asymmetric autocatalysis is sufficiently applicable as a chiral sensor for saturated tertiary hydrocarbons. Various chiral hydrocarbons with  $\pi$ -electrons such as 1,1'-binaphthyls [110], helicenes [82], olefins [83], allenes [111], and [2.2]paracyclophanes [112, 113] serve as chiral initiators in this asymmetric autocatalysis.

## 4.2

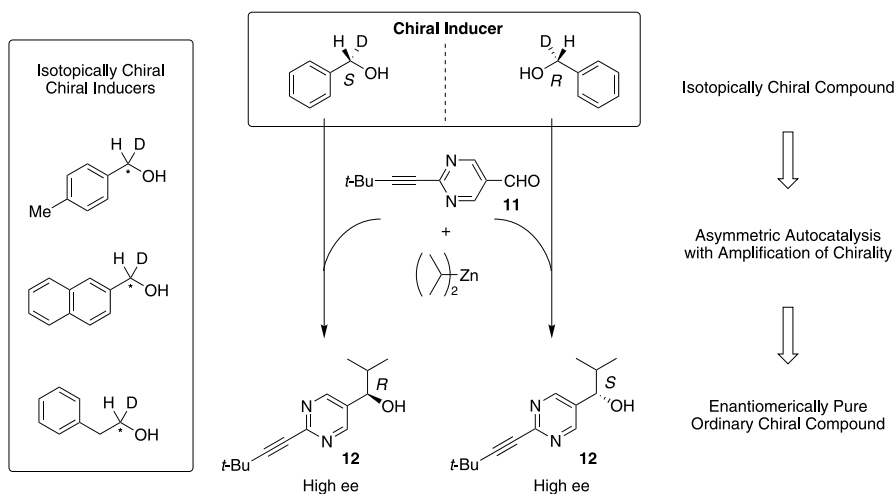
### Asymmetric Autocatalysis Initiated by Isotopically Chiral Primary Alcohols

Chiral compounds whose chirality is due to the replacement of hydrogen by deuterium are important from the standpoint of organic stereochemistry and biochemistry [114, 115]. The chirality of these enantiomers is mainly due to the very small difference between the lengths of carbon–deuterium and carbon–hydrogen bonds; the time-averaged carbon–deuterium bond length (0.1099 nm) is shorter than the carbon–hydrogen bond by only 0.0004 nm [116, 117]. Thus, unlike other enantiomers whose chirality results from the difference in the number of protons in the atomic nucleus, these isotopic enantiomers are considered to show only very small differences in asymmetric reactions and recognition.

We investigated highly enantioselective asymmetric autocatalysis of a chiral compound induced by the isotopic enantiomer of a primary alcohol- $\alpha$ -*d* (Scheme 22) [118]. The correlation between the absolute configurations of the obtained pyrimidyl alkanol and the isotopic chiral compound is reproducible, thus the small isotope chirality can be recognized by asymmetric autocatalysis.

When aldehyde **11** was reacted with *i*-Pr<sub>2</sub>Zn in the presence of chiral (*S*)-benzyl alcohol- $\alpha$ -*d*, (*R*)-alkanol **12** with 96% ee was obtained with a yield of 95%. On the other hand, in the presence of (*R*)-deuterated alcohol (> 95% ee), (*S*)-**12** with 95% ee was obtained in 98% yield. Thus, (*S*)- and (*R*)-benzyl alcohol- $\alpha$ -*d* acted as chiral inducers to give (*R*)- and (*S*)-pyrimidyl alkanols with high ee after consecutive asymmetric autocatalysis, respectively.

Furthermore, the generality of the effect of isotopic enantiomers in chiral initiation was exemplified using chiral tolyl methanol- $\alpha$ -*d*, 2,2-naphthyl



**Scheme 22** Enantioselective addition of diisopropylzinc to aldehyde **11** using chiral  $\alpha$ -deuterated alcohols as chiral inducers

methanol- $\alpha$ -*d* and 3-phenylpropanol- $\alpha$ -*d*. Each isotopically chiral compound acted as a chiral initiator in the enantioselective addition of *i*-Pr<sub>2</sub>Zn to aldehyde **11**, and pyrimidyl alkanol (*R*)-**12** with high ee was synthesized, respectively [118]. Thus asymmetric autocatalysis is an efficient method to discriminate hydrogen isotope chirality.

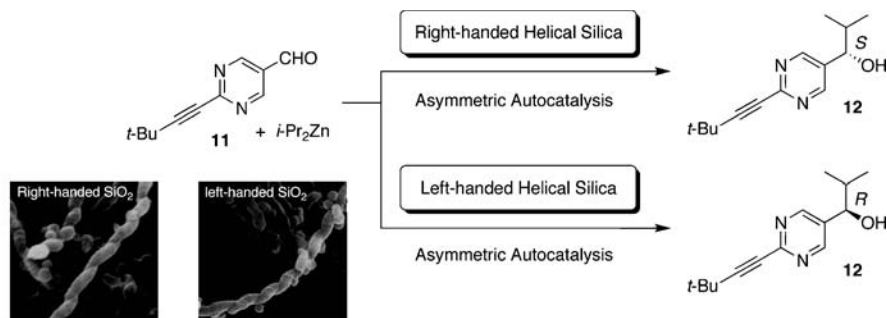
### 4.3

#### Asymmetric Autocatalysis Initiated by Heterogeneous Chiral Substances

Heterogeneous solid materials such as silica play an important role in organic synthesis because they provide suitable environments such as appropriately sized cavities for certain reactions, and they work as catalysts [119–122]. They usually have high (especially thermal) stability. Their insolubility in solvents facilitates separation of the catalyst from the reaction mixture.

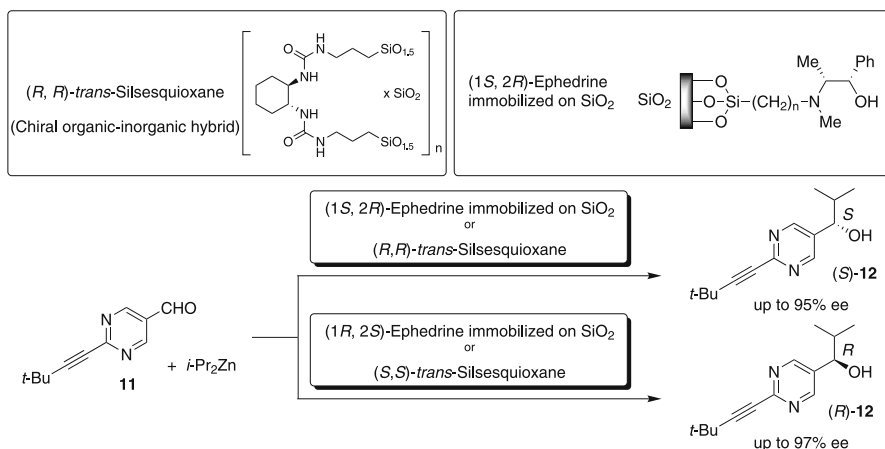
We found that inorganic helical structures such as helical silica serve as chiral triggers for asymmetric autocatalysis (Scheme 23). In the presence of helical silica, the enantioselective addition of *i*-Pr<sub>2</sub>Zn to 2-alkynylpyrimidine-5-carbaldehyde **11** was examined. In the presence of right-handed helical silica, (*S*)-5-pyrimidyl alkanol **12** was formed [123]. In contrast, in the presence of left-handed helical silica, (*S*)-5-pyrimidyl alkanol **12** with high ee was obtained. These results clearly show that asymmetric autocatalysis can discriminate the helical structure in artificially tuned inorganic silica.

Chiral organic–inorganic hybrid materials such as silsesquioxane and ephedrine immobilized on silica gel also act as chiral inducers of asymmetric autocatalysis (Scheme 24) [124–126]. Enantioselective addition of *i*-Pr<sub>2</sub>Zn



Diameters of the helical silica are 100–110 nm.

**Scheme 23** Helical silica-induced highly enantioselective asymmetric autocatalysis of chiral pyrimidyl alkanol



**Scheme 24** Asymmetric autocatalysis initiated with chiral organic–inorganic hybrid materials

to pyrimidine-5-carbaldehyde in the presence of these heterogeneous chiral hybrid materials produce highly enantioenriched (*S*)- and (*R*)-pyrimidyl alkanol **12** following asymmetric autocatalysis with amplification of chirality.

## 5 Summary

We found that chiral 5-pyrimidyl alkanol, 3-quinolyl alkanol and 5-carbamoyl-3-pyridyl alkanol are highly enantioselective asymmetric autocatalysts for the addition of  $i\text{-Pr}_2\text{Zn}$  to the corresponding aldehydes, respectively. Among these, 2-alkynyl-5-pyrimidyl alkanol is a highly efficient asymmetric auto-

catalyst with > 99.5% enantioselectivity. Moreover, asymmetric autocatalysis with amplification of ee from extremely low ee to > 99.5% ee was realized for the first time by consecutive asymmetric autocatalysis without the need for any other chiral auxiliary. Kinetic analysis of pyrimidyl alkanol suggested that the reaction is second order in the zinc monoalkoxide of the pyrimidyl alkanol.

Chiral organic compounds with low ee, when exposed to CPL serve as chiral triggers for asymmetric autocatalysis. The overall process correlates, for the first time, the chirality of CPL with an organic compound with very high ee. Chirality of the CPL was directly correlated with the chirality of the pyrimidyl alkanol with high ee by asymmetric photodegradation of racemic pyrimidyl alkanol in combination with asymmetric autocatalysis. Chiral inorganic crystals such as quartz and sodium chlorate act as chiral triggers and regulate the sense of the asymmetric autocatalysis. The process correlates, for the first time, the chirality of inorganic crystals with an organic compound with very high ee.

Chiral organic crystals composed of achiral compounds such as hippuric acid act as the initial source of chirality of asymmetric autocatalysis to produce the highly enantiomerically pure product. In this reaction, chiral organic crystals are utilized as a chiral inducer, not as a reactant. Therefore, these results are the realization of the process in which the crystal chirality of achiral organic compounds induces asymmetry in another organic compound whose chirality was amplified to produce a large amount of enantiomerically pure organic compound, pyrimidyl alkanol in conjunction with asymmetric autocatalysis.

Highly sensitive chiral discrimination of amino acids with low ee was described. Amino acids with low ee act as a chiral initiator of asymmetric autocatalysis. In the presence of amino acids with low ee, pyrimidine-5-carbaldehyde was treated with *i*-Pr<sub>2</sub>Zn to produce chiral pyrimidyl alkanol with the absolute configuration correlated with that of the amino acid by the consecutive asymmetric autocatalysis with amplification of ee. In addition, direct examination of extraterrestrial chirality was performed using meteorites by applying the asymmetric autocatalysis as the chiral sensor. The results indicated the presence of some chiral factor in the meteorites other than known organic compounds such as amino acids.

Spontaneous absolute asymmetric synthesis was described in the formation of enantiomerically enriched pyrimidyl alkanol from the reaction of pyrimidine-5-carbaldehyde and *i*-Pr<sub>2</sub>Zn without adding a chiral substance in combination with asymmetric autocatalysis. The approximate stochastic distribution of the absolute configurations of pyrimidyl alkanols strongly suggests that the reaction is a spontaneous absolute asymmetric synthesis.

It was shown that the asymmetric autocatalysis of chiral pyrimidyl alkanol is the only possible method to discriminate cryptochiral quaternary saturated hydrocarbons, whose chirality is not capable of determination by any current

method. The discrimination of chirality due to deuterium substitution is also accessible by the highly sensitive asymmetric autocatalysis.

As described, asymmetric autocatalysis is closely related to the origin of the homochirality of organic compounds.

**Acknowledgements** This work was supported by a Grant-in-Aid from the Ministry of Education, Culture, Sports, Science and Technology.

## References

1. Maddox J (1998) What Remains to Be Discovered: Mapping the Secrets of the Universe, the Origins of Life, and the Future of the Human Race, Free Press
2. Kuhn W, Knopf EZ (1930) *Phys Chem B* 7:292
3. Bernstein WJ, Calvin M, Buchardt O (1972) *J Am Chem Soc* 94:494
4. Inoue Y (1992) *Chem Rev* 92:741
5. Bonner WA, Rubenstein E (1987) *BioSystems* 20:99
6. Feringa BL, van Delden RA (1999) *Angew Chem Int Ed* 38:3418
7. Hazen RM (2004) Chiral Crystal Faces of Common Rock-Forming Minerals In: Pályi G, Zucchi C (eds) *Progress in Biological Chirality*, chap 9. Elsevier, Oxford, pp 137–151
8. Cairns-Smith AG (1986) *Chem Ber*, p 559
9. Green BS, Lahav M, Rabinovich D (1972) *Acc Chem Res* 12:191
10. Matsuura T, Koshima H (2005) *J Photochem Photobiol C: Photochem Rev* 6:7
11. Tanaka K, Toda F (2000) *Chem Rev* 100:1025
12. Sakamoto M (1997) *Chem Eur J* 3:684
13. Hasegawa M (1983) *Chem Rev* 83:507
14. Mislow K (2003) *Collect Czech Chem Commun* 68:849–864
15. Islas JS, Lavabre D, Grevy JM, Lamonedá RH, Cabrera HR, Micheau JC, Buhse T (2005) *Proc Natl Acad Sci* 102:13743
16. Mason SF, Tranter GE (1984) *Mol Phys* 53:1091
17. Frank FC (1953) *Biochim Biophys Acta* 11:459
18. Soai K, Shibata T (1999) Asymmetric autocatalysis and biomolecular chirality. In: Pályi G, Zucchi C, Caglioti L (eds) *Advances in biochirality*, chap 11. Elsevier, Oxford, p 125
19. Soai K, Shibata T, Sato I (2000) *Acc Chem Res* 33:382
20. Soai K (1999) *Enantiomer* 4:591
21. Soai K, Shibata T (1997) *J Synth Org Chem Jpn* 55:994
22. Soai K, Shibata T (2000) Asymmetric amplification and autocatalysis In: Ojima I (ed) *Catalytic asymmetric synthesis*, 2nd ed, chap 9. Wiley-VCH, New York, p 699
23. Soai K, Shibata T, Sato I (2001) *J Chem Soc Jpn, Chem Ind Chem*, p 141
24. Soai K, Sato I, Shibata T (2001) *Chem Record* 1:321
25. Soai K, Sato I (2002) *Chirality* 14:548
26. Soai K (2002) Asymmetric autocatalysis and the origin of chiral homogeneity of biologically relevant molecules. In: Pályi G, Zucchi C, Caglioti L (eds) *Fundamentals of life*. Elsevier, Paris, p 427
27. Soai K, Sato I, Shibata T (2002) *J Synth Org Chem Jpn* 60:668
28. Soai K, Sato I (2002) *Viva Origino* 30:186

29. Soai K, Sato I, Shibata T (2004) Asymmetric autocatalysis and the origin of homochirality of biomolecules. In: Malhotra SV (ed) *Methodologies in asymmetric catalysis*. J Am Chem Soc, Washington, DC, p 85
30. Soai K (2004) *J Synth Org Chem Jpn* 62:673
31. Soai K, Shibata T, Sato I (2004) *Bull Chem Soc Jpn* 77:1063
32. Soai K, Kawasaki T (2006) *Chirality* 18:469
33. Soai K, Kawasaki T (2006) *Shokubai (Catalysts & Catalysis)* 48:346
34. Bolm C, Bienewald F, Seger A (1996) *Angew Chem Int Ed Engl* 35:1657
35. Avalos M, Babiano R, Cintas P, Jiménez JL, Palacios JC (2000) *Chem Commun*, p 887
36. Buschmann H, Thede R, Heller D (2000) *Angew Chem Int Ed* 39:4033
37. Todd MH (2002) *Chem Soc Rev* 31:211
38. Blackmond DG (2004) *Proc Nat Acad Sci* 101:5732
39. Podlech J, Gehring T (2005) *Angew Chem Int Ed* 44:5776
40. Mikami K, Yamanaka M (2003) *Chem Rev* 103:3369
41. Gridnev ID (2006) *Chem Lett* 35:148
42. Caglioti L, Zucchi C, Pályi G (2005) *Chemistry Today (Chimica Oggi)* 23:38
43. Pályi G, Micskei K, Zékány L, Zucchi C, Caglioti L (2005) *Magy Kem Lapja* 60:17
44. Stankiewicz J, Eckardt LH (2006) *Angew Chem Int Ed* 45:342
45. Jacobsen EN, Pfaltz A, Yamamoto H (1999) *Comprehensive asymmetric catalysis*. Springer-Verlag, Heidelberg
46. Ojima I (2000) *Catalytic asymmetric synthesis*, 2nd edn. Wiley, New York
47. Malhotra SV (2004) *Methodologies in asymmetric catalysis*. J Am Chem Soc, Washington, DC
48. Soai K, Niwa S (1992) *Chem Rev* 92:833
49. Noyori R, Kitamura M (1991) *Angew Chem Int Ed* 30:49
50. Pu L, Yu HB (2001) *Chem Rev* 101:757
51. Mukaiyama T, Soai K, Sato T, Shimizu H, Suzuki K (1979) *J Am Chem Soc* 101:1455
52. Soai K, Yokoyama S, Ebihara K, Hayasaka T, (1987) *J Chem Soc Chem Commun*, p 1690
53. Soai K, Yokoyama S, Hayasaka T (1991) *J Org Chem* 56:4264
54. Soai K, Hayase T, Takai K, Sugiyama T (1994) *J Org Chem* 59:7908
55. Soai K, Ookawa A, Ogawa K, Kaba T (1987) *J Chem Soc, Chem Commun*, p 467
56. Soai K, Ookawa A, Kaba T, Ogawa K (1987) *J Am Chem Soc* 109:7111
57. Soai K, Hori S, Niwa S (1989) *Heterocycles* 29:2065
58. Shibata T, Choji K, Morioka H, Hayase T, Soai K (1996) *Chem Commun*, p 751
59. Shibata T, Morioka H, Tanji S, Hayase T, Kodaka Y, Soai K (1996) *Tetrahedron Lett* 37:8783
60. Shibata T, Morioka H, Hayase T, Choji K, Soai K (1996) *J Am Chem Soc* 118:471
61. Soai K, Shibata T, Morioka H, Choji K (1995) *Nature* 378:767
62. Shibata T, Hayase T, Yamamoto J, Soai K (1997) *Tetrahedron: Asymm* 8:1717
63. Shibata T, Yonekubo S, Soai K (1999) *Angew Chem Int Ed* 38:659
64. Sato I, Urabe H, Ishiguro S, Shibata T, Soai K (2003) *Angew Chem Int Ed* 42:315
65. Lutz F, Kawasaki T, Soai K (2006) *Tetrahedron: Asymm* 17:486
66. Sato I, Yanagi T, Soai K (2002) *Chirality* 14:166
67. Sato I, Omiya D, Tsukiyama K, Ogi Y, Soai K (2001) *Tetrahedron: Asymm* 12:1965
68. Sato I, Omiya D, Igarashi H, Kato K, Ogi Y, Tsukiyama K, Soai K (2003) *Tetrahedron: Asymm* 14:975
69. Gridnev ID, Serafimov JM, Brown JM (2004) *Angew Chem Int Ed* 43:4884
70. Blackmond DG (2004) *Proc Natl Acad Sci* 101:5732



71. Buhse T (2003) *Tetrahedron: Asymm* 14:1055
72. Saito Y, Hyuga H (2004) *J Phys Soc Jpn* 73:33
73. Lente G (2005) *J Phys Chem A* 109:11058
74. Micskei K, Pota G, Caglioti L, Palyi G (2006) *J Phys Chem A* 110:5982
75. Shibata T, Yamamoto J, Matsumoto N, Yonekubo S, Osanai S, Soai K (1998) *J Am Chem Soc* 120:12157
76. Kawasaki T, Shimizu M, Suzuki K, Sato I, Soai K (2004) *Tetrahedron: Asymm* 15:3699
77. Kawasaki T, Suzuki K, Licandro E, Bossi A, Maiorana S, Soai K (2006) *Tetrahedron Asymm* 17:2050
78. Bailey J, Chrysostomou A, Hough JH, Gledhill TM, McCall A, Clark S, Menard F, Tamura M (1998) *Science* 281:672
79. Nishino H, Kosaka A, Hembury GA, Aoki F, Miyauchi K, Shitomi H, Onuki H, Inoue Y (2002) *J Am Chem Soc* 124:11618
80. Suarez M, Schuster GB (1995) *J Am Chem Soc* 117:6732
81. Kagan H, Moradpour A, Nicoud JF, Balavoine G, Tsoucaris G (1971) *J Am Chem Soc* 93:2353
82. Soai K, Sato I (2001) *Enantiomer* 6:189
83. Sato I, Ohgo Y, Igarashi H, Nishiyama D, Kawasaki T, Soai K (2007) *J Organomet Chem* 692:1783
84. Sato I, Yamashita R, Kadowaki K, Yamamoto J, Shibata T, Soai K (2001) *Angew Chem Int Ed* 40:1096
85. Sato I, Sugie R, Matsueda Y, Furumura Y, Soai K (2004) *Angew Chem Int Ed* 43:4490
86. Kawasaki T, Sato M, Ishiguro S, Saito T, Morishita Y, Sato I, Nishino H, Inoue Y, Soai K (2005) *J Am Chem Soc* 127:3274
87. Hazen RM (2004) Chiral crystal faces of common rock-forming minerals In: Palyi G, Zucchi C (eds) *Progress in biological chirality*, chap 9. Elsevier, Oxford, p 137
88. Bonner WA, Kavasmaneck PR, Martin FS, Flores JJ (1974) *Science* 186:143
89. Soai K, Osanai S, Kadowaki K, Yonekubo S, Shibata T, Sato I (1999) *J Am Chem Soc* 121:11235
90. Pagni RM, Compton RN (2002) *Cryst Growth Des* 2:249
91. Kondepudi DK, Kaufman RJ, Singh N (1990) *Science* 250:975
92. Sato I, Kadowaki K, Soai K (2000) *Angew Chem Int Ed* 39:1510
93. Sato I, Kadowaki K, Ohgo Y, Soai K (2004) *J Mol Cat A Chem* 216:209
94. Penzien K, Schmidt GM (1969) *Angew Chem Int Ed* 8:608
95. Ringertz H (1971) *Acta Crystallogr Sec B* 27:285
96. Kawasaki T, Suzuki K, Hatase K, Otsuka M, Koshima H, Soai K (2006) *Chem Commun*, p 1869
97. Koshima H, Hayashi E, Matsuura T, Tanaka K, Toda F, Kato M, Kiguchi M (1997) *Tetrahedron Lett* 38:5009
98. Koshima H, Nagano M, Asahi T (2005) *J Am Chem Soc* 127:2455
99. Kawasaki T, Jo K, Igarashi H, Sato I, Nagano M, Koshima H, Soai K (2005) *Angew Chem Int Ed* 44:2774
100. Cronin JR, Pizzarello S (1997) *Science* 275:951
101. Kawasaki T, Hatase K, Fujii Y, Jo K, Soai K, Pizzarello S (2006) *Geochim Cosmochim Acta* 70:5395
102. Mills WH (1932) *Chem Ind* 51:750
103. Soai K, Shibata T, Kowata Y (1997) *JP Patent* 9 268 179
104. Soai K, Sato I, Shibata T, Komiya S, Hayashi M, Matsueda Y, Imamura H, Hayase T, Morioka H, Tabira H, Yamamoto J, Kowata Y (2003) *Tetrahedron: Asymm* 14:185

105. Kawasaki T, Suzuki K, Shimizu M, Ishikawa K, Soai K (2006) *Chirality* 18:479
106. Eliel EL, Wilen SW (1994) *Stereochemistry of Organic Compounds*. Wiley, New York (Chap 4)
107. Wynberg H, Hekkert GL, Houbiers JPM, Bosch HW (1965) *J Am Chem Soc* 87:2635
108. Mislow K, Bickart P (1976–1977) *Isr J Chem* 15:1
109. Kawasaki T, Tanaka H, Tsutsumi T, Kasahara T, Sato I, Soai K (2006) *J Am Chem Soc* 128:6032
110. Nishio M, Hirota M, Umezawa Y (1998) *The CH/p Interaction, Evidence, Nature, and Consequences*. Wiley-VCH, New York
111. Sato I, Osanai S, Kadowaki K, Sugiyama T, Shibata T, Soai K (2002) *Chem Lett* 168
112. Sato I, Matsueda Y, Kadowaki K, Yonekubo S, Shibata T, Soai K (2002) *Helv Chim Acta* 85:3383
113. Sato I, Ahno A, Aoyama Y, Kasahara T, Soai K (2003) *Org Biomol Chem* 1:244
114. Tanji S, Ohno A, Sato I, Soai K (2001) *Org Lett* 3:287
115. Arigoni D, Eliel EL (1969) *Top Stereochem* 4:127
116. Verbit L (1970) *Prog Phys Org Chem* 7:51
117. Bartell LS, Roth EA, Hollowell CD, Kuchitsu K, Young JE Jr (1965) *J Chem Phys* 42:2683
118. Bartell L, Roskos RR (1966) *J Chem Phys* 44:457
119. Sato I, Omiya D, Saito T, Soai K (2000) *J Am Chem Soc* 122:11739
120. Davis ME (1993) *Acc Chem Res* 26:111
121. Davis ME, Katz A, Ahmad WR (1996) *Chem Mater* 8:1820
122. Thomas JM, Raja R (2001) *Chem Commun*, p 675
123. Wulff G (2002) *Chem Rev* 102:1
124. Sato I, Kadowaki K, Urabe H, Hwa Jung J, Ono Y, Shinkai S, Soai K (2003) *Tetrahedron Lett* 44:721
125. Soai K, Watanabe M, Yamamoto A (1990) *J Org Chem* 55:4832
126. Kawasaki T, Ishikawa K, Sekibata H, Sato I, Soai K (2004) *Tetrahedron Lett* 45:7939
127. Sato I, Shimizu M, Kawasaki T, Soai K (2004) *Bull Chem Soc Jpn* 77:1587



# Asymmetric Autocatalysis with Organozinc Complexes; Elucidation of the Reaction Pathway

John M. Brown<sup>1</sup> (✉) · Ilya Gridnev<sup>2</sup> · Jürgen Klankermayer<sup>3</sup>

<sup>1</sup>Chemistry Research Laboratory, Mansfield Rd., Oxford OX1 3TA, UK  
*John.brown@chem.ox.ac.uk*

<sup>2</sup>Graduate School of Science and Engineering, Tokyo Institute of Technology,  
 2-12-1 I3-28 O-okayama, Meguro-ku, 152-8552 Tokyo, Japan

<sup>3</sup>Institut fuer Technische und Makromolekulare Chemie (ITMC),  
 RWTH Aachen University, 52074 Aachen, Germany

<b>1</b>	<b>Introduction</b>	36
1.1	Preamble	36
1.2	Background	36
<b>2</b>	<b>Mechanistic Approaches 1. Kinetics</b>	39
<b>3</b>	<b>Mechanistic Approaches 2. NMR Analyses</b>	44
3.1	Background	44
3.2	Solution Structure of the Soai Catalyst	45
3.2.1	NMR Spectra in thf-d <sub>8</sub>	45
3.2.2	NMR Spectra in Toluene-d <sub>8</sub>	48
3.2.3	NMR Studies of Dialkylzinc Binding	48
3.2.4	NMR Exchange Spectroscopy	52
3.3	Correlation of NMR Results and Autocatalysis	53
3.4	NMR in Spontaneous Asymmetric Synthesis	55
<b>4</b>	<b>Mechanistic Approaches 3. Computational Chemistry</b>	56
4.1	Methylzinc Models	56
4.2	Isopropylzinc-Derived Species	58
<b>5</b>	<b>Conclusions and Remaining Problems</b>	61
	<b>References</b>	62

**Abstract** This review describes the development of mechanistic understanding of amplifying asymmetric autocatalysis. After a brief description of kinetics, the main body of the work discusses the application of a variety of NMR techniques to the structure of the resting state in solution. The results are consistent with a dominant square Zn–O bonded dimer at ambient temperature. Furthermore, the energies of homo- and heterochiral dimers is comparable; they exchange slowly on the NMR timescale but fast enough for the lifetime of an individual molecule to be established. The association of alkylzinc with this dimer can be quantified and located, and dynamic alkyl exchanges defined. DFT calculations have been carried out, which underpin the dimer structure and provide further insight into the steric control of autocatalysis by the bulk of diisopropylzinc. NMR, kinetics and computation converge in supporting the role of dimers of the

indicated structure, and in pointing to a mechanism whereby the unique reactivity of the homochiral dimer is the driving force, at least at ambient temperature.

**Keywords** Absolute asymmetric synthesis · DFT calculations · Microcalorimetric kinetics · NMR analyses · Soai autocatalysis

## 1

### Introduction

#### 1.1

##### Preamble

This review is concerned with the development of our understanding of the mechanism of amplifying autocatalysis, and endeavours to provide an explanation of how the original example arising from Soai's work in 1995 has remained unique over 12 years. This implies a highly convergent process, and that is in keeping with the current state of understanding. The demonstration of asymmetric amplifying autocatalysis has excited interest far beyond the organic chemistry community. This arises both from the fact that autocatalysis is an intrinsically interesting phenomenon, and also from its possible connection to the origins of life.

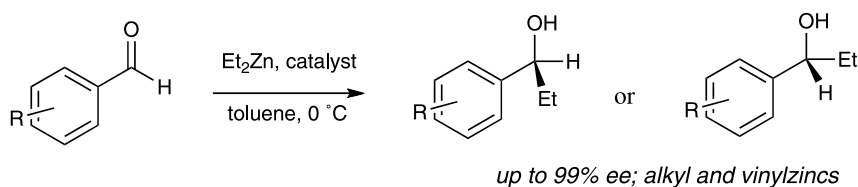
#### 1.2

##### Background

Nobody has yet been able to provide a convincing model for the way in which homochirality evolved in the primordial world so as to permit the development of living organisms. Progress from racemic compounds towards the enantiomerically pure species that characterise the living cell is likely to have occurred at an early stage in molecular evolution. In all probability the triggers were in place prior to the existence of pre-cellular structures, and thus involved purely chemical events. In the absence of experiment, or any real prospect thereof, there has been intense speculation about how prebiotic "symmetry-breaking" might have occurred [1–4]. This speculation has centred on physical mechanisms (parity violation, photolysis with plane polarised light, chirality enhancement through amplifying crystallisation processes, selective homochiral polymerisation) that have been presented by several reviewers, generally without a specific conviction to adopt one explanation over another [5–12]. There has been a recent surge of interest in chiral amplification through crystallisation processes, however [13–20]. One review specifically comments on the relationship between such crystallisations and chirally amplifying autocatalysis [21]. The possibility that homochirality could arise from purely chemical processes was raised by Frank in 1954, and became established

in most later discussions ([22], for an insight into contemporary thinking on non-linear spatiotemporal processes in biology, see [23]). His ground-breaking idea was that an autocatalytic process, one in which the product self-generates more of itself from the reactants, could lead to amplification of one enantiomer if the other was subject to an inhibition process: “The interaction between the antimers (*sic* = enantiomers) ... may be interpreted either as a lethal interaction whenever they meet, or as a tendency of the presence of either to diminish the reproduction rate of the other”. The vagueness of this proposition was removed when mathematical models describing mechanisms leading to amplification of chirality were established [24].

In separate developments, somewhat later on, Kagan provided an overview of the non-linear effects (NLE) that are sometimes observed in catalytic reactions [25–28]. The non-linearity refers to the anomalous relationship between the enantiomer excess (ee) of the product in a catalytic reaction and the ee of the catalyst. This can be positive, with enhancement of ee, or negative with its diminution. The concept was not completely novel at the time it was introduced [29], but Kagan’s contribution was to recognise the importance and generality of NLE, and to devise a logical framework that in turn provided a powerful illumination of reaction mechanism. The most striking examples of positive non-linear effects are to be found in the addition of alkylzinc reagents to aldehydes, catalysed by chiral  $\beta$ -aminoalcohols, and the mechanism is now reasonably well understood (Fig. 1). The catalyst forms a dimeric adduct with the alkylzinc, and the racemic dimer is generally far more stable than the homochiral dimer. The catalyst is a monomer formed by dissociation, and in these circumstances the easier dissociation of the homochiral dimer leads to a “reservoir” effect that enhances the ee of this



**Effective catalysts (benzaldehyde,  $\text{Et}_2\text{Zn}$ ) include**

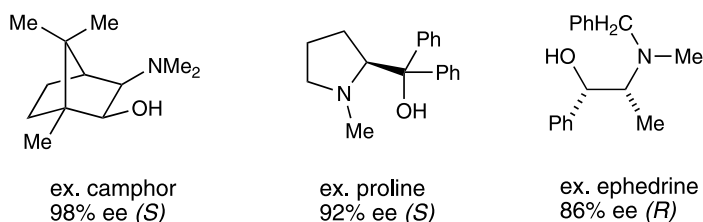


**Fig. 1** Basic features of zinc alkyl addition to aldehydes

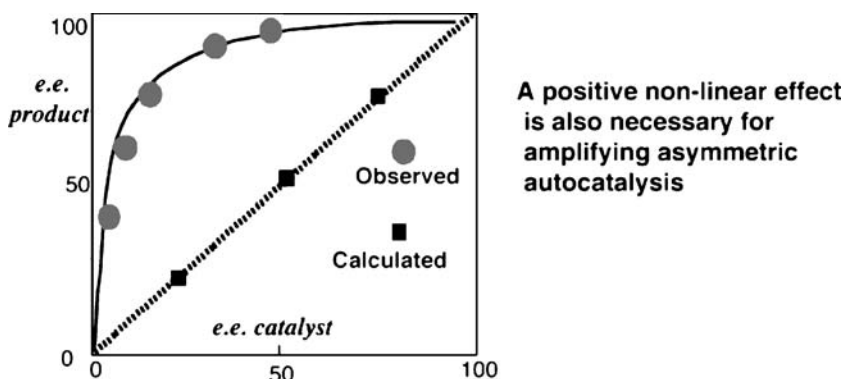


**Fig. 2** Illustration of a positive non-linear effect, where the enantiomer excess in the product exceeds that of the catalyst

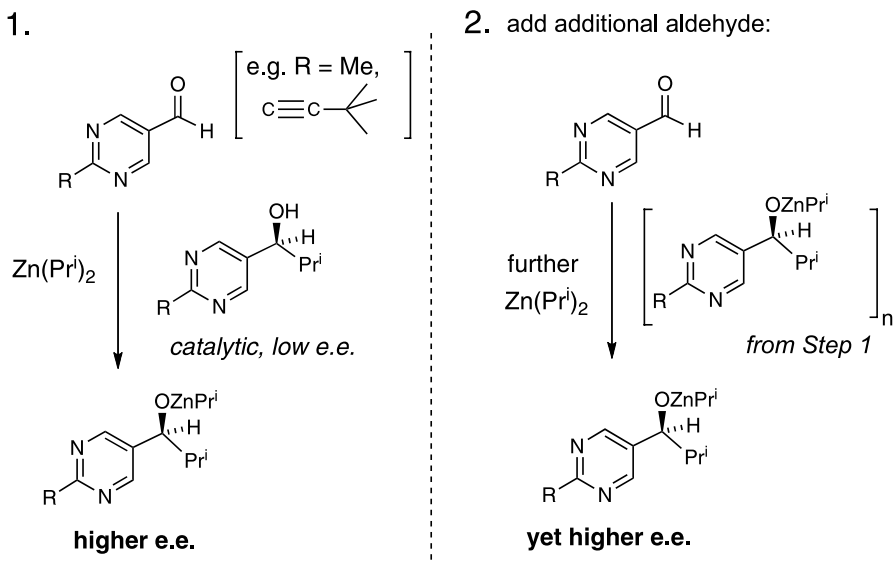


**Fig. 3** Basis of the Soai amplifying autocatalysis illustrated by a two-stage procedure

monomer. The overall effect can be quite dramatic, with ca. 15% ee catalyst leading to 90% ee product in favourable cases. The reservoir mechanism is not the only one that leads to positive NLEs, and a dimeric catalyst that is only operative through the homochiral form may provide an viable alternative pathway.

It is explicit in the definition and formulation of NLEs that an enantio-selective reaction where the product catalyses its own formation will be subject to the same rules; autocatalysis can hence both breed and amplify chirality (Fig. 2). Up to late 1995 examples were lacking, until the work of Soai

and colleagues revealed the first case (Fig. 3). The combination of a specific alkylzinc (diisopropyl) and a class of aldehydes based on the pyrimidine nucleus was shown to lead to effective amplifying autocatalysis. Over several years these observations were extended by Soai, but the initial parameters (nature of the alkylzinc, structural relationship between the nitrogen lone pair and the aldehyde) were barely altered. The elucidation of mechanistic details of this remarkable observation forms the basis of our review.

There have been two additional striking developments arising from the original experimental work. In the absence of preformed catalyst, almost any added enantiomerically pure species can trigger autocatalysis [30–38]. For example, single-handed quartz crystals, enantiomerically pure hydrocarbons lacking functional groups or resolved isotopically chiral alcohols (RCHDOH) are all effective in inducing autocatalysis in the Soai system with high ee product of reproducible configuration. The autocatalytic reaction is also initiated by circularly polarised light as the only external chiral source [39–41]. The second development was demonstration that the Soai system, consisting only of organozinc and aldehyde components in the absence of product catalyst, reacted spontaneously to give an enantiomerically enriched product with random configuration. This was the first time that a reaction in solution had led to asymmetric synthesis; the result has been verified in reports from three separate laboratories [42–46]. Soai's system has additionally found use in the identification and amplification of very low levels of chirality [47, 48].

It is remarkable that 10 years after the demonstration of amplifying (positive NLE) autocatalysis by Soai, the observation has not been extended into other areas. Indeed it remains the only case of its kind. There are, however, several examples of autoinductive catalysis, where the newly formed product becomes integrated with the original catalyst and influences the ensuing product ee [49–53]. Likewise, there are many examples of simple autocatalytic organic reactions not involving chirality [54–58]. Very recently, a true example of asymmetric autocatalysis has been discovered in the simple Mannich reaction between an in-situ generated iminium ion and a ketone. This is efficient, to the extent that product catalyst with a high level of enantiomeric enrichment produces almost equally enriched new product. Amplification is absent, however [59]. This provides an incentive to understand the Soai system, not just in its own right but also in order to predict generalities that can lead to further examples.

## 2

### Mechanistic Approaches 1. Kinetics

The asymmetric alkylation of aldehydes by dialkylzinc reagents is one of the most intensively studied catalytic reactions [60–62]. Following the initial discoveries of Oguni and colleagues, including the recognition that a single



enantiomer of a  $\beta$ -aminoalcohol acted as the catalyst for a normally non-productive reaction pathway [63–65], the extensive work of Noyori's group elucidated the mechanism in detail. Their research demonstrated the key features of the reaction, and in particular made the linkage to Kagan's illuminating essays on non-linear effects [66–71]. To summarise this body of work, the catalytic assembly is dimeric in the ground state, but the active catalyst is a monomer. When the aminoalcohol is enantiomerically impure (suppose the (*S*)-enantiomer predominates), there are three possible dimers, two homo- and one heterochiral. The heterochiral (*R,S*)-dimer is the more stable, and in consequence of this depletes the equilibrium concentration of (*R*)-enantiomer, as illustrated in Fig. 4. Hence the enantiomer excess of the reaction product can be higher than the initial enantiomer excess of the catalyst. As can be seen from Fig. 4, the monomeric catalyst forms zinc chelate, which acts as a template for both the zinc alkyl reactant (the alkyl group is delivered from an exogenous zinc alkyl) and the aldehyde. A combination of steric and electronic effects leads to the observed enantioselectivity. There are a prolific number of chiral aminoalcohols that function as catalysts for the asymmetric alkylation reaction, and the indicated chelation is believed to provide a universal component of the mechanism.

Soai's autocatalytic reaction appears to break a fundamental rule. The observed amplification of ee is a necessary consequence of a positive non-linear effect, and yet the typical reactant is a rigid  $\gamma$ -aminoalcohol that cannot chelate to zinc (Fig. 5). This means that the Noyori mechanism needs to be modified in some way. Elucidation of this problem requires knowledge both

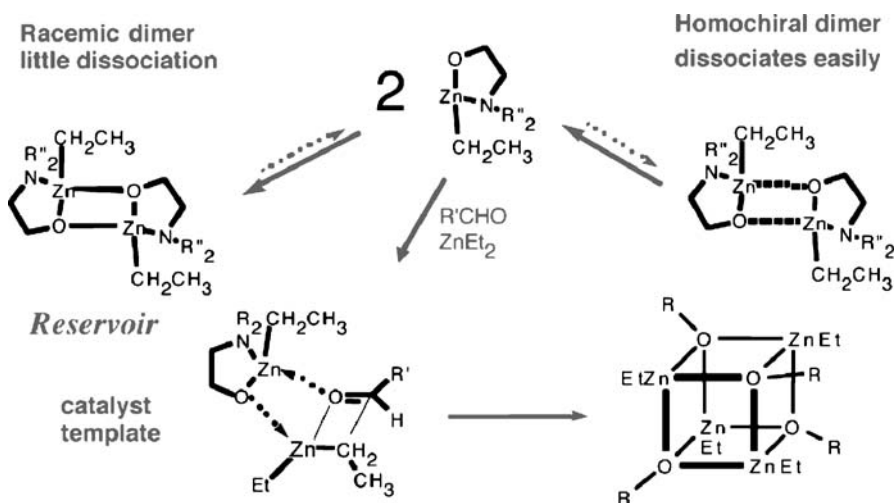


**Fig. 4** Production of a monomeric active catalyst from diethylzinc and a  $\beta$ -aminoalcohol; the resting form is an equilibrating mixture of homochiral and heterochiral dimers, which favours the latter

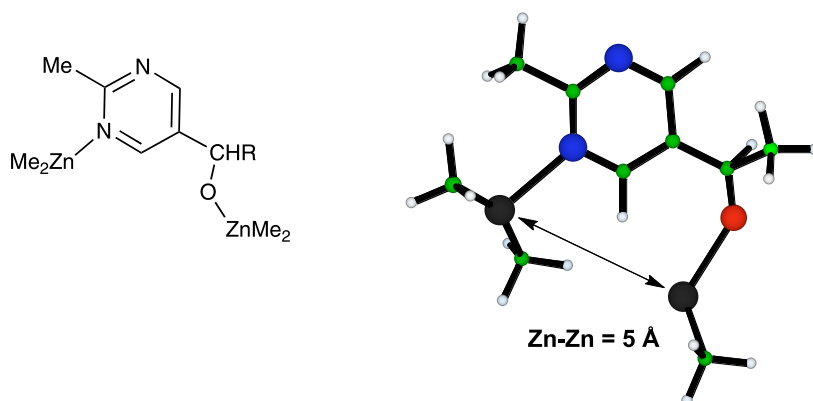


**Fig. 5** The impossibility of forming a monomeric chelate from a 5-substituted pyrimidinyl alcohol

of the catalyst ground state and of the reaction kinetics, so that a clear overall picture may be obtained. The microcalorimetric methodology, popularised by Blackmond [72], is ideal for the study of autocatalytic reactions; under turnover conditions the heat generated as the formal concentration of the catalyst increases should first maximise and then decay through substrate and reagent depletion. A conventional catalytic reaction would demonstrate only constant heat output (zero order in reactants) or decay over time (finite order in reactants).

The first experiments carried out by Blackmond and Brown employing this technique are shown in Fig. 6 [73]. They demonstrate autocatalytic behavior as expected, and much can be learned about the reaction by analysis of the heat output from scalemic, racemic and enantiopure alcohols in separate experiments. The characteristic shapes permit testing against numerical integration of various model mechanisms. There is an excellent fit assuming what is probably the simplest solution. If the true catalyst is dimeric, and there is no selectivity between the binding constants of homochiral and heterochiral forms, yet the heterochiral form is unreactive, a positive non-linear effect ensues. In this case, selectivity is a purely kinetic phenomenon; the positive non-linear effect arises because the statistical distribution between homo- and heterochiral forms causes the excess of (*S,S*)-dimer over (*R,R*)-dimer to exceed the formal ee.

The dimer model was anticipated by Kagan in his analysis of non-linear effects. In simple catalytic cases it is much less common than the reservoir model where the monomeric species is the active catalyst. Figure 7 shows how both of these work in practice for autocatalytic systems, and demonstrate how the two pathways can be distinguished when the catalyst structure is understood. A further consequence of autocatalysis is that (counter-intuitively) the smaller the initial proportion of catalyst, the greater the enhancement of ee.

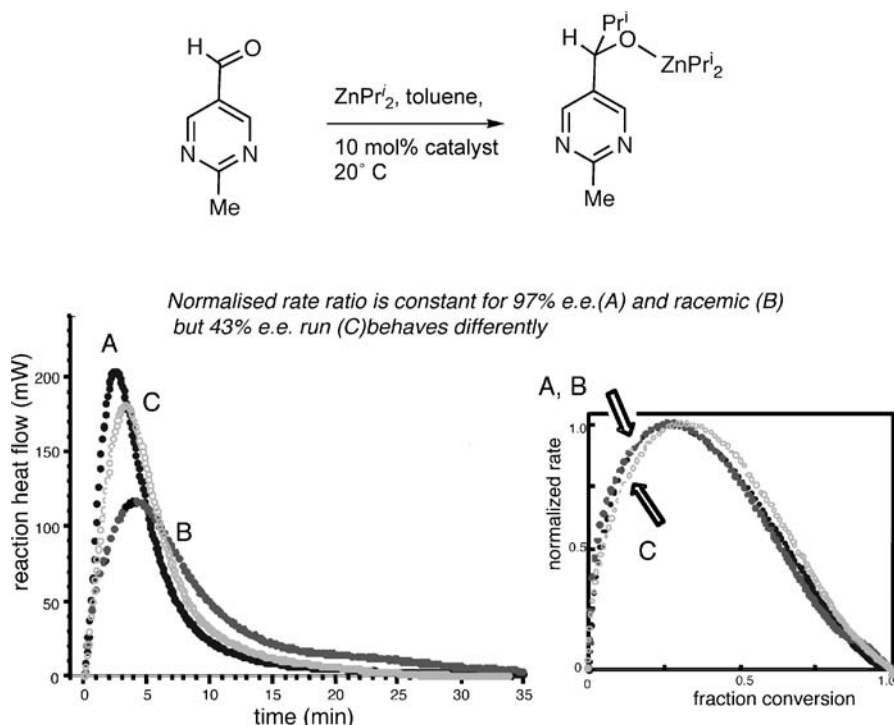


**Fig. 6** Experimental observations made through microcalorimetry of autocatalysis, starting with enantiomerically pure (A), racemic (B) and 43% enantioenriched pyrimidinyl alcohol (C). Conditions as shown in the reaction scheme

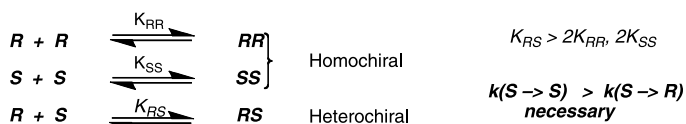
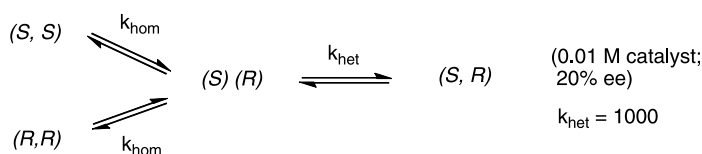
The catalyst term in the rate equation is first order as [dimer] [1–4]. In further analysis of this model, the progress in enantiomer excess over time matches well to that predicted for a dimeric catalyst. This is further augmented by a later paper from Blackmond and Buono [74]. They discovered additional kinetic complexity, in that the kinetics under their chosen conditions fit better to an  $[\text{R}_2\text{Zn}]^0[\text{aldehyde}]^2[\text{dimer}]$  model. Even so, there is a robust correlation between the evolution of ee and the extent of reaction. Notably, the 2-methylpyrimidine was employed in all the kinetic studies described in [20, 21].

As a minimal requirement, analysis of the microcalorimetric kinetics requires the following:

- The active catalyst incorporates two molecules of alkoxide, not one
- The ground state is mainly dimeric under the reaction conditions
- Both racemic and homochiral dimers are formed
- Selectivity is completely kinetic – only the homochiral species is a catalyst

**A(a) Autocatalysis with monomeric catalyst**

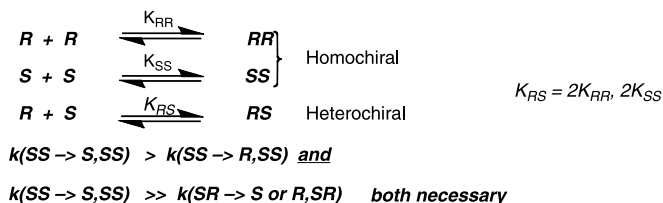
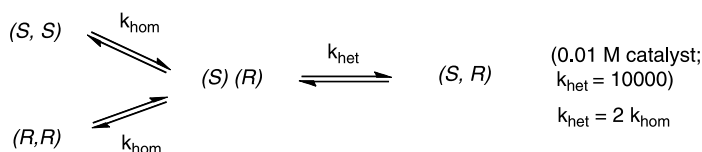
Positive non-linear effect when heterochiral dimer favoured

**A(b)**

$k_{\text{hom}}$	Ee of (S)-monomer
1000	20
100	35
10	48

**B(a) Autocatalysis with dimeric catalyst**

Positive non-linear effect if dimerisation is statistical

**B(b)**

Original ee of alcohol	Ee of homochiral dimer
10	19.8
20	38.5
40	67.0

**Fig. 7** Constraints for autocatalysis by A monomeric (reservoir mechanism) and B dimeric catalysts where the homochiral dimer is the only active form. *a* Indicates the conditions and *b* the typical outcomes for enumeration under illustrative conditions

In his later work, Soai and co-workers showed that other pyrimidine aldehydes were more responsive in the autocatalytic process. In particular, the 4-alkynyl derivatives (e.g.  $\text{CCSiMe}_3$ ,  $\text{CCBu}^t$ ) show a very high stereochemical fidelity,

with >99% ee maintained over several cycles of autocatalysis [75]. In these cases, and starting with low ee reactant, the enhancement is somewhat greater than can be explained by the simple dimer catalyst model, inviting speculation that higher oligomers of autocatalytic zinc species may be involved.

Soai's own work has contributed to kinetic analysis, albeit under conditions significantly different from the ones reported earlier. Reactions were run with the favoured alkynylpyrimidine at  $-25\text{ }^{\circ}\text{C}$  [76]. Reaction progress was analysed by sampling and HPLC, and indicates a strikingly fast process that occurs after an initial burst. The model used in explanation, "under conditions where the concentration of dimers is vanishingly small compared to that of the monomers", involves two Zn alkoxides of the same hand working in tandem in the transition state. An additional input ascribes the auto-amplification to an inhibition process where the "heterotrimeric complex is more stable than the homotrimeric complex" – trimeric complexes being the immediate autocatalytic reaction product. This would require that trimeric structures contribute significantly to the resting state of autocatalysis. In essence, different kinetic studies provide different mechanistic models, and additional physicochemical studies are required in order to distinguish between them.

### 3

## Mechanistic Approaches 2. NMR Analyses

### 3.1

#### Background

The main part of this review concerns the identification of the solution species that must be the active autocatalyst or its progenitor. Like much zinc asymmetric alkylation chemistry, autocatalysis is typically carried out in toluene or related non-polar solvents. This lends itself to NMR analysis under both static and dynamic conditions. Surprisingly, there is relatively little by way of guidance in the parent field of zinc alkylations. In the one detailed study of reactive intermediates [77], Noyori, Kitamura and colleagues demonstrated that both the enantiopure and racemic catalyst (1 : 1  $\text{Me}_2\text{Zn}$ ,  $\beta$ -aminoalcohol) were dimeric (MW in solution, X-ray), and characterised the enantiopure species **A** (see Fig. 8) in  $\text{C}_7\text{D}_8$  by  $^1\text{H}$  and  $^{13}\text{C}$  NMR (note that in Fig. 8 A–E, the chelating ligand is shown in abbreviated form). Several further species in the proposed catalytic cycle were identified. Addition of  $\text{Me}_2\text{Zn}$  breaks the dimeric structure, with formation of an adduct **B** that has distinct and dynamically interconverting Me environments. Likewise, addition of benzaldehyde to the dimer leads rapidly but reversibly to the formation of a monomeric adduct **C**. When both  $\text{Me}_2\text{Zn}$  and benzaldehyde are both added to the dimer below  $0\text{ }^{\circ}\text{C}$ , a further double adduct **D** is formed, and deemed to

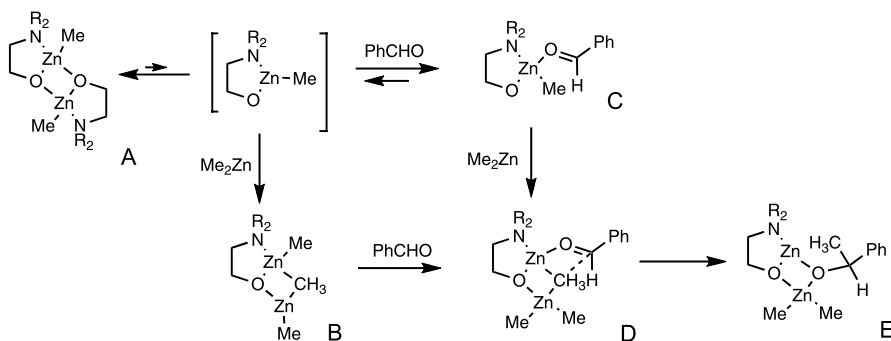


**Fig. 8** Reactive intermediates in asymmetric zinc alkylations observed by NMR

be the true precursor of the addition product **E**. Indeed, this process is observed to occur when the solution is warmed to 20 °C. The double adduct **D** again shows rapid Me-exchange between the two Zn entities. The product of alkyl transfer, **E**, is stable in stoichiometric experiments, but when the reactants are present in excess, turnover occurs with the ultimate formation of an inert tetrameric alkoxide.

In separate experiments, the catalytic reaction was found to be first order in enantiomerically pure  $\beta$ -aminoalcohol catalyst precursor, zero-order in diethylzinc and zero-order in aldehyde above 0.3 M. When racemic catalyst was employed, however, the overall turnover rate was six times slower, and there was a dependency of rate on the concentrations of all three species. This was elaborated further in a quantitative analysis of positive non-linearity, which is one of the classic examples of this effect.

### 3.2

#### Solution Structure of the Soai Catalyst

##### 3.2.1

##### NMR Spectra in $\text{thf-d}_8$

It proved to be technically quite demanding to characterise the autocatalytic species in solution. At concentrations suitable for NMR analysis (0.1 M region) the solubility in  $\text{C}_7\text{D}_8$  was low and there was a tendency to form precipitates on standing. In tetrahydrofuran- $\text{d}_8$  ( $\text{thf-d}_8$ ) this problem was not significant, and in  $\text{C}_7\text{D}_8$  it could be alleviated by addition of excess diisopropylzinc. Autocatalysis is ineffective in  $\text{thf}$ , however. Since  $\text{thf}$  characteristically gave sharp and readily interpretable spectra, much of the early work was carried out in this medium. For comparison, and to ensure generality of the results, two different pyrimidine aldehydes and their enantiopure and racemic alcohol counterparts were employed. The first significant results came when spectra of racemic and enantiopure zinc alkoxides (prepared in situ from

the alcohol and diisopropylzinc) were compared. For the enantiopure 2-Me pyrimidine, an assignable set of signals was observed, in particular CH (aromatic), CH (alkoxide), C (ring methyl) and separate CH, CMe and isopropyl signals. With the racemic species, two signals of comparable intensity were seen for all of the CH (aromatic), CH (alkoxide) and C (ring methyl) signals, clearly corresponding to distinct homo- and heterochiral species (Fig. 9).

The doubling of resonances in the racemate is characteristic of the 2-CCSiMe<sub>3</sub> pyrimidine analogue, and also for both substrates in toluene,

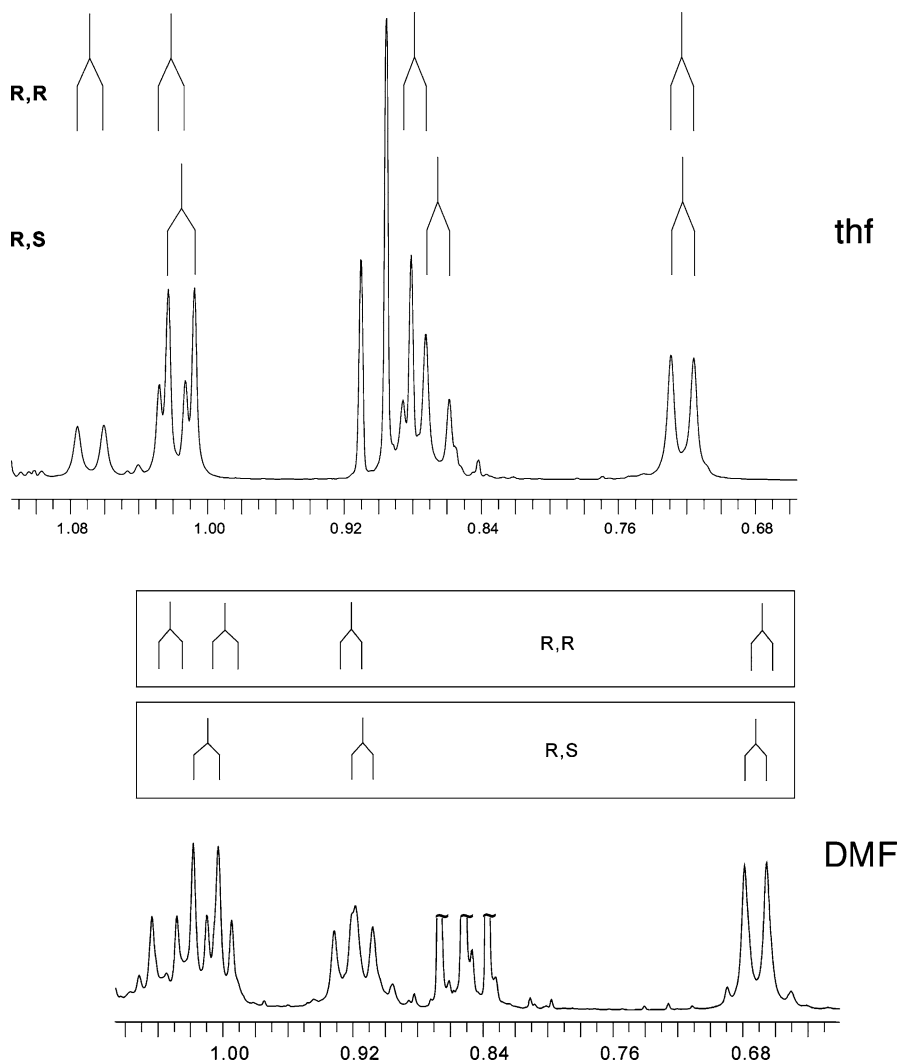


**Fig. 9** Example of the doubling of resonance on going from homochiral to heterochiral 2-TMS-alkynylzinc in thf-d<sub>8</sub> and DMF-d<sub>7</sub>, ZnCHMe<sub>2</sub> and OCHMe<sub>2</sub> region

albeit with broader signals in that medium. The fact that only two sets of resonances are seen indicates formation of (*R,S*) and {(*R,R*), (*S,S*)} dimers in comparable amounts, affirming the model postulated from the microcalorimetry experiments with direct physicochemical evidence. Higher oligomers would be expected to present more signals. It is very hard to envisage trimers or tetramers that possess a single aromatic or alkoxide proton environment distinct for homochiral and heterochiral forms and at the same time exclude all other stereoisomers [78].

Density functional theory (DFT) computational studies (*vide infra*) indicate that there are three viable closed dimeric structures. Since the pyrimidine nitrogen is clearly necessary for autocatalysis, it is tempting to consider a macrocyclic structure where each zinc is N,O-bonded to two distinct pyrimidines. Indeed, a similar structure was postulated in the first mechanism paper [66–71]. For the TMS-ethynyl analogue, a definitive answer can be given on the basis of analysis of the isopropyl Me resonances in *thf-d*<sub>8</sub>. In the enantiomerically pure form there are two separate Me signals associated with the zinc-bound isopropyls and two associated with the alkoxide isopropyl groups. There are only two CH isopropyl environments, and so the observation of four separate Me signals must mean that there are two pairs of isopropyl groups, each exhibiting diastereotopicity. This is in accord with a structure lacking symmetry, or alternatively one possessing a symmetry element that does not render the relevant Me groups equivalent. The corresponding NMR of the racemic Zn alkoxide shows two new signals for the (*R,S*)-alkoxide isopropyl Me groups, but only one at twice intensity for the zinc isopropyl Me groups. A symmetry plane through (CZn – ZnC) is indicated by this result. The only dimer structure compatible with these observations is the Zn – O square shown in Fig. 10.

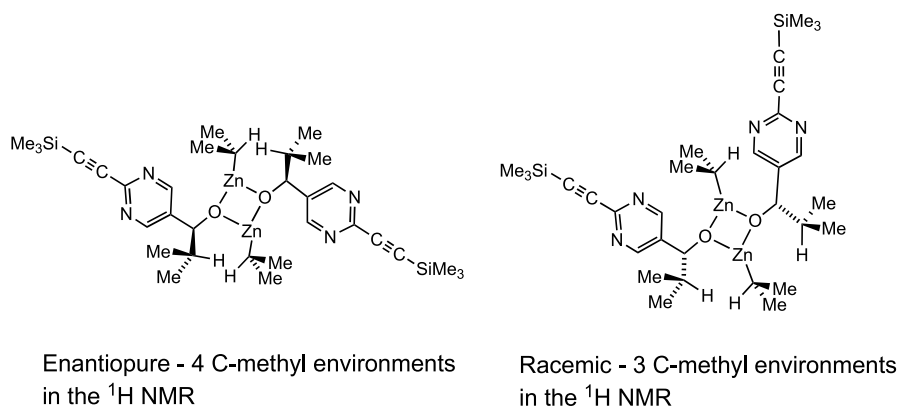


**Fig. 10** Symmetry argument for the square planar dimer structure. A reflection plane bisects CZn – ZnC uniquely in the racemic dimer of square planar structure



### 3.2.2

#### NMR Spectra in Toluene- $d_8$

Zn alkoxide solutions in non-polar solvents have a tendency to precipitate that is alleviated by the addition of excess alkylzinc reagent in the pyrimidine case. The general features of the NMR spectra in  $thf-d_8$  are reproduced in  $C_7D_8$ . For the enantiopure species in  $C_7D_8$ , an interesting difference is that the diastereotopic methyls of Zn-bound isopropyl groups are at 1.4 and 1.3 ppm, strongly deshielded from the 1.07 and 1.01 ppm signals observed in  $thf-d_8$ . DFT calculations indicate the stability of a doubly  $thf$ -solvated structure with additional O – Zn bonding. For racemic dimer in  $C_7D_8$ , prepared from aldehyde synthesized directly without added catalyst, two broadened singlets of similar intensity were observed at 298 K in the 8.5 ppm region, corresponding to the homo- and heterochiral forms (48 : 52). On increasing the temperature these broaden and then coalesce at 348 K (Fig. 11). Similar dynamic behaviour is observed for the sets of alkoxide and methyl protons at 4.5 and 2.6 ppm, respectively. Line-shape analysis of the aryl protons over the range 313–353 K and extrapolation of the slope of  $\ln k(\text{exchange})$  to ambient temperature indicates that the half-life of an individual dimer molecule with respect to  $(R) \leftrightarrow (S)$  exchange is in the region of 15 s at 293 K. The monomer is not observed in this equilibrium, but at the highest temperatures there are small changes in chemical shift that may indicate (dissociative) structural changes. It is noteworthy that the sharpest spectra are obtained in the region of 310–320 K, and at lower temperatures significant broadening sets in. The observation of a single aryl proton environment in all ambient temperature spectra demonstrates a freely rotating ring, and is not compatible with strong N – Zn association.

A second set of VT experiments involved the homochiral TMS-alkynyl dimer, and illustrates the potential complexity of the alkoxide/zinc system outside the ambient temperature range (Fig. 12). As the sample is cooled, all the signals broaden dramatically and then sharpen somewhat, although the low temperature species are not easily defined. The spectra obtained are consistent with the presence of higher oligomers of low symmetry, and probably several such species are present. By way of illustration,  $^1H$  spectra from the low-field aromatic and high-field silylmethyl regions are shown. The complexity of the aryl-H region, and the pairwise connectivities between ring protons involved in the low temperature  $^1H$  EXSY spectra demonstrate that Zn – N association becomes significant at lower temperatures.

### 3.2.3

#### NMR Studies of Dialkylzinc Binding

##### To Aldehyde

The first experiments were carried out with the precursor aldehyde in toluene- $d_8$ , varying the concentration of excess of  $ZnPr_2$  at constant aldehyde

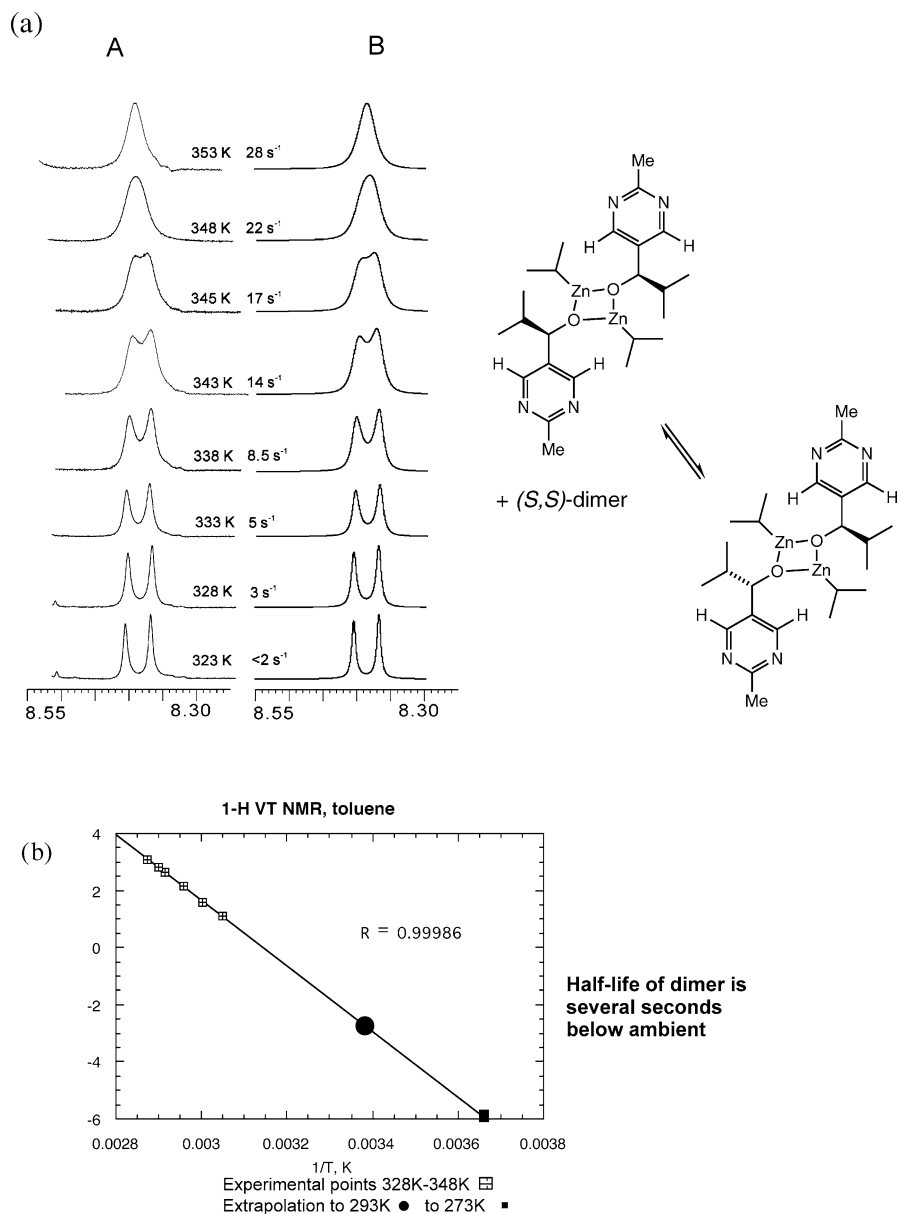


**Fig. 11** VT proton spectra showing dynamic exchange between homo- and heterochiral dimers in the aryl proton region. In **a**, A shows observed and B calculated spectra; **b** is the Arrhenius plot of the data. This gives a half-life for one dimer of ca. 14 s at 20 °C

concentration. In order to obtain significant chemical shift changes, the experiments were conducted at a reduced temperature of 213 K. Under these conditions all three observed nuclei,  $^1\text{H}$ ,  $^{13}\text{C}$  and  $^{15}\text{N}$  shifted in a quantifi-

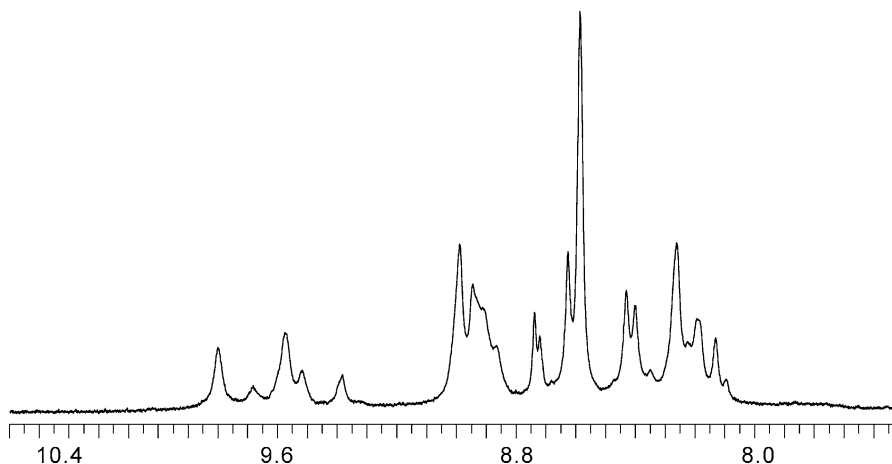


**Fig. 12** Increased complexity of the aromatic protons of the homochiral TMS-ethynylzinc alkoxide  $^1\text{H}$  NMR spectrum below ambient temperature at 208 K in  $\text{C}_7\text{D}_8$ , in contrast to the slightly broadened singlet that is observed in the aromatic region at 298 K

able way (Fig. 13). Measurement of the association constant using a number of independent nuclear probes gave a consistent result, with the outcome:

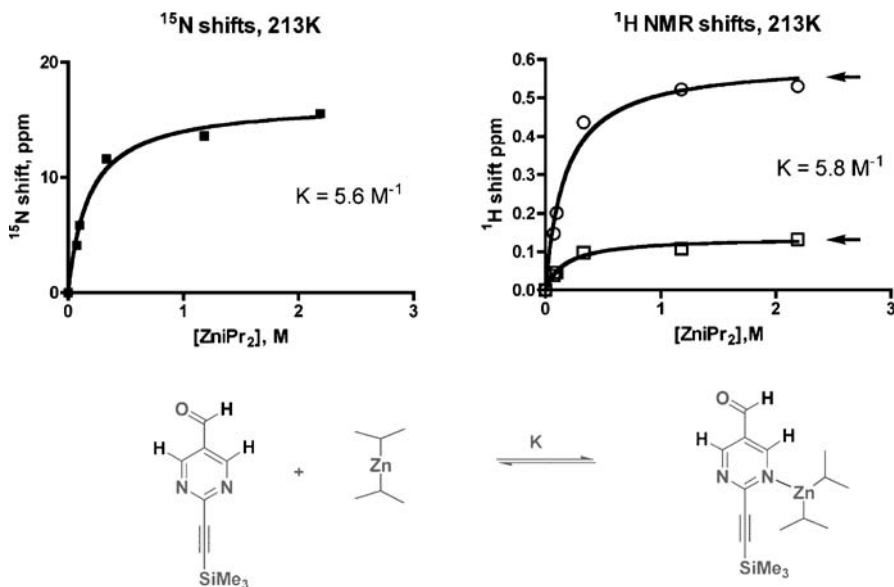
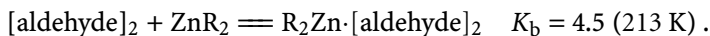
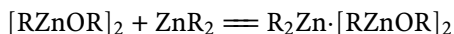


**Fig. 13** Association of diisopropylzinc with the pyrimidine aldehyde. Such significant aryl ring CH chemical shift changes require low temperature analysis

The site of binding is the pyrimidine nitrogen, and not the carbonyl group. The consistency of results with the different nuclear probes indicates that a single association is involved for all the chemical shift changes of different nuclei.

### To Zn Alkoxide

The same procedures were carried out for the Zn alkoxide, monitoring  $^{13}\text{C}$ ,  $^1\text{H}$  and  $^{15}\text{N}$  chemical shift changes against the concentration of excess diisopropylzinc. These experiments proved to be more demanding; it is not possible to provide a stable sample of the alkoxide in the absence of excess zinc alkyl, and the results were carefully gathered to take account of this difficulty. In addition, the best data for  $^{15}\text{N}$  NMR analysis were obtained at a slightly elevated temperature of 308 K. A precursor and a side-product in the  $^{15}\text{N}$ -pyrimidinal were employed as controls for the data in separate experiments, demonstrating the generality of pyrimidine nitrogen to the zinc alkyl reagent. A direct comparison was made between the results obtained in toluene solution, with parallel experiments in thf where the extent of binding is considerably lower (Fig. 14).



$$K_b = 30 \text{ (C}_7\text{D}_8\text{)}; \quad K_b = 0.5 \text{ (thf)}.$$

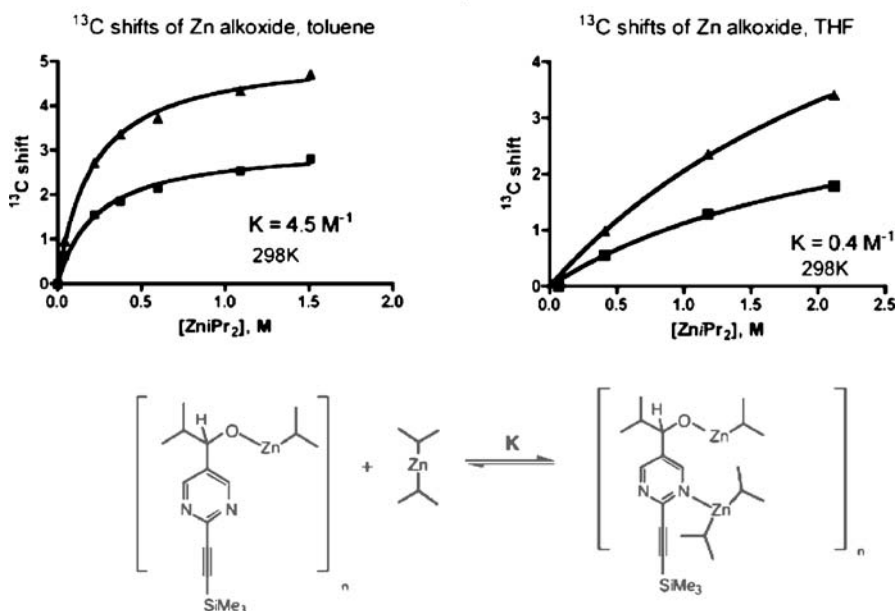


**Fig. 14** Zn binding to the homochiral Zn alkoxide, monitored by the  $^{13}\text{C}$  shifts of the two alkyne protons and demonstrating the higher degree of association in toluene compared to thf

The results of these experiments are recorded below, and show that reactant catalyst interaction must be important under the conditions of asymmetric autocatalysis. It raises a possibility that the true catalytic entity could be the association complex on the right-hand side of the equation.

The strong binding of  $\text{ZnR}_2$  to the zinc alkoxide is reinforced by observations on the  $\text{CHMe}_2$  signal of diisopropylzinc, which experiences a low-field shift proportional to the relative concentration of Zn alkoxide. In addition, the signal is doubled, indicating that the chirality of the enantiomerically pure Zn alkoxide produces an induced diastereotopic shift in the  $\text{CHMe}_2$  groups of the zinc alkyl, engaged in rapidly reversible complexation with the alkoxide. This observation implies a high level of structural specificity in the binding process, and opens up the possibility of Zn binding sites in the alkoxide other than the pyrimidine nitrogen. See Sect. 4.1 for a computational approach to this observation.

### 3.2.4

#### NMR Exchange Spectroscopy

In the presence of excess diisopropylzinc, the EXSY spectrum in both thf and toluene shows rapid interconversion between zinc-bound isopropyl groups of the zinc reagent and alkoxide dimer (Fig. 15). The reaction occurs for both racemic and homochiral dimers with comparable facility. In toluene, the rate

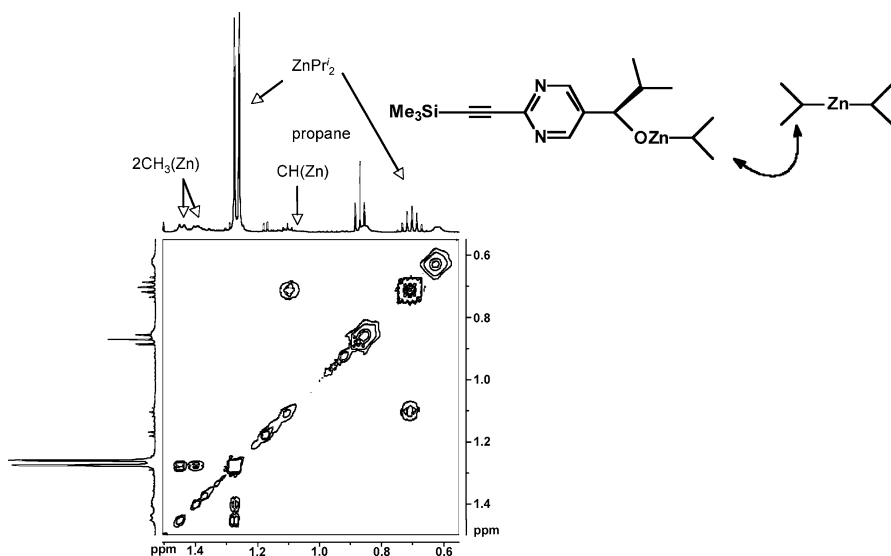


**Fig. 15** EXSY spectrum of a mixture of homochiral Zn alkoxide and excess diisopropylzinc in toluene- $d_8$ . The exchange peaks at 1–1.5 ppm are Zn-bound methyl groups; the high field cross-peak belongs to the isopropyl methine protons

increases monotonically with increasing  $[\text{Zn}/i\text{Pr}_2]$  but for the far slower process in thf saturation is evident above 0.2 M Zn reagent. These observations are consistent with access to trigonal, and therefore coordinatively unsaturated zinc sites, as proposed in the square dimer model. It is likely that these sites are solvated in thf (vide infra), so that ligand dissociation is required in that medium before the formally trigonal zinc site is exposed. A four-centre mechanism is in accord with the dynamic NMR experiments conducted in the presence of  $\text{ZnMe}_2$  for the simple asymmetric zinc catalyst described in a previous section (Sect. 3.1).

In summary, the various NMR experiments provide the following information:

- The autocatalysis resting state is a square  $\text{Zn}_2\text{O}_2$  dimer; racemic and homochiral forms are distinguishable, and are present at the same concentration within experimental error.
- In thf the spectrum is assignable; in toluene the spectrum is more dynamic and hence more difficult to interpret, but mixed toluene/dichloromethane solutions give high quality NMR spectra.
- There is a rapid exchange between  $i\text{Pr}_2\text{Zn}$  and the  $i\text{PrZn}$  of the dimer in both solvents; in thf this reaches a limiting value at high  $i\text{Pr}_2\text{Zn}$  concentration.
- The aldehyde does not bind  $i\text{Pr}_2\text{Zn}$  appreciably; the Zn alkoxide does.
- Homochiral and heterochiral dimers exchange through a monomeric state. At low temperatures further association of dimers to higher oligomers occurs, giving broadened and dispersed spectra.

### 3.3

#### Correlation of NMR Results and Autocatalysis

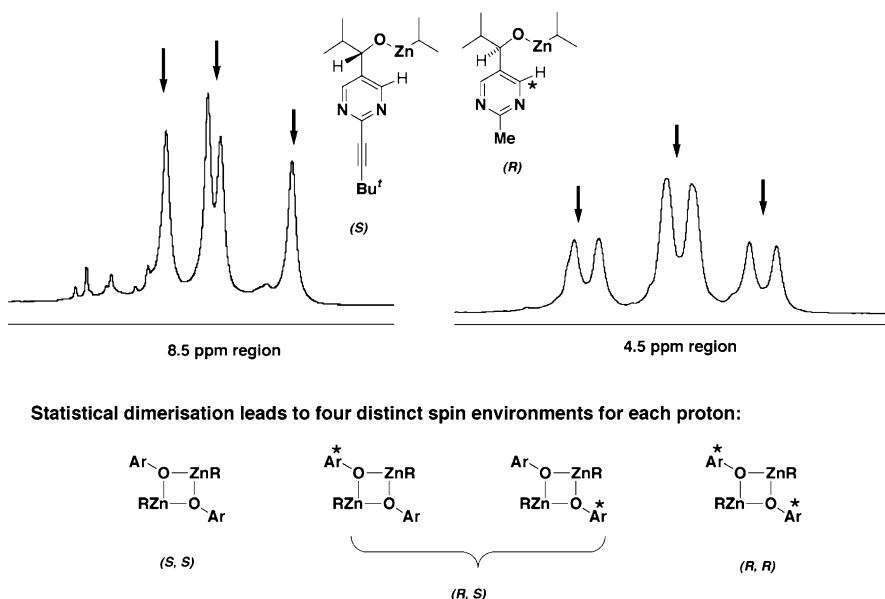
The best resolved NMR spectra were obtained in thf, which is not a solvent for autocatalysis, presumably because of strong reactant binding. Subsequent to these experiments it was found that  $\text{CH}_2\text{Cl}_2$  was a good solvent for the zinc alkoxide. Although it is not an effective medium for autocatalysis, mixtures of toluene and  $\text{CH}_2\text{Cl}_2$  were, enabling a formal link to be made between the NMR work and autocatalytic turnover. Firstly, a comparison of solvent influences on the reaction can be made, as shown in Table 1. This reaffirms that toluene is a good solvent for the autocatalytic reaction, as already known. The tolerance for dilution with up to 60% of  $\text{CH}_2\text{Cl}_2$  was not previously recognised, however. With increasing proportions of the halogenated solvent, the ultimate ee becomes increasingly compromised, although amplification persists even in pure  $\text{CH}_2\text{Cl}_2$ , where catalysis is inefficient. The bonus of working in  $\text{CH}_2\text{Cl}_2$ -containing media lies in the increased quality of  $^1\text{H}$  NMR spectra; for the enantiomerically pure dimer derived from the 2-Bu<sup>t</sup>-pyrimidine, four well-resolved Me signals at 0.588 and 0.869 ppm (CCHMe<sub>2</sub>) and at 1.265

**Table 1** Solvent effects on the course of autocatalytic reaction between the methylpyrimidinal and diisopropylzinc

20 mol%, 12.4 % ee  
solvent  
Zn<sup>i</sup>Pr<sub>2</sub> 3eq.

Solvent	Yield (%)	ee (%)	ee product (%)
Toluene	99	59	68
CH <sub>2</sub> Cl <sub>2</sub>	–40	24	–
Toluene/CH <sub>2</sub> Cl <sub>2</sub> (1.1:0.9)	98	52	60
Toluene/CH <sub>2</sub> Cl <sub>2</sub> (0.8:1.2)	95	46	53
Toluene/CH <sub>2</sub> Cl <sub>2</sub> (0.6:1.4)	~70	36	–

and 1.291 ppm (ZnCHMe<sub>2</sub>) are observed. This encouraged a further test of the dimer model through the preparation of a “pseudoracemate” as outlined in Fig. 16. Both the aromatic and alkoxide CH regions of the spectrum show

**Fig. 16** Crossover experiment demonstrates the expected number of species and the expected number of spin environments for a square dimer structure (with overlap in the 4.5 ppm region)

distinct signals for each of the four possible dimeric components, exactly as would be predicted for an unbiased equilibrium. The parallel experiment, where the two different alkoxides were of the same hand, gave less clear-cut results, since a modest bias towards one dimeric form skewed the equilibrium somewhat (Klankermayer and Brown, unpublished results).

### 3.4

#### NMR in Spontaneous Asymmetric Synthesis

In the course of NMR studies of the autocatalytic system in  $C_7D_8$ , several experiments were carried out in which the 2-TMS-alkynylpyrimidine-5-aldehyde was directly mixed with diisopropylzinc at low temperatures and allowed to warm until the reaction was complete. The dimeric product can then be observed directly, and would be expected to be racemic since there are no internal or external chiral influences on the reaction. This was not the case, and an imbalance in favour of the homochiral form was sometimes observed; a striking example is shown in Fig. 17. Since there is no workup

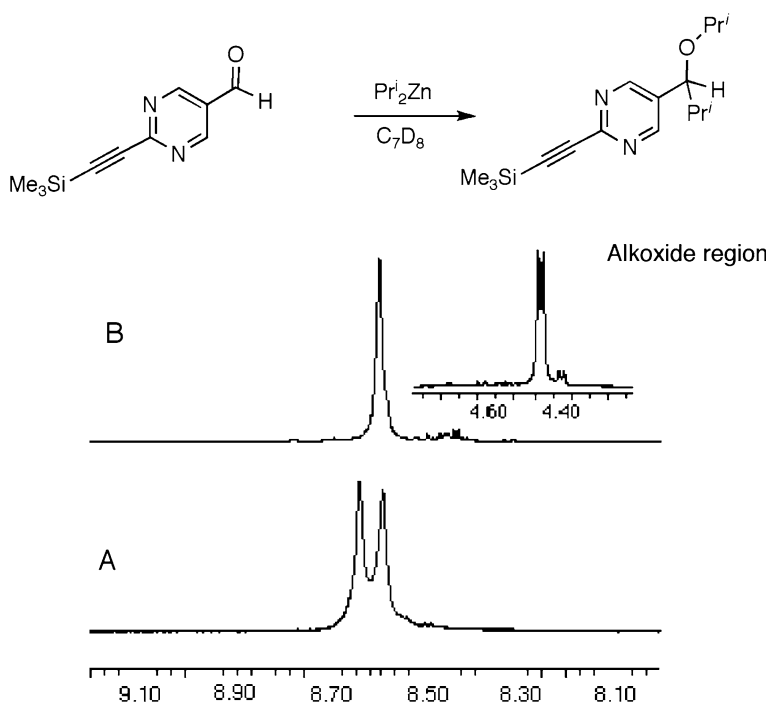


**Fig. 17** Absolute asymmetric synthesis observed by  $^1H$  NMR. The lower trace is a solution of the racemic square planar dimer in toluene- $d_8$  with separate signals for  $(R,S)$  [low field] and  $(R^*,R^*)$  forms. The upper trace shows the final product of autocatalysis without initial added catalyst, giving a product of >80% ee



or other procedure that could involve bias, this presents a very cogent case for absolute asymmetric synthesis. The heterochiral dimer is present to the extent of ca. 10%. Having made this initial observation it was systematised through non-NMR-based controlled experiments that affirmed the generality, and was accompanied by a simple model based on amplification of the random statistical excess in a small molecular pool [46].

## 4

### Mechanistic Approaches 3. Computational Chemistry

#### 4.1

##### Methylzinc Models

The study of intermediate structures in asymmetric autocatalysis may be augmented by computational chemistry, since the enthalpies of formation of putative species can readily be compared. The first paper to address this topic simplified the computation by “reacting” the Soai aldehyde with  $\text{Me}_2\text{Zn}$ , assuming that this would be a good surrogate for the more difficult problem of minimising structures based on the authentic  $i\text{Pr}_2\text{Zn}$  additions. Calculations were carried out using DFT at the B3LYP function level with a 6-31G\* basis

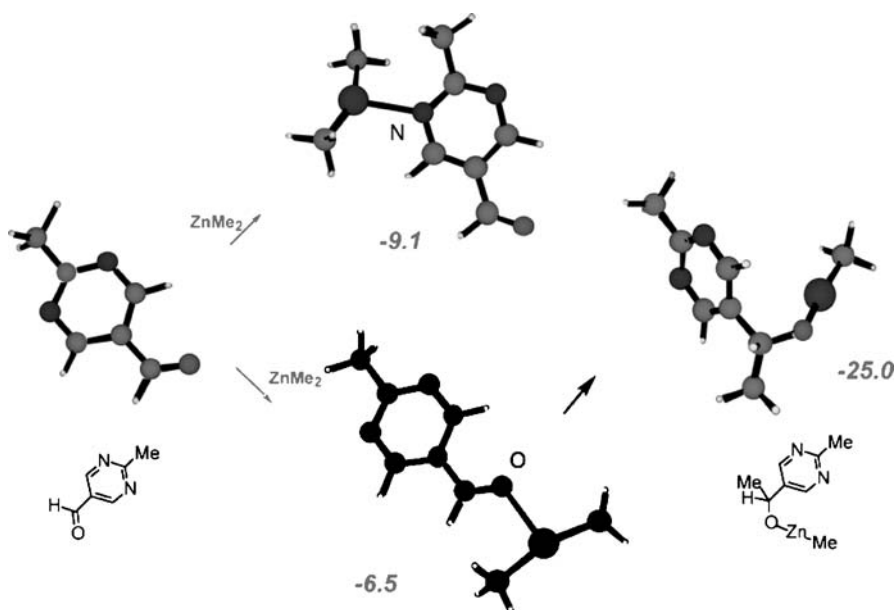


**Fig. 18** Enthalpy of binding  $\text{ZnMe}_2$  to the 2-methylpyrimidinal in units of  $\text{kcal mol}^{-1}$  with N-complexation preferred over O-complexation, from DFT computation

set for all atoms. Both the initial addition and the dimerisation process are strongly exothermic. A comparison with experimental results is possible at this stage. Just as the NMR results indicated, association of zinc reagent with the pyrimidine aldehyde prefers ring-N to ring-O association; the former has the lower enthalpy. These simple conclusions are shown in Fig. 18 [79].

A more relevant conclusion arising from the computational work provides the relative stability of different dimers. There is a clear favouring of the  $(\text{ZnO})_2$  square structure over possible O – Zn – N macrocycles and more markedly over the  $\{\text{OZnO}, \text{NZnN}\}$  isomeric macrocycle. Structures and relative enthalpies are shown in Fig. 19. Within the square model, homo- and heterochiral dimers are closely similar in energy and show no discernable structural differences that could indicate why one is catalytically active and the other not.

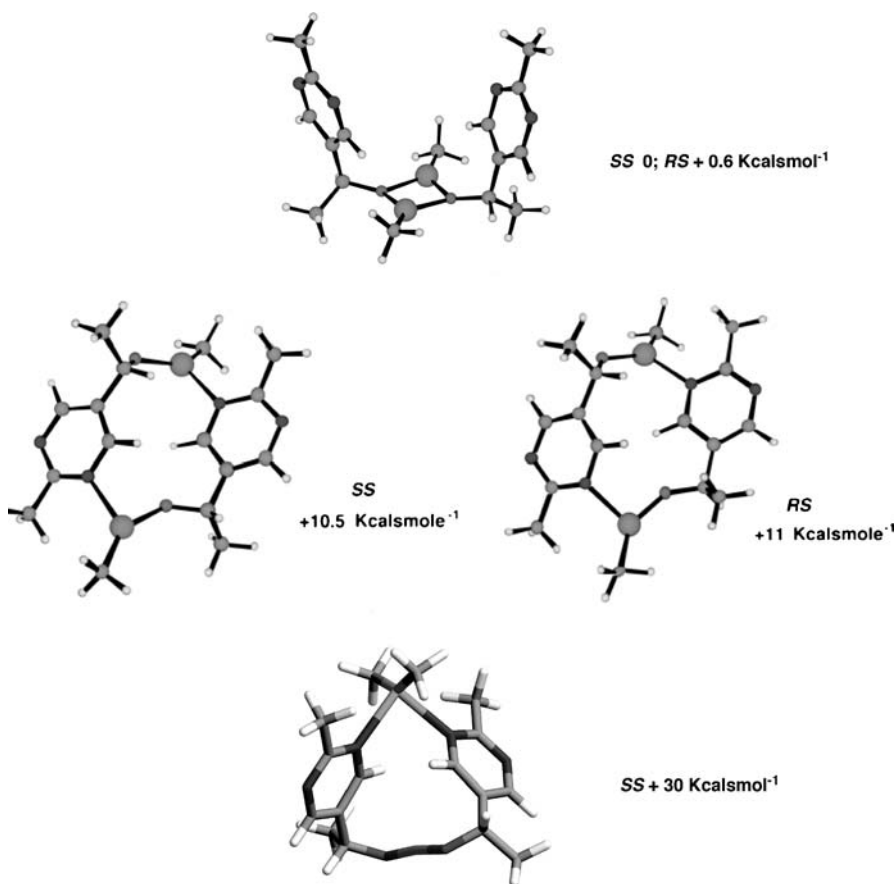


**Fig. 19** DFT-derived energetics of closed cyclic dimers from the 2-methylpyrimidine and dimethylzinc

The enthalpies of trimers and tetramers were also calculated as part of this study. At the trimer level – important because this is the initial product of the reaction [dimer + zinc alkyl + aldehyde] – the most stable structures are macrocyclic. At the tetramer level there are two species of comparable enthalpy. One is the well-described cubic tetramer, and the other a barrel-like species that is conceptually related to two N – Zn lined dimers. The specific value derived from these calculations is only apparent when compared with the later computational work on the “real” diisopropylzinc-derived species. This highlights the importance of steric effects involving the more bulky isopropyl groups as a defining feature of asymmetric autocatalysis [80].

## 4.2

### Isopropylzinc-Derived Species

Superficial analysis at the dimer level indicates that the order of reactivity is the same as observed for the methylzinc DFT calculations. On closer examination of the calculation for the homo- and heterochiral Zn – O squares, a modest discrepancy is apparent; the heterochiral form is less stable than its homochiral counterpart by  $>2 \text{ kcal mol}^{-1}$ . The anomaly was identified by combining DFT calculations with conformational variation of the rotatable bonds in the alkoxide moieties side chains and Zn-bound isopropyl groups, so that the true minimum structures were defined. On this basis, the minimum enthalpies were close, but the preferred conformations quite distinct. The homochiral dimer possesses *syn*-related pyrimidines, whilst the heterochiral form prefers *anti*-related pyrimidines. Only the former has a significant dipole moment and so this distinction may have an influence on autocatalysis, given that the heterochiral form plays no part (Fig. 20). To gain further insight into the NMR observations reported above, the association of diisopropylzinc with the homochiral dimer was examined by DFT. Two stable minima were observed, one the expected Zn-bound adduct, the other an unusual cluster, where the added Zn alkyl is directly associated with the zinc square (Fig. 21). Interestingly this form is without experimental precedent, beyond the unexpected involvement of the homochiral dimer as a shift reagent for diisopropylzinc, as discussed earlier.

The conformational distinction between homo- and heterochiral dimers indicates why a bulky dialkylzinc may be important in limiting the scope of amplifying autocatalysis; the Soai prescription remains unique. Since it is the product of reaction that is also the catalyst, a further question needs to be addressed. In the conventional Oguni–Noyori reaction discussed earlier [60–71] the zinc alkoxide product normally plays no further part in the proceedings because it forms a stable cubic tetramer [81–87]. There are scattered exceptions in zinc-mediated catalysis, arising when the product structure is conducive to its further involvement [88, 89].

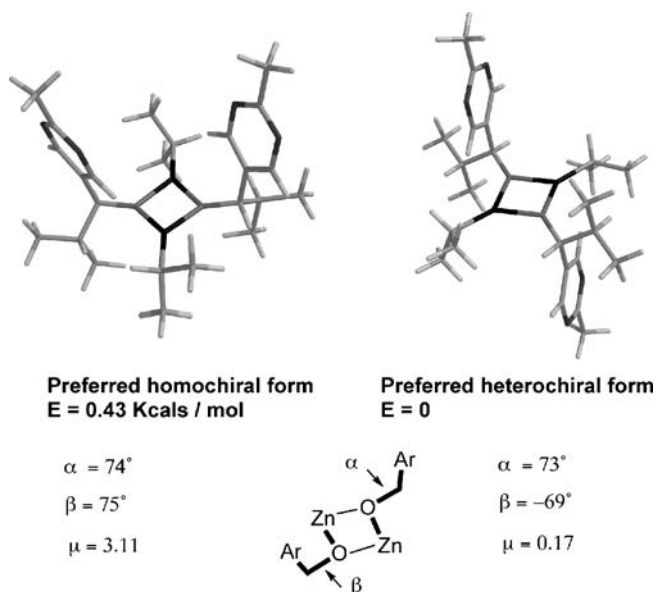


**Fig. 20** Preferred ground-state conformations of the diisopropylzinc-derived homochiral dimer (Ar, Ar' *syn*) and the heterochiral dimer (Ar, Ar' *anti*) from DFT calculations

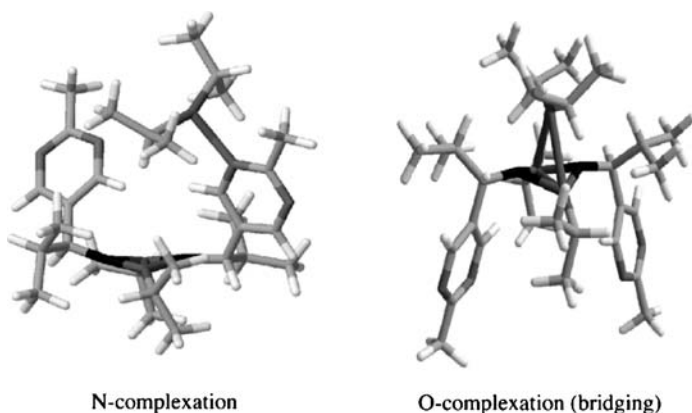


**Fig. 21** DFT-computed structures of the two products of association of further diisopropylzinc with the homochiral square dimers derived from 2-methylpyrimidinal.

In further computational work concerned with isopropylzinc-derived species, the enthalpies and structures of the four possible closed tetramers were derived (Fig. 22). Dramatic differences from the methylzinc analogues were observed, simply because the bulk of the larger alkyl group dictates the level of inter-cluster interactions. Cubic structures directly derived from homochiral isopropyl-dimers possessed severe and inescapable non-bonding

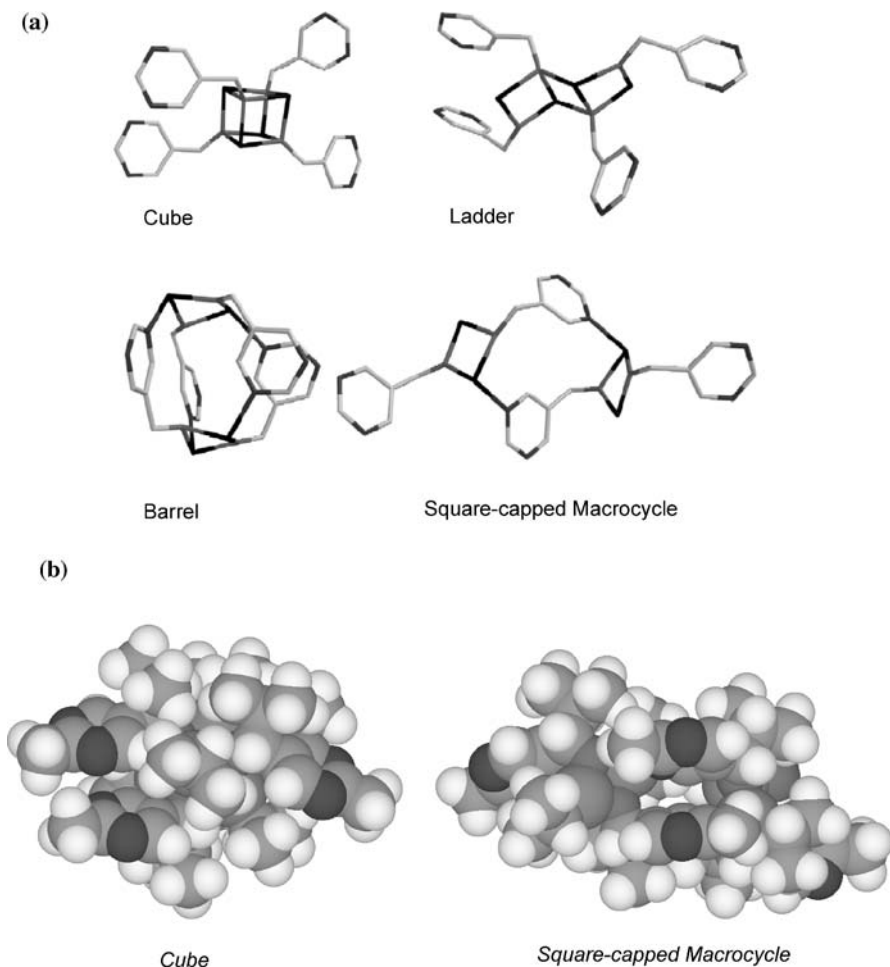


**Fig. 22** **a** Skeletal representations of the four closed tetramers with alkyl substituents removed; **b** space-filling models of the isopropyl-derived cube and the more open square-capped macrocycle; both homochiral and obtained from DFT calculations

H – H interactions, both for all-(*S*) and (*R,R,S,S*) tetramers, even after conformational energy minimisation. Overall, most of the  $>40 \text{ kcal mol}^{-1}$  enthalpic advantage of the [dimer + dimer to tetramer] process is lost on going from methylzinc to isopropylzinc-derived structures, because of the increased steric strain. The remaining  $[\text{Zn} - \text{O}]_2$  square-based tetramers are all more strained in the isopropyl than in the Me series. As an extreme, the latter is less stable than two isolated monomers. What stands out is that the square-capped macrocycle is only modestly more strained in the isopropyl series, and lacks severe H – H interactions (only two H – H contacts are below  $2.3 \text{ \AA}$ ). Forming the barrel isomer from this by making two additional Zn – N

bonds is only marginally advantageous, because of short H – H distances inside the closed macrocycle. Taken together, these considerations make the square-capped macrocyclic form the most probable tetrameric species. This structure notably retains the trigonal coordinatively unsaturated Zn geometry, making it a potentially active autocatalyst.

Soai's work demonstrates high autocatalytic activity at  $-25\text{ }^{\circ}\text{C}$ , and at this lower temperature the NMR work demonstrates that unsymmetrical higher oligomers are evident in the  $^1\text{H}$  NMR spectrum [78]. It is known that bulky ligands can modulate dimer–tetramer equilibria, as seen in the rational design of oligomeric copper clusters [90]. If higher homochiral oligomers contribute to autocatalysis, then the net gain in ee for a given level of turnover is higher than for a simple dimer catalyst, according to models. For the 2-Me pyrimidines and when operating at ambient temperature, the calculated and experimental ees are in good agreement [73, 74]. At lower temperatures and with the 2-alkynylpyrimidines preferentially employed by Soai in his later work, the observed ee is higher than calculated for a purely dimeric catalyst. There are different explanations for this result, but it is consistent with the incursion of tetramers, or other more associated species. Since the square-capped macrocycle seems the most viable tetramer for participation in autocatalysis, the goal of a molecular model for this phenomenon is realisable.

## 5

### Conclusions and Remaining Problems

A combination of physicochemical methods, microcalorimetry and DFT calculations has enabled some inroads to be made into our understanding of asymmetric autocatalysis. The main features of the “catalyst” solution structure – strictly speaking, the observed resting-state – are reasonably well understood, although details of the process of oligomerisation (e.g. ES-MS evidence) are lacking. The X-ray structure of an oligomer would provide a real breakthrough. A satisfactory transition-state model is also lacking at present. Whatever further details are added to this already fascinating story, the uniqueness of the autocatalyst and its simplicity are obvious. This uniqueness derives from the required ingredients: a rigid  $\gamma$ -iminoaldehyde, diisopropylzinc (other dialkylzincs are ineffective) and a non-coordinating solvent. The simplicity resides in the basic model, which underpins the observed equidistribution of homo- and heterochiral dimers, and attributes the enantioselectivity to the reactivity of the homochiral form and the unreactivity of the heterochiral form. A high level of stereoselectivity is required to explain the fidelity of high ee transmission in multiple sequential autocatalytic experiments [75]. An explanation for this most crucial aspect of the process is still lacking, although the structural evidence provided to date is sufficient to encourage future speculations.

A final cautionary comment is worth making. On account of the interest in asymmetric autocatalysis and its significance, there is much current focus on modelling the process, and deriving and applying the models to “chironeogenesis”, namely the origins of homochirality in biology. In earlier protocols, experimental restraints were lacking. With the results reported herein being available, this is no longer the case. Amplifying asymmetric autocatalysis must function as the consequence of a non-linear effect, of one of the types so comprehensively delineated by Kagan and co-workers. This allows for two sets of conditions: (i) The catalyst is a monomer and is formed dissociatively from a dimer or higher oligomer. In this case the non-linearity arises because the heterochiral oligomer(s) is(are) more stable than the homochiral oligomer(s). The heterochiral form acts as a reservoir to enrich the ee of the monomeric catalyst over the ee of the bulk material. (ii) The catalyst itself is oligomeric, most simply a dimer, but the homochiral form is the catalytically active one. The enantiomer enrichment in this case may arise purely through statistical enrichment without concurrent selectivity. This is a consequence of a Frank-type model; the unreactive heterochiral oligomer(s) sequester the disfavoured enantiomer and thus reduce its formal concentration.

The key NMR observations (i) that the proportion of homo- and heterochiral dimers is near-equal, and (ii) that their interconversion by a dissociative process is rapid compared to catalytic turnover, preclude the possibility of a monomer autocatalyst. In Kagan’s classification, monomer catalysis with a positive NLE may only arise when there is an *unequal* concentration of homo- and heterochiral oligomers, in favour of the heterochiral form, which acts as a reservoir for the deficient enantiomer. NMR results show that the resting state for Soai’s autocatalysis is an equal mixture of homo- and heterochiral species, predominantly dimeric. The lack of ground-state stereo-discrimination requires that the number of chiral entities in the resting state must be *less than or equal to* the number in the enantioselectivity-determining transition state, else there is no possibility of the vital non-linear effect. Even after the publication of these results in late 2004, their consequences are not always applied. For recent discussions where a monomeric catalyst for Soai’s system is permitted or promoted, see [91–93].

**Acknowledgements** We thank the Leverhulme Trust for support of the research from our laboratories cited herein.

## References

1. Goldanskii V (1988) Z Phys Chem 269:216 (Leipzig)
2. Mikami K, Yamanaka M (2003) Chem Rev 103:3369
3. Weissbuch I, Leiserowitz L, Lahav M (2005) Stochastic “Mirror-symmetry breaking” via self-assembly, reactivity and amplification of chirality: relevance to abiotic con-

- ditions. In: Walde P (ed) Prebiotic chemistry. Topics in current chemistry, vol 259. Springer, New York, p 123
4. Viedma C (2007) *Astrobiology* 7:312
  5. Bonner WA (1988) *Topics Stereochem* 18:1
  6. Feringa BL, Van Delden RA (1999) *Angew Chem Int Ed* 38:3419
  7. Avalos M, Babiano R, Cintas P, Jimenez JL, Palacios JC, Barron LD (1998) *Chem Rev* 98:2391
  8. Cerf C, Jorissen A (2000) *Space Sci Rev* 92:603
  9. Avalos M, Babiano R, Cintas P, Jimenez JL, Palacios JC (2000) *Tetrahedron: Asymmetry* 11:2845
  10. Quack M (2002) *Angew Chem Int Ed* 41:4618
  11. Cintas P (2002) *Angew Chem Int Ed* 41:1139
  12. Cline DB (2004) *Mendeleev Commun*, p 301
  13. Kondepudi DK, Bullock KL, Digits JA, Yarrowborough PD (1995) *J Am Chem Soc* 117:401
  14. Kondepudi DK, Bullock KL, Digits JA, Hall JK, Miller JM (1993) *J Am Chem Soc* 115:10211
  15. Kondepudi DK, Kaufman RJ, Singh N (1990) *Science* 250:975
  16. Viedma C (2005) *Phys Rev Lett* 94:065504
  17. Blackmond DG (2007) *Chem Eur J* 13:3290
  18. Cartwright JHE, Piro O, Tuval I (2007) *Phys Rev Lett* 98:165501
  19. Viedma C (2007) *Cryst Growth Des* 7:553
  20. Perry RH, Wu C, Neffiu M, Cooks RG (2007) *Chem Commun*, p 1071
  21. Gridnev ID (2006) *Chem Lett* 35:148
  22. Frank FC (1953) *Biochim Biophys Acta* 11:459
  23. Turing AM (1952) *Trans R Soc B* 237:37 (London)
  24. Decker P (1975) *Orig Life* 6:211
  25. Kagan HB (2001) *Synlett*, p 888
  26. Girard C, Kagan HB (1998) *Angew Chem Int Ed* 37:2923
  27. Guillaneux D, Zhao S-H, Samuel O, Rainford D, Kagan HB (1994) *J Am Chem Soc* 116:9430
  28. Puchot C, Samuel O, Dunach E, Zhao S, Agami C, Kagan HB (1986) *J Am Chem Soc* 108:2353
  29. Heller D, Drexler H-J, Fischer C, Buschmann H, Baumann W, Heller B (2000) *Angew Chem Int Ed* 39:495
  30. Sato I, Omiya D, Saito T, Soai K (2000) *J Am Chem Soc* 122:11739
  31. Sato I, Yamashita R, Kadowaki K, Yamamoto J, Shibata T, Soai K (2001) *Angew Chem Int Ed* 40:1096
  32. Tanji S, Ohno A, Sato I, Soai K (2001) *Org Lett* 3:287
  33. Sato I, Kadowaki K, Urabe H, Jung JH, Ono Y, Shinkai S, Soai K (2003) *Tetrahedron Lett* 44:721
  34. Sato I, Kadowaki K, Ohgo Y, Soai K (2004) *J Mol Catal A: Chem* 216:209
  35. Kawasaki T, Jo K, Igarashi H, Sato I, Nagano M, Koshima H, Soai K (2005) *Angew Chem Int Ed* 44:2774
  36. Kawasaki T, Tanaka H, Tsutsumi T, Kasahara T, Sato I, Soai K (2006) *J Am Chem Soc* 128:6032
  37. Kawasaki T, Suzuki K, Licandro E, Bossi A, Maiorana S, Soai K (2006) *Tetrahedron: Asymmetry* 17:2050
  38. Shibata T, Iwahashi K, Kawasaki T, Soai K (2007) *Tetrahedron: Asymmetry* 18:1759
  39. Shibata T, Yamamoto J, Matsumoto N, Yonekubo S, Osanai S, Soai K (1998) *J Am Chem Soc* 120:12157



40. Sato I, Sugie R, Matsueda Y, Furumura Y, Soai K (2004) *Angew Chem Int Ed* 43:4490
41. Kawasaki T, Sato M, Ishiguro S, Saito T, Morishita Y, Sato I, Nishino H, Inoue Y, Soai K (2005) *J Am Chem Soc* 127:3274
42. Soai K (1997) JP Patent 09-268 179
43. Soai K, Sato I, Shibata T, Komiya S, Hayashi M, Matsueda Y, Imamura H, Hayase T, Morioka H, Tabira H, Yamamoto J, Kowata Y (2003) *Tetrahedron: Asymmetry* 14:185
44. Singleton DA, Vo LK (2003) *Org Lett* 5:4337
45. Mislow K (2003) *Coll Czech Chem Commun* 68:849
46. Gridnev ID, Serafimov JM, Quiney H, Brown JM (2003) *Org Biomol Chem* 1:3811
47. Kawasaki T, Hatase K, Fujii Y, Jo K, Soai K, Pizzarello S (2006) *Geochim Cosmochim Acta* 70:5 5395
48. Soai K, Sato I (2001) *Enantiomer* 6:189
49. Danda H, Nishikawa H, Otaka K (1991) *J Org Chem* 56:6740
50. Kogut EF, Thoen JC, Lipton MA (1998) *J Org Chem* 63:4604
51. Szlosek M, Figadere B (2000) *Angew Chem Int Ed* 39:1799
52. De Rosa M, Acocella MR, Soriente A, Scettri A (2001) *Tetrahedron: Asymmetry* 12:1529
53. Costa AM, Garcia C, Carroll PJ, Walsh PJ (2005) *Tetrahedron* 61:6442
54. Simonov AN, Pestunova OP, Matvienko LG, Parmon VN (2007) *Kinetics Catal* 48: 245
55. Weber AL (2007) *Orig Life* 37:105
56. Kassianidis E, Philp D (2006) *Angew Chem Int Ed* 45:6344
57. Kassianidis E, Pearson RJ, Philp D (2005) *Org Lett* 7:3833
58. Kalck P, Urrutigoity M (2004) *Coord Chem Rev* 248:2193
59. Mauksch M, Tsogoeva SB, Martynova IM, Wei S (2007) *Angew Chem Int Ed* 46:393
60. Pu L, Yu HB (2001) *Chem Rev* 101:757
61. Vilaivan T, Bhanthumnavin W, Sritana-Anant Y (2005) *Curr Org Chem* 9:1315
62. Betancort JM, Garcia C, Walsh PJ (2004) *Synlett*, p 749
63. Oguni N, Omi T (1984) *Tetrahedron Lett* 25:2823
64. Hayashi M, Miwata H, Oguni N (1989) *Chem Lett*, p 1969
65. Hayashi M, Miwata H, Oguni N (1991) *J Chem Soc Perkin* 1:1167
66. Jessop PG, Brown RA, Yamakawa M, Xiao J, Ikariya T, Kitamura M, Tucker SC, Noyori R (2002) *J Supercrit Fluids* 24:161
67. Kitamura M, Oka H, Noyori R (1999) *Tetrahedron* 55:3605
68. Kitamura M, Suga S, Oka H, Noyori R (1998) *J Am Chem Soc* 120:9800
69. Kitamura M, Yamakawa M, Oka H, Suga S, Noyori R (1996) *Chem Eur J* 2:1173
70. Kitamura M, Suga S, Niwa M, Noyori R (1995) *J Am Chem Soc* 117:4832
71. Noyori R, Kitamura M (1991) *Angew Chem Int Ed* 30:49
72. Blackmond DG (2005) *Angew Chem Int Ed* 44:4302
73. Blackmond DG, McMillan CR, Ramdeehul S, Schorm A, Brown JM (2001) *J Am Chem Soc* 123:10103
74. Buono FG, Blackmond DG (2003) *J Am Chem Soc* 125:8978
75. Shibata T, Yonekubo S, Soai K (1999) *Angew Chem Int Ed* 38:659
76. Sato I, Omiya D, Igarashi H, Kato K, Ogi Y, Tsukiyama K, Soai K (2003) *Tetrahedron: Asymmetry* 14:975
77. Kitamura M, Okada S, Suga S, Noyori R (1989) *J Am Chem Soc* 111:4028
78. Gridnev ID, Serafimov JM, Brown JM (2004) *Angew Chem Int Ed* 43:4884
79. Gridnev ID, Brown JM (2004) *Proc Natl Acad Sci USA* 101:5727
80. Klankermayer J, Gridnev ID, Brown JM (2007) *Chem Commun*, p 3151
81. Shearer HMM, Spencer CB (1980) *Acta Cryst B* B36:2046

82. Olmstead MM, Power PP, Shoner SC (1991) *J Am Chem Soc* 113:3379
83. Herrmann WA, Bogdanovic S, Behm J, Denk M (1992) *J Organometal Chem* 430:C33
84. Bond AD, Linton DJ, Wheatley AEH (2001) *Acta Cryst* E57:m298
85. Charette AB, Molinaro C, Brochu C (2001) *J Am Chem Soc* 123:12160
86. Boyle TJ, Bunge SD, Andrews NL, Matzen LE, Sieg K, Rodriguez MA, Headley TJ (2004) *Chem Mater* 16:3279
87. Polarz S, Neues F, Van den Berg MWE, Gruenert W, Khodeir L (2005) *J Am Chem Soc* 127:12028
88. Rosner T, Sears PJ, Nugent WA, Blackmond DG (2000) *Org Lett* 2:2511
89. Trost BM, Fettes A, Shireman BT (2004) *J Am Chem Soc* 126:2660
90. Jiang X, Bollinger JC, Lee D (2005) *J Am Chem Soc* 127:15678
91. Islas JR, Lavabre D, Grevy J-M, Lamoneda RH, Cabrera HR, Micheau J-C, Buhse T (2005) *Proc Natl Acad Sci USA* 102:13743
92. Micskei K, Maioli M, Zucchi C, Caglioti L, Palyi G (2006) *Tetrahedron: Asymmetry* 17:2960
93. Saito Y, Hyuga H (2006) *Cond Matter* 12:381



# Kinetic Insight into Specific Features of the Autocatalytic Soai Reaction

Dominique Lavabre<sup>1</sup> · Jean-Claude Micheau<sup>1</sup> (✉) · Jesús Rivera Islas<sup>2</sup> · Thomas Buhse<sup>2</sup> (✉)

<sup>1</sup>Laboratoire des IMRCP, UMR au CNRS No. 5623, Université Paul Sabatier, 118, Route de Narbonne, 31062 Toulouse Cedex, France  
*micheau@chimie.ups-tlse.fr*

<sup>2</sup>Centro de Investigaciones Químicas, Universidad Autónoma del Estado de Morelos, Av. Universidad 1001, Col. Chamilpa, 62209 Cuernavaca, Morelos, Mexico  
*buhse@uaem.mx*

<b>1</b>	<b>Introduction</b>	68
<b>2</b>	<b>Experimental Features of the Soai Reaction</b>	70
2.1	Effect of Aldehyde Structures	70
2.2	Strong Chiral Amplification, Extreme Sensitivity and Mirror-Symmetry Breaking	71
2.3	Effect of Miscellaneous Chiral Additives	74
2.4	Enantioselectivity Reversal	74
<b>3</b>	<b>Short Survey of Proposed Models</b>	79
3.1	General Models	79
3.2	Spontaneous Asymmetric Synthesis	80
3.3	Chiral Amplification in Asymmetric Synthesis	81
3.4	Chiral Symmetry Breaking in Crystallization	82
3.5	Kinetic Recording of the Soai Reaction	82
<b>4</b>	<b>Kinetic Understanding of the Soai Reaction</b>	84
4.1	Proposition of Kinetic Schemes	84
4.2	Properties of the Kinetic Schemes	85
4.3	Mirror-Symmetry Breaking in Simulation	86
4.4	Reproduction of Further Experimental Observations	87
4.5	Reproduction of Enantioselectivity Reversal	89
4.5.1	Additive–Additive Interactions	89
4.5.2	Additive–Product Interactions	90
<b>5</b>	<b>Conclusion</b>	93
	<b>References</b>	94

**Abstract** The addition of diisopropylzinc to prochiral pyrimidine carbaldehydes (Soai reaction) is the only known example of spontaneous asymmetric synthesis in organic chemistry. It serves as a model system for the spontaneous occurrence of chiral asymmetry from achiral initial conditions. This review describes the possible kinetic origin of specific experimental features of this reaction. It is shown that generic kinetic models, including enantioselective autocatalysis and mutual inhibition between the enantiomers,

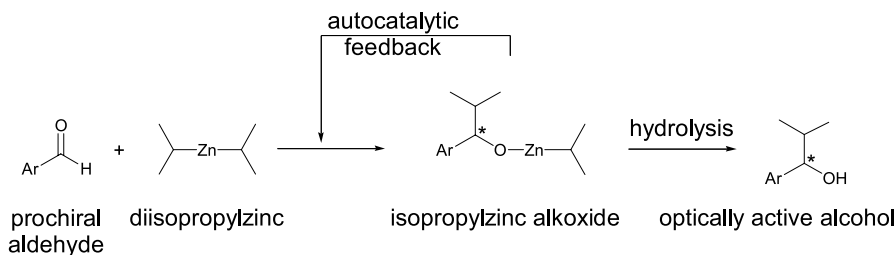
are adequate to describe a variety of the astonishing properties of the Soai reaction. Namely, these are the unprecedented strong chiral amplification, extreme sensitivity to the presence of very small amounts of chiral initiator, mirror-symmetry breaking when starting from achiral conditions, and the reversal of enantioselectivity of chiral catalysts by addition of achiral additives. The described kinetic approach allows a closer insight into the nonlinear dynamics of the Soai reaction. It also reveals that a number of open questions concerning the detailed reaction mechanism are still to be solved and that further experimental studies are required.

## 1

### Introduction

Spontaneous asymmetric synthesis has been envisaged by theoretical models for more than 50 years [1–7]. This process features the generation and amplification of optical activity during the course of a chemical reaction. It stands in contrast to asymmetric procedures, such as stoichiometric resolution, conglomerate crystallization, or chiral chromatography, in which the optical activity can be increased but no additional chiral product is formed [8]. It is also different from classical asymmetric synthesis, in which new chiral product is obtained but the resulting enantiomeric excess (*ee*) is usually less than or, at most, equal to that of the chiral initiator or catalyst<sup>1</sup>.

The first experimental invention of spontaneous asymmetric synthesis was achieved only a little more than a decade ago in an organic reaction system by Soai and coworkers [9–15]. The Soai reaction (Scheme 1) comprises the addition of diisopropylzinc to prochiral pyrimidine carbaldehydes yielding isopropylzinc alkoxides that, after hydrolysis, are usually converted into stable chiral pyrimidyl alkanols.



**Scheme 1** The Soai reaction; Ar = 3-pyridyl, 3-quinolyl, 5-pyrimidinyl, ferrocenyl, 2-alkyl-5-pyrimidinyl (see Table 1)

At first glance, the Soai reaction appears to be one of the prominent examples of catalytic asymmetric organozinc additions to carbonyl com-

<sup>1</sup> On some occasions an exception from this case can be observed by so-called nonlinear effects in asymmetric synthesis, in which the relation between the enantiomeric excess of the chiral catalyst or initiator and that of the product deviates from linearity (see Sect. 3.3)

**Table 1** Relationship between the achieved enantiomeric excess and the structure of the aldehyde in various Soai-type reactions

Aromatic part	R in $\text{ZnR}_2$	% $ee_0$	% $ee_f$	Refs.
3-Pyridyl	Me	42	7	[24]
3-Pyridyl	Et	56	14	[24]
3-Pyridyl	<i>i</i> Pr	86	35	[24]
3-Pyridyl	<i>n</i> Bu	47	6	[24]
3-Quinolyl	<i>i</i> Pr	9	43	[27]
3-Quinolyl	<i>i</i> Pr	43	67	[27]
3-Quinolyl	<i>i</i> Pr	57	89	[27]
5-Pyrimidinyl	<i>i</i> Pr	5	55	[9]
5-Pyrimidinyl	<i>i</i> Pr	39	87	[9]
5-Carbamoyl-3-pyridyl	<i>i</i> Pr	14	22	[28]
Ferrocenyl	<i>i</i> Pr	97.3	26	[29]
Ferrocenyl	<i>i</i> Pr	96.3	39	[29]
2-Methylpyrimidinyl	<i>i</i> Pr	6.4	92.1	[30]
2-Methylpyrimidinyl	<i>i</i> Pr	0.28	87	[30]
2- <i>t</i> -Bu-C $\equiv$ C-5-pyrimidinyl	<i>i</i> Pr	0.00005	57	[31]

pounds [16]. However, there is an essential difference: while asymmetric organozinc additions usually require the intervention of an external chiral catalyst, as for instance amino alcohols [17, 18], the Soai reaction was shown to be catalyzed by the reaction product itself (the pyrimidyl alcohol) [19]. The pyrimidyl alcohol acts as an efficient chiral initiator, where frequently the achieved *ee* of the product exceeds the *ee* of the initially added pyrimidyl alcohol. Such cases represent so-called chiral amplification. Early attempts by Soai and coworkers showed that the initial addition of the enantiomerically enriched pyrimidyl alkanol of 2% can finally lead to a product with an *ee* of 88% when the reaction process was driven in a series of individual reaction cycles in which the *ee* formed in a preceding reaction served as the input of the subsequent one [9].

A reaction process in which the product directly increases the rate of the chemical reaction is called autocatalysis. In the present case, the reaction product plays the role of a catalyst and of a potent chiral auxiliary at the same time. Hence Soai's discovery described the first example of a *chirally* autocatalytic reaction in organic chemistry in which the chiral product and the chiral catalyst are identical.

In this contribution, we will try to give an overview of the possible mechanistic origin of chiral amplification in the Soai reaction. We will present a reaction network derived from simple theoretical models of chiral amplification that can give rise to a plausible description of the combined experimental observations of this reaction. Following our interest in describing the dynamic features of nonlinear reaction systems [20–23], we will emphasize the possible kinetic rea-

son for a number of astonishing properties of the Soai reaction and promote a nonlinear chemical dynamics viewpoint of this reaction system.

## 2

### Experimental Features of the Soai Reaction

#### 2.1

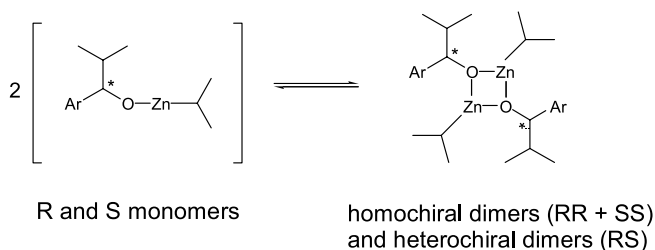
##### Effect of Aldehyde Structures

In recent years, the Soai reaction has been carried out with a number of variations in the starting aldehyde [9, 24–31]. These attempts revealed a certain relationship between the structure of the aldehyde and the achievable *ee*, i.e., the difference between the *ee*<sub>0</sub> of the initially added autocatalyst and the *ee*<sub>f</sub> of the produced autocatalyst (see Table 1).

The presence of N-atoms in the aromatic part of the aldehyde appears essential for chiral amplification. With only one nitrogen, such as in the case of 3-pyridine carbaldehyde, autocatalytic kinetics but no chiral amplification effect has been observed [24, 25]. In the case of 3-quinoline carbaldehyde, i.e., in the presence of two nucleophilic centers, autocatalysis as well as moderate chiral amplification were reported [26, 27]. Highest amplification capacity is observed in the presence of two N-atoms in the aromatic part of the aldehyde, where for the substituent at the 2-position the amplification capacity increases  $H < CH_3 < t-Bu - C\equiv C-$ , i.e., with the size and rigidity of this group. So far, detailed studies that could relate the given observations to the possible mechanism of chiral amplification in Soai's reaction are still to be carried out.

Using an empirical expression for the amplification capacity, Micskei et al. found that the amplification strength of the Soai reaction fluctuates over a wide range when the structure of the aldehyde is varied [32]. The authors excluded the possibility of simple substituent effects but rather assumed that important changes in the reaction mechanism are taking place.

Valuable information concerning a part of the possible reaction mechanism has been obtained by NMR studies, which indicate the formation of zinc



**Scheme 2** Possible zinc alkoxide dimer formation in the Soai reaction by assuming a  $(ZnO)_2$  ring structure

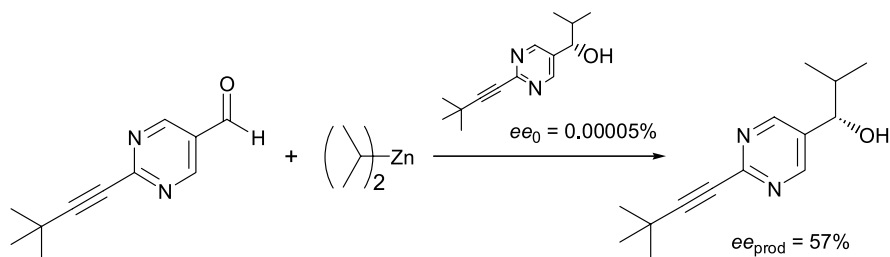
alkoxide dimers (Scheme 2) in which homochiral (*RR* and *SS*) as well as heterochiral (*RS*) species are generated [33].

As outlined in a later section, dimer formation is believed to play an essential role in the chiral amplification mechanism. Since the thermodynamic stabilities as well as the kinetics of formation of the dimers depend on their structural properties, variations in the amplification capacity by taking different aldehyde substrates may appear rational from this point of view.

## 2.2

### Strong Chiral Amplification, Extreme Sensitivity and Mirror-Symmetry Breaking

Among the most impressive examples of chiral amplification, it was shown that an extremely tiny chiral imbalance of the initially added pyrimidyl alkanol of around 0.00005% *ee* can give rise to 57% product *ee* in a single run (Scheme 3) [31]<sup>2</sup>.



**Scheme 3** Strong chiral amplification in the Soai reaction by using a starting *ee* of 0.00005% and obtaining the 2-alkynyl-5-pyrimidyl alkanol with an *ee* of 57% in the first reaction cycle

Further remarkable experimental results have been obtained by Singleton and Vo [34]: starting 48 trials of the Soai reaction with practically achiral initial conditions and conducting these experiments each in a series of four individual reaction cycles, the authors found that at the end of all 48 cases, the final *ee* ranged from 3 to 86%.

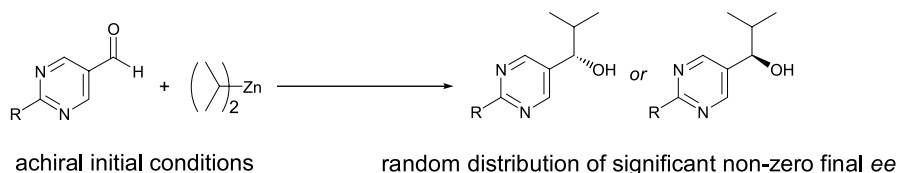
Since the enantiomeric distribution, i.e., the incidence of generating the *R* or *S* product, did not appear clearly as random but seemed to be correlated to the specific set-up used and to the order in which the experiments were carried out, the authors interpreted these results as possibly caused by chiral impurities in the starting mixture [34]. However, attempts to detect these impurities failed. In essence, the experiments of Singleton and Vo showed that

<sup>2</sup> In many cases, the Soai reaction is driven in reaction cycles by which the *ee* obtained in one cycle serves as the starting *ee* in a subsequent one. In the present case, the obtained *ee* was 57% (first cycle), 99% (second cycle), and > 99.5% (third cycle).



the Soai reaction can be susceptible to tiny initial chiral imbalances that can be below the experimental detection limit.

The first experimental evidence of absolute asymmetric synthesis with a truly stochastic enantiomeric product distribution was reported by Soai and coworkers (Scheme 4) [35]. In a total of 37 experiments and without adding any chiral substances, the authors found 19 times the formation of the *S* and 18 times the formation of the *R* product.



**Scheme 4** Soai reaction performed under achiral initial conditions giving rise in repeated experiments to a random distribution of the product enantiomers with significant non-zero final *ee*; R = *t*-Bu-C≡C-

Subsequent attempts by Singleton and Vo supported these results [36]. Also in this case, a clear random distribution of the *R* and *S* enantiomers in a number of the 54 experiments was observed, indicating that a systematic effect coming from chiral impurities may be excluded. Each experimental run afforded a clearly detectable prevalence of either the *R* or the *S* enantiomer, giving rise to a total of 27 events in which the *R* enantiomer dominated and 27 events in which the *S* enantiomer was found in excess (no quantification of the particular *ee* was given).

These findings were sustained by the observation that even a few molecules of the chiral initiator can determine the enantiomeric outcome: in 13 out of 13 reactions in the initial presence of only  $10^{-16}$  M of the *R*-pyrimidyl alkanol, i.e., about 60 000 molecules in 1 mL reaction mixture, the dominating product enantiomer after two to four reaction cycles showed constantly the same *R* configuration. Although a control experiment using the *S*-pyrimidyl alkanol was not reported, it was indicated that an extremely small amount of chiral starter can give rise to a deterministic enantiomeric outcome and can overshadow any chiral impurity or influence that may have caused the above-mentioned random generation of optical activity. Accordingly, the authors conclude that the optical activity arises “based on amplification of the random-chance excess of one enantiomer in the initial ‘racemic’ product” [36]. Hence the Soai reaction consists of both extremely strong amplification capacity and astonishingly high sensitivity towards the chirality sign of very small amounts of chiral starter.

The results of Soai and coworkers [35] as well as those of Singleton and Vo [36] suggest the occurrence of mirror-symmetry breaking in the Soai reaction, which is a rare phenomenon that is basically limited to a few crystallization processes [37]. Under certain kinetic conditions, chiral autocatalysis

can result in the instability of the racemic state. It follows that there is no other option for the system to become and perhaps to remain optically active, even if such a process is started from racemic or achiral initial conditions. Hence the generation of chiral imbalances can occur spontaneously, i.e., without any internal or external asymmetric intervention.

Fluctuations are inherent to any experimental chemical system. Even if these fluctuations are infinitesimally small, they are sufficient to drive the system away from an unstable state. The optically active state is characterized by two equivalent options: starting from an unstable racemic situation, the system can evolve into either an *R* configuration or into an *S* one. However, each individual experiment remains unpredictable as to which of the optically active states the system will move towards. For a large number of experiments an equal and random distribution between *R* and *S* dominance is expected if the initial conditions do not involve any preferences. Due to this unpredictability of the chiral configuration, the phenomenon of mirror-symmetry breaking introduces another element of stochastic behavior into chemical reactions different from that occurring in “clock reactions” [38, 39].

Such spontaneous generation of chiral asymmetry must be distinguished from occasional large fluctuations in the *ee* that can be also observed in asymmetric reactions. These processes generally correspond to a Gaussian distribution of the *ee* around zero, while symmetry breaking results in a bimodal probability distribution around the two optically active situations, and basically no racemic result is observed.

Figure 1 illustrates symmetry breaking in the Soai reaction that has been clearly documented in two cases by bimodal product distributions (black and

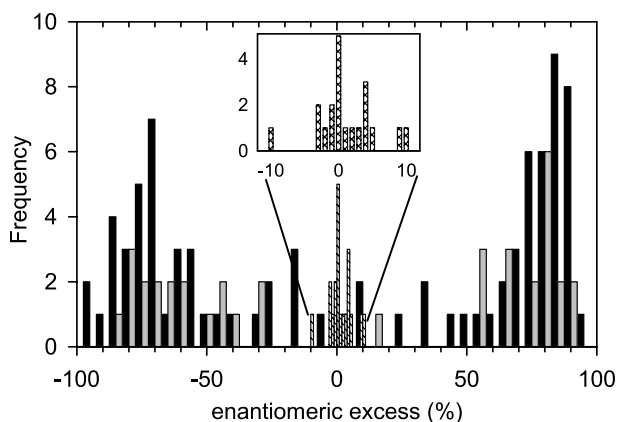


**Fig. 1** Frequency distribution of the %*ee* in repeated experiments of the Soai reaction performed with different starting aldehydes but without initial addition of chiral substances. Gray bars 2-*t*-Bu-C≡C-5-pyrimidinyl aldehyde ([35]); black bars 2-*t*-Bu-C≡C-5-pyrimidinyl aldehyde with achiral silica gel ([40]); patterned bars (CH<sub>3</sub>)<sub>2</sub>Si-C≡C-5-pyrimidinyl aldehyde ([41])

gray bars) [35, 40]. In contrast, Gridnev et al. found deviations from a racemic solution and a statistical distribution of the *R* and *S* products but no clear indication of a bimodal product distribution (patterned bars) [41].

Since there were variations in the experimental conditions (such as the nature of the aldehyde or the number of performed reaction cycles) it remains possible that the event or the extent of symmetry breaking depend on these. Even if the first reaction cycle gives rise to only a small *ee*, further ones will certainly amplify this small bias and push it with its proper enantiomeric direction to the edges. Further influence could come from achiral additives. Kawasaki et al. assume in the case of the addition of achiral silica gel that this additive may provide an improved reaction platform by coordination of the aldehyde and involvement of a zinc atom from the reaction of diisopropylzinc with the acidic hydroxyl group of silica gel [40]. Further systematic experimental studies, which can also shed more light on the basic reaction mechanism, are required to better understand the differences in the results.

## 2.3

### Effect of Miscellaneous Chiral Additives

As listed in Tables 2 and 3, not only the initially added pyrimidyl alkanol but also a wide variety of other chiral substances can act as chiral initiators in the Soai reaction [42–63]. All the experiments reported below have been reproduced several times and were performed by using alternately the *R* and *S* enantiomer of the additives to confirm the inversion of the outcome.

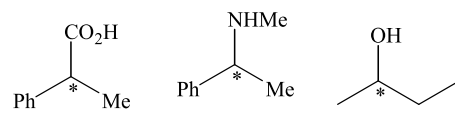
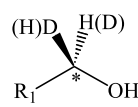
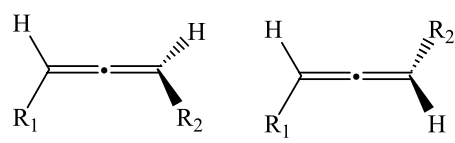
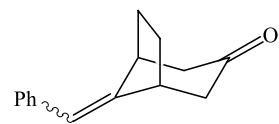
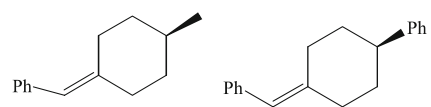
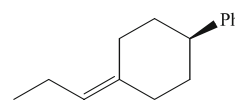
The origin of the various additive effects is still unknown. However, taking into account the wide variety of chiral additives that cause effects with considerable sensitivity, it can be assumed that unspecific rather than specific interactions between the additives and species involved in the reaction mechanism of the Soai reaction take place. These may cause small but directed chiral perturbations where advantage is taken of the extraordinarily strong autocatalytic amplification capacity of the system. As already demonstrated by Singleton and Vo [36], these “perturbations” can be extremely small without losing its enantiomeric direction. In fact, as we describe later, the assumption of interactions between these chiral additives and the Soai reaction product itself, i.e., the autocatalytic species, could provide a tentative explanation for such effects.

## 2.4

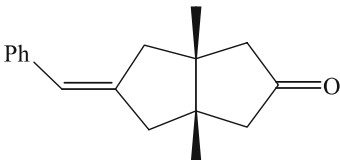
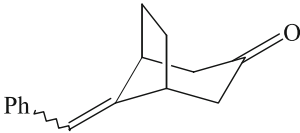
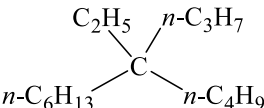
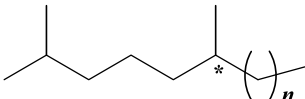
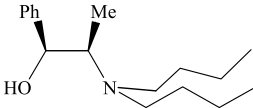
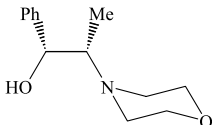
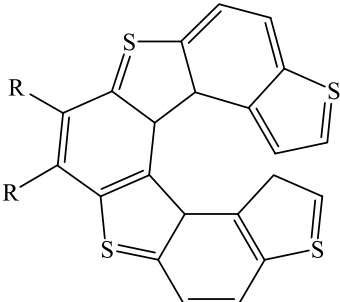
### Enantioselectivity Reversal

Lutz et al. initiated a series of Soai reactions by simultaneously adding a pair of competing chiral  $\beta$ -amino alcohol catalysts of opposite configurations to the initial reaction mixtures that were known to generate predominantly the

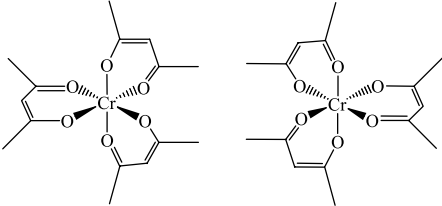
**Table 2** Soluble chiral additives in the Soai reaction that act as chiral initiators

Chiral additive	%ee (additive)	%ee (product)	Refs.
Leucine	2	16–26	[42]
Valine	1	47–51	[42]
Methyl mandelate	0.05–0.1	38–70	[42]
	0.1	73–85	[42]
 $R_1 = \text{Ph}$ $\text{Naphthyl}$ $\text{PhCH}_2\text{CH}_2$ $p\text{-Tolyl}$	56–95	91–96	[43]
[5]- and [6]-helicenes	0.13–95	56–95	[44]
4-Monosubstituted-[2.2]-paracyclophanes	2.5–100	89–99	[45, 46]
 $R_1$ $R_2$ $\text{Ph}$ $\text{Ph}$ $\text{Ph}$ Cyclohexyl $\text{Ph}$ $i\text{-Pr}$ $\text{Ph}$ $\text{PhCH}_2$ $\text{PhCH}_2$ $\text{PhCH}_2$	43–100	90–98	[47]
	Racemic <sup>a</sup>	93–97	[48]
	30–99	95–96	[48]
			

**Table 2** (continued)

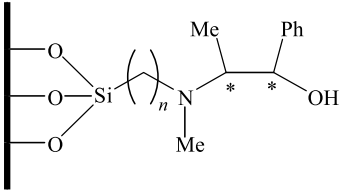
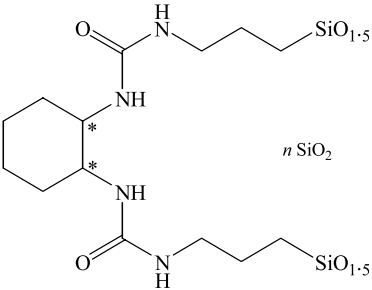
Chiral additive	%ee (additive)	%ee (product)	Refs.
	1.3–98	95–98	[48]
			
Chiral epoxides	2–100	64–96	[49]
Pyrimidylalkanols	Racemic <sup>a</sup>	53–100	[50]
	80–100	94–97	[51]
 $n = 1-7$	82–100	92–99	[51]
	100	98–100	[52]
			
	2–99	23–99	[53]

**Table 2** (continued)

Chiral additive	%ee (additive)	%ee (product)	Refs.
	4–100	45–96	[54]

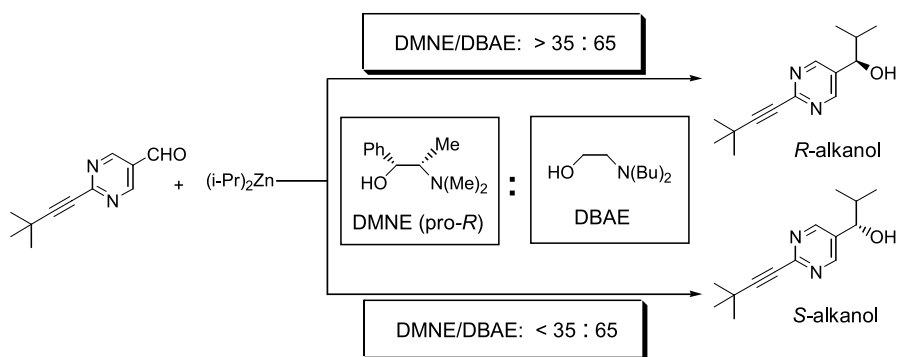
<sup>a</sup> Chiral additives have been employed in racemic form while chiral asymmetry was induced by continuous irradiation with right- or left- circularly polarized light

**Table 3** Insoluble chiral additives in the Soai reaction that act as chiral initiators

Chiral additive	%ee (additive)	%ee (product)	Refs.
Quartz	80–100	80–95	[55]
NaClO <sub>3</sub> , NaBrO <sub>3</sub>	50–100	97–98	[56, 57]
K[Co(edta)], 2H <sub>2</sub> O	100	85–94	[58]
Helical silica	100	96–97	[59]
	100	93–97	[60]
	100	82–95	[61]
Chiral cocrystals (from achiral organic molecules)	100	82–92	[62]
Chiral crystals of achiral hippuric acid	100	23–99	[63]

*R* or *S* product, respectively [64]. Variations in the mole fractions of the two catalysts revealed steep transitions between the two possible product configurations that practically occurred without intermediate values of the *ee*. These transitions did not necessarily occur when the concentrations of both catalysts were equal. Hence, the authors obtained information about the asymmetric power of each of the two competing chiral catalysts.

In a subsequent approach, Lutz et al. conducted a series of reactions in the simultaneous presence of pairs of chiral and achiral  $\beta$ -amino alcohol catalysts that were of similar chemical structure (e.g., DMNE and DBAE) [65]. The authors found that at a certain ratio of the concentrations of the chiral and achiral catalysts a reversal of the enantioselectivity of the chiral catalyst took place (Scheme 5).



**Scheme 5** Enantioselectivity reversal in the Soai reaction in the presence of the chiral catalyst DMNE and the achiral additive DBAE

The use of a pro-*R* catalyst (e.g., (1*R*,2*S*)-DMNE), which usually yields a product with *R* configuration, produces a product with *S* configuration if the achiral additive (e.g., DBAE) surpasses a certain concentration. The equivalent case at the same threshold concentration happened for the use of a pro-*S* catalyst. The *ee* of the reaction product, as a variation of the ratio of the two added compounds, again showed steep transitions between the two enantiomeric product configurations practically without intermediate values of the *ee*.

As a first assumption to explain the unexpected enantioselectivity reversal, Lutz et al. proposed that the chiral and achiral additives interact to form a new dimeric species that catalyzes the formation of the opposite enantiomer of the chiral catalyst [65]. As described in a later section, the interaction between the chiral additive and the reaction product of the Soai reaction could represent a second possibility to explain the phenomenon of enantioselectivity reversal.

### 3 Short Survey of Proposed Models

#### 3.1 General Models

Commenting their discovery of the first case of chiral autocatalysis in organic chemistry, Soai et al. stated that “it seems conceivable that the [Soai] reaction ... may be an example of the scheme proposed by Frank” [9]. Indeed, the so-called Frank model that has been developed in 1953 predicts the spontaneous amplification of an initial enantiomeric excess by means of a simple set of coupled differential equations [1]:

$$\begin{aligned}\frac{dn_1}{dt} &= (k_1 - k_2 n_2) n_1 \\ \frac{dn_2}{dt} &= (k_1 - k_2 n_1) n_2\end{aligned}\tag{1}$$

where  $n_1$  and  $n_2$  stand for the two product enantiomers,  $k_1 n_1$  and  $k_1 n_2$  represent the autocatalytic terms and  $-k_2 n_1 n_2$  stands for the so-called mutual inhibition between the enantiomers, i.e., a cross-inhibition between  $n_1$  and  $n_2$  that could be considered to form an inactive product. Although the Frank scheme is entirely symmetric by employing the same rate constants for both enantioselective processes, it can describe an amplification of *any* initial  $n_1/n_2$  ratio ( $ee = (1 - n_1/n_2)/(1 + n_1/n_2)$ ) – no matter how small – up to nearly  $ee = 100\%$ . On the other hand, the Frank scheme remains entirely general from the chemical point of view, so that Soai et al. concluded: “the detailed mechanism of the autocatalytic steps in our reaction, and in particular, whether an inhibitory mechanism is present, remains to be clarified” [9].

As already implied by the above scheme, it is essential that chiral amplification and symmetry breaking comprising the generic autocatalytic steps  $A + R \rightarrow 2R$  and  $A + S \rightarrow 2S$ , require some sort of cross-inhibition between the two enantiomers, for instance expressed by  $R + S \rightarrow P$ . Here A denotes an achiral substrate and P an unspecified product. In the absence of cross-inhibition, the  $ee$  will at best stay at its initial value but amplification remains impossible [66].

Lente proposed a discrete-state stochastic modeling approach in which chiral amplification could be described by a quadratic autocatalytic model without considering cross-inhibition [67, 68]. However, the discrepancy between the usually employed deterministic kinetic approach, which reinforces the need for cross-inhibition, and the discrete-state stochastic approach is only apparent. The discrete approach considers the repetitive reproduction of single molecules which, in the case of a chiral system, obviously are individually all enantiomerically pure. Hence, basically no amplification of the  $ee$  occurs at all during the discrete scenario. It has been indicated that deter-



ministic simulations using a quadratic autocatalytic model can reproduce this effect in which the cross-inhibition is not active by taking appropriate parameter values, such as considering the initial concentration of a single molecule of the enantiomer [69].

### 3.2

#### Spontaneous Asymmetric Synthesis

According to Mislow [70], the spontaneous generation of optical activity in chirally autocatalytic systems is practically unavoidable on statistical grounds alone. In fact, as shown early on by Mills [71], trivial statistical deviations from the racemic state can become significant, especially when the population of the chiral species is small. In a racemic mixture, there is always a tiny  $ee$ . Its value is proportional to the reciprocal of the square root of  $N$ , the total number of molecules. For instance, the expected  $ee$  ( $ee_{\text{exp}}$ ), which will be observed in more than 50% of the cases is given by:

$$ee_{\text{exp}} = \frac{0.6743}{\sqrt{N}} \quad (2)$$

where  $N$  is the number of molecules and 0.6743 corresponds to the surface under a half Gaussian probability distribution (Fig. 2).

During classical asymmetric synthesis, the amplitude of these fluctuations are expected to decrease during the course of the reaction because more and more chiral molecules are formed and  $ee_{\text{exp}}$  declines. However, in the presence of chiral autocatalysis, the small  $ee$  caused by such fluctuations can be amplified. In such cases, the system is likely to be most sensitive in the initial stage of reaction when the concentration of chiral molecules is still small. If the autocatalytic species are concentrated they can be either in a racemic or optically active state but if they are highly diluted, as at the beginning of the reaction, statistical fluctuations can become significant so that the state

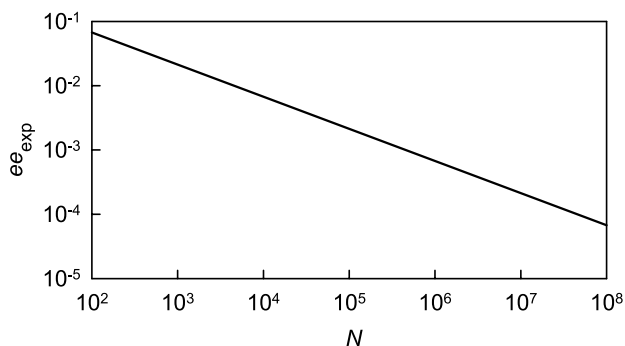


**Fig. 2** Log-log plot for 50% probability to obtain a higher  $ee$ , as indicated by the line as a function of  $N$ , the total number of molecules in a racemic mixture

is not necessarily racemic. Furthermore, the dominating chiral configuration cannot be predicted.

### 3.3

#### Chiral Amplification in Asymmetric Synthesis

It was soon recognized that in specific cases of asymmetric synthesis the relation between the *ee* of a chiral auxiliary and the *ee* of the product can deviate from linearity [17, 18, 72–74]. These so-called nonlinear effects (NLE) in asymmetric synthesis, in which the achievable *ee*<sub>prod</sub> becomes higher than the *ee*<sub>aux</sub>, represent chiral amplification while the opposite case represents chiral depletion. A variety of NLE have been found in asymmetric syntheses involving the interaction between organometallic compounds and chiral ligands to form enantioselective catalysts [74]. NLE reflect the complexity of the reaction mechanism involved and are usually caused by the association between chiral molecules during the course of the reaction. This leads to the formation of diastereoisomeric species (e.g., homochiral and heterochiral dimers) with possibly different relative quantities due to distinct kinetics of formation and thermodynamic stabilities, and also because of different catalytic activities.

In the “reservoir model”, which was confirmed by Noyori and coworkers as the prototype case of catalytic asymmetric organozinc additions to carbonyl compounds in the presence of (–)-3-*exo*-(dimethylamino)isoborneol (DAIB) yielding chiral benzyl alkanols with a higher *ee* than that of the added DAIB [17, 18], there is a reversible equilibration between monomers and dimers. It is assumed that the monomers *r* and *s* are the catalysts and that the heterochiral dimers [*r*·*s*] are of higher thermodynamic stability than their homochiral ([*r*·*r*] and [*s*·*s*]) analogues:



The formation of the comparatively more stable heterochiral dimers generates an optically inactive reservoir that consequently leads to an increase in the *ee* of the free monomers. In this case, the *ee* is increased by building up an inactive racemic pool, as is the case in conglomerate crystallizations.

Similarly, there is the “ML<sub>*n*</sub>” model invented by Kagan and coworkers [72–74]. In this case, no a priori difference in the thermodynamic stabilities between homochiral and heterochiral dimers is assumed, but the dimers instead of monomers are considered to be the catalytic species. The heterochiral and homochiral dimers are allowed to display different catalytic activities, where the heterochiral dimer is assumed to perform without any enantioselectivity.

According to Soai and coworkers [31], the strong chiral amplification sometimes observed in their system cannot be explained by so-called NLE alone since amplification effects in these cases remain at a more moderate level. Hence a more complex reaction mechanism than expressed by the reservoir or the  $ML_n$  model is indicated for the Soai reaction.

### 3.4

#### Chiral Symmetry Breaking in Crystallization

The first laboratory demonstration of mirror-symmetry breaking in a chemical system was the stirred crystallization of sodium chlorate ( $\text{NaClO}_3$ ), discovered by Kondepudi and coworkers [75].  $\text{NaClO}_3$  is achiral on the molecular level but its crystals exhibit a chiral morphology. Normally, crystallization from the achiral solution phase yields a statistically equal amount of left-handed and right-handed crystals. This changes if the solution is stirred during crystallization since fluid motion is believed to give rise to so-called secondary nucleation, which is an autocatalytically driven fast process. In such a case, each crystallization results in an almost 100% *ee* of either L- or D-crystals, where the chirality sign of the major or minor enantiomer of each individual experiment remains unpredictable.

Gridnev argued that the mechanism of mirror-symmetry breaking in the Soai reaction and that in the stirred crystallization of  $\text{NaClO}_3$  might be closely related [76]. It is assumed that in both cases a supramolecular level is involved in the amplification mechanism: the intervention of oligomers or aggregates in the Soai reaction and that of nucleation processes in the  $\text{NaClO}_3$  system. However, chiral amplification in the Soai reaction essentially occurs under homogeneous reaction conditions [48]. Therefore the formation of aggregates or precipitates, as occasionally observed under specific reaction conditions, cannot be considered to be the cause of amplification and so stands in contrast to the characteristics of  $\text{NaClO}_3$  crystallization. Hence both systems are of opposite nature but, nevertheless, are obviously driven by similar autocatalytic dynamics.

### 3.5

#### Kinetic Recording of the Soai Reaction

A number of different kinetic attempts and strategies have been employed to obtain a closer understanding of the Soai reaction. The first efforts were made by Blackmond et al. using microcalorimetric studies [77]. The autocatalytic nature of the reaction was confirmed by the observation of the maxima of the reaction heat flows as a function of time. In particular, it was reported that the reaction rate depends on the enantiomeric purity of the initially added pyrimidyl alkanol, where the rate in the presence of the enantiopure alkanol was roughly twice of that using the racemic alkanol.

Based on these results, Blackmond et al. argued that the autocatalytic species in the Soai reaction were dimeric or oligomeric since in the case of a monomeric autocatalyst, asymmetric amplification would require higher stability of the heterodimer against the homodimer, i.e.,  $K_{\text{HETERO}} > K_{\text{HOMO}}$  [77]. On the other hand, it was claimed that the rate obtained using the enantiopure catalyst can only be twice the rate using the racemic catalyst if  $K_{\text{HETERO}} = K_{\text{HOMO}}$ , i.e., if both dimers exhibit the same stability. Hence, the same stabilities of homo- and heterochiral dimers seemed to exclude the occurrence of chiral amplification because of insufficient cross-inhibition. This idea of a modified  $ML_n$  mechanism was converted into an empirical kinetic approach based on several approximations, such as the assumption of instant dimer formation (pre-equilibration). Furthermore, the catalytic efficiency of the homochiral dimers was a priori assumed to be higher than that of the heterochiral ones.

Sato et al. confirmed the autocatalytic nature of the Soai reaction by showing the sigmoidal time evolution of the product formation and the acceleration of the reaction by initial addition of the pyrimidyl alkanol [19]. The authors also presented a modeling attempt by using fast pre-equilibrium approximations [19, 78].

In the above-cited kinetic attempts, the overall rate of the Soai reaction was expressed by single expressions that were able to describe selected experimental data. On the other hand, it was impossible to rationalize, for instance, the spontaneous generation of *ee* from achiral starting conditions by such simplified reasoning. Moreover, it is pertinent for nonlinear reaction systems that approximations used to arrive at single rate laws can become problematic [79, 80]. For instance, this is the case for the assumption of a fast pre-equilibrium between the monomers and the dimers. In order to describe a nonlinear system such as the Soai reaction, the time of equilibration becomes decisive because of the amplifying character coming from the underlying autocatalytic kinetics.

Rivera Islas et al. proposed an alternative approach, which should be generally employed for the study of nonlinear systems and was believed to respond better to the complexity of the Soai reaction than the consideration of single rate laws [69]. In such an attempt a priori approximations are usually avoided, all possible species are considered, the velocity of equilibria is especially taken into account, and the coupling of chemically realistic reaction steps is not disregarded. On the other hand, a larger number of variables and parameters have to be handled. Hence such an approach can only be conducted numerically but, in the best case, it can mimic the mechanics of the real system because of its similar coupled and multistep design.

As indicated by our previous works [20–23, 81], such a strategy of kinetic modeling is usually less focused on the extraction of rate parameter values than on the exploration of the dynamic behavior of the system. This dynamic behavior can be considered to be the fingerprint of the underlying reaction

mechanism. Hence, sensitive processes and parameters that govern the dynamics of the system can be established and evaluated. As is apparent for each type of kinetic approach, the validity of any proposed model system has to be determined through its accordance with experimentally observed behavior.

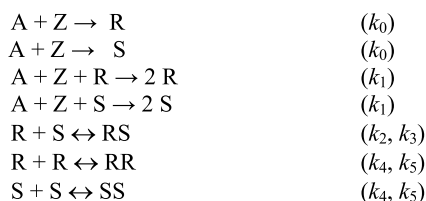
## 4

### Kinetic Understanding of the Soai Reaction

#### 4.1

##### Proposition of Kinetic Schemes

Taking into account basic experimental information, such as the observation of autocatalytic kinetics and the formation of dimers, the Soai reaction was expressed by a minimal kinetic model (Scheme 6) that was considered foremost to consist of chemically realistic steps [69]:



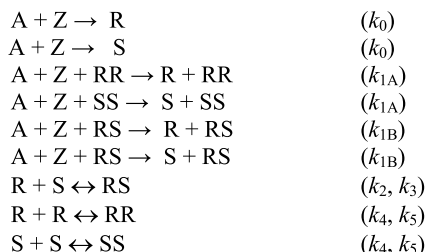
**Scheme 6** Minimal kinetic model for the Soai reaction. A = pyrimidine carbaldehyde, Z = diisopropylzinc, R or S = enantiomeric zinc alkoxide, RR or SS = homochiral zinc alkoxide dimers, and RS = heterochiral zinc alkoxide dimer

The minimal model comprises an uncatalyzed and unspecific direct formation of R and S ( $k_0$ ), a simple and unspecified description of the autocatalytic steps assuming monomers as catalytic species ( $k_1$ ), and the monomer–dimer equilibria ( $k_2, k_3$ ) and ( $k_4, k_5$ ) in which different rates of dimer formation for homochiral and heterochiral species is allowed. This model translates into the following set of differential equations:

$$\begin{aligned}
 dA/dt &= dZ/dt = -2k_0AZ - k_1AZ(R + S) \\
 dR/dt &= k_0AZ + k_1AZR - k_2RS + k_3(RS) + 2k_5(RR) - 2k_4RR \\
 dS/dt &= k_0AZ + k_1AZS - k_2RS + k_3(RS) + 2k_5(SS) - 2k_4SS \\
 d(RS)/dt &= k_2RS - k_3(RS) \\
 d(RR)/dt &= -k_5(RR) + k_4RR \\
 d(SS)/dt &= -k_5(SS) + k_4SS
 \end{aligned} \tag{4}$$

While it is commonly accepted that the required mutual inhibition originates from dimerization as expressed by the minimal model, the exact nature

of the autocatalytic stereoselective process is still open. This question concerns another mechanistic detail, namely whether the reaction is catalyzed by monomers or by dimers. For this reason, an alternative kinetic model (Scheme 7) assuming dimer catalysis has been evaluated [69].



**Scheme 7** Alternative kinetic model for the Soai reaction assuming dimer catalysis

In the alternative kinetic model, the monomer-catalyzed steps ( $k_1$ ) were replaced by dimer-catalyzed steps ( $k_{1A}$  and  $k_{1B}$ ) allowing different rates for the homochiral and heterochiral catalytic processes.

The two models behave very similar in both their dynamic properties and in their capacity to reproduce experimental data. For this reason it was concluded that no definite discrimination between these two options can be made so far [69].

## 4.2

### Properties of the Kinetic Schemes

As demonstrated in Fig. 3, by performing a simple simulation of the minimal model<sup>3</sup>, chiral amplification from initially extremely low to very high values can be readily reproduced using an appropriate set of rate parameter values.

In order to observe the chiral amplification given in Fig. 3, two considerations have to be regarded for the choice of the rate parameters: (i) the rate constant  $k_0$  has to be adequately small. For instance, chiral amplification does not occur if  $k_0 \geq 0.2 \text{ M}^{-1} \text{ s}^{-1}$ . It is apparent that if the chirally unspecific process  $A + Z \rightarrow R$  or  $S$  proceeds too fast it generates a high amount of racemic matter that can overwhelm the enantiospecific amplification process. (ii) The mutual inhibition rate constant  $k_2$  ( $R + S \rightarrow RS$ ) must be higher than  $k_4$  ( $R + R \rightarrow RR$ , or it must occur faster than the homodimerization. Moreover, taking into account the equilibrium constants  $K_{\text{HETERO}} = k_2/k_3$  and  $K_{\text{HOMO}} = k_4/k_5$ , it is vital that  $K_{\text{HETERO}} > K_{\text{HOMO}}$ , i.e., the heterochiral dimer has to be thermodynamically more stable than its homochiral coun-

<sup>3</sup> In the following, only the properties of the minimal model are discussed since the alternative model gives rise to very similar results.

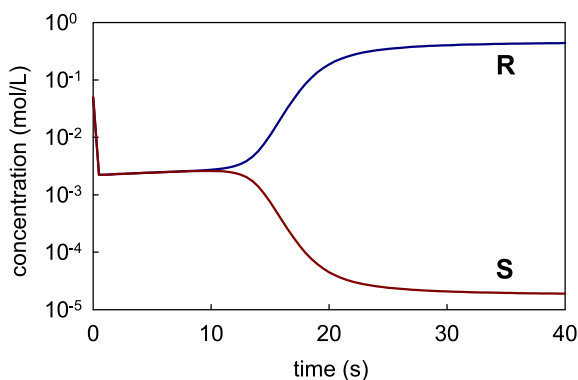


**Fig. 3** Numerical simulation of the time evolution of the concentrations of R and S showing strong amplification starting with  $ee_0 = 10^{-5}\%$ .  $[A]_0 = [Z]_0 = 1\text{ M}$ ,  $[R]_0 = 5.0000005 \times 10^{-2}\text{ M}$ , and  $[S]_0 = 4.9999995 \times 10^{-2}\text{ M}$ ;  $k_0 = 10^{-6}\text{ M}^{-1}\text{ s}^{-1}$ ,  $k_1 = 1\text{ M}^{-2}\text{ s}^{-1}$ ,  $k_2 = 10^5\text{ M}^{-1}\text{ s}^{-1}$ ,  $k_3 = 10\text{ s}^{-1}$ ,  $k_4 = 10\text{ M}^{-1}\text{ s}^{-1}$ , and  $k_5 = 10\text{ s}^{-1}$

terpart. This requirement appears to be in agreement with preliminary semi-empirical energy calculations of the RS and RR or SS dimers [69].

### 4.3

#### Mirror-Symmetry Breaking in Simulation

Besides the effect of strong chiral amplification in the Soai reaction there is the experimental observation of spontaneous generation of  $ee$  from entirely achiral starting conditions. Fig. 4 shows that the kinetic model can give rise to mirror-symmetry breaking.

At first glance, this result appears surprising because numerical simulations are deterministic and if started under symmetric (achiral) initial conditions a symmetric (racemic) result would be expected. However, surpassing a critical value of  $k_2$  of around  $6 \times 10^3\text{ M}^{-1}\text{ s}^{-1}$ , each computational run (started under completely achiral conditions) afforded an optically active result. Analogous to the laboratory experiments, the chirality sign (positive or negative  $ee$ ) remained unpredictable for each individual simulation (here triggered by small changes in the internal calculation parameters only) but resulted equally weighted in R and S over the total number of simulations. Despite this stochastic behavior, each computational run with the same initial conditions and internal calculation parameters was perfectly reproducible.

For Fig. 4, the rate constant for the mutual inhibition ( $k_2$ ) was chosen as the bifurcation parameter; however, all other parameters and the initial reactant concentrations serve as bifurcation parameters as well. Mirror-symmetry breaking in simulation is caused by the intrinsic instability of the autocatalytic model. When placed into the proper parameter domain, this instability can be revealed by the inevitable machine round-off as well as by slightly

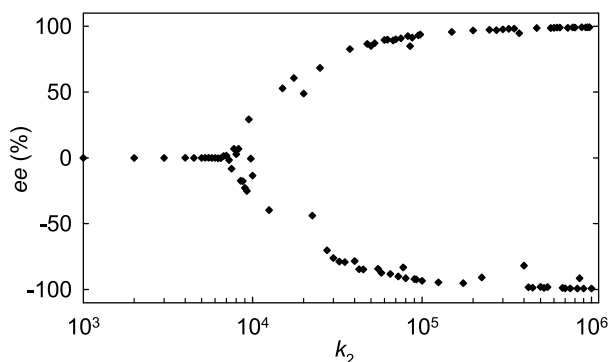


**Fig. 4** Numerical simulation revealing mirror-symmetry breaking in which  $k_2$  acts as a bifurcation parameter (same conditions as in Fig. 3 except  $[R]_0 + [S]_0 = 0$ ). Each *dot* represents the final *ee* of an individual computer simulation. For  $k_2 > 6 \times 10^3 \text{ M}^{-1} \text{ s}^{-1}$  the system becomes optically active, where positive and negative values of the resulting *ee* are equally distributed

shifting the initial values of the concentrations of the chiral species. Hence machine round-off plays the role of fluctuations, while the instability is a dynamic property of the model itself being independent of the computational method.

#### 4.4

#### Reproduction of Further Experimental Observations

After having confirmed that both kinetic models are able to reproduce strong amplification and mirror-symmetry breaking, we looked at whether there was further agreement with experimental observations and whether there was a quantitative accord with time-resolved kinetic data. We attempted to reproduce the, perhaps most comprehensive, kinetic record of the Soai reaction reported by Gridnev et al. [39]. This data originated from NMR-monitored Soai reactions and consists of a high number of experimental points that have been taken in situ and represent a reliable source for data fitting. On the other hand, the authors also noticed variations in the kinetic curves in repeated experiments that were conducted under the same initial conditions. Such an irreproducibility effect may point towards an important intrinsic property of this reaction system, namely an extremely high sensitivity to initial fluctuations, which essentially cannot be controlled and are amplified by the autocatalytic kinetics. As shown in Fig. 5, it was possible to reproduce the non-trivial kinetics reported by Gridnev et al., although the data reproduction of multiple experiments with the same rate parameters appeared impossible because of the experimental irreproducibilities.

Using the same set of parameters given in Fig. 5, it is possible to simulate another NMR experimental result described by Gridnev et al. [33]. Namely,



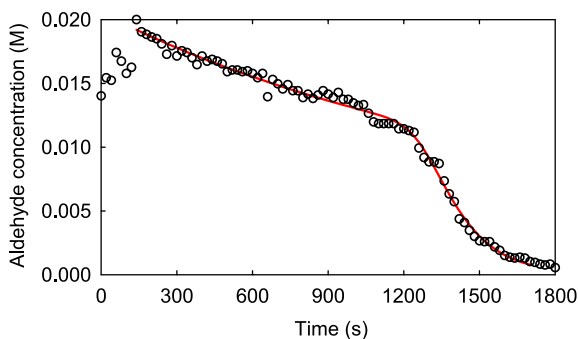


**Fig. 5** Experimentally observed consumption of the aldehyde (dots, [39]) reproduced by the kinetic minimal model (solid line).  $[A]_0 = 1.92 \times 10^2 \text{ M}$  and  $[Z]_0 = 0.04 \text{ M}$ ; rate parameters, minimal model  $k_0 = 5.2 \times 10^{-3} \text{ M}^{-1} \text{ s}^{-1}$ ,  $k_1 = 69 \text{ M}^{-2} \text{ s}^{-1}$ ,  $k_2 = 4.5 \times 10^5 \text{ M}^{-1} \text{ s}^{-1}$ ,  $k_3 = 5.2 \times 10^{-2} \text{ s}^{-1}$ ,  $k_4 = 4.8 \times 10^3 \text{ M}^{-1} \text{ s}^{-1}$ , and  $k_5 = 21 \text{ s}^{-1}$ . The first experimental points were excluded from the fitting procedure

this is the observation of two broadened singlets of similar intensity (52 : 48) in the 8.5 ppm region corresponding to the homo- and heterochiral forms of the dimers prepared from the starting aldehyde and diisopropylzinc without added catalyst. These studies indicated a statistical 1 : 1 distribution of the dimers in solution.

The simulation shown in Fig. 6 demonstrates that a close to 1 : 1 ratio of homo- and heterochiral species can be reproduced, even under conditions in which the thermodynamic stability of the heterochiral dimers is considered higher than that of the homochiral ones. This effect results from the nonlinear dynamics of the reaction and from mirror-symmetry breaking.

In summary, it was confirmed that simple kinetic models derived from the classical Frank scheme can reproduce the variety of unprecedented effects of

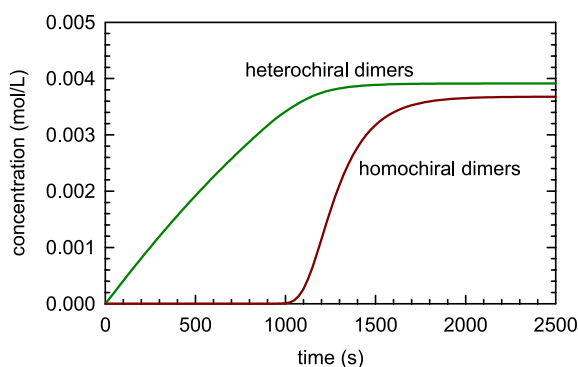


**Fig. 6** Simulated time-evolution of heterochiral and homochiral dimers in the Soai reaction by using the minimal model, giving rise to a nearly 1 : 1 distribution of both types of species. Same initial conditions and parameters used as in Fig. 5

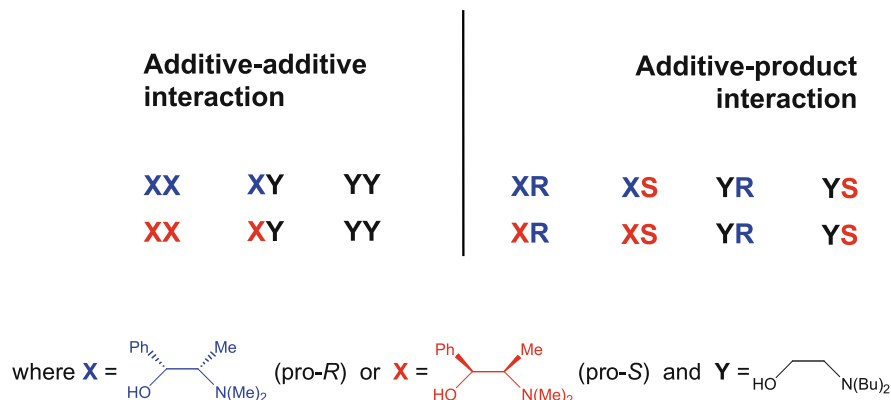
the Soai reaction, such as the astonishingly strong amplification starting from extremely small chiral imbalances as well as the phenomenon of spontaneous mirror-symmetry breaking.

A closer exploration of the parameter space showed that symmetry breaking is sensitive to the thermodynamic stabilities of the dimers but also to the rate of their formation, predicting that the heterochiral dimers are formed faster and are more stable than the homochiral ones [69]. The fitting of the experimentally obtained data (Fig. 5) resulted in rate parameters that confirm these conclusions and that simultaneously give rise to mirror-symmetry breaking.

## 4.5

### Reproduction of Enantioselectivity Reversal

We have provided a possible understanding of the observed reversal of enantioselectivity [82]. Extending the minimal or alternative kinetic model, two mechanistic assumptions have been evaluated from a kinetic point of view: (i) the direct interaction between the two added catalysts X (chiral) and Y (achiral) to form the dimers XX, XY, and YY, or (ii) the interaction between the added catalysts X (chiral) and Y (achiral) and the products of the Soai reaction (R and S) to form the dimers XR, XS, YR and YS (Scheme 8).



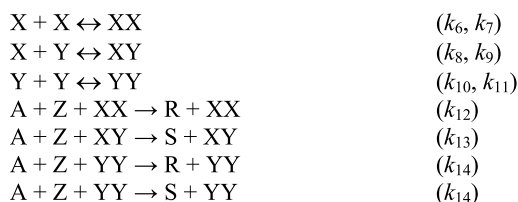
**Scheme 8** Scenarios of additive-additive or additive-product interactions that have been evaluated as the possible cause for enantioselectivity reversal in the Soai reaction in the presence of chiral and achiral additives

### 4.5.1

#### Additive-Additive Interactions

For the assumption of additive-additive interactions, the dimer formation between the chiral and achiral catalyst was translated into a series of kinetic

steps. Considering the case in which X is a pro-R catalyst, the dimer XX is assumed to promote the R product while YY, which is composed of two achiral entities, does not display any enantioselectivity (Scheme 9).



**Scheme 9** Kinetic steps expressing an additive–additive interaction that were added to the minimal or alternative kinetic model. X = enantioselective catalyst, Y = achiral catalyst

According to Lutz et al. [65], the mixed aggregate XY is assumed to promote the product with opposite configuration to that of the chiral catalyst X alone, i.e., in the present example the S product. The kinetic steps denoted in Scheme 9, together with the minimal or alternative kinetic model, can give rise to a simulation of the experimentally observed enantioselectivity reversal.

In the case of additive–additive interactions, the equilibrium distribution of the dimers XX, XY, and YY depends only on their relative stabilities since R or S are not involved in their formation. Hence at a high concentration of X, the dimerization of X monomers dominates and leads to the formation of the reaction product with the same configuration of X. In contrast, at a high concentration of Y, the formation of XY dimers governs the process and provides a large amount of mixed XY aggregates that catalyze the product with opposite configuration to X.

The key point of this scenario is to assume a priori that XY promotes the product of opposite configuration to X. In addition, additive dimers and not monomers are considered as catalytically active species, opposing the commonly accepted mechanism for typical dialkylzinc additions to aldehydes catalyzed by  $\beta$ -amino alcohols [18].

#### 4.5.2

##### Additive–Product Interactions

In the second option, additive–product interactions are assumed. These can lead to the reproduction of enantioselectivity reversal by considering only *one* additive. The driving force for the enantioselectivity reversal in this case originates from a competition between kinetic steps that give rise to the product R on one hand and to the product S on the other. Due to mutual inhibition, as expressed by the minimal or alternative kinetic model, i.e.,  $\text{R} + \text{S} \leftrightarrow \text{RS}$  ( $k_2$ ,  $k_3$ ), a process that gives rise to the formation of R is in some way equivalent to an inhibition of the S formation and vice versa. Due to additive–product

interactions, R and S become partially trapped to form dimers with the additives. Because of diastereomeric effects, XR and XS may display different rates of formation and dissociation and different thermodynamic stabilities that cause a shift in the enantiomeric ratio of the alkoxide monomers R and S. This effect occurs even when the diastereomeric recognition ability of X vs. R or S is extremely small, i.e., even if the respective association rate constants differ less than  $10^{-11} \text{ M}^{-1} \text{ s}^{-1}$ . Hence, additive-product interaction could also be a possible explanation for the miscellaneous chiral additive effects exhibited by the Soai reaction (see Tables 2 and 3).

The dynamic trapping of R and S can be understood in terms of a poisoning of the autocatalytic species R and S since those that are complexed to X are disabled from contributing to the autocatalytic processes  $A + Z + R \rightarrow 2R$  and  $A + Z + S \rightarrow 2S$ .

In the following, we will exemplify this effect by considering an enantiopure pro-R catalyst (X) as the only additive. The main additive-product interaction is given by the two equilibria:



As we have already shown [82], these two equilibria alone can be sufficient to cause the enantioselectivity reversal if very special kinetic properties such as the slower formation of the thermodynamically more stable dimer are considered. A more general situation is given when the pro-R additive is additionally allowed to display catalytic properties in the formation of the Soai products such as:



The simplest situation occurs if X is highly stereoselective regarding the formation of R and if it shows an overwhelming preference to form the XR over the XS dimer. In this case, the competition between  $k'_6$  and  $k'_{10}$  alone gives rise to the enantioselectivity reversal. Here, R is inhibited by the process  $X + R \leftrightarrow XR$  but promoted by  $A + Z + X \rightarrow R + X$ . In this particular case, a stepwise transition between the two optically active states can be obtained by simulation within a certain range of the involved rate parameters when the concentration of the additive is gradually increased. A more general case where all the realistic processes are operative is shown in Fig. 7.

To account for a chemically more realistic situation, it should be assumed that X is an asymmetric catalyst with limited stereoselectivity and reduced capacity to discriminate between R and S so that the kinetic steps involving the S ( $k'_8$ ,  $k'_9$ , and  $k'_{11}$ ) can no longer be ignored. Under this consideration, the rate parameters have been equipped with stereoselectivity parameters  $\varepsilon_1$  and  $\varepsilon_2$  in such a way that  $k'_6 = (1 + \varepsilon_1) \times k'_8$  and  $k'_{10} = (1 + \varepsilon_2) \times k'_{11}$ , where

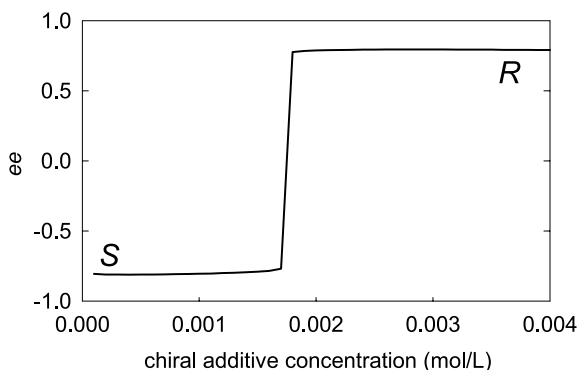


**Fig. 7** Simulation of enantioselectivity reversal by considering additive–product interactions and poorly pronounced chiral discrimination and stereoselectivity of the chiral additive.  $[A]_0 = 0.02$  M,  $[Z]_0 = 0.04$  M,  $k_0 = 5.2 \times 10^{-3} \text{ M}^{-1} \text{ s}^{-1}$ ,  $k_1 = 69 \text{ M}^{-2} \text{ s}^{-1}$ ,  $k_2 = 4.5 \times 10^5 \text{ M}^{-1} \text{ s}^{-1}$ ,  $k_3 = 0.052 \text{ s}^{-1}$ ,  $k_4 = 4.8 \times 10^3 \text{ M}^{-1} \text{ s}^{-1}$ ,  $k_5 = 21 \text{ s}^{-1}$ ,  $k'_6 = 9.52 \times 10^3 \text{ M}^{-1} \text{ s}^{-1}$ ,  $k'_7 = 100 \text{ s}^{-1}$ ,  $k'_8 = 9.48 \times 10^3 \text{ M}^{-1} \text{ s}^{-1}$ ,  $k'_9 = 100 \text{ s}^{-1}$ ,  $k'_{10} = 0.02375 \text{ M}^{-2} \text{ s}^{-1}$ , and  $k'_{11} = 0.02365 \text{ M}^{-2} \text{ s}^{-1}$ . Note that  $\varepsilon_1 = \varepsilon_2 = 4 \times 10^{-3}$

$\varepsilon_1 > 0$  and  $\varepsilon_2 > 0$ . An interesting situation occurs when both  $\varepsilon_1$  and  $\varepsilon_2$  are almost zero, i.e., when X interacts with R and S and catalyzes the formation of both enantiomers but its discrimination capability and stereoselectivity is extremely poor. In such a case, the additive–product interaction still gives rise to enantioselectivity reversal (see example shown in Fig. 7).

Figure 8 shows the corresponding dynamic evolution of R and S below and above the chiral additive concentration at which the enantioselectivity rever-

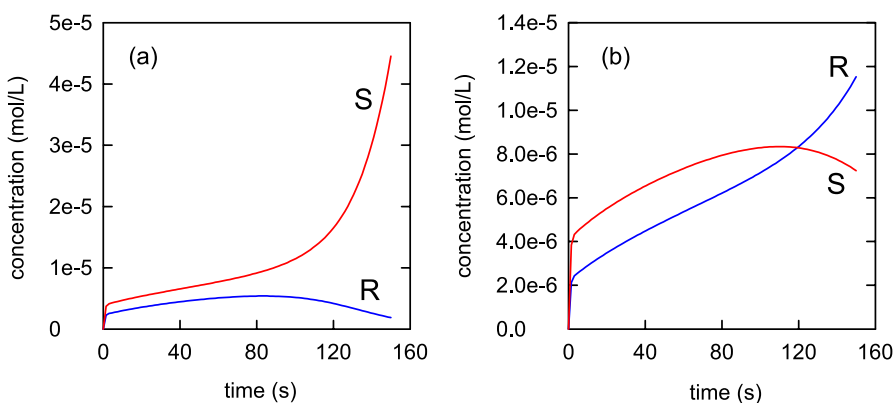


**Fig. 8** Early time evolution of the R and S Soai reaction products on both sides of the stepwise transition as shown in Fig. 7. **a** R-trapping is dominant giving rise to enantioselectivity reversal (pro-R catalyst  $[X]_0 = 1.55 \times 10^{-3}$  M); **b** R-catalysis is dominant resulting in the preservation of enantioselectivity (pro-R catalyst  $[X]_0 = 1.95 \times 10^{-3}$ ). Same initial conditions and rate parameters as in Fig. 7

sal occurs. At the initial stage of reaction, R is strongly inhibited resulting in a higher concentration of S over R in both enantioselectivity reversal and enantioselectivity preservation, i.e., in the case in which pro-R gives R. Since X is a pro-R catalyst, enantioselectivity reversal takes place at a lower concentration of X (Fig. 8a) and the formation of S is favored. Enantioselectivity is preserved at a higher concentration of X where, as expected, R is formed (Fig. 8b).

Further attempts by introducing Y + R and Y + S interactions showed that both the enantioselectivity reversal in the presence of competing chiral or achiral catalysts as well as the experimentally observed variation of the transition step as a function of the structure of the chiral catalyst can be addressed by the same approach [82].

## 5 Conclusion

We have given kinetic insight into a number of experimental features of the Soai reaction. It was shown that chiral amplification and mirror-symmetry breaking are driven by a reaction network that contains enantioselective autocatalysis and mutual inhibition as the essential ingredients. In this sense, the Soai reaction moves the early concepts of Frank forward into experimental reality. Taking into account the formation of isopropylzinc alkoxide dimers, an evaluation of the parameter space in which amplification and symmetry-breaking are observed indicates that the heterochiral dimers display a higher thermodynamic stability and have to be formed faster than the homochiral ones. The necessity of such sensitive interplay may explain why such reactions systems are so scarce.

Further insight into the structural aspects of the basic reaction process was given by NMR studies, which indicate that additional equilibria between the alkoxide dimers and diisopropylzinc molecules should be taken into account yielding RR-Z, SS-Z, and RS-Z association complexes [33, 83]. Further studies in such a direction combined with kinetic experiments will be needed to decide about the closer reaction network in the Soai reaction (especially about the autocatalytic steps) in order to shine light on the possible catalytic action of monomer or oligomer species.

The effect of enantioselectivity reversal serves as an additional experimental observation that gives a possible clue for the reaction mechanism. By the proposed additive–product interactions it was predicted that even poor stereoselectivity and discriminating capability of the catalytic additive can give rise to enantioselectivity reversal. This also gives a possible kinetic explanation for the effect of miscellaneous chiral additives in the Soai reaction and their role as potent chiral initiators.

The observed sensitivity towards almost any chiral compound can be regarded as an example of so-called chiral propagation, which is of immediate

importance for the disputed origin of biomolecular homochirality [84–89]. Three open questions still govern the discussion about this matter:

1. The fundamental (initial) cause of universal chiral asymmetry
2. Whether the enantiomeric preference, such as found in the L-configuration of amino acids or the D-configuration of sugars, comes from a deterministic or a random process
3. How chiral asymmetry has been propagated through the diverse levels of biomolecular systems

For the latter question, the observed various additive effects in the Soai reaction could perhaps serve as a prototype model. In these cases, the chiral asymmetry of an external precursor (e.g., mandelate) is propagated and amplified by another system (the Soai reaction) and becomes apparent with a higher *ee* in a different compound (the Soai reaction product). This could perhaps be the key principle governing how chiral asymmetry spread out efficiently during an evolutionary scenario. Although it is not likely that the Soai reaction was involved in a prebiotic chemical scenario in which chiral asymmetry evolved, a better understanding of the mechanistic and kinetic principles of chiral propagation could contribute to resolving an important open question on the origin of asymmetry in nature.

In turn, the Soai reaction could have an impact in an opposite sense. As recently reported [90], the sensitivity of the system can be used to detect the smallest chiral imbalances, as for instance found in the unknown organics of meteorites, and can throw light on the question of delivery of chiral asymmetry to the early Earth.

Without a doubt, these effects deserve further experimental investigation and kinetic analysis. They are not only of interest for the origin of biomolecular homochirality but also as a possible innovation in enantioselective synthesis, as well as a remarkable example of nonlinear behavior through autocatalytic reaction kinetics.

## References

1. Frank FC (1953) *Biochim Biophys Acta* 11:459
2. Calvin M (1969) *Molecular evolution*. Oxford University Press, Oxford
3. Seelig FF (1971) *J Theor Biol* 31:355
4. Decker P (1979) In: Walker DC (ed) *Origins of optical activity in nature*. Elsevier, Amsterdam, p 109
5. Iwamoto K, Seno M (1982) *J Chem Phys* 76:2347
6. Kondepudi DK, Nelson GW (1984) *Physica A* 125:465
7. Feringa BL, van Delden RA (1999) *Angew Chem Int Ed* 38:3418
8. De Min M, Levy G, Micheau JC (1988) *J Chim Phys* 85:603
9. Soai K, Shibata T, Morioka H, Choji K (1995) *Nature* 378:767
10. Soai K, Shibata T, Sato I (2000) *Acc Chem Res* 33:382
11. Soai K, Sato I, Shibata T (2001) *Chem Record* 1:321
12. Soai K, Sato I (2002) *Chirality* 14:548

13. Soai K, Shibata T, Sato I (2004) *Bull Chem Soc Jpn* 77:1063
14. Podlech J, Gehring T (2005) *Angew Chem Int Ed* 44:2
15. Soai K, Kawasaki T (2006) *Chirality* 18:469
16. Soai K, Niwa S (1992) *Chem Rev* 92:833
17. Kitamura M, Suga S, Oka H, Noyori R (1998) *J Am Chem Soc* 120:9800
18. Noyori R, Suga S, Oka H, Kitamura M (2001) *Chem Record* 1:85
19. Sato I, Omiya D, Tsukiyama K, Ogi Y, Soai K (2001) *Tetrahedron: Asymmetry* 12:1965
20. Buhse T, Lavabre D, Micheau JC, Thiemann W (1993) *Chirality* 5:341
21. Rivera Islas J, Pimienta V, Micheau JC, Buhse T (2003) *Biophys Chem* 103:191
22. Rivera Islas J, Pimienta V, Micheau JC, Buhse T (2003) *Biophys Chem* 103:201
23. Rivera Islas J, Micheau JC, Buhse T (2004) *Origins Life Evol Biosphere* 34:497
24. Soai K, Hori H, Niwa S (1989) *Heterocycles* 29:2065
25. Soai K, Hori H, Niwa S (1990) *J Chem Soc Chem Commun*, p 982
26. Shibata T, Choji K, Morioka H, Hayase T, Soai K (1996) *Chem Commun*, p 751
27. Shibata T, Choji K, Hayase T, Aizu Y, Soai K (1996) *Chem Commun*, p 1235
28. Shigehisa T, Kodaka Y, Ohno A, Takanori S, Sato I, Soai K (2000) *Tetrahedron: Asymmetry* 11:4249
29. Soai K, Hayase T, Takai K (1995) *Tetrahedron: Asymmetry* 6:637
30. Shibata T, Hayase T, Yamamoto J, Soai K (1997) *Tetrahedron: Asymmetry* 8:1717
31. Sato I, Urabe H, Ishiguro S, Shibata T, Soai K (2003) *Angew Chem Int Ed* 42:315
32. Micskei K, Póta G, Caglioti L, Pályi G (2006) *J Phys Chem A* 110:5982
33. Gridnev ID, Serafimov JM, Brown JM (2004) *Angew Chem Int Ed* 43:4884
34. Singleton DA, Vo LK (2002) *J Am Chem Soc* 124:10010
35. Soai K, Sato I, Shibata T, Komiya S, Hayashi M, Matsueda Y, Imamura H, Hayase T, Morioka H, Tabira H, Yamamoto J, Kowata Y (2003) *Tetrahedron: Asymmetry* 14:185
36. Singleton DA, Vo LK (2003) *Org Lett* 5:4337
37. Kondepudi DK, Asakura K (2001) *Acc Chem Res* 34:946
38. Nagypál I, Epstein IR (1988) *J Chem Phys* 89:6925
39. Epstein IR (1995) *Nature* 374:321
40. Kawasaki T, Suzuki K, Shimizu M, Ishikawa K, Soai K (2006) *Chirality* 18:479
41. Gridnev ID, Serfimov JM, Quiney H, Brown JM (2003) *Org Biomol Chem* 1:3811
42. Shibata T, Yamamoto J, Matsumoto N, Yonekubo S, Osanai S, Soai K (1998) *J Am Chem Soc* 120:12157
43. Sato I, Omiya D, Saito T, Soai K (2000) *J Am Chem Soc* 122:11739
44. Sato I, Yamashima R, Kadowki K, Yamamoto J, Shibata T, Soai K (2000) *Angew Chem Int Ed* 40:1096
45. Tanji S, Ohno A, Sato I, Soai K (2001) *Org Lett* 3:287
46. Sato I, Ohno A, Aoyama Y, Kasahara T, Soai K (2003) *Org Biomol Chem* 1:244
47. Sato I, Matsueda Y, Kadowaki K, Yonekubo S, Shibata T, Soai K (2002) *Helv Chim Acta* 85:3383
48. Sato I, Sugie R, Matsueda Y, Furumura Y, Soai K (2004) *Angew Chem Int Ed* 43:4490
49. Kawasaki T, Shimizu M, Suzuki K, Sato I, Soai K (2004) *Tetrahedron: Asymmetry* 15:3699
50. Kawasaki T, Sato M, Ishiguro S, Saito T, Morishita Y, Sato I, Nishino H, Inoue Y, Soai K (2005) *J Am Chem Soc* 127:3274
51. Kawasaki T, Tanaka H, Tsutsumi T, Kasahara T, Sato I, Soai K (2006) *J Am Chem Soc* 128:6032
52. Lutz F, Kawasaki T, Soai K (2006) *Tetrahedron: Asymmetry* 17:486
53. Kawasaki T, Suzuki K, Licandro E, Bossi A, Maiorana S, Soai K (2006) *Tetrahedron: Asymmetry* 17:2050



54. Kawasaki T, Omine T, Sato M, Morishita Y, Soai K (2007) *Chem Lett* 36:30
55. Soai K, Osanai S, Kadawaki K, Yonekubo S, Shibata T, Sato I (1999) *J Am Chem Soc* 121:11235
56. Sato I, Kadowaki K, Soai K (2000) *Angew Chem Int Ed* 39:1510
57. Sato I, Kadowaki K, Ohgo Y, Soai K (2004) *J Mol Cat A* 216:209
58. Sato I, Kadowaki K, Ohgo Y, Soai K, Ogino H (2001) *Chem Commun*, p 1022
59. Sato I, Kadowaki K, Urabe H, Jung JH, Ono Y, Shinkai S, Soai K (2003) *Tetrahedron Lett* 44:721
60. Sato I, Shimizu M, Kawasaki T, Soai K (2004) *Bull Chem Soc Jpn* 77:1587
61. Kawasaki T, Ishikawa K, Sekibata H, Sato I, Soai K (2004) *Tetrahedron Lett* 45:7939
62. Kawasaki T, Jo K, Igarashi H, Sato I, Nagano M, Koshima H, Soai K (2005) *Angew Chem Int Ed* 44:2774
63. Kawasaki T, Suzuki K, Hatase K, Otsuka M, Koshima H, Soai K (2006) *Chem Commun*, p 1869
64. Lutz F, Sato I, Soai K (2004) *Org Lett* 6:1613
65. Lutz F, Igarashi T, Kawasaki T, Soai K (2005) *J Am Chem Soc* 127:12206
66. Blackmond DG (2002) *Adv Synth Catal* 344:156
67. Lente G (2004) *J Phys Chem A* 108:9475
68. Lente G (2005) *J Phys Chem A* 109:11058
69. Rivera Islas J, Lavabre D, Grevy JM, Hernández Lamonedá R, Rojas Cabrera H, Micheau JC, Buhse T (2005) *Proc Natl Acad Sci USA* 102:13743
70. Mislow K (2003) *Collect Czech Chem Commun*, p 68:849
71. Mills W (1932) *Chem Ind (London)* 51:750
72. Puchot C, Samuel O, Duñach E, Zhao S, Agami C, Kagan HB (1986) *J Am Chem Soc* 108:2353
73. Guillaneux D, Zhao SH, Samuel O, Rainford D, Kagan HB (1994) *J Am Chem Soc* 116:9430
74. Girard C, Kagan HB (1998) *Angew Chem Int Ed* 37:2922
75. Kondepudi DK, Kaufman RJ, Singh N (1990) *Science* 250:975
76. Gridnev ID (2006) *Chem Lett* 35:148
77. Blackmond DG, McMillan CR, Ramdeehul S, Schorm A, Brown JM (2001) *J Am Chem Soc* 123:10103
78. Sato I, Omiya D, Igarashi H, Kato K, Ogi Y, Tsukiyama K, Soai K (2003) *Tetrahedron: Asymmetry* 14:975
79. Gray P, Scott SK (1994) *Chemical oscillations and instabilities. Non-linear chemical kinetics*. Clarendon, Oxford
80. Epstein IR, Pojman JA (1998) *An introduction to nonlinear chemical dynamics. Oscillations, waves, patterns, and chaos*. Oxford University Press, New York
81. Buhse T (2003) *Tetrahedron: Asymmetry* 14:1055
82. Lavabre D, Micheau JC, Rivera Islas J, Buhse T (2007) *J Phys Chem A* 111:281
83. Gridnev ID, Brown JM (2004) *Proc Natl Acad Sci USA* 101:5727
84. Bonner WA (1991) *Origins Life Evol Biosphere* 21:59
85. Keszthely L (1995) *Q Rev Biophys* 28:473
86. Siegel JS (1998) *Chirality* 10:24
87. Avalos M, Babiano R, Cintas P, Jiménez JL, Palacio PC (2000) *Tetrahedron: Asymmetry* 11:2845
88. Sandars PGH (2005) *Int J Astrobiol* 4:49
89. Lente G (2006) *J Phys Chem A* 110:12711
90. Kawasaki T, Hatase K, Fujii Y, Jo K, Soai K, Pizzarello S (2006) *Geochim Cosmochim Acta* 70:5395

# Rate Equation Approaches to Amplification of Enantiomeric Excess and Chiral Symmetry Breaking

Yukio Saito (✉) · Hiroyuki Hyuga

Department of Physics, Keio University, 3-14-1 Hiyoshi, Kohokuku, 223-8522 Yokohama, Japan  
*yukio@rk.phys.keio.ac.jp*

<b>1</b>	<b>Introduction</b>	98
<b>2</b>	<b>Amplification in Monomeric Systems</b>	100
2.1	Reaction Schemes	101
2.2	Rate Equations and an Order Parameter	102
2.3	Flow Trajectory in a $r-s$ Phase Space	103
2.3.1	Spontaneous Production	104
2.3.2	Linear Autocatalysis	104
2.3.3	Quadratic Autocatalysis	106
<b>3</b>	<b>Amplification with Homodimer Catalyst</b>	107
<b>4</b>	<b>Amplification with Antagonistic Heterodimers</b>	109
<b>5</b>	<b>Recycling and Flow: Chiral Symmetry Breaking</b>	110
<b>6</b>	<b>Summary and Discussions</b>	115
	<b>References</b>	117

**Abstract** Theoretical models and rate equations relevant to the Soai reaction are reviewed. It is found that in production of chiral molecules from an achiral substrate autocatalytic processes can induce either enantiomeric excess (ee) amplification or chiral symmetry breaking. The former means that the final ee value is larger than the initial value but is dependent upon it, whereas the latter means the selection of a unique value of the final ee, independent of the initial value. The ee amplification takes place in an irreversible reaction such that all the substrate molecules are converted to chiral products and the reaction comes to a halt. Chiral symmetry breaking is possible when recycling processes are incorporated. Reactions become reversible and the system relaxes slowly to a unique final state. The difference between the two behaviors is apparent in the flow diagram in the phase space of chiral molecule concentrations. The ee amplification takes place when the flow terminates on a line of fixed points (or a fixed line), whereas symmetry breaking corresponds to the dissolution of the fixed line accompanied by the appearance of fixed points. The relevance of the Soai reaction to the homochirality in life is also discussed.

**Keywords** Flow trajectory · Homochirality · Nonlinear autocatalysis · Recycling · Soai reaction

**Abbreviations**

ee Enantiomeric excess

**1****Introduction**

In the Human Genome Project (from the year 1990 to 2003) sequences of chemical base pairs that make up human DNA were intensively analyzed and determined, as they carry important genetic information. DNA is a polymer made up of a large number of deoxyribonucleotides, each of which is composed of a nitrogenous base, a sugar, and one or more phosphate groups [1]. Similar ribonucleotides polymerize to form RNA, which is also an important substance for producing a template for protein synthesis. RNA sometimes carries genetic information but rarely shows enzymatic functions [1].

One big issue of the post-Genome Project era is proteomics since proteins play crucial roles in virtually all biological processes such as enzymatic catalysis, coordinated motion, mechanical support, etc. [1]. A protein is a long polymer of amino acids, and folds into a regular structure for its biological function.

Sugars and amino acids in these biological polymers contain carbon atoms, each of which is connected to four different groups, and consequently are able to take two kinds of stereostructures. The two stereoisomers are mirror images or enantiomers of each other, and are called the D- and L-isomers. The two isomers should have the same physical properties except for their optical response to polarized light. Therefore, a simple symmetry argument leads to the conclusion that there are equal amounts of D- and L-amino acids or sugars in life. But the standard biochemical textbook [1] tells us that “only L-amino acids are constituents of proteins” [1] (p 17) and that “nearly all naturally occurring sugars belong to the D-series” [1] (p 346). There is no explanation why chiral symmetry is broken in life and how the homochirality has been brought about on earth.

It was Pasteur, in the middle of the 19th century, who first recognized the breaking of chiral symmetry in life. By crystallizing optically inactive sodium ammonium racemates, he separated two enantiomers of sodium ammonium tartrates, with opposite optical activities, by means of their asymmetric crystalline shapes [2]. Since the activity was observed even in solution, it was concluded that optical activity is due to the molecular asymmetry or chirality, not due to the crystalline symmetry. Because two enantiomers with different chiralities are identical in every chemical and physical property except for optical activity, in 1860 Pasteur stated that “artificial products have no molecular asymmetry” and continued that “the molecular asymmetry of natural organic products” establishes “the only well-marked line of demarcation that can at present be drawn between the chemistry of dead matter and the chemistry

of living matter” [3]. Also, by using the fact that asymmetric chemical agents react differently with two types of enantiomers, he separated enantiomers by fermentation. Therefore, once one has an asymmetric substance, further separation of two enantiomers or even production of a single type of enantiomer may follow [4]. But how was the first asymmetric organic compound chosen in a prebiotic world?

Since Pasteur’s discovery this problem of the origin of homochirality in life has attracted the attention of many scientists in relation to the origin of life itself [3, 5–7]. Japp expected a “directive force” when “life first arose” [3], and various “directive forces” have been proposed later, such as different intensities of circularly polarized light in a primordial era, adsorption on optically active crystals, or parity breaking in the weak interaction. However, the expected degree of chiral asymmetry or the value of the enantiomeric excess (ee) turns out to be very small [6], and one needs a mechanism to amplify ee enormously to a level of homochirality.

Another scenario for the origin of homochirality was suggested by Pearson [8, 9] such that chance breaks the chiral symmetry. Though the mean number of right- and left-handed enantiomers are the same, there is a nonzero probability of deviation from the equal populations of both enantiomers. The probability of establishing homochirality in a macroscopic system is, of course, very small [10], but “chance produces a slight majority of one type of” enantiomer and “asymmetric compounds when they have once arisen” act as “breeders, with a power of selecting their own kind of asymmetry form” [8, 9]. In this scenario, produced enantiomer acts as a chiral catalyst for the production of its own kind and hence this process should be autocatalytic.

Nearly a century later, a long-sought autocatalytic system with spontaneous amplification of chiral asymmetry was found by Soai and his coworkers [11]: In a closed reactor with achiral substrates, addition of a small amount of chiral products with a slight enantiomeric imbalance yielded final products with an overwhelmingly amplified ee [11]. The autocatalytic system also showed significant ee amplification under a variety of organic and inorganic chiral initiators with a small enantiomeric imbalance [12]. When many reaction runs were performed without chiral additives, about half of the runs ended up with the majority of one enantiomer, and the other half with the opposite enantiomer. The probability distribution of the ee is bimodal with double peaks, showing amplification of ee and further indicating the occurrence of chiral symmetry breaking [13–15].

As for theoretical research on the chiral symmetry breaking, Frank was the first to show that a linear autocatalysis with an antagonistic nonlinear chemical reaction can lead to homochirality [16]. His formulation with rate equations corresponds to the mean-field analysis of the phase transition in a nonequilibrium situation [17], and other variants have been proposed [6, 18–23]. All these analyses have been carried out only for open systems where

**Table 1** The ee amplification and the chiral symmetry breaking in an open and a closed system

		Initial condition	
		Dependent	Independent
System	Open		Chiral symmetry breaking
	Closed	ee amplification	Chiral symmetry breaking

the concentration of an achiral substrate is kept constant. Asymptotically the system approaches a unique steady state [6, 18–21] or even an oscillatory state [22, 23], independent of the initial condition. When the final state is chirally asymmetric, one may call this a chiral symmetry breaking in the sense of statistical mechanics, and it is indicated in the upper right corner in Table 1. On the other hand, the Soai reaction is performed in a closed system and an achiral substrate is converted to chiral products irreversibly: The substrate concentration decreases with time, and eventually the reaction comes to a halt. After the reaction, the ee value increases but its final value is found to depend on the initial state. Even though the ee is amplified, the history-dependent behavior is different from what we expect from phase transitions in statistical mechanics, so that we write “ee amplification” in the lower left corner in Table 1. We have analyzed theoretically the chiral symmetry breaking in a closed system in general, and found that with an irreversible nonlinear autocatalysis the system may show an ee amplification as in the Soai reaction. Furthermore, with an additional recycling back reaction, a unique final state with a finite ee value is found possible, which we call a chiral symmetry breaking, as shown in the lower right corner in Table 1 [24–29]. There are also many theoretical works on the Soai reaction in a closed system [30–36]. Here we give a brief survey of various theoretical models of the ee amplification and the chiral symmetry breaking in a closed system, though it is by no means exhaustive.

## 2

### Amplification in Monomeric Systems

Two stereostructural isomers are called D- and L-enantiomers for sugars and amino acids, but, for general organic compounds, R and S representation is common. We adopt the R and S representation hereafter.

We consider a production of chiral enantiomers R and S from an achiral substrate A in a closed system. Actually, in the Soai reaction, chiral molecules are produced by the reaction of two achiral reactants A and B as  $A + B \rightarrow R$  or  $A + B \rightarrow S$ . But in a closed system a substrate of smaller amount controls

the reaction, since it is first consumed and thus prevents the reaction from proceeding further. Therefore, in order to grasp the main features of chirality selection, it is sufficient to assume that an achiral substrate  $A$  of a smaller amount converts to  $R$  or  $S$ . The process may further involve formation of intermediate complexes, oligomers etc., but for the purpose of discussing the relationships and differences between amplification and symmetry breaking in chirality, we restrict our consideration in this section to the simplest case where only monomers are involved.

## 2.1

### Reaction Schemes

The spontaneous production of chiral molecules  $R$  or  $S$  from an achiral substrate  $A$  is described by reactions:



We assume the same reaction rate  $k_0$  for the nonautocatalytic spontaneous production of  $R$  and  $S$  enantiomers. Since both of them are identical in every chemical and physical aspects, no advantage factor [6] is assumed.

Since the spontaneous production (Eq. 1) yields only a racemic mixture of two enantiomers, one has to assume some autocatalytic processes. The simplest is a linear autocatalysis with a reaction coefficient  $k_1$ :



There may be a linear cross-catalytic reaction or erroneous linear catalysis with a coefficient  $k'_1$ :

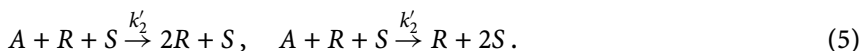


As will be discussed later, these linear autocatalyses alone are insufficient not only to break the chiral symmetry but also to amplify ee.

Beyond the linear autocatalyses, nonlinear effects such as a quadratic autocatalysis have been considered [6, 24, 31]:



and a cross-catalysis:



These higher order autocatalytic processes may actually be brought about by the dimer catalysts [19], but we confine ourselves to the simplest description (Eqs. 4 and 5) in terms of only monomers  $R$  and  $S$  in this section. Consideration of dimers is postponed in the following sections. The reaction Eq. 4 alone can give rise to the amplification of chirality as will be discussed. One

notes that all these processes (Eqs. 1 to 5) unidirectionally produce chiral enantiomers and thus the reaction comes to a halt when the whole achiral substrate is consumed; the total process is irreversible.

## 2.2

### Rate Equations and an Order Parameter

Concentrations  $r$  and  $s$  of two enantiomers  $R$  and  $S$  vary according to the reaction processes described in the previous subsection. In an open system, the achiral substrate  $A$  is steadily supplied in such a way that its concentration  $a$  is kept constant. In contrast, in a closed system, achiral substrates are transformed to chiral products and only the total concentration  $c = a + r + s$  of reactive chemical species is kept constant. By denoting the total concentration of monomeric chiral products with a subscript 1 as:

$$q_1 = r + s \quad (6)$$

the concentration of the substrate  $a$  is determined as:

$$a = c - q_1, \quad (7)$$

which should be nonnegative. Then, the development of reactions in a closed system can be depicted as a flow in the triangular region in the  $r - s$  phase space:

$$0 \leq r, s, r + s \leq c. \quad (8)$$

The reaction schemes Eqs. 1 to 5 induce rate equations for  $r$  and  $s$ :

$$\begin{aligned} \frac{dr}{dt} &= [f(r) + k'_1 s + k'_2 rs] a \\ \frac{ds}{dt} &= [f(s) + k'_1 r + k'_2 rs] a \end{aligned} \quad (9)$$

with an effective rate coefficient:

$$f(r) = k_0 + k_1 r + k_2 r^2. \quad (10)$$

Since the right-hand side of Eq. 9 for velocities  $\dot{r} = dr/dt$  and  $\dot{s} = ds/dt$  are always nonnegative and in proportion to the concentration of the achiral substrate  $a$ , both  $r$  and  $s$  never decrease and stop growing after  $a$  vanishes ( $a = 0$ ).

The asymptotic behavior of a two-dimensional autonomous dynamical system is, in general, known to have fixed points or lines where  $\dot{r} = \dot{s} = 0$ , or to have limit cycles where  $\dot{r}, \dot{s} \neq 0$ . Since the system is irreversible as the concentrations of chiral products always increase at the cost of the substrate  $A$ :

$$\frac{da}{dt} = -[f(r) + f(s) + k'_1(r + s) + 2k'_2 rs] a \leq 0 \quad (11)$$

and no epimerization process  $R \leftrightarrow S$  is assumed, limit cycle is impossible: Production stops when all the substrate molecules are transformed to chiral ones;  $a(t = \infty) = 0$ . Since  $\dot{r} = \dot{s} = 0$  for  $a = 0 = c - r - s$ , the diagonal line  $r + s = c$  is a fixed line for this irreversible system. Any points on the fixed line are marginally stable because they have no guaranteed stability along the fixed line.

Our interest is the dynamical behavior of ee or the chiral symmetry breaking and, in particular, as to whether ee increases asymptotically. In order to quantify the monomeric ee or the degree of chiral symmetry breaking, we define a monomeric order parameter  $\phi_1$  as:

$$\phi_1 = \frac{r - s}{r + s} = \frac{r - s}{q_1}, \quad (12)$$

which is zero for a symmetric or racemic state ( $r = s$ ), and is nonzero for a symmetry-broken or chiral state. The evolution equation of  $\phi_1$  is immediately derived from Eq. 9:

$$\frac{d\phi_1}{dt} = A\phi_1 - B\phi_1^3 \quad (13)$$

with coefficients:

$$A(t) = -2 \frac{k_0 + k'_1 q_1}{q_1} a + B(t), \quad B(t) = \frac{1}{2} (k_2 - k'_2) q_1 a. \quad (14)$$

However, as  $a(t = \infty) = 0$ , both the coefficients  $A$  and  $B$  vanish asymptotically, and one cannot determine a unique final value of ee from the evolution Eq. 13. On a fixed line  $r + s = c$  the ee value varies from  $\phi_1 = -1$  at a point  $(r, s) = (0, c)$  to  $\phi_1 = 1$  at  $(c, 0)$ , and the final values of  $\phi_1$  can be anything between  $+1$  and  $-1$ . In order to obtain the final value of ee, one has to solve the evolution Eq. 9 and especially to determine the trajectory of the dynamical flow in  $r - s$  phase space. The final value of  $\phi_1$ , in fact, turns out to depend on the initial condition.

## 2.3

### Flow Trajectory in a $r - s$ Phase Space

As the first step in analyzing flow trajectories in a phase space, we consider the simplest case when reactions such as spontaneous production (Eq. 1), linearly autocatalytic (Eq. 2), or quadratically autocatalytic (Eq. 4) reactions are active. Then the rate equations are simplified as:

$$\frac{dr}{dt} = f(r)a, \quad \frac{ds}{dt} = f(s)a \quad (15)$$



with the rate coefficient  $f$  defined in Eq. 10. Flow trajectories are obtained by integrating a trajectory equation:

$$\frac{ds}{dr} = \frac{f(s)}{f(r)} . \quad (16)$$

In the following, an initial condition is set as  $r = r_0$ ,  $s = s_0$ ,  $a_0 = c - r_0 - s_0$  (or  $q_1 = q_{1,0} = r_0 + s_0$ ,  $\phi_1 = \phi_{1,0} = (r_0 - s_0)/q_{1,0}$ ,  $a_0 = c - q_{1,0}$ ), and we discuss how the final ee value  $\phi_{1,\infty}$  depends on the initial value  $\phi_{1,0}$  for a few typical cases.

### 2.3.1

#### Spontaneous Production

When chiral molecules are produced only spontaneously and the system has no autocatalytic processes ( $k_0 > 0$ ,  $k_1 = k_2 = 0$ ), the trajectory in the  $r-s$  phase space is obtained:

$$r - s = r_0 - s_0 = \text{const} . \quad (17)$$

The flow diagram is a straight line with a unit slope, terminating at the fixed line  $r + s = c$ , as shown in Fig. 1a. Half of the substrate  $a_0$  initially present converts to  $R$  and the remaining half to  $S$ , and the ee decreases to the value  $\phi_{1,\infty} = (q_{1,0}/c)\phi_{1,0}$ . The smaller the ratio  $q_{1,0}/c$  of the initial amount of chiral species to the total amount of active reactants, the more ee decreases, as shown in Fig. 2a.

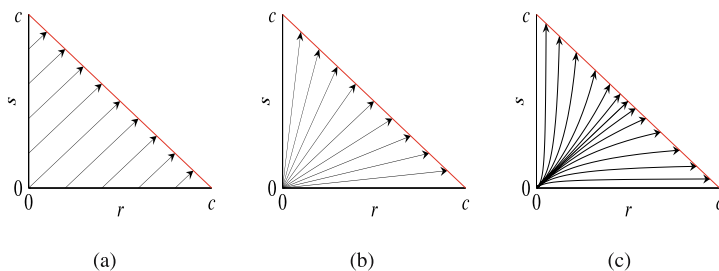


**Fig. 1** Flow diagrams for **a** spontaneous production ( $k_0 > 0$ ,  $k_1 = k_2 = 0$ ), **b** linearly autocatalytic ( $k_1 > 0$ ,  $k_0 = k_2 = 0$ ), and **c** quadratically autocatalytic ( $k_2 > 0$ ,  $k_0 = k_1 = 0$ ) reactions

### 2.3.2

#### Linear Autocatalysis

When only the linearly autocatalytic production of chiral molecules is active ( $k_1 > 0$ ,  $k_0 = k_2 = 0$ ), the trajectory is obtained:

$$\frac{s}{r} = \frac{s_0}{r_0} = \text{const} . \quad (18)$$

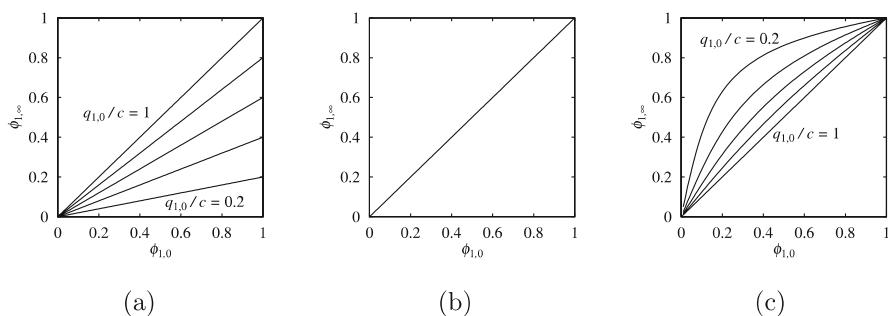


**Fig. 2** Final ee  $\phi_{1,\infty}$  versus initial ee  $\phi_{1,0}$  for **a** spontaneous production ( $k_0 > 0$ ,  $k_1 = k_2 = 0$ ), **b** linearly autocatalytic ( $k_1 > 0$ ,  $k_0 = k_2 = 0$ ), and **c** quadratically autocatalytic ( $k_2 > 0$ ,  $k_0 = k_1 = 0$ ) reactions. Each curve corresponds to a fixed ratio of the initial amount of chiral species to the total amount of active reactants  $q_{1,0}/c$ . As the ratio decreases, the initial slope of the curve decreases in **a**, does not change in **b**, and increases in **c**

and the flow diagram is a straight line radiating from the origin and terminating at the fixed line  $r + s = c$ , as shown in Fig. 1b. The ee value remains constant:

$$\phi_{1,\infty} = \phi_{1,0} = \text{const.} \quad (19)$$

and is independent of the initial ratio  $q_{1,0}/c$ , as shown in Fig. 2b.

If the erroneous linear catalysis (Eq. 3) is at work in addition to the linear autocatalysis (Eq. 2), rate equations are modified:

$$\frac{dr}{dt} = (k_1 r + k'_1 s) a, \quad \frac{ds}{dt} = (k_1 s + k'_1 r) a. \quad (20)$$

These equations can be combined to yield:

$$\frac{d\phi_1}{dq_1} = - (1 - f) \frac{\phi_1}{q_1} \quad (21)$$

with a fidelity factor  $f$  defined by:

$$f = \frac{k_1 - k'_1}{k_1 + k'_1}, \quad (22)$$

which is unity without the error  $k'_1 = 0$  and vanishes when  $k_1 = k'_1$ . The ee value  $\phi_1$  is easily integrated:

$$\phi_{1,\infty} = \phi_{1,0} \left( \frac{q_{1,0}}{c} \right)^{1-f} \leq \phi_{1,0}. \quad (23)$$

This result shows that the final value is less than the initial  $\phi_{1,0}$  whenever there is a finite error process  $f < 1$ . In particular, if  $f = 0$ , the final ee behaves the same as that of the spontaneous production.

### 2.3.3

#### Quadratic Autocatalysis

With only a quadratic autocatalysis ( $k_2 > 0$ ,  $k_0 = k_1 = 0$ ), the trajectory is obtained as:

$$\frac{1}{r} - \frac{1}{s} = \frac{1}{r_0} - \frac{1}{s_0} = \text{const} \quad (24)$$

and the flow diagram is hyperbolae radiating out from the origin and terminating at the fixed line  $r + s = c$ , as shown in Fig. 1c. Below the diagonal  $r = s$  line, the flow bends downward and the ratio  $s/r$  decreases as time passes, and consequently the ee value  $\phi_1$  increases. In other words, by using the relation  $r = q_1(1 + \phi_1)/2$  and  $s = q_1(1 - \phi_1)/2$ , the ee value is easily found from Eq. 24 to satisfy the relation:

$$\frac{\phi_1}{1 - \phi_1^2} = Aq_1 \quad (25)$$

with a constant  $A$  determined by an initial condition. For a given value of  $q_1$ , the ee value  $\phi_1$  is determined graphically as a cross point of two curves representing both sides of Eq. 25, as shown in Fig. 3. Then, it is evident that  $\phi_1$  increases as  $q_1$  increases. The asymptotic value corresponding to  $q_1 = c$  is obtained:

$$\phi_{1,\infty} = \frac{1}{2cA} \left[ \sqrt{1 + (2cA)^2} - 1 \right]. \quad (26)$$

The relation between the initial value  $\phi_{1,0}$  of the ee and its final value  $\phi_{1,\infty}$  is depicted in Fig. 2c for fixed values of the initial amount  $q_{1,0}$  of chiral species relative to the total amount  $c$ . The smaller the initial ratio  $q_{1,0}/c$ , the more prominent the ee amplification.

The ee amplification curves possess a remarkable property in that they depend on the initial ratio  $q_{1,0}/c$  but are independent of the rate coefficient  $k_2$ .

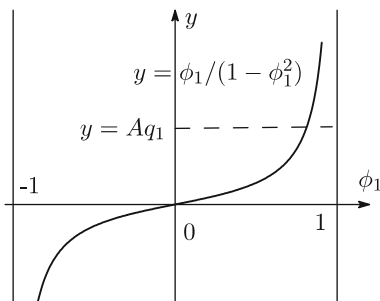


**Fig. 3** The ee value  $\phi_1$  is obtained at a cross point of two curves,  $y = \phi_1/(1 - \phi_1^2)$  and  $y = Aq_1$

The latter determines the time evolution of  $\phi_1$  but not its final value. If there are other processes involved, for instance the spontaneous production  $k_0 \neq 0$ , then amplification curves should depend on the ratio  $k_0/k_2c^2$ .

If there is a racemizing cross-catalysis (Eq. 5) with  $k'_2$ , the trajectory equation is rewritten as:

$$\frac{d\phi_1}{dq_1} = \frac{\phi_1 (1 - \phi_1^2)}{f_X^{-1} + \phi_1^2} \frac{1}{q_1} \quad (27)$$

with a crossing effect factor defined by:

$$f_X = \frac{k_2 - k'_2}{k_2 + k'_2}, \quad (28)$$

which is unity without a cross-catalysis term ( $k'_2 = 0$ ) and vanishes when  $k_2 = k'_2$ . The solution of Eq. 27 is given by:

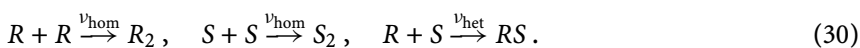
$$\frac{\phi_1}{(1 - \phi_1^2)^{(1+f_X)/2}} = Aq_1^{f_X}. \quad (29)$$

From this result one can see that the asymptotic value  $\phi_{1,\infty}$  decreases as  $f_X$  decreases. In particular, when  $f_X = 0$ ,  $\phi_1$  is independent of  $q_1$  and does not vary;  $\phi_{1,\infty} = \phi_{1,0}$ . Namely, chirality amplification by  $k_2$  is completely canceled out by the racemization effect caused by  $k'_2$ .

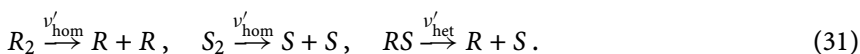
### 3

#### Amplification with Homodimer Catalyst

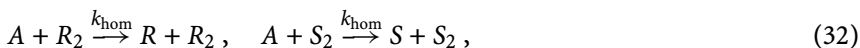
In order to understand the molecular mechanisms of how the quadratic auto-catalysis is brought about, the concept of dimer catalyst introduced by Kagan and coworkers, may be relevant [19, 30, 32, 33]. Assume that monomers  $R$  and  $S$  react to form homodimers  $R_2$  and  $S_2$  with a rate  $\nu_{\text{hom}}$  and a heterodimer  $RS$  with a rate  $\nu_{\text{het}}$ :



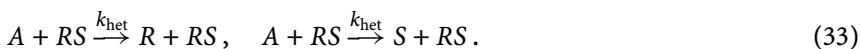
Corresponding decomposition processes are described as:



Homodimers thus formed are assumed to catalyze their own enantiomeric type:



whereas heterodimers have no preference in enantioselectivity:



Now, the state of the system is described not only by the concentrations of monomers  $r$  and  $s$ , but also by those of dimers denoted as  $[R_2]$ ,  $[S_2]$ , and  $[RS]$ . The rate equations are:

$$\begin{aligned} \frac{dr}{dt} &= k_0 a + k_{\text{hom}} a [R_2] - 2\nu_{\text{hom}} r^2 + 2\nu'_{\text{hom}} [R_2] \\ &\quad - \nu_{\text{het}} rs + \nu'_{\text{het}} [RS] + k_{\text{het}} a [RS], \\ \frac{d[R_2]}{dt} &= \nu_{\text{hom}} r^2 - \nu'_{\text{hom}} [R_2], \quad \frac{d[RS]}{dt} = \nu_{\text{het}} rs - \nu'_{\text{het}} [RS] \end{aligned} \quad (34)$$

and the corresponding ones for the  $S$  enantiomer. The ee or the chiral order parameter is now defined by:

$$\phi = \frac{r + 2[R_2] - s - 2[S_2]}{q}, \quad (35)$$

where  $q$  is the total concentration of chiral molecules, given as:

$$q = r + s + 2[R_2] + 2[RS] + 2[S_2]. \quad (36)$$

If the dimerization and decomposition proceed very fast, the dimer concentrations take quasi-equilibrium values that satisfy  $[\dot{R}_2] = [\dot{RS}] = [\dot{S}_2] = 0$  and are determined by the instantaneous monomer concentrations  $r$  and  $s$ :

$$[R_2] = \frac{\nu_{\text{hom}}}{\nu'_{\text{hom}}} r^2, \quad [RS] = \frac{\nu_{\text{het}}}{\nu'_{\text{het}}} rs, \quad [S_2] = \frac{\nu_{\text{hom}}}{\nu'_{\text{hom}}} s^2. \quad (37)$$

Then, the equations for monomers in Eq. 34 reduce to Eq. 9 with the coefficients  $k_2$  and  $k'_2$  given as:

$$k_2 = k_{\text{hom}} \frac{\nu_{\text{hom}}}{\nu'_{\text{hom}}}, \quad k'_2 = k_{\text{het}} \frac{\nu_{\text{het}}}{\nu'_{\text{het}}} \quad (38)$$

and with  $k_1 = k'_1 = 0$ . As the reaction proceeds, the whole achiral substrate is ultimately transformed to chiral products so that  $a = c - q_\infty = 0$ . This represents a quadratic curve of fixed points in  $r - s$  phase space. When there is solely a homodimer catalytic effect  $k_2 > 0$  without spontaneous production nor heterodimer racemization  $k_0 = k'_2 = 0$ , the initial state with  $(r_0, s_0)$  follows the hyperbolic flow trajectory (Eq. 24) and ends up on the curve of fixed points,  $q = c$ , as shown in Fig. 4a.

The ratio  $r/s$  increases along the flow trajectory if it is initially larger than unity. Thus the  $r - s$  asymmetry increases, and the final value of the ee  $|\phi_\infty|$  is larger than the initial value  $|\phi_0|$ . Figure 4b shows  $\phi_0 - \phi_\infty$  for cases of positive  $\phi$ . The enhancement is more evident when the initial ratio  $q_0/c$  is smaller. These essential features are the same with the monomeric system, discussed in Sect. 2.3.3.

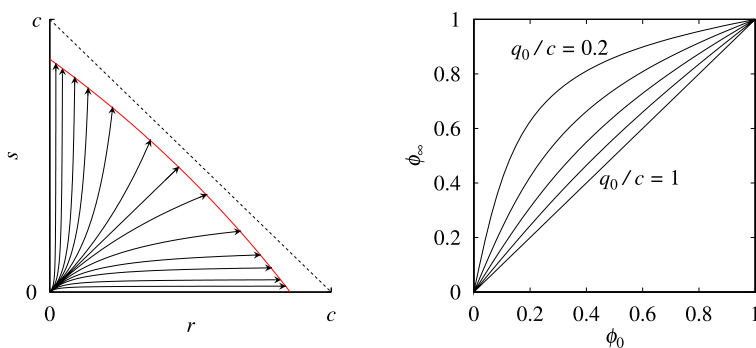


**Fig. 4** **a** Flow diagram for homodimer catalyst with  $v_{\text{hom}}c/v'_{\text{hom}} = 0.1$  and  $v_{\text{het}} = v'_{\text{het}} = 0$ . Flow terminates on a curve of fixed points  $q = c$ . **b** Final ee value  $\phi_\infty$  as a function of its initial value  $\phi_0$  for various amount of initial chiral species  $q_0$ . The less  $q_0$  is, the more amplified  $\phi_\infty$  is

#### 4

#### Amplification with Antagonistic Heterodimers

Another model for the chiral asymmetry amplification is a variant of the Frank model in a closed system [34]. In its simplest form, the model consists of reaction schemes of spontaneous production (Eq. 1), linear autocatalysis (Eq. 2), and heterodimer formation (Eq. 31). Then, the rate equations for monomers are the same as those of the original Frank model [16], but they are supplemented with the heterodimer formation:

$$\frac{dr}{dt} = k_0a + k_1ar - v_{\text{het}}rs, \quad \frac{ds}{dt} = k_0a + k_1as - v_{\text{het}}rs, \quad \frac{d[\text{RS}]}{dt} = v_{\text{het}}rs. \quad (39)$$

Since every achiral substrate is eventually consumed  $a(t = \infty) = 0$  and all the reactions stop asymptotically, Eq. 39 tells us that the product  $rs$  should vanish. If there is more  $R$  than  $S$  initially,  $S$  monomer disappears ultimately, for instance. But  $S$  molecules do not disappear nor decompose back into achiral substrate. They are only incorporated into the heterodimer  $RS$ . The system is not determined solely by monomer concentrations  $r$  and  $s$ , (or  $\phi_1$  and  $q_1$ ) but also depends on heterodimer concentration  $[\text{RS}]$ . The flow takes place in a three-dimensional phase space of  $r, s, [\text{RS}]$ , as shown in Fig. 5a.

The asymptotics discussed above force both the concentrations of the substrate  $a = c - r - s - 2[\text{RS}]$  and the product  $rs$  to vanish ultimately. These two conditions define a line of fixed points in the three-dimensional  $r - s - [\text{RS}]$  phase space. If the initial state has a prejudice to  $R$  enantiomer such as  $r_0 > s_0$ , then the system ends up on a fixed line  $r + 2[\text{RS}] = c$  on a  $s = 0$  plane, as shown in Fig. 5a. Otherwise with  $r_0 < s_0$ , the system flows to another fixed

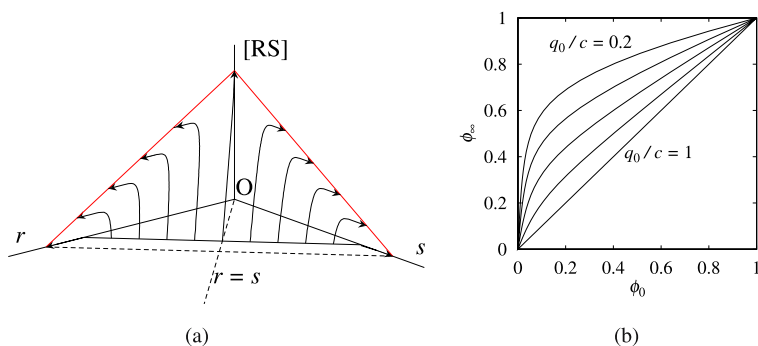


**Fig. 5** **a** 3D flow diagram for reactions with antagonistic heterodimers  $RS$ . Red lines represent fixed lines. Initial amount of achiral substrate is  $0.2c$ , and the remaining  $q_0 = 0.8c$  is shared by  $R$  and  $S$  monomers. There are no heterodimers initially. Rate coefficients are  $k_0 = 0$ ,  $k_1c = 1$ ,  $\nu_{\text{het}}c = 10$ . **b** Final ee  $\phi_\infty$  versus its initial value  $\phi_0$  for a given initial ratio  $q_0/c$ . As  $q_0/c$  decreases, the ee amplification increases

line  $s + 2[RS] = c$  on a  $r = 0$  plane. The plane  $r = s$  is a dividing surface that determines the final preference of chirality.

One can readily find that ee is amplified by the reaction involving antagonistic heterodimer, as shown in Fig. 5b. For a given amount of initial total concentration of chiral species  $q_0 = r_0 + s_0$ , the ee value  $\phi$  increases by the completion of a reaction. No heterodimer is assumed to exist initially,  $[RS]_0 = 0$ . The amplification is more significant for smaller amounts of  $q_0/c$  and  $\phi_0$ . We note that the rate constant of heterodimerization  $\nu_{\text{het}}$  has to be large in order to produce strong ee amplification. Minority enantiomer should be quickly incorporated into heterodimers before the achiral substrate is consumed. Otherwise, both enantiomers consume the achiral resource  $A$  and slowly form heterodimers afterwards, but without significant ee amplification. For a large  $\nu_{\text{het}}$ , minority enantiomers are incorporated into heterodimers in an early stage. Therefore, flow trajectories first point upwards in Fig. 5a, indicating the rapid increase of heterodimer concentration  $[RS]$ . The trajectory is in fact inclined such that the minority enantiomer decreases its monomeric concentration. When it almost disappears, then the trajectory makes a quick turn in the vicinity of the  $r = 0$  plane or  $s = 0$  plane, indicating the concentration growth of the surviving majority enantiomer.

## 5

### Recycling and Flow: Chiral Symmetry Breaking

So far, we have discussed several models for ee amplification. The irreversibility of the dynamical system is essential to make the final state dependent on the initial condition. In this section, we consider the effect induced by intro-

ducing reversibility into the system by including various types of recycling processes. For simplicity, we will consider a monomeric system.

In addition to the catalytic production processes (Eqs. 1 to 5), we include the recycling process such that enantiomeric products  $R$  or  $S$  undergo a back reaction to the substrate  $A$  [24] with a reaction rate  $\lambda$ :



Hereafter, we will call this reaction linear recycling. One can also assume a nonlinear type of recycling process [28] such that different chiral species by their encounter react back to achiral molecules:



This back reaction can be a combined effect of the following two processes:



The rate equations now read:

$$\begin{aligned} \frac{dr}{dt} &= [f(r) + k'_1 s + k'_2 rs] a - \mu rs - \lambda r, \\ \frac{ds}{dt} &= [f(s) + k'_1 r + k'_2 rs] a - \mu rs - \lambda s. \end{aligned} \quad (43)$$

The term with  $\mu$  has the same form as the contribution of Frank's mutual inhibition [16]. The corresponding time evolution of  $\phi_1$  is readily derived in the form of Eq. 13 with coefficients  $A$  and  $B$  determined by symmetric quantities  $q_1$  and  $a = c - q_1$ :

$$A(t) = -2 \frac{a}{q_1} (k_0 + k'_1 q_1) + B(t), \quad B(t) = \frac{1}{2} [(k_2 - k'_2) a + \mu] q_1. \quad (44)$$

The evolution Eq. 13 of the order parameter has a similar form to the time-dependent Landau equation [17], which is fundamental in nonequilibrium phase transitions. The asymptotic value of the order parameter  $\phi_{1,\infty}$  is determined as the zero of the velocity  $\dot{\phi}_1$ . The main difference from the standard model of phase transitions lies in the time dependence in the coefficients  $A(t)$  and  $B(t)$  induced by that of the achiral concentration  $a(t)$  and the total chiral concentration  $q_1(t)$ . Because the concentrations  $a$  and  $q_1$  are nonnegative,  $A(t)$  cannot exceed  $B(t)$ ;  $A(t) \leq B(t)$ .

In previous sections we have focused on the cases with  $\lambda = \mu = 0$ . In these cases, the asymptotic value of  $a$  vanishes,  $a(t = \infty) = 0$  so that  $A(t = \infty) = B(t = \infty) = 0$ , and the asymptotic value of the order parameter  $\phi_1$  cannot be determined from Eq. 13. Another example with  $A = B = 0$  happens for a special case with  $k_0 = k'_1 = \mu = 0$  and  $k_2 = k'_2$ . In this case, we can calculate trajectories and find a fixed line shifted from  $a = 0$  to the one with a finite value of  $a(t = \infty)$  [28]: Flow trajectories are along lines passing through the origin, similar to those shown in Fig. 1b, but terminating at a shifted fixed



line. Since  $a = 0$  is no longer a fixed line, trajectories not only point out from the origin, but also come out from the line  $a = 0$ .

In all the other cases, with either a linear or a nonlinear recycling process or with both, the coefficients  $A$  and  $B$  are no longer zero at the same time, and a definite value of the order parameter  $\phi_1$  is obtained asymptotically. The reason for the above is as follows: If the nonlinear recycling exists as  $\mu > 0$ ,  $B$  becomes nonzero since  $\mu q_{1,\infty} > 0$ . If the linear recycling exists as  $\lambda > 0$ , not all the achiral substrate transform to chiral products but a finite amount remains asymptotically as  $a(t = \infty) > 0$ . Therefore, nonzero values of  $k_0$ ,  $k'_1$  or  $k_2 \neq k'_2$  give contributions to the coefficients  $A$  or  $B$ .

For nonzero  $A$  and/or  $B$ , the velocity  $\dot{\phi}_1 = d\phi_1/dt$  has three typical behaviors as a function of the order parameter  $\phi_1$ , as shown in Fig. 6. In the region with a positive (negative) velocity  $\dot{\phi}_1$ ,  $\phi_1$  increases (decreases) and moves to the right (left), as indicated by arrows on the  $\phi_1$  axis in Fig. 6. When  $A$  is negative, as in Fig. 6a or b,  $\phi_1$  eventually approaches the racemic value  $\phi_1 = 0$  within its range of definition  $|\phi_1| \leq 1$ : The racemic state is a stable fixed point for  $A < 0$ . Equation 44 tells us that this happens when the spontaneous production  $k_0$  or error in a linear autocatalytic process  $k'_1$  are sufficiently strong, or quadratic catalysis  $k_2$  is weaker than the cross-catalysis  $k'_2$ . The coefficient of the linear autocatalysis  $k_1$  as well as the linear recycling process  $\lambda$  are absent in the coefficients  $A$  and  $B$ , and cannot directly affect the chirality of the system. These linear processes with  $k_1$  and  $\lambda$  affect the chirality only implicitly through  $a$  and  $q_1$ .

When  $A$  is positive, as in the case of Fig. 6c, the coefficient of the cubic term  $B$  is also positive, and the velocity  $\dot{\phi}_1$  vanishes at three values of  $\phi_1$  in the range of  $-1 \leq \phi_1 \leq 1$ . This is possible if a strong quadratic autocatalysis  $k_2 > k'_2$  exists together with a linear recycling  $\lambda > 0$ , or if a linear autocatalysis  $k_1$  and a nonlinear recycling  $\mu > 0$  coexist. By following the direction indicated by the arrows for positive  $\phi_1$ , the order parameter ends up at a definite value:

$$\phi_{1,\infty} = \sqrt{\frac{A(t = \infty)}{B(t = \infty)}} \quad (45)$$

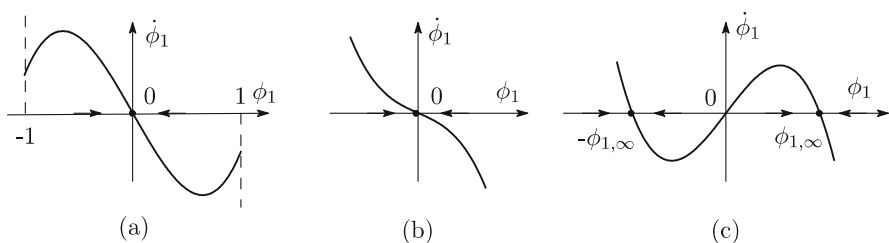


**Fig. 6**  $\phi_1$  versus the velocity  $\dot{\phi}_1 = A\phi_1 - B\phi_1^3$  for three typical cases: **a**  $A < B < 0$ , **b**  $A < 0 < B$ , and **c**  $0 < A < B$

and chiral symmetry breaking takes place. If the system starts with a negative  $\phi_1$ , it stops at  $-\phi_{1,\infty}$ . The final state of the system depends on the initial sign of  $\phi_{1,0}$ , but is independent of its magnitude  $|\phi_{1,0}|$ . We note that the asymptotic values of the coefficients  $A(t = \infty)$  and  $B(t = \infty)$  are independent of the initial condition and so is  $|\phi_{1,\infty}|$ . This situation is what we mean by “chiral symmetry breaking” in the sense of statistical mechanics.

We will first discuss chiral symmetry breaking when there is a nonlinear recycling,  $\mu > 0$  [16, 28]. The rate (Eq. 43) tells us that  $a = c - r - s = 0$  is no more a fixed line, but we have many fixed points. The simplest is the case with only a linear autocatalysis  $k_1 > 0$  but nothing else ( $k_0 = k'_1 = k_2 = k'_2 = \lambda = 0$ ). In this case we have four fixed points in the  $r - s$  phase space: two unstable ones,  $O$  and  $U$ , and two stable ones at  $(r, s) = (c, 0)$  or  $(0, c)$ , as shown in Fig. 7a. At the stable fixed points the final ee take values  $\phi_{1,\infty} = \pm 1$ . These values agree with those expected from Eq. 45 with  $A(t) = B(t) = \mu q_1/2$ , as determined from Eq. 44. The nonlinear recycling (Eq. 42) returns the same amount of enantiomers back to the achiral substrate, but the relative decrease in concentration is larger for the minority enantiomer than for the majority one. The damage is further amplified by a large reduction of the linear autocatalytic effect for the minority enantiomer, and it finally disappears.

As for the second example, we consider the case with a quadratic autocatalysis  $k_2 > 0$  and a linear recycling  $\lambda > 0$ . Because the linear recycling takes place whenever there is nonzero concentrations of enantiomers, a few achiral substrate always remain,  $a(t = \infty) \neq 0$ . Thus, the diagonal line  $q_1 = r + s = c$  is no longer a fixed line. Instead, there appear fixed points in general. In the present case with a finite  $\lambda > 0$ , a total of seven fixed points appear; three stable ( $O, S_{1,2}$ ) and four unstable ones ( $U_{1-4}$ ), as shown in Fig. 7b. As the reaction proceeds, the system approaches a state associated with one of the stable fixed points. The origin  $O$  is not interesting, since all the chiral products are recycled back to the achiral substrate. Also its influence extends only in a small

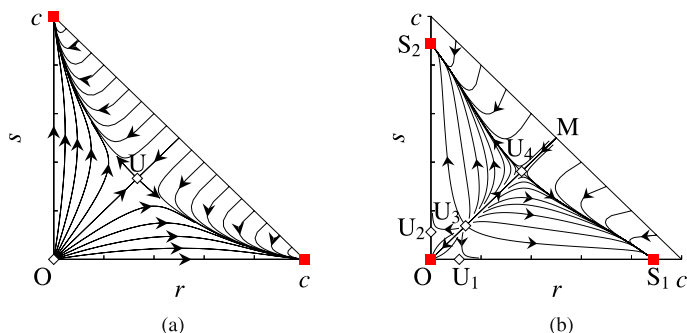


**Fig. 7** Flow diagrams with **a** linear autocatalysis and nonlinear recycling ( $k_1 = \mu > 0$ ,  $k_0 = k_2 = \lambda = 0$ ) similar to the Frank model, and **b** quadratic autocatalysis and linear recycling ( $k_2 c^2 = \lambda > 0$ ,  $k_0 = k_1 = \mu = 0$ ).  $O$  origin,  $S$  stable fixed points,  $U$  unstable fixed points

region around  $O$ , bounded by  $U_{1-3}$ , if the life time  $1/\lambda$  of chiral products is long enough. Close to this fixed point, the influence of the spontaneous production process with  $k_0$  should anyhow be taken into account.

When the initial system is sufficiently far from  $O$ , the system approaches  $S_1$  or  $S_2$ ; Both correspond to homochiral states with  $\phi_{1,\infty} = \pm 1$ . When the initial configuration is close to the racemic state or the diagonal line  $r = s$ , the system approaches a racemic fixed point  $U_4$  at first. But, while the recycling process returns the chiral enantiomers back to achiral substrate, the majority enantiomer increases its population at the cost of the minority one along the flow curve diverging from  $U_4$  to  $S_1$  or to  $S_2$ , and eventually the whole system becomes homochiral.

One may wonder whether recycling processes such as a linear or a non-linear back reaction exist in relevant autocatalytic systems. So far, we are not aware of their existence. It is, however, possible that the back reaction rates  $\lambda$  or  $\mu$  are nonzero but too exceedingly small to be detected in laboratory experiments. Concerning the problem of homochirality in life, very small  $\lambda$  or  $\mu$  are not unimaginable, considering the geological time scale for its establishment on earth.

On the other hand, a possibility for providing a system with a recycling process has been proposed theoretically [27]: One simply lets the reaction with ee amplification run in an open flow reactor. In an open system there is reactant flow between the system and the environment  $E$ . Let the solution with the achiral substrate  $A$  be supplied by an inflow with an influx  $F$ :



and the products  $R$  and  $S$ , as well as the substrate  $A$ , be taken out by an outflow with a flow out rate  $\lambda$ :



In terms of rate equations the processes are described as:

$$\frac{dr}{dt} = f(r)a - \lambda r, \quad \frac{ds}{dt} = f(s)a - \lambda s, \quad \frac{da}{dt} = -[f(r) + f(s)]a + F - \lambda a. \quad (48)$$

Since the total concentration  $a + r + s$  follows the time evolution  $d(a + r + s)/dt = F - \lambda(a + r + s)$ , it approaches the steady state value  $F/\lambda$  with a relaxation time  $1/\lambda$ . This is a consequence of unbiased outflow (Eq. 47) of all reactants with the same rate  $\lambda$ . Consequently, even though we are dealing with an open system under a flow, the analysis is similar to the closed system by replacing the total concentration  $c$  with the steady state value  $F/\lambda$ . Instead of recycling, therefore, constant supply of the substrate allows the system to reach a certain fixed point with a definite value of the order parameter  $\phi_1$ , independent of the initial condition.

## 6

## Summary and Discussions

We have presented various simple scenarios that we are aware of in relevance to the ee amplification of the Soai reaction: a quadratic autocatalytic model in a monomer or homodimer system, and a linear autocatalytic model in an antagonistic heterodimer system. All these models can realize ee amplification such that the final value of the ee  $|\phi_\infty|$  depends on, but is larger than, the initial value  $|\phi_0|$ , as schematically shown in Fig. 8. The curve in the figure represents  $\phi_0 - \phi_\infty$  for a given initial ratio  $q_0/c$ , namely the ratio of the amount  $q_0$  of the total chiral initiators  $R$  and  $S$  relative to that of the total reactants  $c$ . Amplification is more enhanced if the ratio of the chiral initiator  $q_0/c$  is smaller. This plot also shows the possibility of increasing the final ee by repeating the reaction.

To achieve high ee values, Soai et al. performed experiments of consecutive autocatalytic reactions, where after each run of the reactions, the resulting solutions were quenched by adding acid and purified and reused in the next reactions. How the high ee value is attained in this type of experimental procedure is explained illustratively in Fig. 8. By choosing a specified initial condition  $\phi_0^{(1)}$ , the autocatalytic reaction ends up giving a final ee as  $\phi = \phi_\infty^{(1)}$ , determined by the intersection between the vertical line starting from  $\phi_0^{(1)}$  point and the round curve. The consecutive reaction starts with the purified products, with the ee  $\phi_\infty^{(1)}$  as the initial ee  $\phi_0^{(2)}$ . This feature is illustrated by extending a horizontal line from  $\phi_\infty^{(1)}$  on the round curve to the  $\phi_0 = \phi_\infty$  straight slope. This second reaction yields the ee value  $\phi_\infty^{(2)}$ , which is determined by the intersection between the vertical line starting from  $\phi_0^{(2)} = \phi_\infty^{(1)}$  point and the round curve. Repeating these procedures, the ee rapidly approaches the perfect  $|\phi_\infty| = 1$  with the speed depending on the curvature of the curve, which is determined by  $q_0/c$ . This is a mechanism of ee amplification and consecutive autocatalytic reactions, in contrast to the chiral symmetry break-

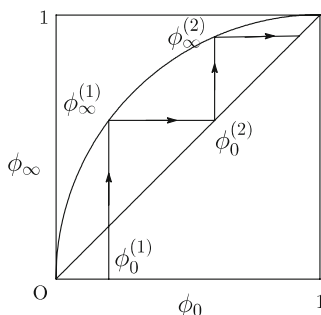


**Fig. 8** Schematics of enantiomeric excess amplification

ing in the sense of statistical mechanics, where the final ee is unique and is reached by a single procedure.

In all the cases considered, autocatalytic processes must be present, whether linear or nonlinear. To understand the actual mechanism of autocatalysis for the Soai reaction, identification of the process at a molecular level is necessary, but is out of scope of the present review.

We would like to point out another interesting feature, namely the spatial aspect of the reaction [25, 29, 37]. In usual experiments, the reactor is stirred to keep the system homogeneous. If there is no stirring, inhomogeneous patterns may develop between domains of two enantiomers. Analysis of these patterns may give some insight into the mechanism of reaction dynamics. Let us imagine, for instance, a time evolution of patterns of chiral domains for diffusionless systems with ee amplification and with chiral symmetry breaking. In an initial stage, chiral domains are nucleated randomly, and the domain pattern may look similar for both systems. After domains come into contact with each other, they behave differently: For a system with ee amplification, the domain pattern freezes because there remains no achiral substrate for further reactions. On the other hand, for a system with the chiral symmetry breaking, neighboring domains compete with each other at domain boundaries to extend their own territories, and the domain pattern evolves to selection slowly. When diffusion or hydrodynamic flow effects are taken into account, the system with ee amplification simply homogenizes and the ee value is averaged out. For the system with chiral symmetry breaking, these transport processes speed up the chirality selection and enhance the final value of ee [29, 37].

So far we have discussed the ee amplification by starting from an initial state with a finite enantiomeric imbalance, and the effect of spontaneous reaction is mostly neglected,  $k_0 = 0$ . However, reaction experiments without adding chiral substances do produce chiral species [13–15], implying that the coefficient  $k_0$  of the spontaneous reaction should be nonzero. In these experiments, it is found that values of the ee order parameter  $\phi$  of many runs are distributed widely between  $-1$  and  $+1$ , and the probability distribution function has double peaks at positive and negative values of  $\phi$ .

There is a theoretical study on the asymptotic shape of probability distribution for nonautocatalytic and linearly autocatalytic systems with a specific initial condition of no chiral enantiomers [35, 36]. Even though no ee amplification is expected in these cases, the probability distribution with a linear autocatalysis has symmetric double peaks at  $\phi = \pm 1$  when  $k_0$  is far smaller than  $k_1$ ;  $k_0 \ll k_1/N$  with  $N$  being the total number of all reactive chemical species,  $A$ ,  $R$ , and  $S$ . This can be explained by the “single-mother” scenario for the realization of homochirality, as follows: From a completely achiral state, one of the chiral molecules, say  $R$ , is produced spontaneously and randomly after an average time  $1/2k_0N$ . Then, the second  $R$  is produced by the autocatalytic process, whereas for the production of the first  $S$  molecule the

spontaneous production is necessary. The waiting time for the second *R* is shorter than that for the first *S* by a factor of about  $k_0/k_1$ . If this factor is far smaller than  $1/N$ , there is only a negligible chance for the production of *S* enantiomer until all the achiral substrates turn into *R*. All the chiral products are the descendants of the first mother *R* produced by the autocatalysis, and no second mother is born by the spontaneous production: This is a single-mother scenario. It strongly reflects the stochastic character of the chemical reaction, and is not contained in the average description using rate equations. Further studies are necessary as for the stochastic aspects of the Soai reaction [38].

In relation to the origin of homochirality in life, an interesting question is whether ee amplification is sufficient to achieve homochirality. From the experimental results of the Soai reaction without chiral initiator, the magnitude of the final ee  $|\phi_\infty|$  is distributed from a small value to a value close to unity. It is rather difficult to imagine that a value close to unity was accidentally selected on various places on earth in the prebiotic era. It seems rather natural that chiral symmetry breaking took place and a unique value of  $|\phi|$  has been finally selected. As discussed in the previous section, the flow in the open system can alter a system with ee amplification to one with chiral symmetry breaking. So we may say that the system with ee amplification in an open flow is one possibility. Recently, there have appeared several theoretical proposals, such as polymerization models [27, 39, 40] or a polymerization–epimerization model [41], to realize chirality selection in polymer synthesis. Although we are still far from a satisfactory understanding of the origin of homochirality in life, the discovery of the autocatalytic reaction by Soai gives us great impetus and imparts a sense of reality to this problem.

## References

1. Stryer L (1998) Biochemistry. Feeman and Company, New York
2. Pasteur L (1849) Comptes Rendus 28:477
3. Japp FR (1898) Nature 58:452
4. Noyori R (2002) Angew Chem Int Ed 41:2008
5. Calvin M (1969) Chemical Evolution. Oxford University Press, Oxford
6. Goldanskii VI, Kuz'min VV (1988) Z Phys Chem (Leipzig) 269:216
7. Gridnev ID (2006) Chem Lett 35:148
8. Pearson K (1898) Nature 58:496
9. Pearson K (1898) Nature 59:30
10. Mills WH (1932) Chem Ind (London) 51:750
11. Soai K, Shibata T, Morioka H, Choji K (1995) Nature 378:767
12. Soai K, Shibata T, Sato I (2000) Acc Chem Res 33:382
13. Soai K, Sato I, Shibata T, Komiya S, Hayashi M, Matsueda Y, Imamura H, Hayase T, Morioka H, Tabira H, Yamamoto J, Kowata Y (2003) Tetrahedron: Asymmetry 14:185
14. Gridnev ID, Serafimov JM, Quiney H, Brown JM (2003) Org Biomol Chem 1:3811
15. Singleton DA, Vo LK (2003) Org Lett 5:4337

16. Frank FC (1953) *Biochim Biophys Acta* 11:459
17. Landau LD, Khalatnikov IM (1954) *Dokl Akad Nauk SSSR* 96:469
18. Avetisov V, Goldanskii V (1996) *Proc Natl Acad Sci USA* 93:11435
19. Girard C, Kagan HB (1998) *Angew Chem Int Ed* 37:2922
20. Kondepudi DK, Asakura K (2001) *Acc Chem Res* 34:946
21. Todd MH (2002) *Chem Soc Rev* 31:211
22. Iwamoto K (2002) *Phys Chem Chem Phys* 4:3975
23. Iwamoto K (2003) *Phys Chem Chem Phys* 5:3616
24. Saito Y, Hyuga H (2004) *J Phys Soc Jpn* 73:33
25. Saito Y, Hyuga H (2004) *J Phys Soc Jpn* 73:1685
26. Saito Y, Hyuga H (2005) *J Phys Soc Jpn* 74:535
27. Saito Y, Hyuga H (2005) *J Phys Soc Jpn* 74:1629
28. Saito Y, Hyuga H (2005) Chirality selection models in a closed system. In: Linke AN (ed) *Progress in chemical physics research*, Chap 3. NOVA, New York, p 65
29. Shibata R, Saito Y, Hyuga H (2006) *Phys Rev* 74:026117-1
30. Sato I, Omiya D, Tsukiyama K, Ogi Y, Soai K (2001) *Tetrahedron: Asymmetry* 12:1965
31. Sato I, Omiya D, Igarashi H, Kato K, Ogi Y, Tsukiyama K, Soai K (2003) *Tetrahedron: Asymmetry* 14:975
32. Blackmond DG, McMillan CR, Ramdeehul S, Shorm A, Brown JM (2001) *J Am Chem Soc* 123:10103
33. Buhse T (2003) *Tetrahedron: Asymmetry* 14:1055
34. Islas JR, Lavabre D, Grevy J-M, Lamoneda RH, Cabrera HR, Micheau J-C, Buhse T (2005) *Proc Natl Acad Sci USA* 102:13743
35. Lente G (2004) *J Phys Chem* 108:9475
36. Lente G (2005) *J Phys Chem* 109:11058
37. Brandenburg A, Multamaki T (2004) *Int J Astrobiol* 3:209
38. Saito Y, Sugimori T, Hyuga H (2007) <http://arXiv.org/abs/cond-mat/0612385>
39. Sandars PGH (2003) *Orig Life Evol Biosph* 33:575
40. Brandenburg A, Andersen AC, Hofner S, Nilsson M (2005) *Orig Life Evol Biosph* 35:225
41. Plasson R, Bersini H, Commeyras A (2004) *Proc Natl Acad Sci USA* 101:16733

# Helix Generation, Amplification, Switching, and Memory of Chromophoric Polymers

Michiya Fujiki

Graduate School of Materials Science, Nara Institute of Science and Technology,  
 8916-5 Takayama, Ikoma, 630-0101 Nara, Japan  
[fujikim@ms.naist.jp](mailto:fujikim@ms.naist.jp)

<b>1</b>	<b>Introduction</b>	120
<b>2</b>	<b>Optically Active Helical Polysilanes</b>	124
2.1	Preparation of Polysilanes	125
2.2	Helical Polysilane and Circular Dichroism	126
2.3	Preferential Screw Sense Helical Ordering	127
2.4	Correlation Between Global Conformation and Optical Characteristics	128
2.5	Optically Active Homopolymers with a Preferential Screw Sense	131
2.5.1	Preferential Screw Sense Homopolymers with Enantiopure Chiral Side Chains	131
2.5.2	AFM Imaging of a Single Rod-like Helical Polymer Molecule on a Surface	134
2.5.3	Helix Recombination of Optically Active Helical Polymer with Opposite Screw Senses and Different Screw Pitches	135
<b>3</b>	<b>Helix Amplification of Polysilanes in Solution</b>	137
3.1	“ <i>Sergeants and Soldiers</i> ” Experiments in Copolymers with Preferential Screw Sense	137
3.2	“ <i>Majority Rule</i> ” Experiments in Copolymers with Preferential Screw Sense	143
3.3	“ <i>Sergeants and Soldiers</i> ” Experiments in Homopolymer Bearing Chiral Termini	143
<b>4</b>	<b>Helix Switching of Polysilane in Solution</b>	144
4.1	Preferential Screw Sense Switching in Homopolymers	144
4.2	Controlled Helix Switching in Copolymers	151
4.3	Quantized and Superposed Helicity	153
<b>5</b>	<b>“Chiroptical Switching and Memory” of Polysilane Aggregates in Solution</b>	159
5.1	Chiroptical Switching and Memory of Aggregates in Solution	159
5.2	Molecular Chirality Transcription and Memory to Polymer Aggregates	165
<b>6</b>	<b>“Helix Command Surface” Experiments of Polysilane Binary Film at the Surface</b>	168
<b>7</b>	<b>Tunable Cholesteric Liquid Crystallinity of Helical Polysilane</b>	172
<b>8</b>	<b>Parity Question—Subtle Left-Right Differences by Physical Origins</b>	174
<b>9</b>	<b>Concluding Remarks</b>	182
	<b>References</b>	183



**Abstract** The origin of biomolecular handedness known as homochirality in the animate world may be one of the most puzzling issues among scientists. The cooperativity of amplification, switching, and memory in biopolymers and synthetic helical polymers might be shared with ideas of a scenario for the biomolecular homochirality, autocatalytic mechanism in chiral chemical synthesis, and bifurcation equilibrium mechanisms in crystallization of chiral crystals. This work focuses on several chiroptical amplification phenomena exemplified in optically active chromophoric helical polysilanes bearing chiral and achiral side groups, which exist in isotropic dilute solution, as aggregate forms dispersed in isotropic solution, in double layered films deposited onto a solid surface, in the thermotropic cholesteric liquid crystal film state, and ultimately by dictating invisible chiral weak and ultraweak interactions at subatomic, atomic, and molecular levels.

**Keywords** Amplification · Helix · Optically active · Polymer · Polysilane

## 1

### Introduction

Since the time of Pasteur, the origin of biomolecular handedness which is known as homochirality in the animate world (de facto) may be one of the most puzzling issues among scientists. This is because biopolymers are derived from the same handedness of building blocks, although mirror-image molecules have long been thought to be energetically identical. Indeed, naturally occurring proteins adopt 19 types of L-amino acids and achiral glycine. Naturally occurring DNA and RNA are also made of only D-ribose and 2-deoxy-D-ribose sugars, respectively. The homochirality of these living constituents might lead to various hierarchical helical architectures, for example,  $\alpha$ -helices of protein, double helices of DNA, triple helices of collagen, and  $\alpha$ -helical coiled-coils of myosin and keratin on the molecular level [1–3]. Alternatively, the homochirality of chiral amphiphilic compounds, including: phospholipids, amino acids, nucleic acid derivatives, and carbohydrate compounds, is the key to fabricate helical superstructures and organizations, such as tubes, disks, bundles, fibers, and cholesteric liquid crystals. Nature's elegant bottom up preferences have thus inspired the development of various hierarchical superhelical assemblies and various functional advanced materials in inanimate systems with efficiency in fabrication under ambient conditions and in a controlled manner [4–6].

Recent advances in scanning probe microscopic (SPM) techniques, including scanning tunnelling microscopy (STM) [7] and atomic force microscopy (AFM) [8, 9], facilitate observation of the real polymer shapes at a molecular level on surfaces and even in solution. Although the visualization of several biopolymers such as DNA, polypeptides, and polysaccharides have been successfully reported in recent years, SPM observation of synthetic helical polymers remains a challenging issue. Shinohara et al. first reported STM imaging of the hierarchical helical structure of high molecular weight poly(phenylacetylene) bearing a *l*-(-)-menthoxycarbonylamino group [10].

Kumaki, Yashima, and coworkers reported formation of hierarchical helix bundles of high molecular weight poly(phenylacetylene) derivatives bearing L- and D-alanine residues by high resolution AFM [11]. Soluble disk-shaped, nickel phthalocyanine bearing four chiral aralkyl groups with the same handedness can form hierarchical supramolecular helical fibers. The phthalocyanine supramolecules were programmed based on the homochiral intermolecular quadruple hydrogen bonding [12].

In sharp contrast, recent knowledge and understanding on a broad range of chemical forces and interactions led to the new idea that weak CH/ $\pi$  (and CH/X, X = F, O, N, Cl) interactions with weak directionality may play an essential role in stabilizing secondary, tertiary, and more higher order structures of proteins and DNAs because of the ubiquitous existence of CH and  $\pi$ -containing groups in biochemistry. Nishio pointed out the importance of CH/ $\pi$  and CH/X interactions among small molecules in crystals [13]. Desiraju and Steiner classified several types of hydrogen bonds into very strong, strong, and weak forces and/or into conventional and nonconventional interactions [14]. In this case, strong forces refer to ordinary hydrogen bonding, coordination bonding, dipole–dipole, electrostatic, and  $\pi$ – $\pi$  stacking forces. Although the CH– $\pi$  interaction (down to  $\sim 0.2$  kcal/mol) is classified as one of the weakest forces, this weakness may be responsible for increased structural adaptability.

A programmed highly ordered hierarchical helical architecture of synthetic polymers is now a major challenge in materials science [6]. Akagi et al. reported the synthesis of hierarchical helical polyacetylene fiber under an asymmetric reaction field of chiral nematic (N\*) liquid crystal [15]. Nolte et al. demonstrated formation of various helical superstructures composed of amphiphilic block copolymer containing a polystyrene tail and a charged helical polyisocyanide head group derived from isocyano-L-alanine-L-alanine and isocyano-L-alanine-L-histidine [16]. In these cases, chiral and strongly polar solute-solvent and solute-solute interactions are responsible for these helical assembled structures. If weak and ultraweak intermolecular interactions of nonpolar artificial constituents were able to solely afford hierarchical helical structures onto an achiral substrate, it might be drawn to a new viewpoint with more common insights that homochirality of constituents is responsible for spontaneous formation of hierarchical helix architecture regardless of the strength and weakness of those chemical forces in animate and inanimate worlds.

Thus far, much effort in the area of asymmetric chemical synthesis has been devoted to efficiently produce chiral molecules with a significant ee of either left-handed or right-handed chirality. To achieve this goal, the use of chiral auxiliaries or catalysts, with high ee purity, are usually required, leading to the product purity linearly responding to the ee of the auxiliary or catalyst used. Although several theoretical models have long suggested that autocatalytic processes may result in kinetically controlled asymmetric amplification, these predictions have now been verified experimentally. Indeed,

it is now well-known that a nonlinear relationship in ee values between the products and chiral catalysts occurs in many asymmetric chemical reactions due to autocatalytic amplification of product chirality.

On the other hand, polymers should essentially show this kind of cooperativity in chirality, helicity, and higher order helical structures [17, 18], suggesting the origin of homochirality in biological polymers. Such self organization takes particular importance as each repeating unit of polymer are linked together with covalent single, double, and/or triple bonds and do not dissipate to solution. Polymer systems, which exist in dilute solution, aggregate and small particle forms in isotropic solution, on surfaces, and in the solid film state, are thus ideal molecular systems to reproducibly elucidate various cooperative phenomena, including amplification, switching, and memory of chirality, helicity, and chiroptical properties.

In particular, synthetic helical polymer made of a chromophoric and fluorophoric main chain seem ultimately much simpler than biological polymers to clarify this kind of cooperativity. This is because a large number of invisible weak and ultraweak forces from intramolecular and intermolecular interactions efficiently *add up* to a strong force, enabling a system to overcome thermal fluctuation energy of  $\sim 0.6$  kcal/mol [17, 18]. This cooperativity is directly detectable by ordinary circular dichroism (CD) and other physicochemical measurements. In case of two optically active polyisocyanate homopolymers bearing chirally deuterated side groups in solution, a tiny energy, on the order of only several cal/mol (not kcal!) can distinguish the right-handed (*P*-, plus) and left-handed (*M*-, minus) screw sense helical structures and greatly amplify a helical structure with a preferential screw-sense.

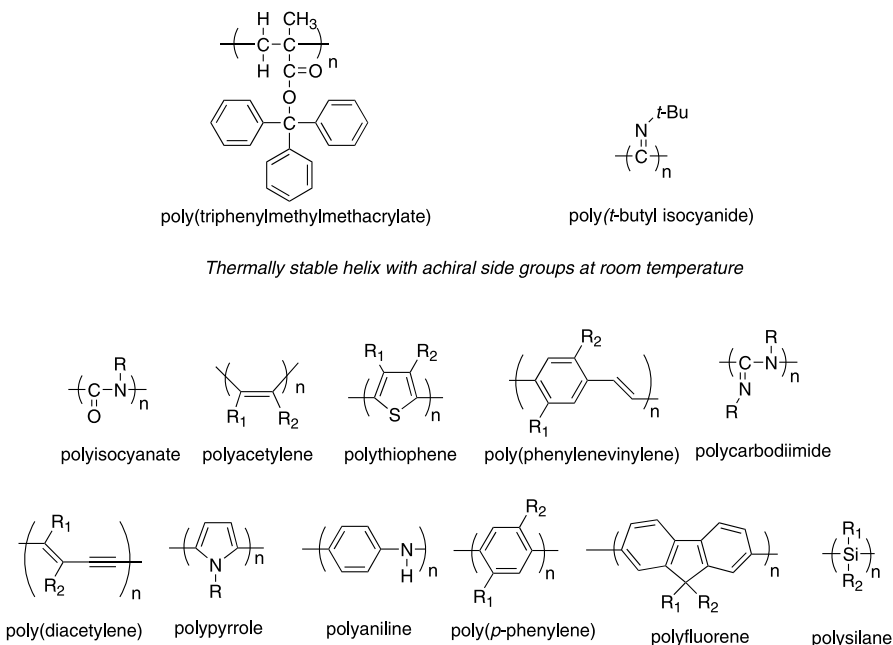
The cooperativity of amplification, switching, and memory in synthetic helical polymers might thus be shared with ideas of a scenario for the biomolecular homochirality, autocatalytic mechanism in chiral chemical synthesis, and bifurcation equilibrium mechanisms in crystallization of chiral crystals. Indeed, amplification phenomena in several optical activity and helicity of synthetic polymers in isotropic solution appears to be common and are now established as “*sergeants and soldiers experiment*” and “*majority rules*” in polymer stereochemistry [17, 18]. Any minute chiral forces caused by intramolecular and intermolecular systems can be detectable, when a proper model polymer system is chosen to elucidate the cooperativity of amplification, switching, and memory.

For example, the *sergeants and soldiers experiment* features a preferential screw-sense helical amplification in optical active copolymers with racemic helical structures named by Green et al. [17, 18]. This effect means that a small portion of enantiopure chiral side groups determines the overall screw sense (*P* or *M*) of the helical main chain bearing a majority of achiral side groups, and a population of helicity with one preferential screw-sense is nonlinearly amplified as a function of the chiral impurity. Since the first report of this phenomenon in poly- $\alpha$ -olefin copolymers by Pino et al. [21],

poly(alkylisocyanate) [17, 18] and polyacetylenes [20] are known to be the most typical examples.

Another significant helical amplification in optically active copolymers with preferential screw-sense helicity is known as the *majority rule* phenomenon [17, 18]. In this case, the screw sense of a helical main chain bearing nonracemic chiral side groups is controlled by the ee only and a population of preferential screw-sense helicity and optical activity were nonlinearly amplified by ee of chiral side groups. Since Pino et al. first reported this phenomenon in poly- $\alpha$ -olefins made of vinyl co-monomers bearing nonracemic chiral moieties [21], this *majority rule* has already been established in stiff polyisocyanates bearing a nonracemic chiral side chain [17, 18].

In the early stage of helical polymer stereochemistry, a few polymers were known to retain a helical main chain with a predominantly single screw sense in solution at room temperature. For example, in cases of poly(*t*-butyl isocyanides) [22], poly(triphenylmethyl methacrylate) [23], polyisocyanate [24], and poly- $\alpha$ -olefins [19], helical structures are kept through side group interactions. Since these pioneering works, many synthetic optically active polymers with a chromophoric main chain bearing chiral and/or bulky side



*Preferential screw sense helix induced by chiral side groups and/or chiral chemical influence*

**Scheme 1** Typical optically active polymers with chromophoric main chain and/or side chain

groups or chiral additives have emerged, such as polyisocyanide [25, 26], polyisocyanate [17, 18], polyacetylene [20, 27], polythiophene [20], poly(*p*-phenylenevinylene) [21], polycarbodiimides [22], polydiacetylenes [28–30], polypyrroles [31], polyanilines [32], poly(*p*-phenylene) [33], polyfluorenes [34], and polysilanes [28, 29].

Among these helical polymers, a series of single strand helical polysilanes [36–41], which have various main chain stiffness (globule, coil, stiff, and rod-like) and are obtained in a wide range of molecular weights ( $10^3$ – $10^7$ ), may be one of the best synthetic stereogenic bonding helical polymer systems to elucidate the cooperativity of amplification, switching, helicity memory, and chiroptical properties. This is because polysilanes exhibit intense CD/UV/fluorescence (FL) bands around 320–400 nm because the main chain itself is chromophoric and fluorophoric. The helices' CD/UV/FL spectroscopic properties in dilute solution features along with viscometric measurement, NMR ( $^{29}\text{Si}$  and  $^{13}\text{C}$ ) experiments, and AFM observation thus have a great advantage for quantitative helical conformational analysis in dilute solution.

This work mainly highlights optically active cooperativity of several helical polysilane systems, which exist in various states including: in dilute solution, as aggregates formed in isotropic solution, onto surfaces, and in film states, as dictated by invisible chiral weak and ultraweak intramolecular and intermolecular interactions. The present knowledge on chiroptical amplification, switching, and memory, including the *sergeants and soldiers experiment* and *majority rule* phenomena on the surface and in the film state, are programmed manifestations of polymer helicity amplification, pointing to the potent applications that chiral polymeric materials might be developed into in which enantiomeric excess, enantiomeric content, and screw-sense may be nonlinearly related to uses such as chiral chromatography, asymmetric catalysis, and new kinds of chiroptical sensors and switches induced by physical origin chirality, involving circularly polarized light, temperature, and electroweak force, as well as by chemical origin chirality.

## 2

### Optically Active Helical Polysilanes

One may have a question of whether an optically active helical polymer obtained from an enantiopure monomer adopts a purely *P*- (or *M*-) screw sense helical main chain in solution at a given temperature, or is composed of an ensemble of pseudo-diastereomeric mixed helical motifs containing *P*- and *M*-screw senses. Fluorescence (FL) studies combined with circular dichroism (CD), UV, and NMR spectra of the main chain constitute a powerful probe in identifying the main chain chirality (screw sense, uniformity, and rigidity) and optical purity of helical polymers, since the photoexcited energy above

the optical band gap should relax to the lowest energetic domain in a polymer chain, and then be emitted from that domain.

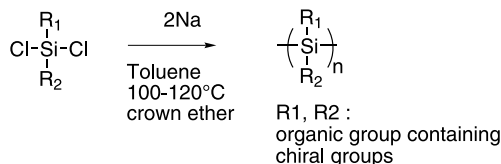
Chromophoric helical polysilanes whose optical activity is induced by nonchromophoric chiral side chains are particularly suitable chiroptical polymers for elucidating the inherent nature of the polymer helix, because they embody a fluorophoric and chromophoric main chain, exhibiting intense UV, CD, and FL bands due to the  $\text{Si}\sigma\text{--Si}\sigma^*$  transition around 300–400 nm [43–47]. Additionally, samples with any desired molecular weight can be obtained by simple fractional precipitation procedure, since the molecular weights of helical polysilanes are widely distributed in the range from  $10^3$  to  $10^7$ . Compared with other optically active  $\pi$ -conjugating polymers, the uniqueness of helical polysilanes may facilitate characterization of helical cooperativity such as helical amplification, switching, and memory. It has been recently established that the spectral characteristics of several helical polysilane homopolymers and copolymers, including intensity, spectral width, peak position, Stokes shift, and linewidth, vary intensely with changes in the main chain stiffness, population of *P*- and *M*-helical motifs and helix reversals, degree of polymerization, temperature, and solvent polarity.

Although main chain chirality refers to both polymers with stereogenic centers in the main chain and polymers with main chains consisting of helical stereogenic bonds induced by chiral side groups this work mainly focuses on polysilanes exhibiting this latter type of chirality.

## 2.1

### Preparation of Polysilanes

The synthesis of organopolysilanes with a high degree of stereogenic control is still a challenging issue with relatively few reports [44] in contrast to the well-documented and successful methods employed in organic polymer chemistry. Most organopolysilanes including poly(dialkylsilane)s, poly(alkylarylsilane)s, and poly(diarylsilane)s are prepared by the Wurtz-type condensation of the corresponding diorganodichlorosilanes with sodium in inert solvent [44–47]. This reaction is essentially identical to the procedure of Kipping more than 80 years ago [48, 49] as shown in Scheme 2. Although the reaction is highly exothermic and usually carried out in hot toluene, an advanced modification of the reaction is to use a small amount of crown ether



**Scheme 2** Wurtz-type reduction preparation of optically active polysilanes

or diglyme as an effective additive, leading to significant improvement of polymerization yields, shortening of polymerization times, and modification of molecular weight distributions [50].

## 2.2

### Helical Polysilane and Circular Dichroism

In the case of synthetic optically active polymers, the intuitive meaning of a CD signal intensity is very similar to that of UV spectroscopy, with the additional dimension of the subtracted absorption between left and right circularly polarized light [36, 44]. Absorption of light obeys the Beer–Lambert law and thus CD intensity is defined as  $\Delta\varepsilon = \varepsilon_L - \varepsilon_R = (A_L - A_R)/cl$ , where  $\Delta\varepsilon$  is the molar circular dichroism intensity,  $\varepsilon_L$  and  $\varepsilon_R$  are the molar absorptivities for L and R circularly polarized light, respectively,  $A_L$  and  $A_R$  are the absorbances of L and R light,  $c$  is the molar concentration per repeat unit and  $l$  is the path length. CD bands are commonly referred to as either positive or negative Cotton effects and the peaks as extrema.

Another useful characteristic is expressed as the ratio of the absorption strength of unpolarized UV-Vis over the magnitude of CD (polarized) absorption. This is formalized in the dimensionless parameter, Kuhn's dissymmetry ratio,  $g_{\text{abs}} = 2\Delta\varepsilon/(\varepsilon_L + \varepsilon_R) = \Delta\varepsilon/\varepsilon$ , where  $\varepsilon$  is the molar absorptivity per repeat unit. The dissymmetry ratio is also a function of the magnetic and electric dipole moments ( $m$  and  $\mu$ , respectively) and the angle  $\theta$  between them, such that  $g_{\text{abs}} = 4 \cdot R/D = 4|m||\mu| \cos\theta(m^2 + \mu^2)^{-1}$ , where  $R$  and  $D$  are the rotatory strength and the dipole strength, respectively. For chromophoric helical polymers, this  $g_{\text{abs}}$  value gives information on the helical characteristics (screw pitch, screw sense, and diastereomeric and/or enantiomeric optical purities). When polysilanes constitute the chromophoric main chain, the observation of CD signal thus indicates chirality in the main chain with the preferential screw sense of the helical conformation. The idealized CD and UV spectra for single *P*- and *M*-screw sense polymers (arbitrarily assigned to *P*- and *M*-CD signals) are illustrated in Fig. 1a. However, particular attention should be paid to the interpretation of  $g_{\text{abs}}$  due to an equal amount of the opposite screw sense helical segments with helix reversals. This is because, if absorptions of *P* and *M* occur at the same wavelength, the magnitude of  $g_{\text{abs}}$  will result in a smaller, or possibly zero CD signal, as illustrated in Fig. 1b.

Bisignate Cotton CD signals have two possible origins. Firstly, in a polymer containing both *P*- and *M*-screw senses with slightly different absorption wavelengths, the positive and negative Cotton effects will be slightly offset with respect to each other, resulting in an apparent bisignate signal [37]. Secondly, for two adjacent chromophores, coupling between the stronger electronic dipole moments will occur to give bisignate split-type CD signals: the so-called exciton couplet signal [51]. This could be classified as either an intramolecular interaction in the same molecule at a kink upon chain folding,

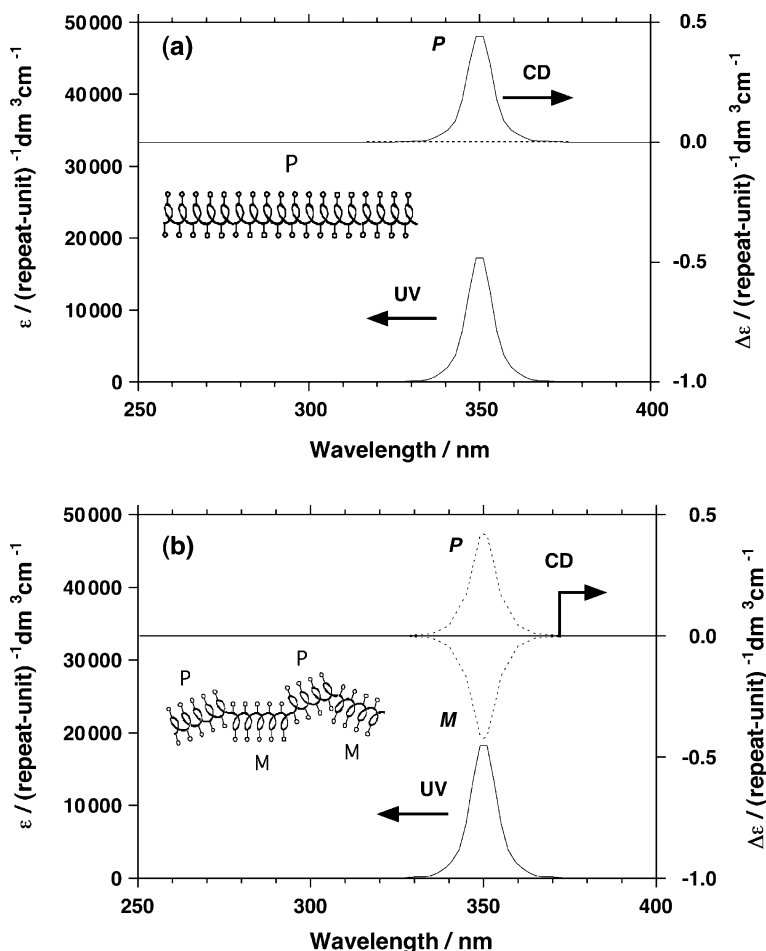


**Fig. 1** Illustrations of coincident CD and UV absorption profiles for chromophoric main chain with **a** *P*-screw sense, **b** equal proportion of *P*- and *M*-screw senses

or an intermolecular interaction in aggregate phases. The sign of an exciton couplet bisignate signal affords a simple, direct method for determining the absolute configuration (right-handed or left-handed configuration) of the two interacting chromophores.

### 2.3

#### Preferential Screw Sense Helical Ordering

Although the main chain conformations of polysilanes have been described as random coil,  $7_3$ - (deviant helical),  $15_7$ - (transoid helical), and  $2_1$ - (all anti, planar) structures, it is now generally accepted that most polysilanes tend to



adopt helical main chain structures in solution, regardless of side groups and temperature [52]. Although poly(dichlorosilane) can adopt an all-anti conformation in the solid state by single crystal X-ray diffraction analysis [53], the vast majority of polysilanes do not show any Cotton effects in their CD spectra, due to the adoption of equal numbers of *P*- and *M*-segments, resulting in an average racemic helical conformation and optical inactivity. If the helical main chain is driven by a chiral chemical influence to adopt a preferential screw sense with an ee of either *P* or *M*-screw sense, a Cotton effect can be seen in the CD spectrum. Thus, the interaction between side groups, solvents, temperature, and helical main chain structures of polysilane in isotropic solution can be probed by means of CD spectroscopy, combined with UV, FL, and  $^{29}\text{Si}$ -NMR spectroscopies and viscometry.

The main chain chirality and helicity of polypeptides is inherent since the stereogenic centers are incorporated into the main chain. In poly(triphenylmethyl methacrylate) and polyisocyanide synthesized by screw-sense selective polymerization, the helical structures are maintained through the stereochemical locking effect of bulky achiral side groups, while poly(triphenylmethyl methacrylate) contains stereogenic centers in the main chain associated with the tacticity [23]. In the cases of polyisocyanates, polyacetylenes, polythiophenes, polyphenylenevinyls, polycarbodiimides, and polysilanes, the main chain helical structures are induced by chiral side chains. Such optically active helical polymers can be obtained in a number of ways, including (a) polymerization with enantiopure chiral catalyst or initiator, (b) chiral doping of optically inactive polymers with enantiopure chiral ions, (c) separation of a racemic mixture of enantiomeric helices using chiral stationary phase chromatography for nondynamic helical systems, (d) chiral complexation of achiral or racemic polymers with nonracemic chiral ligands, (e) post-polymerization functionalization with chiral moieties, (f) incorporation of enantiopure chiral end groups, (g) polymerization of nonracemic chiral monomers, (h) copolymerization of nonracemic chiral monomers with achiral monomers or with nonracemic monomers, and (i) circularly polarized irradiation of polymers bearing racemic sensitizers. In the case of optically active polysilanes, synthetic techniques from (e) to (h) have been carried out.

## 2.4

### Correlation Between Global Conformation and Optical Characteristics

The conformational mobility of a chromophoric main chain polymer is often connected to its electronic structure. Therefore, changes in the UV-visible absorption spectra and/or chiroptical properties are spectroscopically observable as thermo-, solvato-, piezo-, or/and electrochromisms. It is widely reported that  $\sigma$ -conjugating polysilanes exhibit these phenomena remarkably clearly [54]. However, their structural origins were controversial until recently, since limited information was available on the correlation between the conformational prop-

erties of the main chain, electronic state, and (chir)optical characteristics. It was reported in 1996 that in various polysilanes in THF at 30 °C, the main chain peak intensity per silicon repeat unit,  $\epsilon$  (Si – repeat – unit) $^{-1} \cdot \text{dm}^3 \cdot \text{cm}^{-1}$ ,

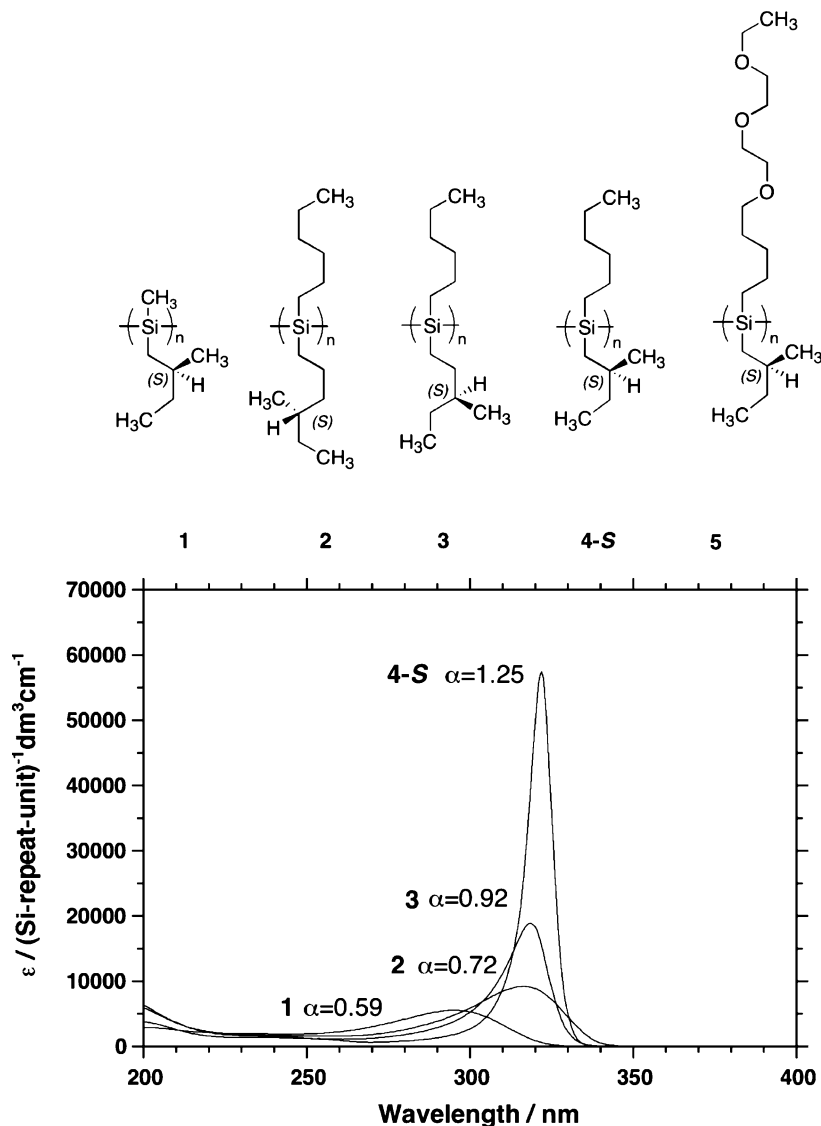


**Fig. 2** Comparison of UV absorption spectra of four optically active polysilanes in THF at 30 °C: Poly{methyl-(S)-2-methylbutylsilane} (1,  $\alpha$  of 0.59), poly{n-hexyl-(S)-4-methylpentylsilane} (2,  $\alpha$  of 0.75), poly{n-hexyl-(S)-3-methylpentylsilane} (3,  $\alpha$  of 0.92), poly{n-hexyl-(S)-2-methyl-butylsilane} (4-S,  $\alpha$  of 1.25)

increases exponentially as the viscosity index,  $\alpha$ , increases [39]. Although conventional viscometric measurements often require a wide range of low dispersity molecular weight polymer samples, a size exclusion chromatography (SEC) machine equipped with a viscometric detector can afford the intrinsic viscosity,  $[\eta]$ , as a function of the molecular weight of the polymer,  $M_w$ , in real time, from the Mark–Houwink–Sakurada plot [39].

Figure 2 shows the UV absorption spectra of four optically active poly(dialkylsilane)s bearing different chiral side groups in THF at 30 °C [45]. It is evident that as the value of  $\alpha$  increases from 0.59 to 1.25, the UV absorption intensity increases, whereas the full width at half maximum (*fwhm*) decreases. These results led to the finding of the semi-empirical relationship between the main chain absorption characteristics and the global conformation of various polysilanes in solution.

Figure 3 shows a correlation between the values of  $\epsilon$ , *fwhm* and  $\alpha$  of various poly(dialkylsilane)s and poly(alkylaryl)silane)s in THF at 30 °C [41]. The polymers include seven optically active helical poly(dialkylsilane)s with four different types of chiral  $\beta$ -,  $\gamma$ -, or  $\delta$ -branched alkyl substituents, 11 optically inactive poly(dialkylsilane)s with six different types of achiral  $\beta$ -,  $\gamma$ -, or  $\delta$ -branched substituents, an optically inactive helical poly(dialkylsilane) with racemic chiral side groups, and two optically inactive helical poly(alkylphenyl)silane)s. It is evident that, for the polysilanes whose  $\lambda_{\max}$  ranges from 290 to 352 nm, although the value of  $\epsilon$  increases exponentially with an in-

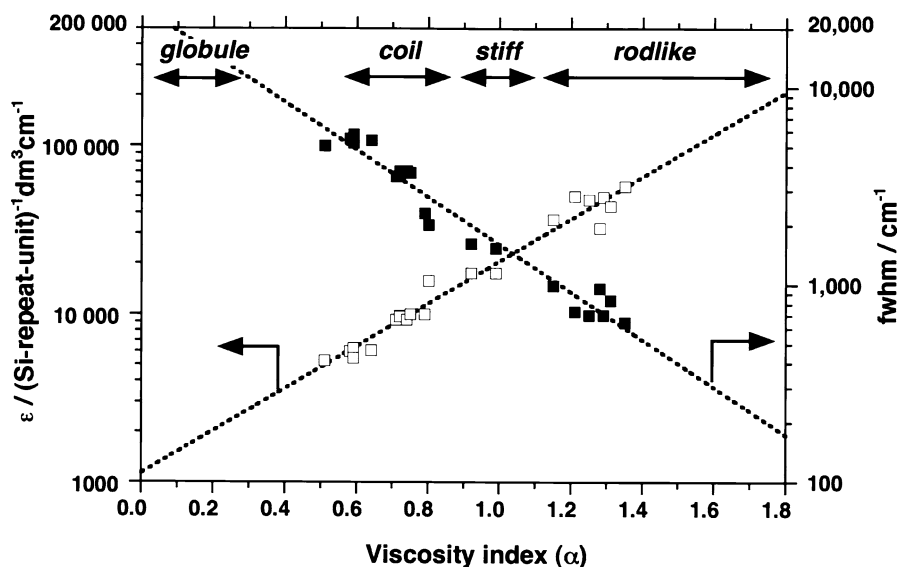


**Fig. 3** Correlation between UV peak intensity ( $\epsilon$ ), full width at half maximum (*fwhm*), and  $\alpha$  of various poly(dialkylsilane)s and poly(alkyl(aryl)silane)s in THF at 30 °C

crease of the  $\alpha$  value, the value of the *fwhm* decreases exponentially. Thus, the degree of  $\sigma$ -conjugation, global conformation, and UV absorption characteristics in polysilanes are controllable by the choice of side groups, regardless of chirality and achirality in the side groups. For example, poly{methyl-(S)-2-methylbutylsilane} (1) has the most shrunken shape with  $\alpha = 0.59$ , whereas its longer *n*-alkyl chain derivative, poly{*n*-hexyl-(S)-2-methylbutylsilane} (4-S) adopts a rigid rod-like conformation with  $\alpha = 1.25$ . Poly{*n*-hexyl-(S)-4-methylpentylsilane} (2) with  $\alpha = 0.75$  has a random coiled conformation similar to conventional optically inactive polysilanes. Poly{*n*-hexyl-(S)-3-methylpentylsilane} (3) with  $\alpha = 0.92$  is stiff (semi-flexible or semi-rigid) and shows intermediate properties between 2 and 4-S.

From the semi-empirical  $\varepsilon$ - $\alpha$ -*fwhm* relationship, either value of  $\varepsilon$  or *fwhm* provides very useful information on the degree of chain coiling in solution at a given condition and is important for discussing the global conformational properties of polysilane in any condition. Also, the relationship assists in predicting the upper limit of the  $\varepsilon$ -value for an ideal rigid rod polysilane. From the extrapolation of the  $\varepsilon$ - $\alpha$  relationship, it is expected that the  $\varepsilon$ -value may reach  $150\,000\ (\text{Si} - \text{repeat} - \text{unit})^{-1} \cdot \text{dm}^3 \cdot \text{cm}^{-1}$ , since the maximum  $\alpha$ -value for the ideal rigid rod polymer may attain 1.7–1.8 [39] and indeed the  $\varepsilon$ -value for rod-like optically active poly(6,9,12-trioxatetradecyl-(S)-2-methylbutyl)silane (5) in ethanol progressively increases from 42 000 with a *fwhm* of  $800\ \text{cm}^{-1}$  (8 nm) at 323 nm to 102 000 with a *fwhm* of  $400\ \text{cm}^{-1}$  (4 nm) at 318 nm when the temperature is cooled from 25 to  $-104\ ^\circ\text{C}$  [55]. This  $\varepsilon$  value, the highest among all polysilanes, is believed to correspond to an ideal perfect rigid rod structure.

## 2.5

### Optically Active Homopolymers with a Preferential Screw Sense

#### 2.5.1

##### Preferential Screw Sense Homopolymers with Enantiopure Chiral Side Chains

In 1994, two research groups independently reported the synthesis and chiroptical properties of poly(dialkylsilane)s bearing (S)-2-methylbutyl side groups. Copolymers were studied originally by Möller, Matyjaszewski and co-workers [35], and homopolymers were prepared by our group [36–38]. Since most of the fundamental features are clarified in a series of our works concerning poly(*n*-decyl-(S)-2-methylbutylsilane) (6) and its derivatives [36, 38], the results concerning dialkyl homopolymers derived from monomers with enantiopure chiral alkyl substituents are first described.

Polymer 6 showed the ideal UV, CD, and FL spectral characteristics of a rod-like chromophore and fluorophore due to the single-screw sense helical structure induced by preferential side group interactions in dilute isooctane

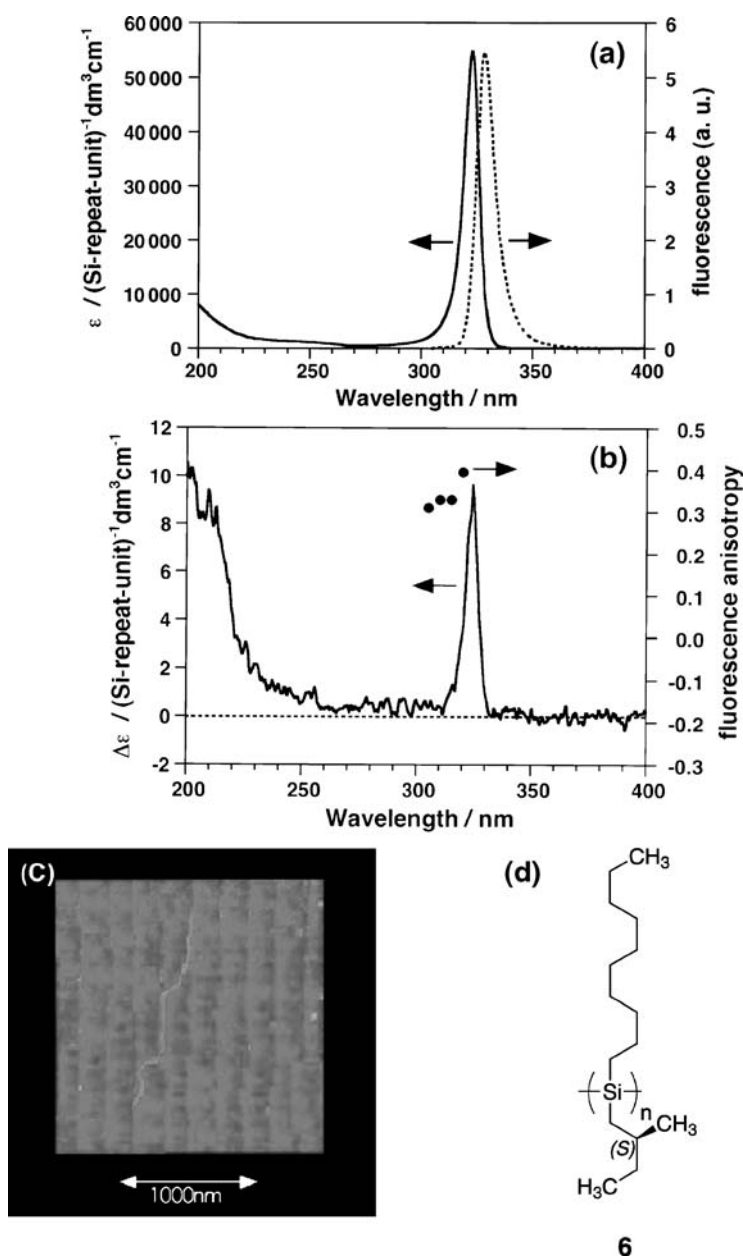


**Fig. 4** **a** UV absorption and Cotton CD spectra and **b** FL spectrum with FL anisotropy of poly(*n*-decyl-(*S*)-2-methylbutylsilane) (**6**,  $M_w = 5\,330\,000$ ,  $M_n = 4\,110\,000$ ,  $\alpha = 1.35$  in THF at 30 °C) in isooctane at 20 °C. **c** AFM molecular image of this high  $M_w$  **6** on the surface of ultraflat sapphire and chemical structure of **6**

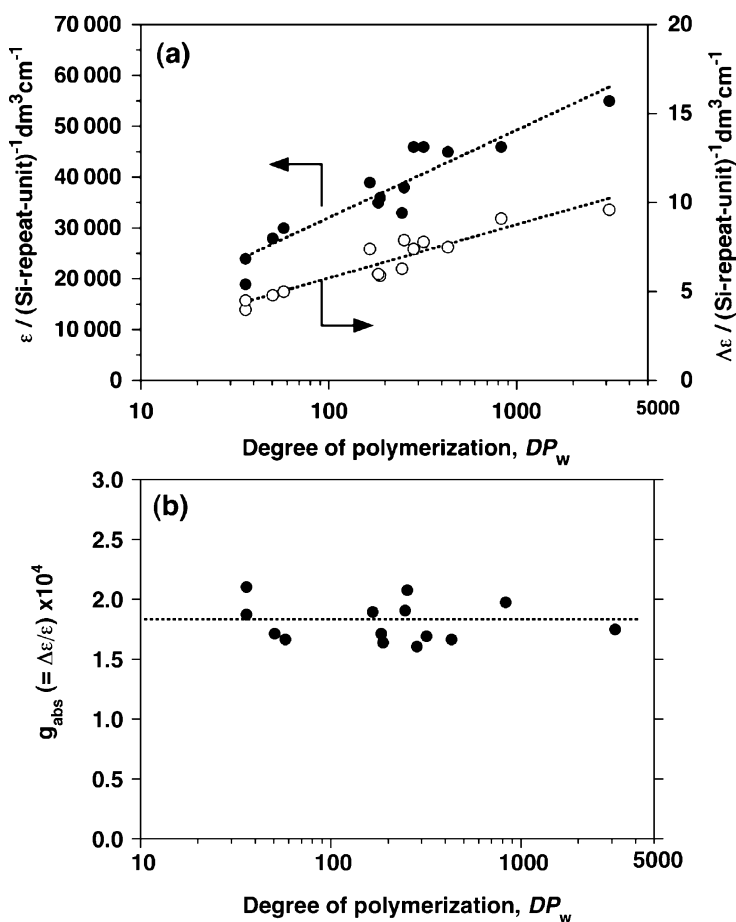


**Fig. 5** Characteristics of the UV and CD intensities at around 323 nm in isooctane at 20 °C of 14 samples isolated from nine poly(*n*-alkyl(*S*)-2-methylbutylsilane) derivatives as a function of the degree of polymerization ( $DP_w$ ) in isooctane at 20 °C: **a**  $\epsilon$  and  $\Delta\epsilon$  and **b** the dissymmetry ratio

at 20 °C. As is evident in Fig. 4a and b, (i) **6** exhibits a very intense, narrow UV absorption at 323 nm, with  $\epsilon = 55\,000 (\text{Si} - \text{repeat} - \text{unit})^{-1} \cdot \text{dm}^3 \cdot \text{cm}^{-1}$  and an *fwhm* value of 8 nm ( $\epsilon$  is ca. six times greater and the *fwhm* narrower by one sixth than conventional random coil poly(dialkylsilane)s); (ii) its CD spectral profile at 323 nm fits completely within the UV spectrum; (iii) the FL spectral profile at 328 nm is the mirror image of the UV and CD band profiles, and (iv) the FL anisotropy (FLA) value around the 323-nm UV-CD bands reaches the theoretical limit of 0.4 expected for the random distribution of a rigid rod chromophore being collinear with the fluorophore in a rigid medium. These novel UV-CD-FL characteristics of **6** could be the first demonstration

of uniqueness among other optically active polysilanes and optically active organic polymers.

Additionally, the UV, CD, FL, and FL excitation (FLE) spectral characteristics of poly(*n*-alkyl-(*S*)-2-methylbutylsilane) derivatives in isooctane at 20 °C revealed that the rigid rod-like helical structure was kept, when the *n*-alkyl side group length was increased from *n*-propyl to *n*-dodecyl and when the main chain length is increased from 20 to 3000 Si units length [38]. This idea was supported by the unique UV-CD-FL-FLE spectroscopic features characteristic of **4** and the fact that the  $g_{\text{abs}}$  value of  $\sim 1.9 \times 10^{-4}$  was almost independent of both *n*-alkyl side group length and Si main chain repeat length, as is evident in Fig. 5b. On the other hand, the peak intensities of UV and CD bands at 323 nm increased nonlinearly as the main chain repeat number increased, as shown in Fig. 5a, while the respective values of the UV peak wavelength and *fwhm* of the band converged to limiting values of 322 nm and 8 nm in isooctane at 20 °C.

The dipole strength of the UV absorption band appears to be independent of the *n*-alkyl side group length and main chain repeat numbers. Indeed, integration of the 323 nm UV absorption band of the poly(*n*-alkyl-(*S*)-2-methylbutylsilane) derivatives depends only very weakly on the repeat number. These results led to the important idea that in the case of optically active polysilanes, the  $g_{\text{abs}}$  value can be used to characterize helical parameters such as the population of *P*- and *M*-motifs and their regularity, rather than the values of  $\Delta\epsilon$  or optical rotation. It was recently established that in a series of dimensionality of polysilane in solution, the persistence length *q* of **4** is as large as 85 nm in isooctane at 20 °C by Sato et al. [56] and this high *q* value is greater than that of polyisocyanate (*q* = 76 nm) bearing  $\beta$ -branched (*R*)-2,6-dimethylheptyl groups.

### 2.5.2

#### AFM Imaging of a Single Rod-like Helical Polymer Molecule on a Surface

Although chain dimensional parameters such as persistence length in solution can be evaluated by well-established light scattering and viscometric techniques, molecular imaging of individual polymer chains is an important issue in the design and control of the inherent optoelectronic properties of functional polymers and nanomaterials. Fortunately, recent advances in atomic force microscopy (AFM) and scanning tunnelling microscopy (STM) have now enabled the direct observation of single molecular images of such insulating polymers as cyclic DNA, random coiled polystyrene-block-poly(methylmethacrylate) on mica, monolayer images of soluble poly(*para*-phenylene) on a gold surface, and twinned chiral polyacetylene placed on a highly oriented pyrolytic graphite substrate [7–9, 57].

The first AFM molecular images of a single molecule of **6** with a high molecular weight sample ( $M_w = 5\,330\,000$ ,  $M_n = 4\,110\,000$ ) deposited onto

a sapphire surface [58] was observed by Koshihara et al. in 1997. Figure 4c shows an AFM molecular image of **6** with a high  $M_w$  on the surface of ultra-flat sapphire. It was found that, although the total molecular contour length of **6** reached ca. 2000 nm in length, the chain consisted of several segments separated by kinks. The individual molecular image appears to indicate rod-like structures accompanied by slight structural fluctuations. The longest segment length between the kinks reached ca. 800 nm and the shortest was ca. 150 nm. Such very long segment structures and persistent lengths might be responsible for the unique UV-CD-FL spectroscopic features of rod-like polysilanes that show several cooperative phenomena, such as helix amplification, switching, and memory due to entanglement and disentanglement of multiple main chains. Recently, Furukawa, Ebata and coworkers successfully obtained a similar AFM molecular image of **6**, one end terminus of which had been chemically immobilized onto a crystal Si surface, as well as of other flexible polysilanes immobilized on solid substrates [59].

### 2.5.3

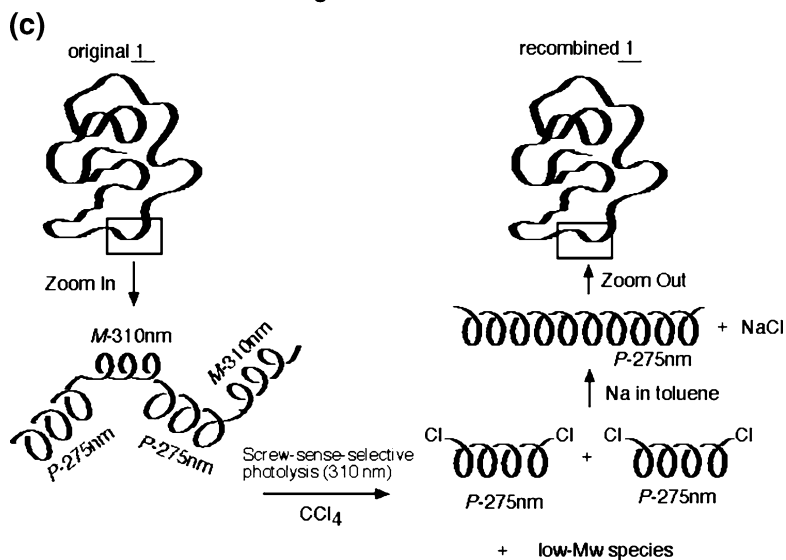
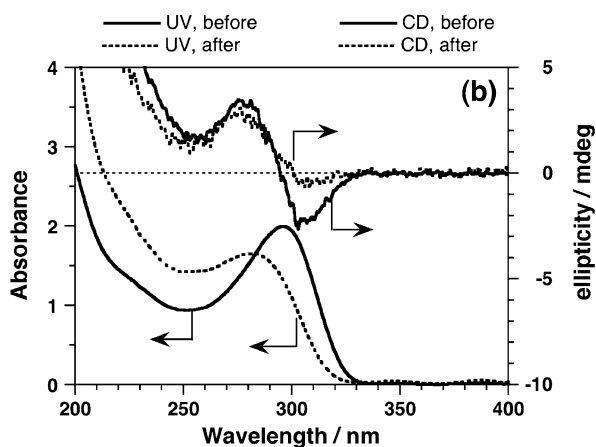
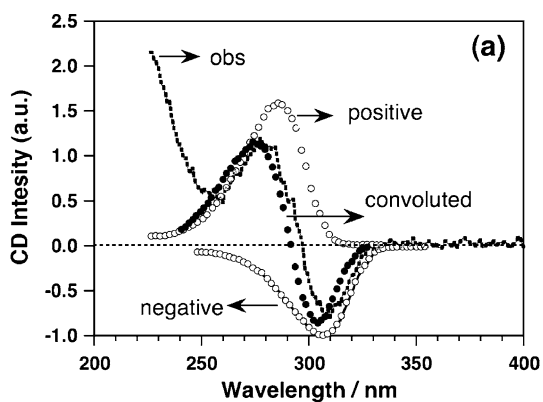
#### **Helix Recombination of Optically Active Helical Polymer with Opposite Screw Senses and Different Screw Pitches**

In a series of poly(alkyl(S)-2-methylbutylsilane)s, only **1** exhibited a very different CD spectrum around the UV absorption at 300 nm [37]: an apparent bisignate CD band with positive and negative signals was observed, as shown in Fig. 6a. From a deconvolutional analysis of the CD, and UV spectra, it was considered that both tight *P*- and loose *M*-helical segments may coexist in the same main chain of **1** in a diastereomeric helical block containing opposite screw senses and different screw pitches. From the Mark-Houwink-Sakurada plot of **1** [39], the  $\alpha$ -value of 0.59 in THF at 30 °C is typical of a coiled global conformation. On the basis of this assumption, a screw-sense-selective “cut-and-paste” experiment allowed a modified **1** to be recombined containing an almost single *P*-screw sense.

The cut-and-paste technique has two steps: (i) *M* (or *P*) screw sense-selective photolysis at the longer  $\lambda_{\max}$  region in  $\text{CCl}_4$  to form *P* (or *M*) screw sense telomeres with Si-Cl termini, and (ii) Na-mediated re-condensation of the telomeres in hot toluene. Formation of an optically active helical polysilane with an almost single screw sense was evidenced by significant changes in the UV and CD spectra after the cut-and-paste technique, as shown in Fig. 6b.

The present knowledge and understanding of **1** may help us to elucidate chiroptical amplification of other optically active polysilanes in isotropic dilute solution, as aggregate forms dispersed in solution, and in a solid film. Indeed, poly(methyl(-)- $\beta$ -pinanylsilane) ((+)-**7**;  $M_w = 10\,200$ ) prepared by Aoki, Oikawa and coworkers showed a bisignate Cotton CD band at 280 and 303 nm, associated with a broad UV absorption at 300 nm in chloroform at





- ◀ **Fig. 6** **a** Original and deconvoluted CD spectra of original **1**, **b** change in UV and CD spectra of original and recombined **1** in isoctane at 25 °C using the “cut-and-paste” technique. **c** key ideas for recombination of **1** with single screw sense from original **1** with diastereomeric helices with opposite screw-sense by the cut-and-paste technique, featuring (i) *M*-screw sense-selective photolysis in CCl<sub>4</sub>, (ii) formation of *P*-screw sense telomers with Si–Cl termini, and (iii) Na-mediated re-condensation of telomers in hot toluene

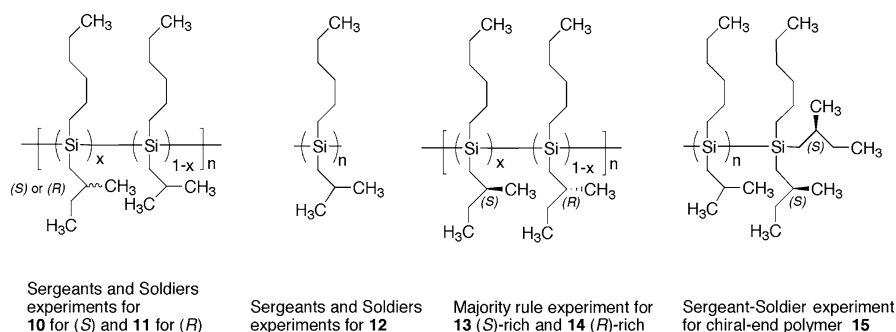
– 15 °C [60]. The spectroscopic similarity between **7** and **1** led to the idea that the main chain of **7** may contain diastereomeric *P*- and *M*-helical segments with opposite screw senses and different screw pitches.

### 3 Helix Amplification of Polysilanes in Solution

#### 3.1 “Sergeants and Soldiers” Experiments in Copolymers with Preferential Screw Sense

As described in the introduction, the most striking cooperative helix amplification featuring a dramatic preferential screw-sense helical ordering in optically active helical copolymers is the “*sergeants and soldiers*” phenomenon named by Green et al. [17, 18]. In this effect, a minority of enantiopure *chiral* side groups determines the overall screw sense (*P* or *M*) of a helical main chain bearing a majority of *achiral* side groups. Since the first report of this phenomenon in poly- $\alpha$ -olefin copolymers by Pino et al. [21], it has also been established in polyisocyanates [17, 18] and polyacetylenes [20]. In 1994, although Möller, Matyjaszewski and coworkers originally prepared two types of copolymers, poly([bis{(S)-2-methylbutyl}silane]-*co*-(di-*n*-pentylsilane)) (**8**) and poly[{(S)-2-methylbutyl-*n*-pentylsilane}-*co*-(di-*n*-pentylsilane)] (**9**) [35], these copolymers revealed an almost linear increment of CD intensity around 320 nm in cyclohexane with increase of the molar fraction of the silicon repeat unit with chiral side chains, indicating no significant *sergeants and soldiers* phenomenon. This may be due to very limited chiral and achiral side chain interactions between flexible di-*n*-pentylsilane and rod-like (S)-2-methylbutyl-*n*-pentylsilane segments, as discussed later.

On the other hand, noticeable helix amplification— *sergeants and soldiers*—was reported in rod-like polysilane copolymers bearing (S)-2-methylbutyl and 2-methylpropyl groups (**10**) and (R)-2-methylbutyl and 2-methylpropyl groups (**11**) in isoctane (Scheme 3). Since the UV-CD spectral features of the polysilane copolymers are almost identical with those of **4–6** and the  $\lambda_{\text{max}}$  varies sensitively with changes in the molar fraction of chiral substituents and temperature [45, 46], the copolymer systems are suitable for testing the *sergeants and soldiers* phenomenon by their CD-UV



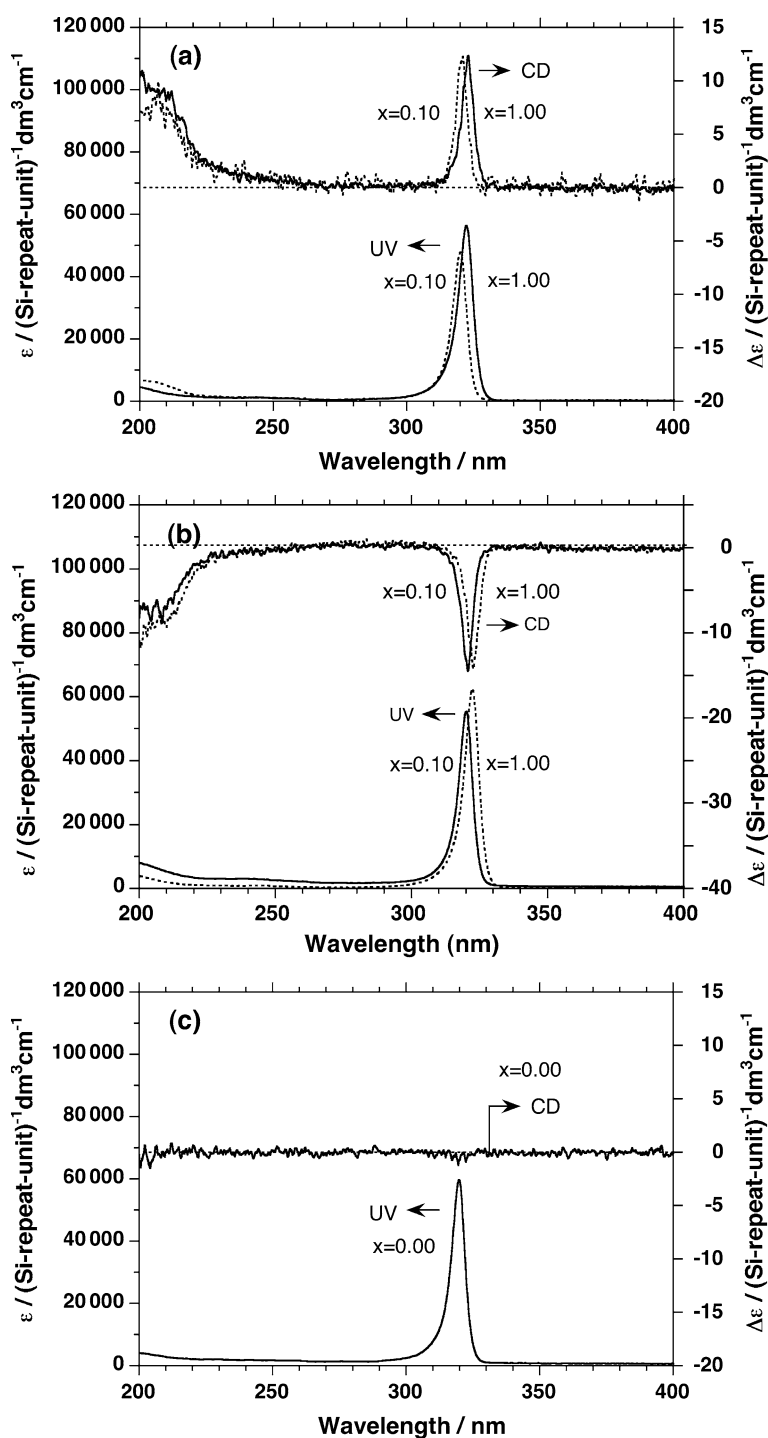
**Scheme 3** Helix amplification experiments for chemical structure of poly(dialkylsilane)s (**10**–**15**) comprising chiral and achiral groups

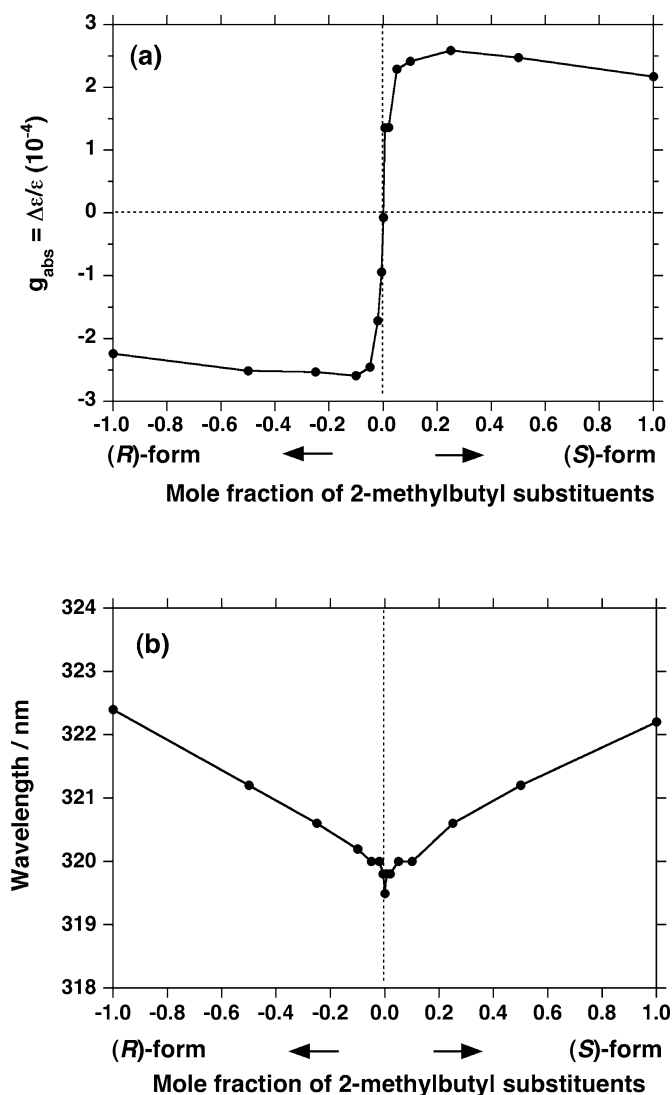
spectra. This may arise from very effective chiral and achiral side chain interactions between *n*-hexyl-(S)-2-methylbutylsilane and rod-like *n*-hexyl-2-methylpropylsilane comonomer segments. Both the comonomer repeating units have commonly  $\beta$ -branched side chains, regardless of chiral and achiral side chains.

Figure 7a compares the UV and CD spectra of homopolymer **4-S** and copolymer **10** with 10 mol % of (S)-2-methylbutyl and 90 mol % of 2-methylpropyl side groups in isooctane at  $-5^\circ\text{C}$ . The UV-CD spectra of **10** are almost identical to those of **4-S**, with the CD signal profile matching the corresponding UV absorption, except for their  $\lambda_{\text{max}}$  values. As expected, the UV and CD spectra of copolymer **11** bearing (R)-2-methylbutyl side groups reveal almost identical features to those in **4-R**, the corresponding antipode of **4-S**, except for the sign of the CD band, as shown in Fig. 9b. For comparison, UV and CD spectra of poly(*n*-hexyl-2-methylpropylsilane) (**12**) in isooctane at  $-5^\circ\text{C}$  are displayed in Fig. 7c. It is evident that UV spectral characteristics ( $\lambda_{\text{max}}$ ,  $\varepsilon$ , and *fwhm*) of all homopolymers **4-S**, **4-R**, **12** and their copolymers **10** and **11** are almost identical, although **12** shows no detectable Cotton CD signals at 320 nm, indicating an equal population of *P*- and *M*- $7_3$  helical segments in the main chain.

Figure 8a plots the  $g_{\text{abs}}$  values in copolymer **10** and **11** as a function of the mole fraction of *n*-hexyl-(S)-2-methylbutylsilane or *n*-hexyl-(R)-2-methylbutylsilane in the copolymers. It is evident that only 5–10 mol % chiral

**Fig. 7** **a** UV and CD spectra of polysilane homopolymer **4-S** (solid lines) and copolymer **10** (dotted lines) containing 10 mol % of (S)-2-methylbutyl and 90 mol % of 2-methylpropyl groups in isooctane at  $-5^\circ\text{C}$ . **b** UV and CD spectra of poly(*n*-hexyl-(R)-2-methylbutylsilane) (**4-R**) (solid lines), which is the antipode of **4**, and copolymer **10** (dotted lines) containing 10 mol % of (R)-2-methylbutyl and 90 mol % of 2-methylpropyl groups in isooctane at  $-5^\circ\text{C}$ . **c** UV and CD spectra of poly(*n*-hexyl-2-methylpropylsilane) (**12**) in isooctane at  $-5^\circ\text{C}$





**Fig. 8** Values of **a** dissymmetry ratio ( $g_{\text{abs}}$ ) and **b**  $\lambda_{\text{max}}$  in a series of copolymer **10** and **11** as a function of mole fraction of *n*-hexyl-(*S*)-2-methylbutylsilane and *n*-hexyl-(*R*)-2-methylbutylsilane in isooctane at  $-5\text{ }^{\circ}\text{C}$

moieties in **10** and **11** almost completely determines the screw sense. Moreover, even as little as 0.6 mol % of chiral side groups induces a marked preferential screw sense helical conformation in the copolymers at temperatures below  $0\text{ }^{\circ}\text{C}$ . The greater flexibility of the di-*n*-pentylsilane moieties might be responsible for the lack of a *sergeants and soldiers* effect in **8** and **9**, since the  $\alpha$  value of poly(di-*n*-pentylsilane) may be similar to that of random coil poly(di-*n*-butylsilane)

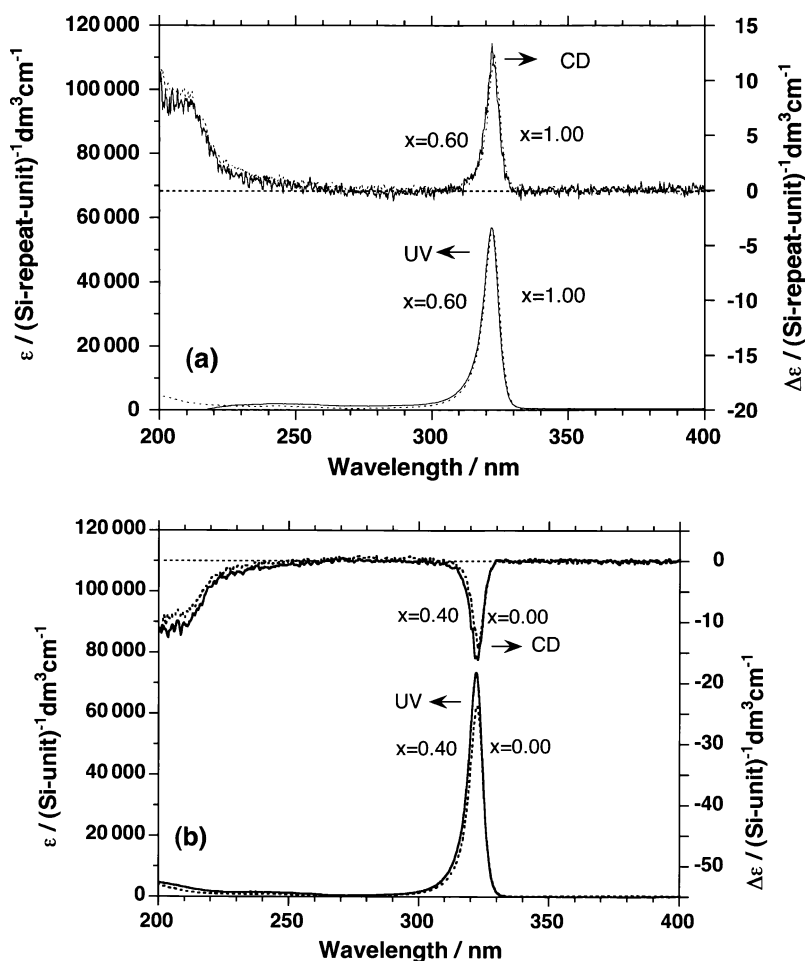


**Fig. 9** **a** UV and CD spectra of polysilane homopolymer **4-S** (solid lines) and copolymer **13** (dotted lines) containing 60 mol % of *n*-hexyl-(*S*)-2-methylbutylsilane and 40 mol % of *n*-hexyl-(*R*)-2-methylbutylsilane in isoctane at  $-5^{\circ}\text{C}$ . **b** UV and CD spectra of polysilane homopolymer **4-R** (solid lines) and copolymer **14** (dotted lines) containing 60 mol % of *n*-hexyl-(*R*)-2-methylbutylsilane and 40 mol % of *n*-hexyl-(*S*)-2-methylbutylsilane in isoctane at  $-5^{\circ}\text{C}$

( $\alpha \sim 0.71$ ) and poly(di-*n*-hexylsilane) ( $\alpha \sim 0.74$ ) [39]. Structural similarity between chiral and branched achiral side groups and a stiffer main chain in copolymer systems may be needed to reveal effective *sergeants and soldiers* cooperativity. In our case, because all mother homopolymers, **4-S**, **4-R**, and poly(*n*-hexyl-2-methylpropylsilane) (**12**), can adopt rod-like helical conformation in solution at room temperature suggested from high viscosity indices of 1.2–1.3 [39], these rod-like natures might be responsible for marked *sergeants and soldiers* helix amplification in their copolymer systems.

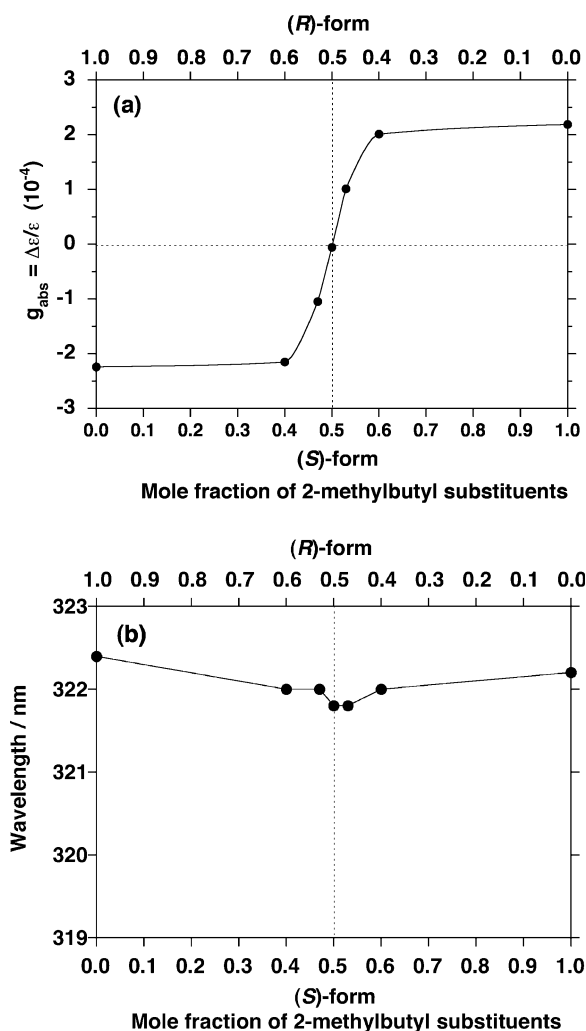


**Fig. 10** The values of **a** dissymmetry ratio ( $g_{\text{abs}}$ ) and **b**  $\lambda_{\text{max}}$  in a series of copolymer 13 as a function of the mole fraction of *n*-hexyl-(*S*)-2-methylbutylsilane and *n*-hexyl-(*R*)-2-methylbutylsilane in isooctane at  $-5^\circ\text{C}$

Figure 8b plots the  $\lambda_{\text{max}}$  values of **10** and **11** as a function of the molar fraction of *n*-hexyl(*S*)-2-methylbutylsilane or *n*-hexyl(*R*)-2-methylbutylsilane. The value of  $\lambda_{\text{max}}$  redshifts slightly, but progressively, with increase in the fraction of the silane with chiral side chains in the copolymers. These features are associated with a decrease in screw-pitch of the main chain, because the  $\text{Si}\sigma-\text{Si}\sigma^*$  absorption is shown from ab initio calculations [45] to blueshift progressively with change in the main chain dihedral angle from planar all-anti ( $180^\circ$ ) to  $4_1$  helix ( $60^\circ$ ) [52].

### 3.2

#### **"Majority Rule" Experiments in Copolymers with Preferential Screw Sense**

The other significant cooperative helix amplification in preferential helical screw-sense ordering of optically active copolymers is the *majority rule* phenomenon [17, 18]. In this case, the screw sense of a helical main chain with nonracemic chiral side groups is controlled by the ee only of the side groups. Since this phenomenon was first reported from poly- $\alpha$ -olefins made of vinyl co-monomers bearing nonenantiopure chiral moieties by Pino et al. [21], this *majority rule* has been established in stiff polyisocyanates bearing a non-racemic chiral side chain [17, 18]. Similarly, noticeable *majority rule* effects were found in rod-like polysilane copolymers **13** and **14** containing (S)- and (R)-2-methylbutyl side groups in different proportions [45].

A comparison of the UV and CD spectra between homopolymer **4** and copolymer **13** with 60 mol % of (S)- and 40 mol % of (R)-2-methylbutyl side groups (20% (S)-ee) in isooctane at  $-5^{\circ}\text{C}$  is shown in Fig. 9a. The UV and CD spectra of **13** are almost identical to those of **4**, the CD peak profile almost matching the corresponding UV absorption, including their  $\lambda_{\text{max}}$  values. As expected, the UV and CD spectra of the corresponding (R)-rich **14** copolymer containing 40 mol % of (S)- and 60 mol % of (R)-2-methylbutyl side groups (20% (R) ee) exhibit almost identical features to those in the (S)-rich **13** copolymer, except for the sign of the CD band, as shown in Fig. 9b.

As shown in Fig. 10a, from the plot of the  $g_{\text{abs}}$  values of **13** as a function of the molar fraction of *n*-hexyl-(S)-2-methylbutyl or *n*-hexyl-(R)-2-methylbutylsilane, it is evident that only 20% ee of (R)- or (S)-2-methylbutyl group in **13** completely determines the overall screw sense and even only 6% ee of (R)- or (S)-2-methylbutyl group induces a significant preferential screw sense helical conformation in the copolymers. The structural identity between the (S)- and mirror image (R)-chiral side group in the stiffer main chain of the copolymer systems appear essential to induce an effective *majority rule* phenomenon. Also, as shown in Fig. 10b, from the plot of the  $\lambda_{\text{max}}$  value of **13** and **14** as a function of the molar fraction of *n*-hexyl-(S)-2-methylbutylsilane or *n*-hexyl-(R)-2-methylbutylsilane, the value of  $\lambda_{\text{max}}$  is very weakly blueshifted, though the ee value of *n*-hexyl-2-methylbutylsilane changes from 100% to 0% ee in the copolymers, indicating minimal change in the screw-pitch of the main chain, in accordance with the ab initio calculation [61].

### 3.3

#### **"Sergeants and Soldiers" Experiments in Homopolymer Bearing Chiral Termini**

Kira and coworkers described the first single crystal X-ray structure, CD and UV spectra of hexasilane oligomers with preferential screw sense induced



by cooperativity between achiral side chains and chiral chain termini and also extended the cooperativity system to high molecular weight poly(di-*n*-hexylsilane) with the same chiral termini [62]. Their works provide important experimental evidence for the adoption of a  $15_7$  helical conformation in solution at lower temperature, which was long believed to adopt an all-anti conformation in solution [52, 54]. Apparent bisignate Cotton effects observed for the oligomers below 153 K and the polymers below 233 K are interpreted in terms of an exciton couplet for spatially interacting polysilane chromophores [51]. They led to the idea that this polysilane at low temperatures is composed of loose helical segments divided by one-handed approximately  $90^\circ$  preferential kinks.

An intriguing chiral termini effect in rod-like poly(*n*-hexyl-(2-methylpropyl)silane) with (*S*)-2-methylbutyl termini (**15**) was also reported [63]. Although the value of  $g_{\text{abs}}$  is only  $+1 \times 10^{-5}$  which indicates a weak helix amplification with a preferential screw sense in **15**, it is noted that the preferential screw sense of **15** was opposite to that of **4-S** bearing the same (*S*)-2-methylbutyl side groups.

## 4 Helix Switching of Polysilane in Solution

### 4.1 Preferential Screw Sense Switching in Homopolymers

The design and controlled synthesis of helical polymers with dynamic properties are currently challenging issues. Successful polymer systems include polyisocyanates and certain recently established polyacetylenes bearing aryl and alkyl ester moieties. However, the most striking helix amplification phenomenon of a helical polymer may be preferential screw sense switching controlled by physical and/or chemical biases, as a consequence of the opposite directions in helix amplifications [64, 65]. This intriguing phenomenon was called *helix-helix* (*PM*) transition in response to external physical and/or chemical stimuli, affording almost mirror-image helical motifs. Although, in 1968 and 1972, biochemists originally discovered this phenomenon and recently in synthetic DNA (driven by a change in NaCl concentration) [64], poly(*L*-aspartic acid ester)s (driven by changes in temperature and organic acid) [65], and a calf thymus DNA [66], several synthetic polymers [67–71] have been found to undergo a *PM*-transition. This might be due to limited knowledge and understanding of the nature of *PM*-transition characteristics. Recently, it was demonstrated that, by controlling their composition and side chains, certain poly(dialkylsilane) homopolymers and copolymers [40, 41, 47] and a poly(diarylsilane) copolymer [72] undergo a thermo-driven *PM*-transition in solution state. This section highlights

the poly(dialkylsilane)s for quantitatively discussing thermo-responsive *PM*-transition characteristics.

Poly{(S)-3,7-dimethyloctyl-3-methylbutylsilane} (16) may be classified as a rod-like helical main chain polymer bearing enantiopure alkyl side groups. The polymer affords an intense, narrow UV absorption band, completely matching the corresponding CD and FL band mirror image profiles, similar to the rigid rod-like helical polysilanes described above. The occurrence of the

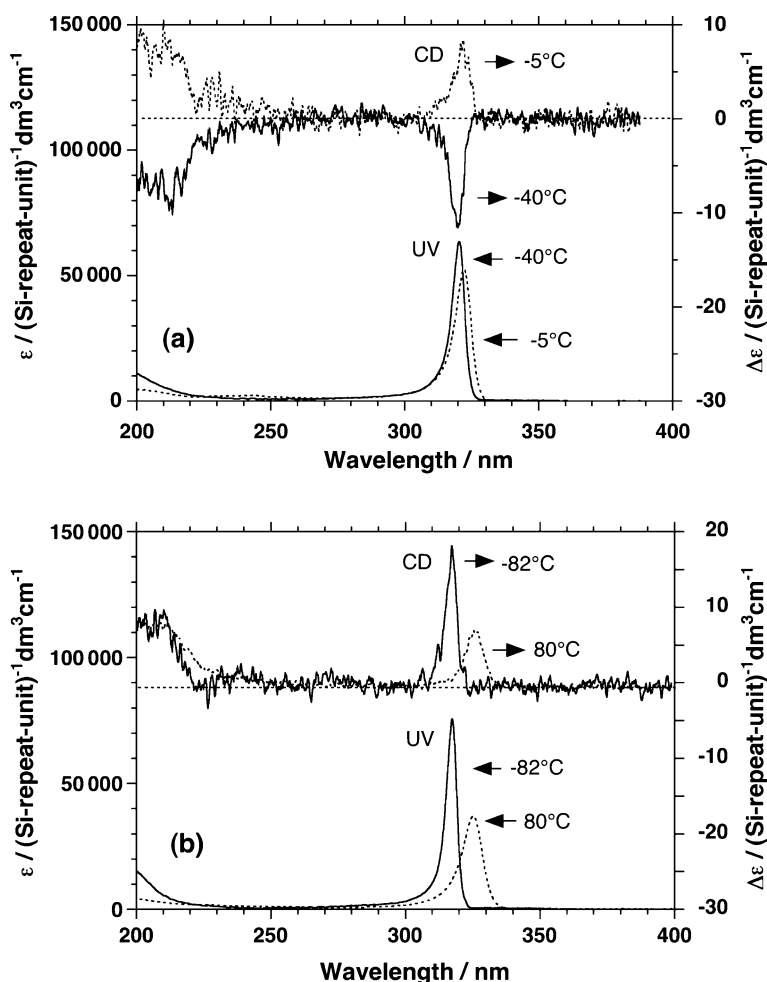
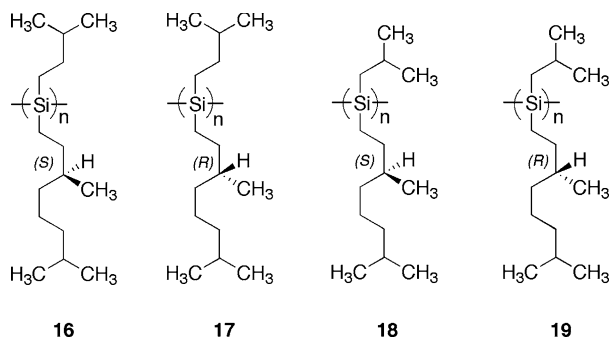


**Fig. 11** **a** CD and UV absorption spectra of poly{(S)-3,7-dimethyloctyl-3-methylbutylsilane} (16,  $M_w = 1.6 \times 10^6$  and  $M_w/M_n = 1.53$ ) at  $-40^\circ\text{C}$  (solid line) and  $-5^\circ\text{C}$  (dotted line) in isoctane; **b** CD and UV absorption spectra of poly{(S)-3,7-dimethyloctyl-2-methylpropylsilane} (18,  $M_w = 4.2 \times 10^4$  and  $M_w/M_n = 1.51$ ) at  $-82^\circ\text{C}$  (solid line) and  $80^\circ\text{C}$  (dotted line) in isoctane

*PM*-transition is spectroscopically detectable as an inversion of the CD band profile. Figures 11a and 11b compare the CD and UV absorption spectra of **16** at  $-40$  and  $-5$  °C and of poly{(*S*)-3,7-dimethyloctyl-2-methylpropylsilane} (**18**) at  $-82$  and  $+80$  °C in isooctane. The positive-signed CD spectrum of **16** with  $\lambda_{\text{ext}}$  of 320 nm at  $-40$  °C is almost the inverse of the negative-signed CD spectrum with  $\lambda_{\text{ext}}$  of 322 nm at  $-5$  °C. It is evident that **16** undergoes a *PM*-transition between the two temperatures, though the helical motifs at  $-40$  and  $-5$  °C are energetically and spectroscopically nonequivalent. On the other hand, neither **18** nor its mirror-image poly{(*R*)-3,7-dimethyloctyl-2-methylpropylsilane} (**17**) undergo any such inversion of the CD spectra in isooctane between  $-90$  and  $+80$  °C.



**Scheme 4** Polysilanes bearing (*S*)- or (*R*)-3,7-dimethyloctyl side groups

Moreover, introduction of additional silane with chiral/achiral side groups to the **16**-based copolymers permits fine control of the transition temperature ( $T_c$ ) between  $-64$  and  $+79$  °C. These results may open new methodologies in designing *PM*-transition polymers that may be promising in diverse screw-sense related applications, such as thermo-driven chiroptical switch and memory, a thermo-driven switching chiral separation column, and molecular recognition ability.

Polysilanes **6**, **16**, and **18** can adopt rod-like  $7_3$ -helical conformations (dihedral angle of ca.  $150^\circ$  or  $210^\circ$ ) in solution, because the  $\lambda_{\text{max}}$  near 320 nm is almost identical to that of poly(di-*n*-butylsilane) (**19**) adopting a  $7_3$ -helical form in the solid state [52]. The rod-like behavior of these materials is evidenced by the high values of  $\alpha$ ; for **16** and **18** in  $\text{CHCl}_3$  at  $30$  °C, the  $\alpha$  values reached 1.11 and 1.29, respectively, and for **6** in THF at  $30$  °C, the  $\alpha$  value was 1.35. However, **16** (and **17**), might be more flexible than **18** (and **19**), according to the following  $^{29}\text{Si}$  NMR results.

Figure 12 displays the  $^{29}\text{Si}$  NMR spectra of **16**, **18**, and **6** in  $\text{CDCl}_3$  at  $30$  °C. Since these polysilanes have two different types of side groups attached to the main chain, they may essentially comprise isotactic (*it*-), syndiotactic (*st*-), and heterotactic (*ht*-) sequences. Nevertheless, both **16** and **18** exhibit single

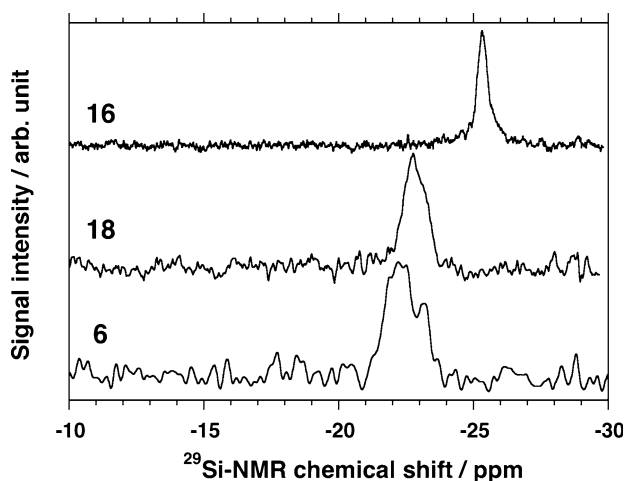


**Fig. 12** Comparison of  $^{29}\text{Si}$  NMR spectra between (*top*) poly{(S)-3,7-dimethyloctyl-3-methylbutylsilane} (**16**), (*middle*) poly{(S)-3,7-dimethyloctyl-2-methylpropylsilane} (**18**), and (*bottom*) poly(*n*-decyl-(S)-2-methylbutylsilane) (**6**) in  $\text{CDCl}_3$  at  $30^\circ\text{C}$

$^{29}\text{Si}$  NMR signals near  $-23$  to  $-25$  ppm, implying mainly *it*- or *st*-sequence. On the other hand, **6** exhibits a major signal at  $-22.2$  ppm and a weak signal at  $-23.1$  ppm, suggesting an almost single configurational sequence with a minor fraction of another sequence in the same main chain. A marked difference in  $^{29}\text{Si}$  NMR linewidth ( $\nu_{1/2}$ ) between **16**, **18**, and **6** is evident. The greater flexibility of **16** compared to **18** and **6** is suggested by the narrower  $\Delta\nu_{1/2}$ : for **16**,  $\nu_{1/2} = 29$  Hz at  $-25.3$  ppm, while for **18**,  $\nu_{1/2} = 65$  Hz at  $-22.7$  ppm and for **6**,  $\nu_{1/2} = 90$  Hz at  $-22.3$  ppm. Although homopolymers bearing two  $\gamma$ -branched side groups per repeat unit can undergo a *PM* transition, polymers with a combination of  $\beta$ - and nonbranched side groups do not undergo a *PM*-transition. Subtle modification in the side groups of polysilanes definitively determines the capability of the *PM*-transition and CD inversion characteristics.

From the temperature dependency of the  $\lambda_{\text{ext}}$ ,  $\lambda_{\text{max}}$ , and intensities of  $\Delta\varepsilon$  and  $\varepsilon$  of **16** and **18** in isoctane, it is evident that the  $\lambda_{\text{ext}}$  and  $\lambda_{\text{max}}$  values of **16** and **18** linearly blue-shift from 325 to 318 nm, and the  $\varepsilon$  values of **16** and **18** increase monotonically from 40 000 to 80 000, as the temperature decreases from  $+80$  to  $-82^\circ\text{C}$ . The former may be ascribed to a slight decrease in screw-pitch, deviating from an ideal  $7_3$ -helical structure, and the latter is due to a progressive increase in dimension of the main chain. The  $\Delta\varepsilon$  value of **16** monotonically, however, increases from ca. 3 at  $80^\circ\text{C}$  to ca. 8 at  $-5^\circ\text{C}$ , and goes to zero abruptly at  $-20^\circ\text{C}$ , and then decreases monotonically to ca.  $-15^\circ\text{C}$ , while that of **18** monotonically increases from 7 to 18. Mutual cancellation of positive and negative CD signals is indeed occurring at  $T_c$ , resulting from an equal population of *P*- and *M*-motifs with the same  $\lambda_{\text{ext}}$  and  $\lambda_{\text{max}}$  values.

To quantitatively characterize the *PM*-populations using chiroptical characteristics, it is useful to use the  $g_{\text{abs}}$  values of **16** at each temperature with reference to the regression curve of these  $g_{\text{abs}}$  values in **18** adopting a purely *P*-7<sub>3</sub> helical structure, in place of the  $\Delta\varepsilon$  value. The analysis is based on the assumption that the weak temperature dependence of the  $g_{\text{max}}$  for **18** is due to a minute modification in the screw-pitch of the *P*-helix, rather than any formation of the opposite *M*-helical motif.

Figure 13 plots the temperature dependence of the dissymmetry ratios and the *PM*-populations in three different samples of **16** with different  $M_w$

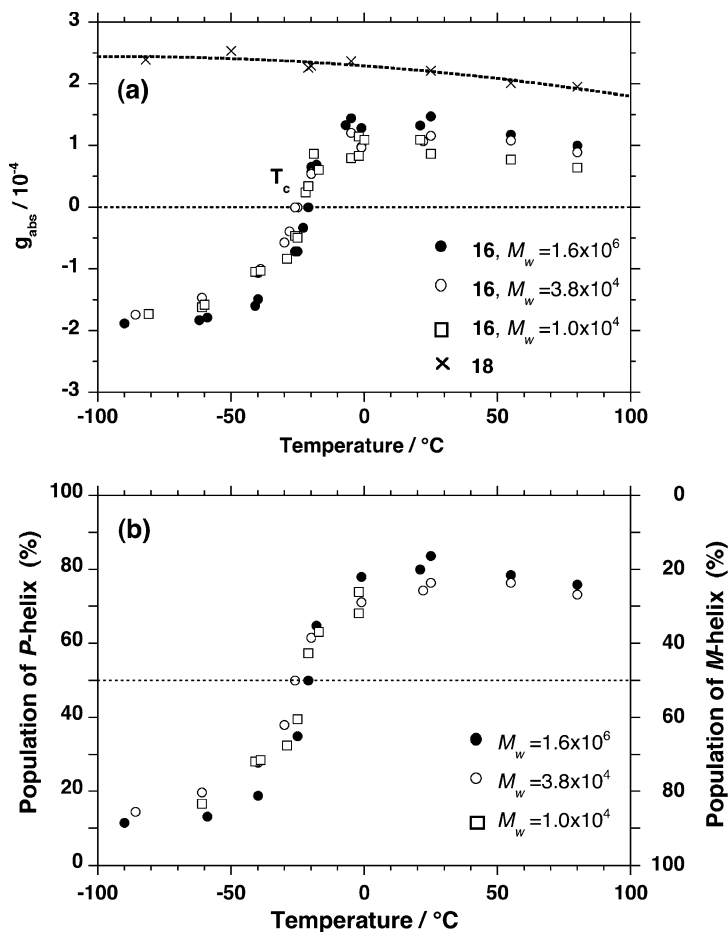


**Fig. 13** **a** Temperature dependent dissymmetry ratios of poly{(S)-3,7-dimethyloctyl-3-methylbutylsilane} (**16**) (three different  $M_w$  samples) and poly{(S)-3,7-dimethyloctyl-2-methylpropylsilane} (**18**) (assumed to be a purely *P*-helix) in isooctane. **b** Temperature dependent *P*- and *M*-populations of **16** in isooctane by reference to the regression  $g_{\text{abs}}$ -Temp curve of  $g_{\text{abs}}$  values in **18**

in isoctane based on the above analysis. Although the *PM*-populations in the three samples depend slightly on  $M_w$ , a steep *PM*-transition clearly occurs at  $-20\text{ }^{\circ}\text{C}$ . The highest  $M_w$  polymer contains 12% *P*- and 88% *M*-motifs at  $-90\text{ }^{\circ}\text{C}$ , while these values are 84% *P*- and 16% *M*-motifs at  $25\text{ }^{\circ}\text{C}$ . The medium and lower  $M_w$  samples contain 15% *P*- and 85% *M*-motifs at  $-90\text{ }^{\circ}\text{C}$ , while at  $25\text{ }^{\circ}\text{C}$  these values are 76% *P*- and 24% *M*-motifs. The transition temperature width ( $\Delta T_c$ ), however, tends to slightly broaden as  $M_w$  decreases. It is concluded that the *PM*-transition characteristics including  $T_c$ ,  $\Delta T_c$ , and *PM*-populations weakly depend on the molecular weight, and the *PM*-transition characteristics may vary with segment length, for segments shorter than 50 silicon repeat units and/or the nature of the chiral termini.

Although the intrinsic origin of the *PM*-transition remains obscure, the subtle differences in potential energy curves and main chain stiffness between **16** and **18** may be critical. Figure 14 compares the main chain dihedral angle dependence on the potential energy of (S)-3,7-dimethyloctyl-3-methylbutylsilane (31 repeat units with hydrogen termini) (**20**) and (S)-3,7-dimethyloctyl(2-methylpropyl)silane (31 repeat units with hydrogen termini) (**21**) for their *it*- and *st*-sequences, respectively. An *it*-**20** clearly shows a double-well potential curve, i.e. two local energy minima with almost enantiomeric helices at dihedral angles of *P*- $157^{\circ}$  and *M*- $210^{\circ}$ . The global minimum *M* is slightly more stable than that of *P* by ca. 0.67 kcal per repeat unit and the barrier heights of the *M*- and *P*-screw senses are 2.3 and 1.7 kcal per repeat unit, respectively.

*St*-**20** also has a similar double-well potential curve at ca. *P*- $160^{\circ}$  and *M*- $200^{\circ}$  dihedral angles and the global minimum *M* is slightly more stable than the corresponding *P* by ca. 1.3 kcal per repeat unit. The barrier heights for the respective *M*- and *P*-screw senses are ca. 4.6 and 3.4 kcal per repeat unit. The calculation of **21** suggests that both pseudo-enantiomeric *P*- and *M*-motifs are likely to stably coexist in the same main chain at any temperature, regardless of tacticity and molecular weight.

Contrarily, *it*-**21** shows an unclear double-well potential curve with minima at dihedral angles of ca. *P*- $160^{\circ}$  and *M*- $200^{\circ}$ . The *P*-helix is much more stable compared to the corresponding *M* by ca. 2.3 kcal per repeat unit. The barrier heights of the respective *M* and *P* are ca. 3.9 and 1.4 kcal per repeat unit, leading to the idea that *P*-helix might be more stable. An *st*-**21** has an almost single well potential curve with dihedral angles of *P*- $160^{\circ}$ . These calculations assume that the *P*-motifs of **16** and **18** are more stable at all temperatures, regardless of tacticity, while the *M*-motifs of **17** and **19** are more stable at all temperatures, as expected.

By using very simple energy parameters of the *P*- and *M*-states of **20** and **21**, the origin of the *PM*-transition may be discussed. Here,  $\Delta G$  is the difference in free energy between the *P*- and *M*-states. Similarly,  $\Delta H$  and  $\Delta S$  are the differences in enthalpy and entropy between the *P*- and *M*-states,

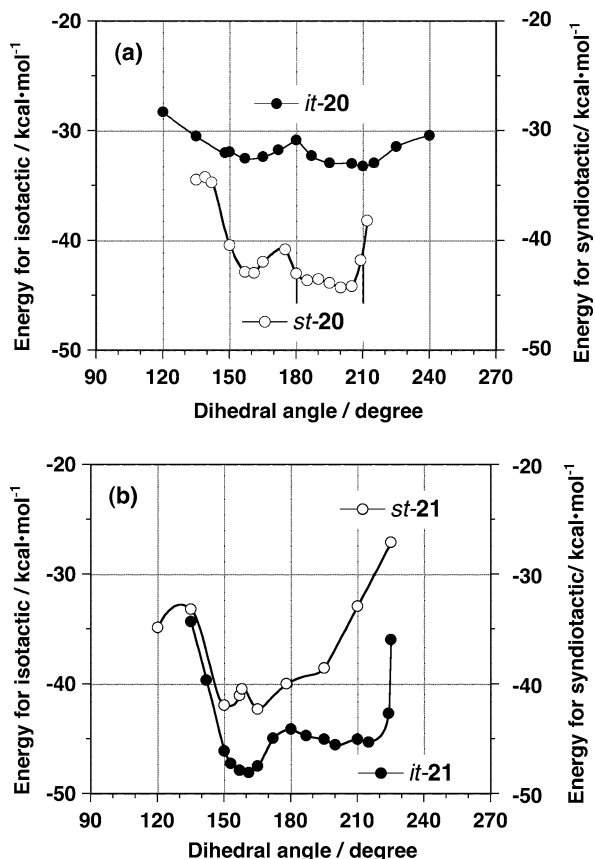


**Fig. 14** Results of molecular mechanics calculation. Main chain dihedral angle dependence on the potential energy of **a** *it*- and *st*-(S)-3,7-dimethyloctyl-3-methylbutylsilane 31 repeat units with hydrogen termini (20), and **b** *it*- and *st*-(S)-3,7-dimethyloctyl-2-methylpropylsilane 31 repeat units with hydrogen termini (21)

respectively.

$$\Delta G = G_P - G_M = \Delta H - T\Delta S = H_P - H_M - T(S_P - S_M), \quad (1)$$

$$\text{where } \Delta H = H_P - H_M, \quad \Delta S = S_P - S_M \quad (2)$$

$$\text{at } T_c, \Delta G = 0, \quad \text{then } T_c = \Delta H / \Delta S. \quad (3)$$

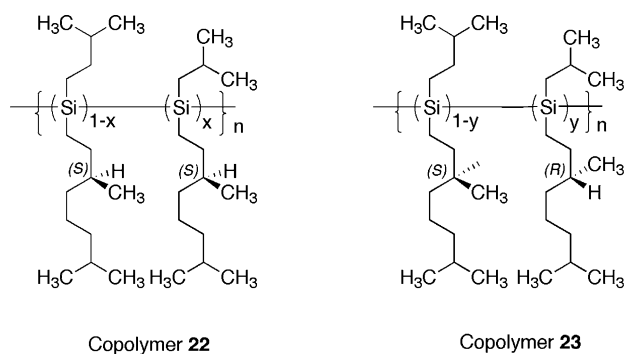
Using the values of  $T_c = 253$  K from 16 and  $\Delta H = -0.67$  kcal per repeat unit for its model 20,  $\Delta S = -2.6$  cal K<sup>-1</sup> at  $T_c$ . Since the sign of the  $\Delta G$  term below  $T_c$  is negative, *P* is more stable than *M*, and vice versa. To design a thermo-driven *PM*-transition polysilane for switching at a desired temperature, it seems to be essential that the polysilane has a double-well potential curve, small  $\Delta H$ , and small potential barrier height. If the  $\Delta S$  term is responsible for the inver-

sion of preferential screw-sense, *P*-polysilane in a low entropy state below  $T_c$  may have a highly ordered packing structure of side groups, whereas *M*-polysilane in a high entropy state above  $T_c$  may be in a disordered arrangement of side groups. Entropy considerations may need to consider polymer-solvent interactions.

## 4.2

### Controlled Helix Switching in Copolymers

Semi-empirical understanding of *PM*-transition characteristics and main chain stiffness of rod-like polysilanes thus leads to the new idea that minute structural modification of the achiral and chiral alkyl side groups could critically modify the transition characteristics, as indeed demonstrated in a series of **16**-based copolymers, poly{((*S*)-3,7-dimethyloctyl-3-methylbutylsilane)-*co*-((*S*)-3,7-dimethyloctyl-2-methylpropylsilane)} (**22**) and poly{((*S*)-3,7-dimethyloctyl-3-methylbutylsilane)-*co*-((*R*)-3,7-dimethyloctyl-2-methylpropylsilane)} (**23**) (see Scheme 5).



**Scheme 5** Chemical structures of poly(dialkylsilane) copolymers (**22** and **23**) with *helix-helix* transition ability

Figure 15 shows the temperature dependence of the  $g_{\text{abs}}$  values and *PM*-populations in **22** (with 80 mol % of **16** and 20 mol % of **18**), **16**, and **23** (with 80 mol % of **16** and 20 mol % of **19**) in isoctane between  $-82$  and  $+80$  °C. It is evident that, compared to the  $T_c$  of **16**, that of **22** containing two identical (*S*)-chiral side groups is lower by  $16$  °C, whereas that of **23** containing the opposite (*S*)- and (*R*)-chiral side groups is higher by  $16$  °C. The CD spectral profile for the respective copolymers still matches the corresponding UV absorption spectrum at all temperatures. When **18** or **19** moieties were introduced to pure **16**, the  $\Delta T_c$  value increased due to the randomness of the two silane repeat units in the same copolymers.

Figure 16 plots the values of  $T_c$  and  $\Delta T_c$  as a function of the molar fraction of **18** in **22**, and **19** in **23**. It is obvious that, as the molar fraction of **18**



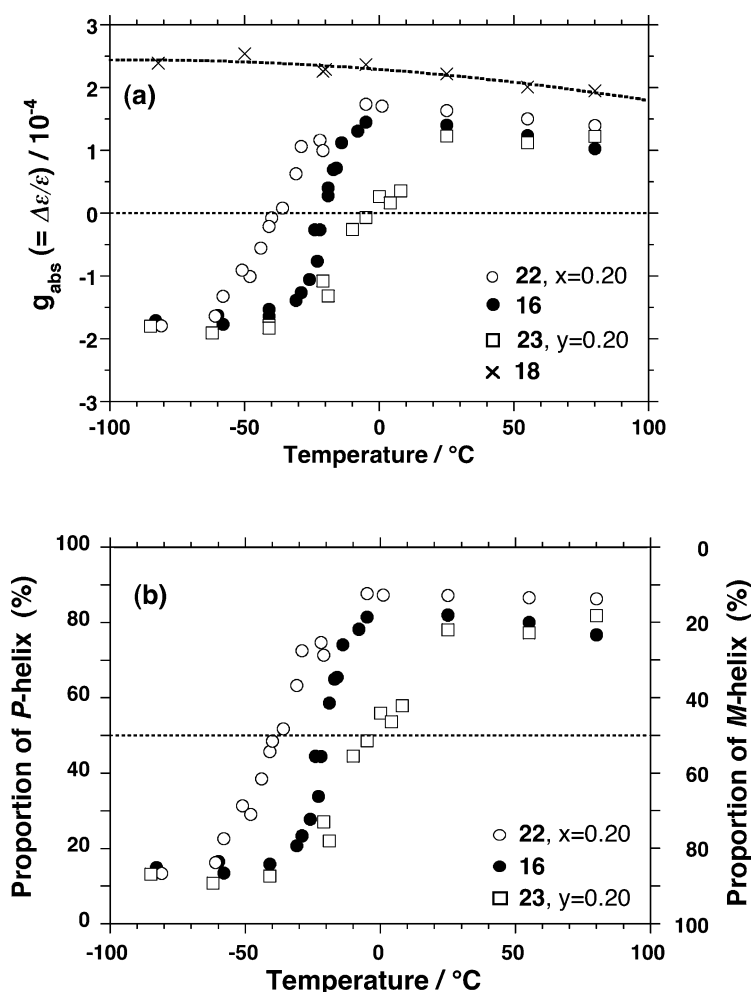


**Fig. 15** **a** Temperature-dependent  $g_{\text{abs}}$  values of 22 (with 80% of 16 and 20% of 18,  $M_w = 5.0 \times 10^4$ , open squares), 16 ( $M_w = 3.8 \times 10^4$ , filled circles), 23 (with 80% of 16, 20% of 19,  $M_w = 4.8 \times 10^4$ , open circles), and 18 ( $M_w = 4.2 \times 10^4$ , crosses and solid curve) in isooctane. **b** Temperature-dependent populations of P(%) and M(%) of the 22, 16, and 23 samples in isooctane by reference to the regression curve of  $g_{\text{abs}}$ -Temp values in 18

in 22 and 19 in 23 increases, the value of  $T_c$  changes nonlinearly from  $-64$  to  $+79$  °C and the value of  $\Delta T_c$  broadened nonlinearly. It was clarified in a PM-transition mechanistic study that was carried out from the viewpoint of linear chain cooperative transition theory [56, 73], as well as demonstrated in stiff poly(alkyl isocyanate) copolymers [69], that the existence of two local free energy minima with respect to the helical dihedral angle and entropy term in the free energy stability might be responsible for the transition characteris-

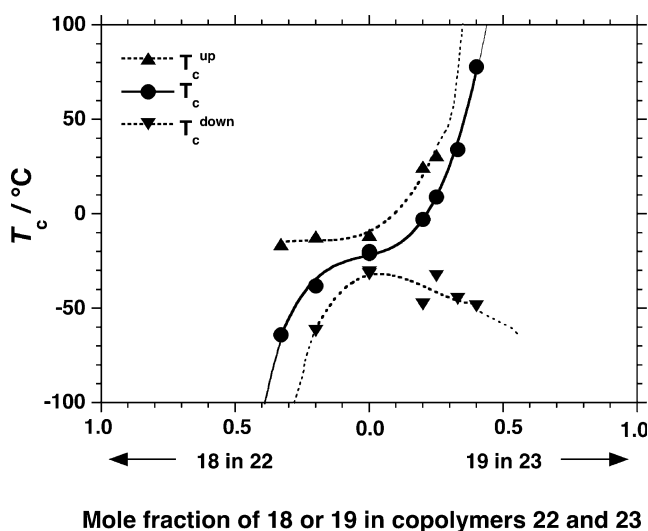


**Fig. 16** Values of  $T_c$  and  $\Delta T_c$  as a function of mole fraction of 18 in 22, and 19 in 23 in isooctane. The  $M_w$  values in all the copolymers ranged from  $8.5 \times 10^4$  to  $3.5 \times 10^4$

tics. In addition, the coexistence of *P*- and *M*-motifs in the same main chain at any temperature, even sufficiently below  $T_c$  or above  $T_c$ , may be essential for the polymers ability to undergo the *PM*-transition.

### 4.3

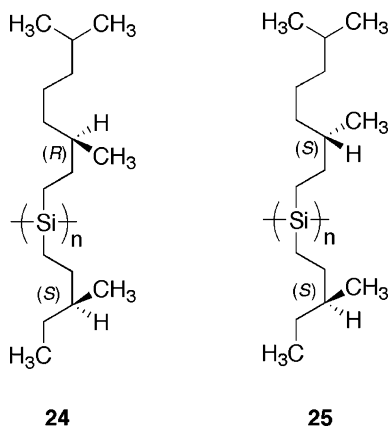
#### Quantized and Superposed Helicity

A knowledge and understanding on the nature of the helix switching may be helpful in designing *PM*-transition capability and characteristics in diverse screw-sense inversion related applications, such as: chiroptical switches and memory, switchable chiral separation columns, molecular recognition and molecular motor applications.

Designing and realizing nano-scale computing devices are now the most challenging issues in nanoscience and nanotechnology. An optically active molecular switch and memory with bi- and multi-stable switching function associated with molecular motions such as twist, rotate, fold, shrink, stack, and shuttle may be candidates as basic elements in these devices. Generally, great problems remain in the design and manufacture of such molecular elements, due to difficulties in the wiring of these elements with functions of “memory and storage”, defining thresholds, processing, and error corrections. To date, understanding and measuring the superposition of quantum states in nano-systems based on semiconductors and superconductors directed towards the realization of quantum computing have been achieved theoretically and experimentally [74, 75]. If the essence of “quantum com-

puting” is the controlled mixing of two quantum states by physical and/or chemical biases [76], this may serve as important research in the realm of molecular and polymer sciences. Before these boom studies, several quantum physicists and chemists had already discussed quantum tunnelling and oscillation [78], and the preparation and detection of superposed optical activity for a hypothetical chiral molecule with a double-well potential using an ultra-short light pulse [76], although they had not extended these ideas to the possibility of chiral molecule-based quantum computing.

As noted earlier, it is reasonable to use the dimensionless parameter to quantitatively evaluate the *PM*-population of **24** and **25** in solution by reference to the regression curve of the  $g_{\text{abs}}$  values for **18**, which is assumed to be in a purely *P*-motif over the temperature range, although the temperature dependence of the  $g_{\text{abs}}$  values in **18** shows a slight change in screw-pitch. Variable temperature  $g_{\text{abs}}$  values and the proportion of *P*- and *M*-motifs of **24**, **25**, and **18** in isooctane between  $-80$  and  $80$  °C are plotted in Figs. 17a and 17b. It is evident that **24** features three distinct switching regions; 1 ( $-80$  to  $-10$  °C), 2 ( $-10$  to  $+10$  °C), and 3 ( $+10$  to  $+80$  °C). Polymer **24** in region 1 contains a constant 80% *P* and 20% *M* (60% *P* excess over *M*), but contrarily in region 3, it has 80% *M* and 20% *P* (60% *M* excess over *P*). However, **25** invariably contains 80% *P* and 20% *M* (60% *P* excess) over the entire temperature range. This behavior may be related to greater differences seen in the potential energy curve between **24** and **25**.



**Scheme 6** Chemical structures of flexible rod-like helical polysilanes bearing 3,7-dimethyloctyl ((*S*)- and (*R*)-forms) and (*S*)-3-methylpentyl side groups

This led to the idea that see-saw-like switching states between region 1 and 3 may be quantized as the stationary state of *P*- and *M*-superposition, but not due to the transition between 100% pure *P*- and 100% pure *M*-states. These switching properties may be interpreted as the consequence of the superpo-

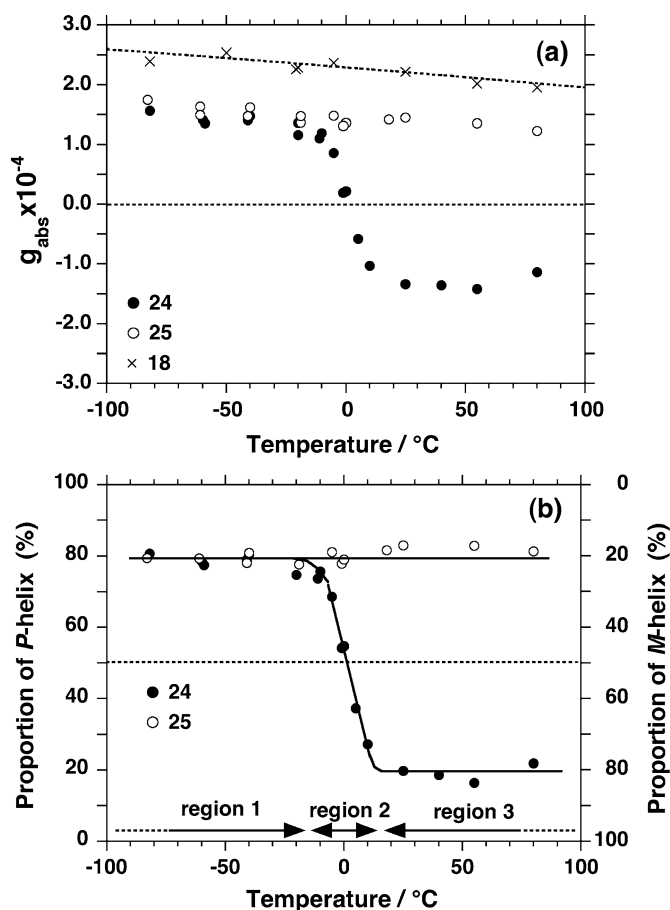


**Fig. 17** **a** Variable temperature  $g_{\text{abs}}$  values of **24** ( $M_w = 5.8 \times 10^6$ ,  $M_n = 3.4 \times 10^6$ , filled circles), **25** ( $M_w = 4.7 \times 10^6$ ,  $M_n = 2.1 \times 10^6$ , open circles), and **18** (crosses) in isooctane in the range of -80 and +80  $^{\circ}\text{C}$ . **b** Proportion of P- and M-motifs of **24** (filled circles) and **25** (open circles) as a function of solution temperature

sition of P- and M-helicities. Presumably, other PM-transition polysilanes, such as **16**, **17**, **22**, and **23**, should exhibit similar thermal energy biased superposed states between purely P- and M-helicities in the main chain around the PM-transition temperatures.

The most important feature of **24** exists in region 2, because the superposed state almost linearly varies with thermal energy bias, ranging from 60% M- to 60% P-excess. It is noted that PM-switching characteristics of **24** can sensitively recognize the topology of small solvent molecules due to the two branched side chain structures and indeed lead to great amplification of the superposed Cotton CD signals. This unique superposed helical state linked by twisting motions is regarded as a “dynamic memory” function,

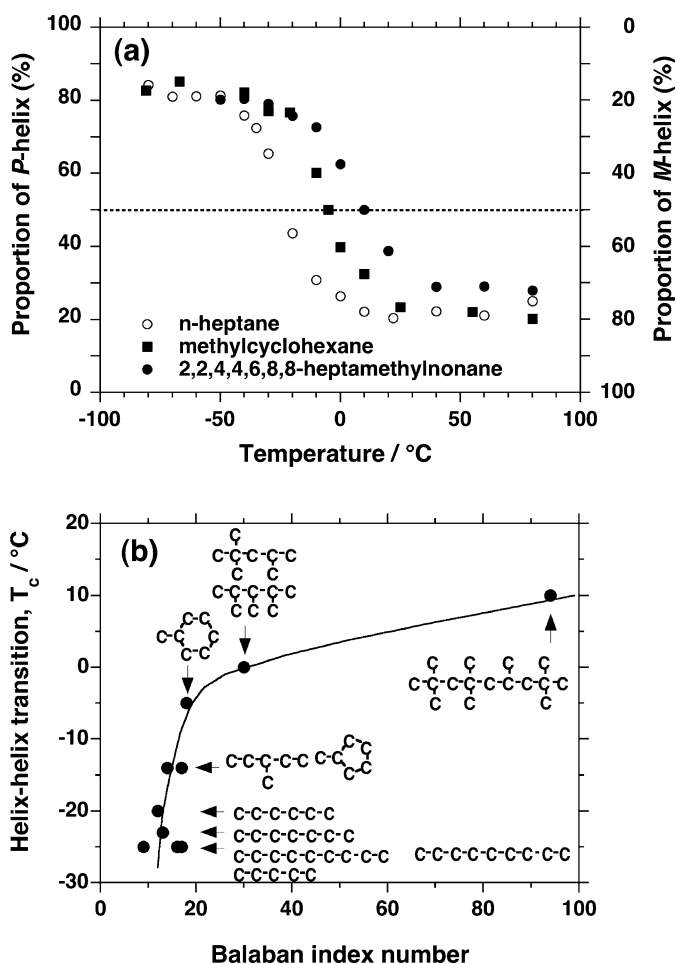
since, if the solvent molecules (external chemical bias) are taken away, the superposed state may modify the *PM*-population. This led to a change in  $T_c$  value with a range of nonpolar hydrocarbon solvent molecules with different degrees of branching. This “solvent effect” of optically active polymers able to alter a preferential screw-sense was demonstrated in the optical activity of poly(*n*-hexyl isocyanate) induced by enantiopure chiral, racemic, and achiral solvents [18].

Figure 18a compares the variable temperature *P-M* population of **24** ( $M_w = 7.4 \times 10^4$ ,  $M_n = 2.5 \times 10^4$ ) in three solvents with different degrees of branching, including *n*-heptane (linear hydrocarbon), methylcyclohexane (cyclic hydrocarbon), and 2,2,4,4,6,8,8-heptamethylnonane (highly branched hydrocarbon). The quantized helicity below and above  $T_c$ , and the superposed helicity around  $T_c$  are conserved in these solvents. Although the value of  $T_c$  considerably varies with the degree of branching of the solvent, the *P-M* population below  $T_c$  is insensitive to the degree of branching, but, above  $T_c$ , it is sensitive to this branching.

Figure 18b plots the effects of solvent topology on  $T_c$  for various solvents as a function of the Balaban index number which is a measure of degree of branching [79]. Qualitatively, although  $T_c$  increases nonlinearly with increasing index number, straight chain alkyl molecules afford a lower  $T_c$ , whereas branched chain alkyl molecules tend to give a higher  $T_c$  and branched cyclic solvents lie at intermediate values.

To explain these quantized and superposed helicities, cooperativity in coupled electronic and conformational transitions is assumed to be the origin of the step-like switching response to the thermal energy bias. Molecular mechanics calculations were made on 31-mers of *it*-**24** and *it*-**25**, with the results shown in Fig. 19a. Both 31-mers are characterized by double-well potentials. The *P* minimum for *it*-**24** is slightly deeper than the *M* minimum, indicating that both *M*- and *P*-conformers may coexist. On the other hand, the *P* minimum for *it*-**25** is significantly deeper than the *M* minimum, suggesting that the chain conformation adopts predominantly *P*-helicity. If the double-well potential of *it*-**24** is assumed to change with temperature as shown in Fig. 19b, the three temperature regions noted for **24** are qualitatively explained.

In an electronically conjugated stiff helical polysilane with discrete energy levels in a double-well potential, it is possible that the wavefunction of the lowest ground-state of an *M*-state electronically communicates with that of a *P*-state through quantum mechanical tunnelling between the *P*- and *M*-electronic states. The original idea on the superposition of chirality and optical activity was discussed theoretically by Hund in 1927 [78], and later by several quantum physicists for wavefunctions of hypothetical chiral molecules [76]. It is necessary to invoke the presence of helix reversals in the case of helical polymers. The helix reversal, presumably consisting of several silicon–silicon single bonds (corresponding to a sub-nm barrier thickness),



**Fig. 18** **a** Variable temperature *P*-*M* proportion of **24** ( $M_w = 7.4 \times 10^4$ ,  $M_n = 2.5 \times 10^4$ ) in 2,2,4,4,6,8,8-heptamethylnonane (filled circles), methylcyclohexane (filled squares), and *n*-heptane (open circles) in the range of  $-80$  and  $+80$  °C. **b** Change in the  $T_c$  value of **24** ( $M_w = 7.4 \times 10^4$ ,  $M_n = 2.5 \times 10^4$ ) as a function of degree of branching in a range of hydrocarbon solvent molecules in which the degree of branching is evaluated by the Balaban index number

is the section in which the screw sense changes direction, and might act as a small tunnelling barrier. The reversal may play a crucial role in correcting errors from thermal noise through dynamic twisting motions from one screw sense to the other. The helix reversal may exist as a very short all-*anti*, or transoid sequence. Time-averaged optical inactivity at  $T_c$ , resulting from a rapid interconversion between *P*- and *M*-segments, is regarded as oscillating helicity or dynamic pseudo-racemization. In this quasi-stationary state,

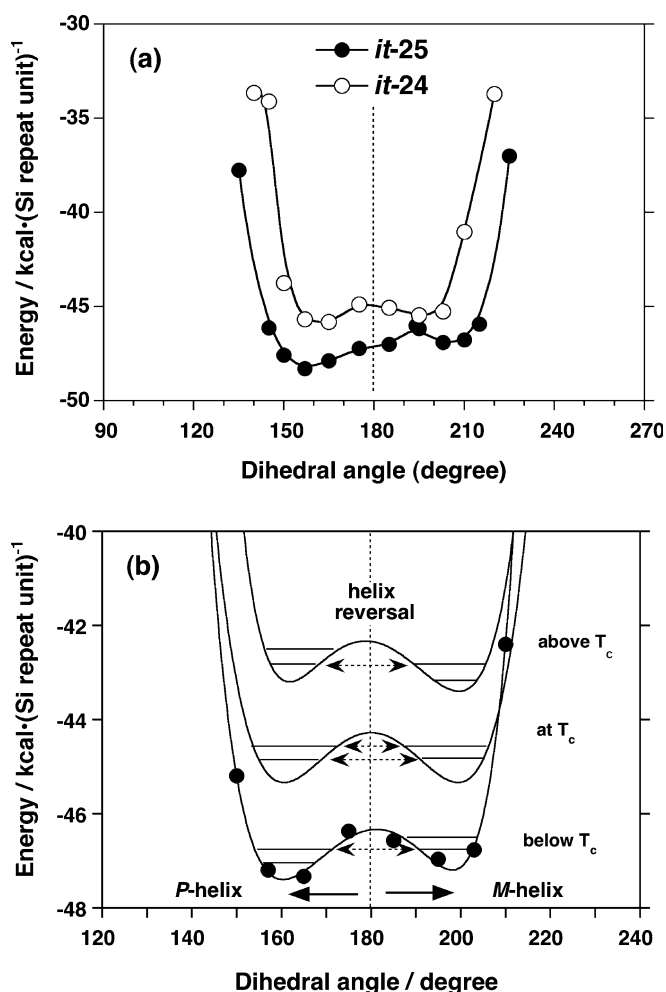


**Fig. 19** **a** Dihedral angle dependence of the potential energy for *it-24* and *it-25* model molecules with 31 repeating units and hydrogen termini (oligo-24 or oligo-25). **b** Schematic tunnelling illustration between *P*- and *M*-helical states. Potential energy as a function of main chain dihedral angles of *it-oligo-24* with three switching regions. Below  $T_c$  (bottom trace with filled circles), at  $T_c$  (middle trace, hypothetical curve), and above  $T_c$  (upper trace, hypothetical curve). Dotted arrows indicate tunnelling processes between wavefunctions of *P*- and *M*-segments existing in the same main chain

the wavefunctions of the superposed *P*- and *M*-states ( $P_s$ - and  $M_s$ -states) can produce two splitting sub-levels,  $\Psi = 1/\sqrt{2}[\Psi_{P_s} \pm i\Psi_{M_s}]$ , as illustrated in Fig. 19b. This is a consequence of electronic coupling between the lowest energy levels of almost degenerate *P*- and *M*-states in the same helical main chain.

## 5

### **“Chiroptical Switching and Memory” of Polysilane Aggregates in Solution**

The dynamic and superposed helicity of *PM*-switching and *sergeant-soldier* and *majority rule* type helix amplifications occurring in flexible rod-like helical dilakylpolysilanes with double-well potential may belong to the autocatalytic asymmetric chemical reactions and bifurcation equilibrium mechanisms in the chiral crystallization from achiral substances. This is because the chromophoric helical polysilane main chains are made of numbers of monomer repeating units, and have similar numbers of small molecules in a crystal and tiny chiral bias by internal and external chemical origins might amplify and invert their chirality to polysilane main chain dispersed in isotropic solution at ambient temperature. At specific  $T_c$  of *PM*-switching an apparent CD signal inactivity may indicate a dynamically equal population of *P*- and *M*-helical segments, regardless of chiral side groups. At all *temperatures* of optically inactive helical polysilanes, an apparent CD signal inactivity may indicate a dynamically equal population of *P*- and *M*-helical segments, regardless of achiral side groups.

Knowledge of dynamic and superposed helicity in helical polysilanes with double-well potential is applicable to polymer aggregate systems, which are regarded as small particles (crystalline and glassy solids) dispersed in isotropic solution. If helical polysilanes made of numbers of repeating units can be confined within the aggregates, an extremely tiny chiral bias due to internal and external chemical origins may greatly amplify helical structure and Cotton CD signals [80–82]. The CD signals from helical polymer aggregates dispersed in isotropic solution are detectable by ordinary CD spectroscopy with minimal artifact signals due to interaction between CD polarized light and a partial orientation of the solid in the films.

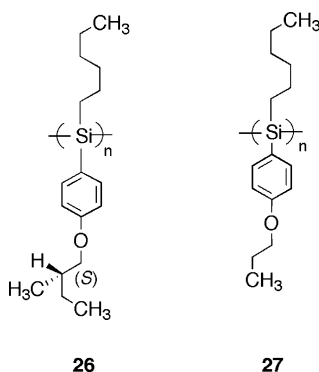
#### 5.1

##### **Chiroptical Switching and Memory of Aggregates in Solution**

The conformational structures of polysilane main chains at the macro- and microscopic levels are controllable by suitable choice of the side chain structures. Similarly, it is also the side chain which controls the optoelectronic properties by effecting the optical band gap. In the case of phenyl-substituted polysilanes, electronic interaction between the delocalized Si chain  $\sigma$ -bonding orbitals and the  $\pi$ -orbitals of the aryl groups causes a dramatic modification of both the band gap and conformational properties [61, 83]. These aryl-containing polysilanes may be potential candidates for applications in a molecular-based chiroptical switch and memory in the UV/visible region. On the other hand, the precise control of helical polymers is now a subject of great interest and importance, due to the tech-



nological importance of polymeric materials in the analysis and preparation of chiral drugs. Indeed, a few synthetic helical polymers are able to act as chiral selectors tuned for a particular chiral drug and its mirror image substance. Aiming at chiral selection, it is necessary to introduce some functional groups capable of discriminating between a pair of the guest enantiomers through intermolecular physicochemical interactions such as hydrogen bonding, phenyl  $\pi$ - $\pi$ , dipole-dipole, ionic, and acid-base interactions. Helical poly(alkyl-(alkoxyphenyl)silane)s bearing chiral side chains are potential candidates for use as a chiral selector since the polysilanes have multiple chiral recognition sites such as aryl groups, oxygen atoms, enantiopure chiral groups, and a chiral matrix due to the preferential helical conformation of the main chain. Therefore, this type of polysilane may open new concepts in the design of new polymer-based chiral stationary phases in gas or liquid chromatography, or in molecular chirality sensors.



**Scheme 7** Chemical structures of semi-flexible helical alkylarylpolysilanes bearing an alkoxy group at the remote *p*-position on the aryl group

Poly{alkyl(alkoxyphenyl)silane}s bearing enantiopure chiral substituents in the *para* position on the phenyl ring, in contrast to poly(dialkylsilane)s or poly(diarylsilane)s, are optically inactive in dilute solution due to the presence of equivalent proportions of *P*- and *M*-helical segments [81, 84]. However, it is well established for several  $\pi$ -conjugated polymers bearing chiral side chains that, even though the polymer may be optically inactive in the single molecule state, optical activity may be observed in an aggregated form due to greater ordering. Interestingly, aggregation of polymers bearing chiral side chains into chiral superstructures considerably influences the optical and chiroptical properties. For instance, the sign and magnitude of the bisignate CD signal switching of polythiophene [30] or poly(*L*-aspartate) [68] aggregates and/or liquid crystals in response to the cooling rate and/or temperature of the thin film or the ratio of good/poor co-solvents have been described. The poly{alkyl(alkoxyphenyl)silane}s aggregates also show switchable and

memorizable CD properties in good/poor cosolvent systems, controllable by various experimental factors, such as solvent polarity, solvation, solubility, solvent addition order, thermal effects and polysilane structure and stereochemistry [80, 81]. Detailed experimental investigations of polysilane aggregates may help in the design of future generations of synthetic polymers with unique and functional chiroptical properties.

The CD spectra of poly[*n*-hexyl(*p*-(*S*)-2-methylbutoxyphenyl)silane] (26) aggregates exhibit a well-resolved bisignate CD signal in a THF (THF)/metha-

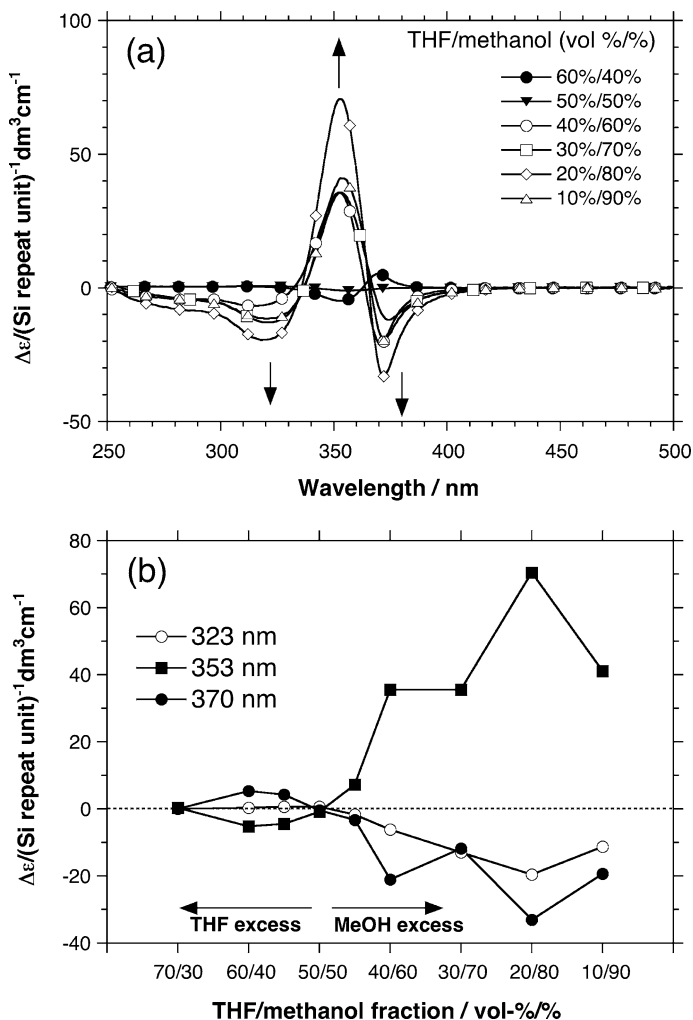


**Fig. 20** **a** CD spectra and **b** CD intensities of poly[*n*-hexyl(*p*-(*S*)-2-methylbutoxyphenyl)silane] (26) aggregates at different THF/methanol volume fractions at 20 °C

nol cosolvent system, although no CD signal is evident in pure THF solution [80]. The observed positive Cotton effect in excess THF becomes a negative Cotton effect above 60% methanol, and the bisignate CD intensities change continuously with increasing methanol concentration, as shown in Fig. 20a, the CD reversal point occurring at ca. 50%/50% THF/methanol. Previously, thermally reversible aggregation and gelation were reported for stiff poly(*n*-hexyl isocyanate) [17] and also intermolecular association and supra-

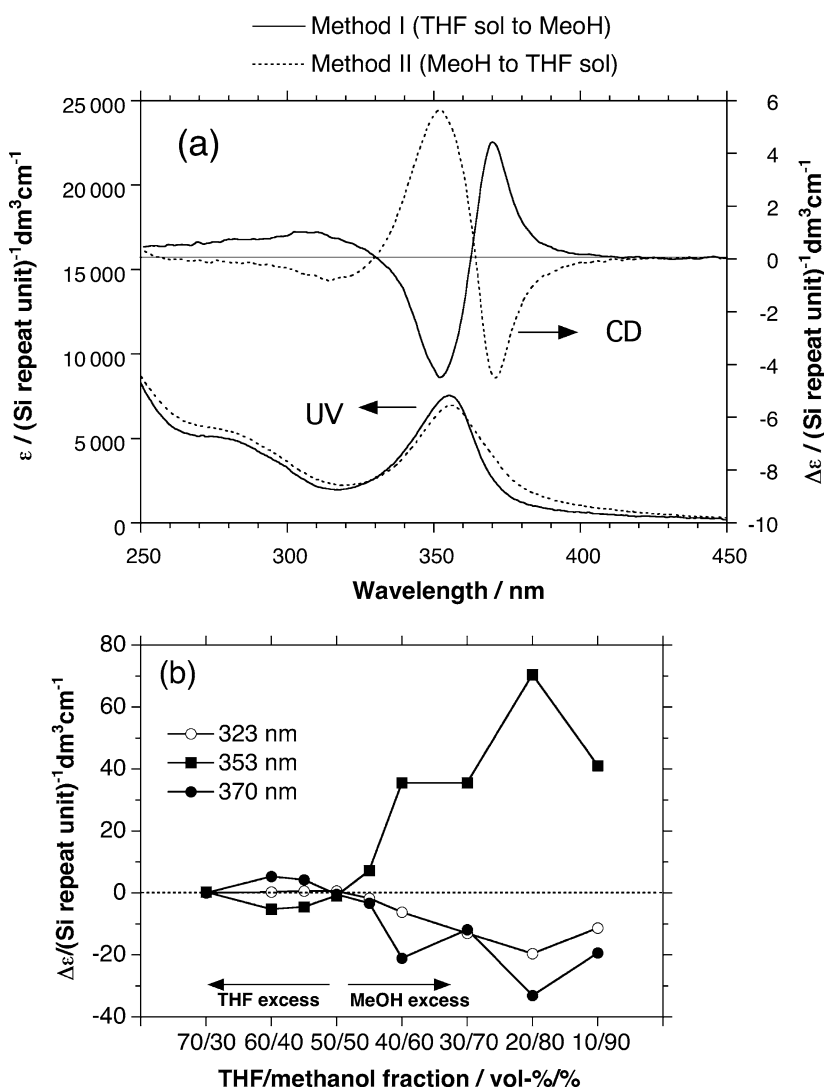


**Fig. 21** UV-Vis and CD spectra of poly[*n*-hexyl(*p*-(*S*)-2-methylbutoxyphenyl)silane] (26) aggregates prepared by Methods I and II at 55%/45% THF/methanol volume ratio at 20 °C

molecular organization of poly(*p*-biphenylmethyl-*L*-glutamate) in solution has been investigated by means of light scattering and optical activity [85]. Even optically inactive polysilane bearing chiral side groups in a good solvent can thus form optically active polysilane aggregates in a mixed good/poor solvent system. Additionally, the chirality of the aggregates can be switchable by the choice of solvent polarity, as has also been reported for a polythiophene [86]. The bisignate nature of the CD spectra is characteristic of exciton coupling between closely situated transition dipole moments on neighboring polymer segments in a chiral configuration [51]. The CD splitting originated mainly from the *intermolecular* interaction between neighboring polysilane helices since the CD spectra originates from  $\mu\text{m}$ -scale chiral aggregate particles (as shown by filtration experiments using several different pore size filters).

We found that the CD sign of the chiral aggregates around the CD reversal point (THF/methanol 55%/45%) is switchable, depending on the solvent addition order: either *Method I* (methanol added into THF solution of the polysilane) or *Method II* (THF solution of the polysilane added into methanol), as shown in Fig. 21. This solvent polarity dependent CD switching may be related to the “polymeric seed chirality” in the initial stage of the polymer chirality amplification process, which can be detected as Cotton CD signal active polymer aggregates.

Two possible origins of the CD switching phenomenon (relating to the oppositely oriented chiral aggregates) dependent on solvent polarity are proposed [80, 81]. (i) The dynamic equilibrium between *P*- and *M*-helical screw senses in **26** may incline to a preferential helical screw sense upon aggregation by locking effects of the *p*-chiral ether moieties, while the solvent polarity may control the slight preference of the polysilane for *P*- or *M*-helicity. Consequently, the preferred chiral orientation of the aggregates may be a result of the preferred helicity of single molecules of polysilane, as shown in Fig. 22. (ii) The helix angle  $\phi$  may govern the handedness of the packing between the preferential helical main chains of contiguous polysilane chains (there

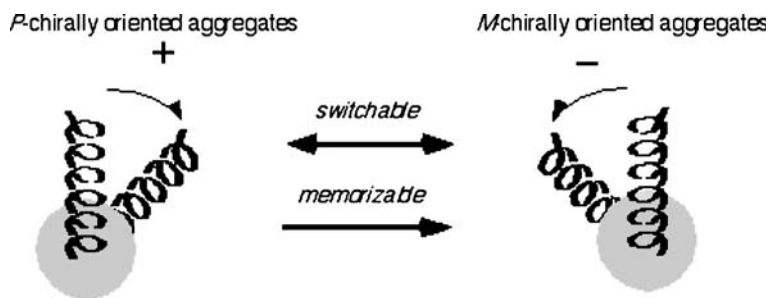


**Fig. 22** Chiral orientation of the preferred helicity of single molecules of the polysilane aggregates

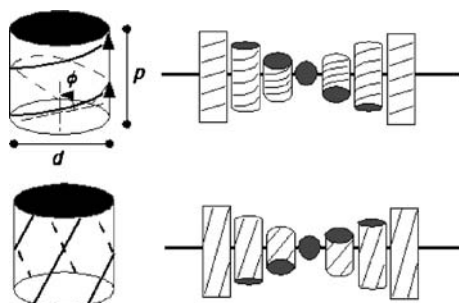
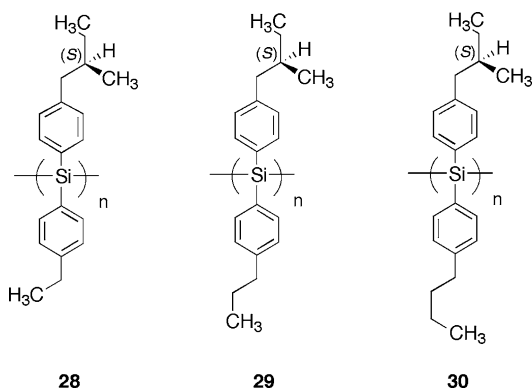


**Fig. 23** Superhelix with helix angle  $\phi$  governing the handedness of the packing between the preferential helical main chains of contiguous polysilane chains for polysilane aggregates

is no helix inversion of the single main chain), as shown in Fig. 23. In this model, the handedness of the superhelix depends on only two critical factors: the ratio of polymer helical screw pitch,  $p$ , to helical diameter,  $d$ , as has also been proposed for cholesteric liquid crystal phases of DNA [87]. Concerning polysilane aggregates in a good/poor cosolvent system, the screw pitch ( $p$ ) of the preferential helicity could greatly depend on the amount of poor solvent, since the polysilane chains may shrink and fold ( $p$  becomes shorter) in excess poor solvent.

Recent studies have validated the idea that the superhelix model is responsible for chiroptical switching of polysilane aggregates in a series of diarylpolysilanes, **28–30**, in which only the length of the *para*-substituent in the aryl side chain varies, decreasing monotonically in the order of **28** (ethyl), **29** (*n*-propyl), **30** (*n*-butyl) with the intention to effect a chirality switch by reduction of  $d$  alone [82]. The proper structural tuning results in a  $p/d$  ratio,



**Scheme 8** Chemical structures of semi-flexible helical diarylpolysilanes bearing (*S*)-2-methylbutyl and alkyl moieties at the *p*-position of aryl side groups

enabling the aggregate chirality to be further amplified as aggregated by the choice of mixed poor-good solvent. These results led to the notion that the aggregate chirality is controllable, not only by selection of the achiral phenyl substituent chain length, but also by solvent under certain conditions.

## 5.2

### Molecular Chirality Transcription and Memory to Polymer Aggregates

A few synthetic helical polymers are known to act as chiral selectors, and are widely used as chiral stationary phases (CSP) in gas or liquid chromatography [88, 89]. Recently, it has been reported that the preference of one helical sense in isotropic solution can be induced by some interaction between optically inactive polymers and chiral solvents/additives. Examples of this include poly(*n*-hexyl isocyanate) [17, 18] and poly(phenylacetylene)s bearing functional groups [20, 27]. The polysilane derivatives also show chiral recognition ability in solution at room temperature. Poly(methyl- $\beta$ -pinanylsilane) which includes two chiral centers per bulky hydrophobic pinanyl side group [60] exhibits an enantio-recognition ability for hydrophobic  $\beta$ -pinene, but none for hydrophilic methanol.

Such examples demonstrate the practical recognition of chiral alcohols using aggregates of optically inactive, chromophoric poly[*n*-hexyl(*p*-*n*-propoxyphenyl)silane] (27) [81]. Aggregates of this polysilane complexed with various chiral alcohols exhibit remarkable, bisignate induced circular dichroism (ICD) based on amplified chiral ordering as shown in Fig. 25a. Additionally, the sign of the ICD depends on the absolute configuration of the

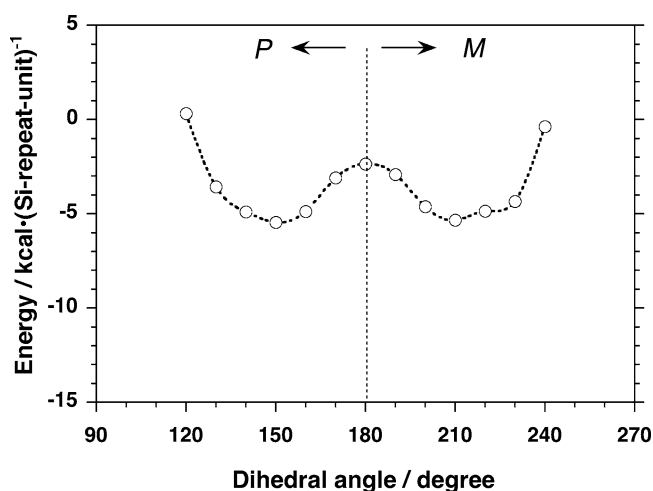


**Fig. 24** Dihedral angle dependence of the potential energy for *it*-27 model molecules with 31 repeating units and hydrogen termini (oligo-27)

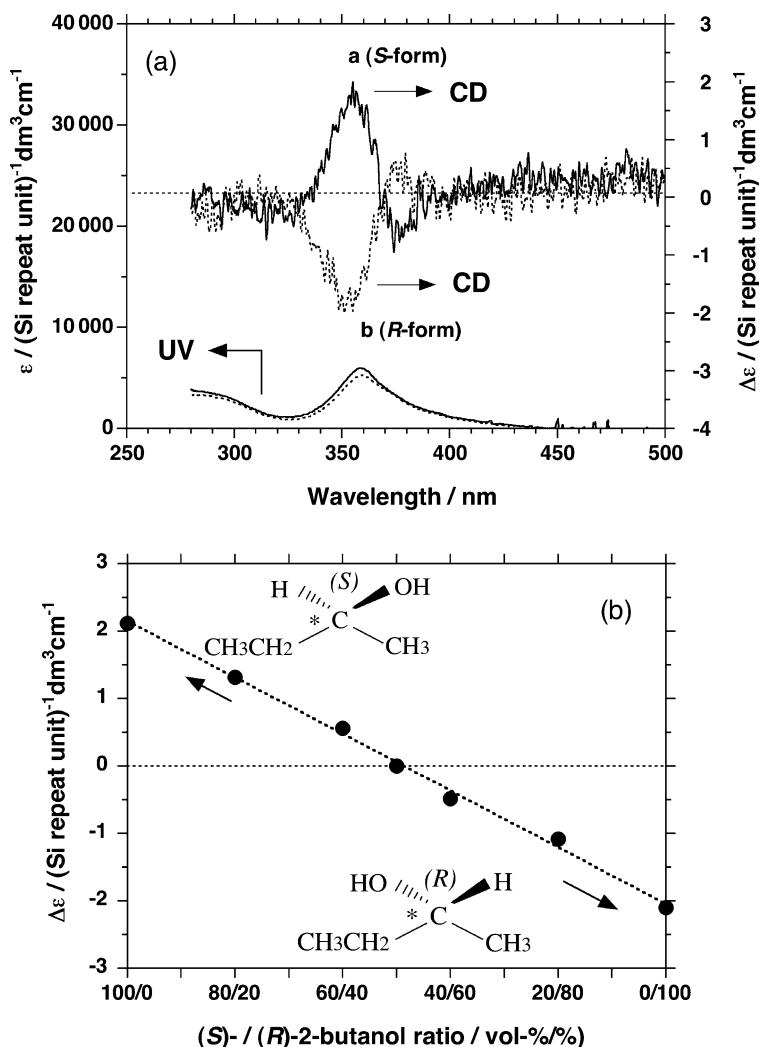


**Fig. 25** **a** CD and UV spectra of poly{*n*-hexyl(*p*-*n*-propoxyphenyl)silane} (27) aggregates in toluene/(*S*)- (a; solid line) or (*R*)-2-butanol (b; dotted line)/methanol mixtures at 20 °C and **b** the ee purity dependency of 2-butanol to CD intensities at 354 nm of the polysilane aggregates dispersed in a ternary solvent composed of toluene/2-butanol ((*S*)- or (*R*)-form)/methanol at 20 °C

chiral alcohol, indicating clearly that the polysilane forms chiral oriented aggregates due to the transfer of information by the weak hydrogen-bonding interaction between the ether oxygen moieties of the polysilane and the OH group of the chiral alcohols. Chiral polysilane aggregates show a linear relation between the ee of chiral 2-butanol and the ICD intensities, as shown in

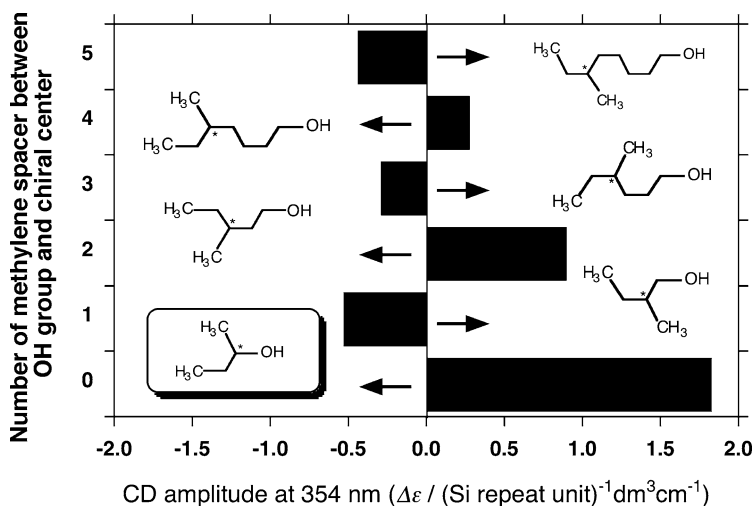


**Fig. 26** CD intensities of poly{*n*-hexyl(*p*-*n*-propoxyphenyl)silane} (27) aggregates in toluene/series of (*S*)-primary chiral alkyl alcohols/methanol mixtures at 20 °C. For comparison, the CD intensity with (*S*)-2-butanol is inserted

Fig. 25b. This system can thus determine the optical purity of chiral targets quantitatively.

Interestingly, in a series of (*S*)-chiral primary alkyl alcohols with monotonically increasing numbers of methylene spacer groups, the ICD sign of the polysilane aggregates oscillated according to the number of methylene carbons from the OH group to the chiral center, as shown in Fig. 27. Such CD phenomena have been referred to as the “odd-even” effect and have been observed in certain helical superstructures [90, 91]. From exciton theory and model studies, it is empirically suggested that the odd-even effect originates in the transition between *P*- and *M*-handed supramolecular helicity, and therefore these results mean that the position of the chiral center might gov-

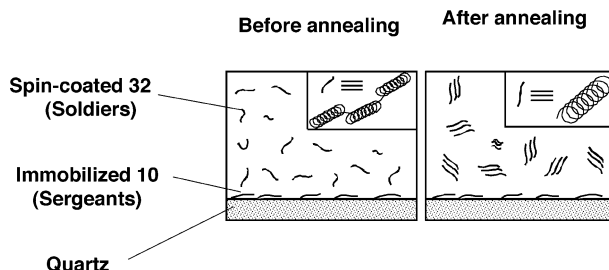


**Fig. 27** Schematic presentation of thermo-driven chiroptical transfer and amplification in “soldier” optically inactive polysilane (32) from “sergeant” optically active helical polysilane (10) on quartz



ern the chirality of the polysilane aggregates. The preparation of a library by screening against various chiral guests (by combinatorial techniques) using 27 aggregates might assist in the design of new polymer-based CSPs or chiral sensors.

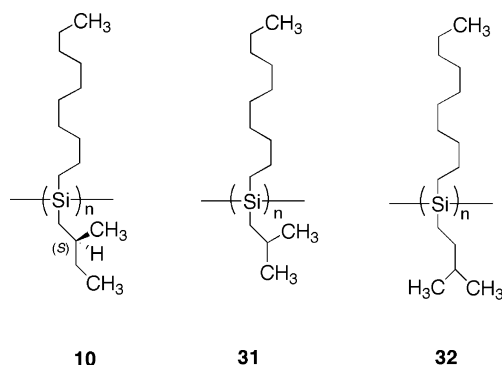
## 6

### **“Helix Command Surface” Experiments of Polysilane Binary Film at the Surface**

Helicity in synthetic polymers is typically induced by chiral centers present either in the main chain or in the side chains. Polymers bearing sterically bulky substituents with no chiral centers can adopt a helical conformation with an equal population of *P*- and *M*-handed screw senses [22]. However, it was well-demonstrated that such helical polymers with a preferential screw sense can be achieved by *sergeants and soldiers* amplification by the proper choice of comonomers [17, 18]. The chiral side group of monomer units act as effective “sergeants” which control the handedness of “soldier” achiral monomer units with a majority of chiral side groups in solution. Indeed, *sergeants and soldiers*-type rod-like helical polysilane copolymers in solution at ambient temperature are necessary to randomly copolymerize optically inactive soldier monomers bearing  $\beta$ -branched achiral side chains with optically active sergeant monomers bearing enantiopure  $\beta$ -branched chiral side groups. Alternatively, it was already established that, in several polymer systems, molecular chirality into achiral polymers in solution can be transferred in the presence of a small amount of chiral additives, known as induced helicity [20]. Molecular chirality transfer and amplification in polymer systems have recently been studied in aggregates [81]. Amplification and transfer of chiral information, however, has not been exploited in polymer solid films, which have several potent applications in chiroptical switch and memory, nonlinear optics, and data storage.

This section will demonstrate the first “*sergeants and soldiers*-type helix command surface” experiment, in which thermo-driven chiroptical transfer and amplification in optically inactive polysilane film from grafted (or spin-coated) optically active helical polysilane onto quartz substrate [92]. Although helix and optical activity amplification phenomena based on the *sergeants and soldiers* principle was mainly investigated in polymer stereochemistry, the orientation and physical properties of a thick layer deposited onto a solid surface and controlled by a monolayer command film based on “command surface” principles was established in photochemical material and surface science [93, 94]. Both *sergeants and soldiers* and *command surface* experiments appear to have been developed independently.

Optically active poly(*n*-decyl-(*S*)-2-methylbutylsilane) (10) with an almost pure *P*-7<sub>3</sub> helix, optically inactive poly(*n*-decyl-*i*-pentylsilane) (32), and op-



**Scheme 9** Chemical structures of rigid rod-like dialkylpolysilanes (**10** and **31**) and semi-flexible dialkylpolysilane (**32**) used for the *sergeants and soldiers-helix command surface* experiments

tically inactive poly(*n*-decyl-2-methylpropylsilane) (**31**) were chosen for this study (Scheme 9). Although **32** and **31** have an equal population of *P*- and *M*- $7_3$  helices due to no CD signals at 320 nm, the rigidity of **10**, **31**, and **32** are very different. Polymers **10** and **31**, with  $\beta$ -branching methyl groups in the side chains, are classified as rigid rod-like polymers with a persistent length of ca. 70 nm, while **32** is classified as a semi-flexible polymer with a persistent length of only 6 nm [39, 56]. Although **32** showed a clear melting point (mp) at  $\sim 40^\circ\text{C}$  in both heating and cooling cycles, no mp was observed for **31** in the range  $-50$  to  $150^\circ\text{C}$ , presumably due to rigid rod-like architecture.

The double layer of polysilane samples were prepared by chemically grafting [95] or spin-coating **10** ( $M_w = 2.11 \times 10^5$ ,  $M_w/M_n = 1.77$ ) onto the quartz substrate (an initial intensity of UV absorbance at 320 nm was ca. 0.04), followed by spin-coating of **32** ( $M_w = 1.11 \times 10^5$ ,  $M_w/M_n = 1.75$ ) or **31** ( $M_w = 3.36 \times 10^4$ ,  $M_w/M_n = 1.17$ ) onto the surface of **10** (total UV absorbance at 320 nm was adjusted between 0.39 and 1.50). Terms “g” and “sc” mean “chemically grafted at the surface” and “a spin-coated film onto the surface”, respectively, in the following discussion.

Figure 28 shows the changes in the CD spectra of **10(g)**-**32(sc)** and **10(g)** (which means that only **10** was grafted onto the quartz surface) films before and after the annealing process. The spectra did not significantly affect the spectral intensity with rotation of the solid films at different angles. The samples were then annealed in a vacuum at  $80^\circ\text{C}$  for 1 h and were cooled down gradually to room temperature. CD spectra of these samples were measured again after the thermal treatment at the same angles as before annealing.

From Fig. 28a, it is evident that both **10(g)**-**32(sc)** and **10(g)** show a bisignate CD band with a positive-signal at 309 nm and a negative-signal at 324 nm, which are characteristics of an exciton couplet Cotton band due to a helical polysilane  $\sigma-\sigma^*$  transition. For **10(g)**-**32(sc)**, both positive-Cotton

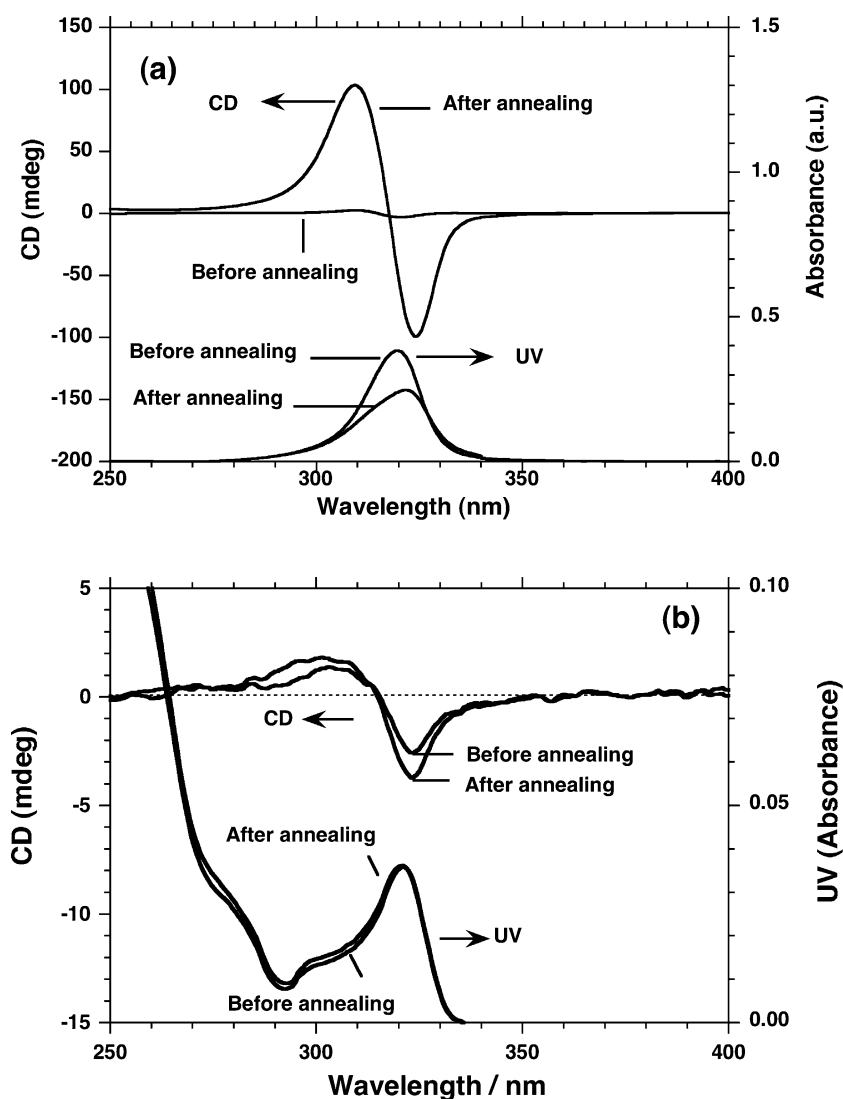


**Fig. 28** **a** CD and UV spectra of chemically grafted polysilane (**10**) and spin-coated polysilane (**32**) binary film onto quartz surface before and after annealing, the initial UV absorbance of **10** was 0.04, and total UV absorbance of grafted **10**/spin-coated **32** double layer was 0.39. **b** CD and UV spectra of spin-coated polysilane (**10**) on quartz surface before and after annealing, the initial UV absorbance of spin-coated **10** was 0.030

CD and negative-Cotton CD intensities were greatly increased after thermal annealing. The enhancement in the CD signal intensities is a consequence of chirality transfer to **32** from the chiral side chain of **10** and/or helical main chain itself and is drastically amplified after annealing. Contrarily, minimal

changes in CD signal intensities, however, were observed for only immobilized **10(g)** after annealing, as shown in Fig. 28b.

It is noted that the UV absorbance of the **10(g)**-**32(sc)** sample decreased after the annealing treatment, as shown in Fig. 28a. Presumably, most polysilane chains lie down before annealing in the quartz substrate plane, as the film was prepared by the spin-coating technique. However, the thermal annealing treatment of semi-flexible **32** tends to orient some of the polymer chain segments perpendicularly and/or tilt them to the substrate plane, leading to the decrease in the apparent UV absorbance at 321 nm, as illustrated in Fig. 27.

The effect of the thickness of **32** (ranging from 10 to 50 nm) on almost uniformly formed thick optically active **10(g)** and/or **10(sc)** films (1–2 nm) was examined. Figure 29 plots the change in relative Kuhn dissymmetry ratios ( $g_{AA}/g_{BA}$ ) at 320 nm after annealing ( $g_{AA}$ ) and before annealing ( $g_{BA}$ ) with the film thickness, which was evaluated by height bar of AFM image onto quartz. It is evident that the ratios increase as the thickness of **32** decreases. However, the magnitude of the  $g_{AA}/g_{BA}$  value was greater in **10(g)** (filled square) than **10(sc)** (filled circle), presumably due to partial penetration of **10(sc)** polymer chains into the surface during the spin-coating process of **32** due to similar solvent solubility behavior between **10** and **32**.

A tiny amount of immobilized optically active **10** is thus able to effectively induce and greatly amplify the Cotton CD signals in an optically inactive **32**

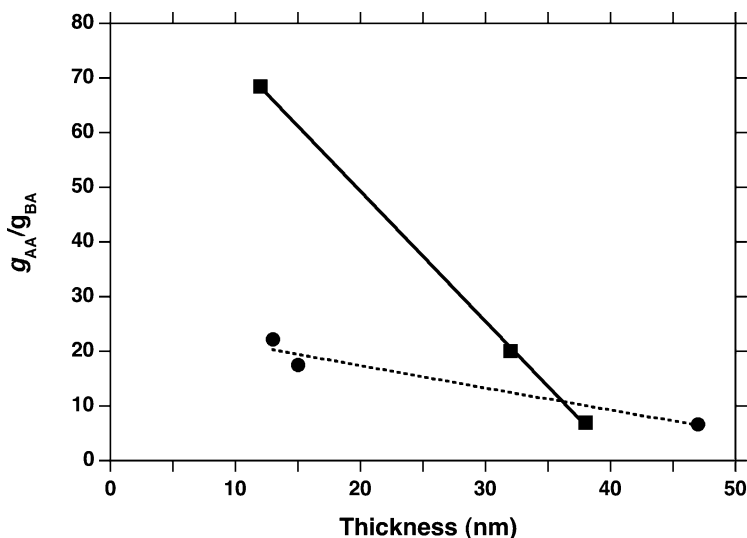


**Fig. 29** Relative Kuhn dissymmetry ratios of chemically grafted **10** – spin-coated **32** (filled square) and spin-coated **10** – spin-coated **32** (filled circle) on quartz surface before annealing ( $g_{BA}$ ) and after annealing ( $g_{AA}$ ) as a function of total film thickness

layer by thermal treatment. Invisible weak van der Waals interaction between **10** (sergeants) and **32** (soldiers) at the quartz surface might be responsible for the transfer and amplification of optical activity in **32**. The positional segmental movement of polymer chains in **32** (mp  $\sim 40^\circ\text{C}$ ) would easily occur, which is the key for the helix command surface experiment in the **10**–**32** binary system in the solid film state. Indeed, the optical activity transfer phenomenon in the **10(sc)**–**31(sc)** system was not observed. The CD signals of the **10(sc)**–**31(sc)** sample were markedly influenced by linear dichroism signals, which is responsible for artifact CD signals of oriented solid film. Even after a prolonged annealing time (overnight) and increased annealing temperature (as high as  $150^\circ\text{C}$ ), the LD influence was not reduced and could not be eliminated.

These experiments prove a similarity between helix amplification by the *sergeants and soldiers* principle in solution and helix amplification by the *command surface* principle at the solid surface.

## 7

### Tunable Cholesteric Liquid Crystallinity of Helical Polysilane

Stiff rod-like helical polymers are expected to spontaneously form a thermotropic cholesteric liquid crystalline (TChLC) phase under specific conditions as well as a lyotropic liquid crystal phase. A certain rod-like poly(*L*-glutamate) with long alkyl side chains was recently reported to form a TChLC phase in addition to hexagonal columnar and/or smectic phases [97, 98]. These properties have already been observed in other organic polymers such as cellulose and aromatic polymers.

Since the persistence length,  $q$ , of **6** in isooctane was determined to be 70 nm, this value is similar to that of **4-S** ( $q = 85$  nm) and much longer than that of **3** ( $q = 6.2$  nm), confirming the previous conclusion that polysilanes with  $\beta$ -branched alkyl side chains are much stiffer compared to those without such branching [56]. The persistence length of helical polymers can be determined by the steepness of the internal rotation potential in the main chain [56]. The slightly shorter  $q$  of **6** than that of **4-S** implies that the longer nonbranched alkyl side chain makes the internal rotation double-well potential of the silicon main chain less steep.

Polymer **6** is the first TChLC polysilane in the range of 70 and  $140^\circ\text{C}$  [96]. The polymer **6** (with a relatively low molecular weight:  $M_w = 1.11 \times 10^4$ ,  $DP_w = 46$ , and  $M_w/M_n = 1.19$ ) indeed showed a TChLC property as proved by the iridescent colors observed due to the reflection of light from many helicoidal periods in randomly aligned textures. This is further supported by the observation using an optical microscope, of a Grandjean mono-domain optical image including partly oily streaks between 70 and  $140^\circ\text{C}$ , which are characteristic of the TChLC phase [97, 98].

Further evidence was obtained by observing the variable temperature CD reflection band characteristic of a cholesteric Grandjean domain, as shown in Fig. 30a. The CD reflection spectra are sharp at any temperature, and the reflection wavelength corresponding to the optical pitch of the TChLC phase greatly depends on film temperature. The optical cholesteric pitch decreases progressively with temperature from 500 nm at 70 °C to 1000 nm at 140 °C. The positive sign of the CD reflection band indicates an *M*-helicity of the cholesteric phase. The optical pitch below 70 °C in the cooling run from

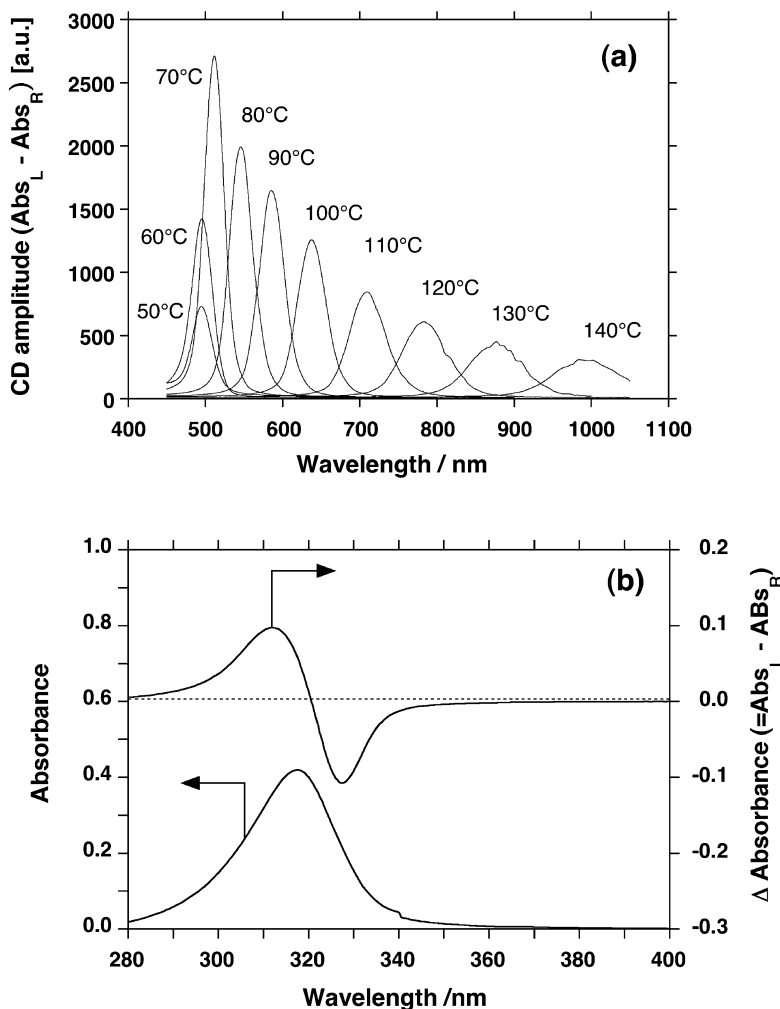


**Fig. 30** **a** Cotton CD reflection bands of **6** ( $M_w = 11\,100$ ,  $DP_w = 46$ , and  $M_w/M_n = 1.19$ ) due to cholesteric phases at various temperatures on cooling run and **b** UV absorption and Cotton CD signal intensity at 80 °C

120 °C is insensitive to change in temperature and the intensity of the CD reflection band in the visible region decreases markedly.

Polysilane **6** in the TChLC phase at 80 °C exhibits a UV band at 318 nm, and a bisignate CD band with equal rotational strengths with extrema at 313 and 327 nm, respectively, as shown in Fig. 30b. The bisignate CD band results from the couplet Cotton CD signals of a chirally ordered motif between two interacting excited states of adjacent **6** molecules in the chiral environment. These led to the idea that the chiral motif adopts an *M*-helicity based on the exciton couplet assignment, which is consistent with the assignment of *M*-helicity to the TChLC phase above 70 °C. On the assumption that  $\lambda = n_{\text{av}} \cdot p$ ,  $\Delta\lambda = \lambda \cdot \Delta n / n_{\text{av}}$ , and  $n_{\text{av}} = 2$  for **6**, while  $\lambda$  is a reflection wavelength in nm,  $p$  pitch,  $n_{\text{av}}$  average refractive index,  $\Delta\lambda$  bandwidth,  $\Delta n$  difference in refractive index between extraordinary and ordinary light, ca. 175 and 350 molecules of **6** at 70 and 120 °C, respectively, are included per half-pitch in the TChLC phase.

The *M*-cholesteric pitch quickly altered in response to the change in temperature with little hysteresis on either heating or cooling runs. Upon rapid cooling, the recovery time of the cholesteric pitch was less than 1–2 min. The absence of strong intermolecular forces, such as hydrogen bonding, dipole–dipole, and  $\pi$ – $\pi$  interactions, and the existence of only weak van der Waals interaction are responsible for the uniqueness of TChLC characteristics. These quick and no-hysteresis response CD band characteristics in the visible and near infrared regions are indeed useful in a practical-level circular polarizing band notch filter. These tunable helix amplifications may open new ways for chiral polysilane-based applications, if proper modification of helical polysilanes was made by the choice of comonomers and proportion, molecular weight and polydispersity, and chiral and achiral side chains.

Rod-like **6**, adopting an almost  $7_3$  helical conformation, belongs to a unique set of stiff polymers, exhibiting both TChLC and lyotropic liquid crystallinity. Indeed, experiments demonstrated that solutions of **6** became cholesteric at high concentrations [99]. The isotropic-biphasic phase boundary concentration increases as the molecular weight is increased. This increase has been described theoretically using the molecular parameters determined from dilute solution data.

## 8

### Parity Question—Subtle Left-Right Differences by Physical Origins

Since the enantiomeric resolution of tartaric acid in 1848 by Pasteur, a long-standing issue is whether mirror-image molecules are energetically identical with respect to the origin of biomolecular homochirality [100]. In 1860 Pasteur first conjectured that the homochirality may come from certain intrinsically handed force existing in the Universe [1]. In 1898, Kipping and Pope reported experimental results in relation to NaClO<sub>3</sub> with L- and D-

form crystals formed by evaporation of aqueous solution to test a validity of a relationship between stereochemistry (racemism, pseudoracemism, enantiomorphism) and vitalism. However, although the yield of L- and D-crystals varied widely from 24% to 77%, the average value for the number of D-crystals was almost 50% over 3206 crystals in 46 independent crystallization experiments. After this initial work to seek inorganic silicon-based double bond compounds ( $\text{Si}=\text{Si}$  and  $\text{Si}=\text{O}$ ) in analogy with organic ( $\text{C}=\text{O}$ ) ketone and  $\text{C}=\text{C}$  double bonds, Kipping initiated organosilicon chemistry. He first synthesized numbers of Si-catenates known as poly(oligo)silane ( $\text{Si}-\text{Si}$ ) and siloxane compounds ( $\text{Si}-\text{O}-\text{Si}$ ) from the viewpoint of the hypothetical  $\text{Si}=\text{Si}$  and  $\text{Si}=\text{O}$  related compounds.

Hund, one of the pioneers in quantum mechanics, had a fundamental question of relation between the molecular chirality and optical activity [78]. He proposed that all chiral molecules in a double well potential are energetically inequivalent due to a mixed parity state between symmetric and anti-symmetric forms. If the quantum tunnelling barrier is sufficiently small, such chiral molecules oscillate between one enantiomer and the other enantiomer with time through spatial inversion and exist in a superposed structure, as exemplified in Figs. 19 and 24. Hund's theory may be responsible for dynamic helicity, dynamic racemization, and epimerization.

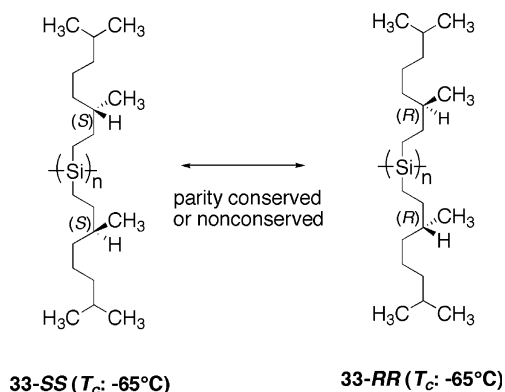
It is now widely accepted among physicists that the interactions in the Universe are governed by four fundamental forces with strong, weak, electromagnetic, and gravitational forces [104]. Between 1956–1957 inequality in emission intensity of electrons in  $\beta$ -decay experiments of  $^{60}\text{Co}$  at 0.01 K was first proven theoretically and experimentally [105, 106], and it is well known that parity (left-right symmetry) of weak nuclear forces is not conserved at a subatomic level. Similar parity-violations (PV) at the atomic level and upwards were assumed to occur. Indeed, in the early 1980s natural optical rotation of heavy metal atoms (Bi, Pb, Tl, and Cs) in the vapor phase was detected in expected sign and magnitude [107, 108], due to the parity-violating weak natural current (WNC) that is amplified by the sixth power of the atomic number due to spin-orbit interaction and relativity [109].

Since the historical PV weak force origin  $\beta$ -decay experiment of  $^{60}\text{Co}$  [106], theoreticians presumed that the tiny parity violating WNC at molecular and subatomic levels may also allow a distinction between mirror image molecules at the macroscopic level as well. This is because PV-WNC at the molecular level may be a candidate for the homochiral scenario under terrestrial and extraterrestrial conditions [1, 2, 104, 109–118]. The WNC, however, did not induce any observable PV effects between enantiomers in their ground states because of the minuscule PV energy difference (PVED) of  $\sim 10^{-19}$  eV and/or negligibly small  $10^{-15}\%$  ee in racemates. Theoreticians also proposed several possible amplification mechanisms at reproducible detection levels within laboratory time scales and at terrestrial locations [113, 117, 118].



The electroweak force, which is now known to be the unified force between the parity-conserving electromagnetic and parity-violating weak nuclear forces, can distinguish between mirror images at atomic and subatomic levels [103, 104]. Typical model systems suited for testing these theoretical proposals may be polymerization and crystallization [113], molecules comprising heavy atoms [114], double-well energy potential systems [115, 116], nonequilibrium autocatalytic chemical reactions [117], and phase transition systems [118]. Although many attempts have been undertaken in several laboratories, little may be known for molecular systems in solution suitable for solving the parity question. In order to observe the consequence of the tiny PVED and/or other macroscopic PV effects between mirror-image molecules, a significant amplification system susceptible to small perturbations is inevitably required.

In 2001, a possibility of detectable differences in chiroptical and achiral physicochemical experiments between an enantiomeric pair of poly[bis{(S)-3,7-dimethyloctyl}silylene] (**33-SS**) and poly[bis{(R)-3,7-dimethyloctyl}silylene] (**33-RR**) (Scheme 10) was reported [119]. The polymers bearing two identical chiral side groups with 96% ee have nearly degenerate double-well energy potentials, leading to *PM*-transition at  $-65^{\circ}\text{C}$  in isoctane. Recently, Shinitzky et al. reported positive experimental results that show distinct differences in helix-coil transition behavior between synthetic D- and L-oligopeptides with 24 identical residues dissolved in water by CD and isothermal titration calorimetry experiments [120]. They assumed that *ortho*-water in the triplet state (75% of bulk water) is responsible for the LD-differences [121].



**Scheme 10** A pair of rod-like dialkylpolysilanes (**33-SS** and **33-RR**) undergoing helix-helix transition at  $-65^{\circ}\text{C}$  in isoctane used for molecular parity test experiment

This section focuses on subtle differences in the chiroptical,  $^{29}\text{Si}$ - and  $^{13}\text{C}$ -NMR spectra for the pair in solution, inferred by the consequences of those

parity-violation mechanisms [18]. Polymers **33-SS** and **33-RR** have several advantages to test the parity question at molecular level. This is because,

- (i) The polymers constitute a bridge between inanimate and biomolecular worlds, because (*S* or *R*)-3,7-dimethyloctyl groups (95.7<sub>4</sub> and 95.8<sub>8</sub>% ee with experimental error of  $\pm 0.2\%$ , respectively) from  $\beta$ -citronellol are highly enantiopure biomolecules available commercially (Fluka and now Aldrich). The *l*- $\beta$ -citronellol is a constituent of rose and geranium oils, and the *d*- $\beta$ -citronellol occurs in Ceylon and Java citronella oils. It is possible that the use of  $\beta$ -citronellols enables us to reproducibly obtain the present results in laboratories on the earth in real time, regardless of time, hemispheres, radioactive sources [122–124], circularly polarized light [125–127], intense magnetic field [128], very cold interstellar universe and long travel from nebula [129], and meteorite [130];
- (ii) The sharp CD signal of the polysilanes completely matches the corresponding near-UV absorption profile, as described in previous sections. To chiroptically detect the macroscopic PV effects excluding chiral chemical auxiliary and seeding effects, a comparison of the absolute  $g_{\text{abs}}$  values between the enantiomeric pair *in isotropic solution* is necessary. The absolute  $g_{\text{abs}}$  values of the enantiomeric pair may be directly connected to the contribution of ( $g_{\text{PV}} + |g_{\text{PC}}|$ ) for polysilane bearing one of the chiral side groups and ( $g_{\text{PV}} - |g_{\text{PC}}|$ ) for the other, because the  $g_{\text{PV}}$  term induced by PVED has the same sign and magnitude for the enantiomeric pair, while  $g_{\text{PV}}$  and  $g_{\text{PC}}$  are dissymmetry ratios relating to PV and PC terms, respectively. The  $g_{\text{abs}}$  of *PM*-transition polysilanes is directly connected to the difference in population between *P*-7<sub>3</sub> (with dihedral angles of  $\sim 150^\circ$ ) and *M*-7<sub>3</sub> (with  $\sim 210^\circ$ ) helical motifs, because *PM*-transition polysilanes are in double-well potential;
- (iii) In the case of molecules,  $\text{PVED} \sim \langle S|V_{\text{PV}}|T \rangle \langle T|V_{\text{SO}}|S \rangle / \Delta E_{\text{ST}}$ , where  $V_{\text{PV}}$  refers to the WNC interaction proportional to  $Z^3$ ,  $V_{\text{SO}}$  the spin-orbit interaction proportional to  $Z^2$  ( $Z$  the atomic or neutron number),  $|S \rangle$  and  $|T \rangle$  singlet and triplet states separated by  $\Delta E_{\text{ST}}$ , respectively [2, 110–114]. Of particular importance would be that the  $|T \rangle$  must partly mix to  $|S \rangle$  [112]. For a certain polysilane, the  $\Delta E_{\text{ST}}$  is reported to be 3.4 eV [132]. Moreover, the heavier silicon atoms and the large effective conjugating numbers ( $N_{\text{eff}}$ ) of  $\sim 10^3$  may linearly enhance PVED [113], relative to carbon-based small molecules, since PVED will be proportional to  $N_{\text{eff}}$ . Therefore, the preliminary expected advantage ratio,  $g_{\text{adv}} = \text{PVED}/kT \sim 10^{-12}$  at 300 K, may exceed a detectable limit of  $\sim 10^{-17}$  [117]. Hopefully, 4.7% of natural abundant  $^{29}\text{Si}$  with  $-1/2$  spin may further enhance this PVED by several times in analogy with neutron optical rotation enhancement, as observed in  $^{117}\text{Sn}$  isotope [133].

Figure 31 gives a comparison of the UV and CD spectra between **33-SS** and **33-RR** with sufficiently high molecular weight samples in isooctane below and above the *PM*-transition temperature. The positive-signed Cotton CD

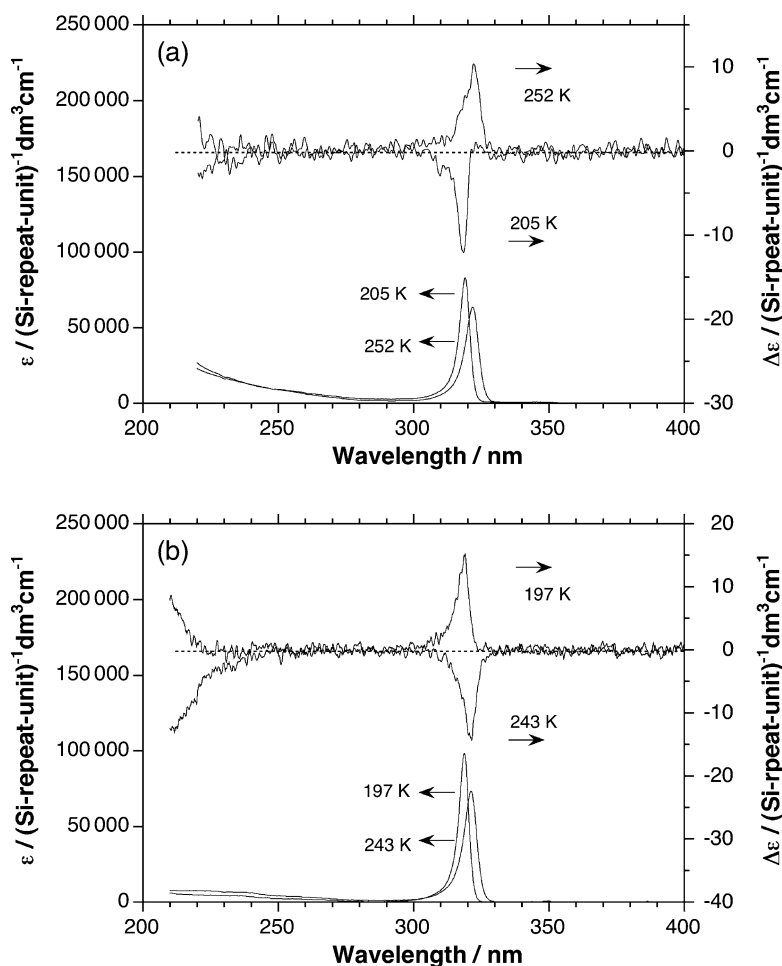


**Fig. 31** The UV and CD spectra of **a** 33-SS ( $M_w = 863\,000$ ,  $M_n = 147\,000$ ) and **b** 33-RR ( $M_w = 394\,000$ ,  $M_n = 85\,800$ ) in isooctane below and above helix-helix transition temperature ( $\sim -65^\circ\text{C}$ )

band of 33-SS, with an extremum of 322 nm at 252 K, is almost the inverse of the negative-signed CD band, which has an extremum of 318 nm at 205 K, over the whole 220 to 350 nm range. Conversely, the negative-signed CD spectrum of 33-RR, with an extremum of 322 nm at 243 K, is almost the inverse of the positive-signed CD spectrum, which has an extremum of 319 nm at 197 K. Thus, it is evident that both 33-SS and 33-RR undergo a *PM*-transition between the two temperatures.

Figure 32a compares the apparent  $g_{\text{abs}}$  around 320 nm for 33-SS and 33-RR in isooctane as a function of temperature. Although both 33-SS and 33-RR have the slightly different *PM*-transition temperature of around 208 K, the ab-

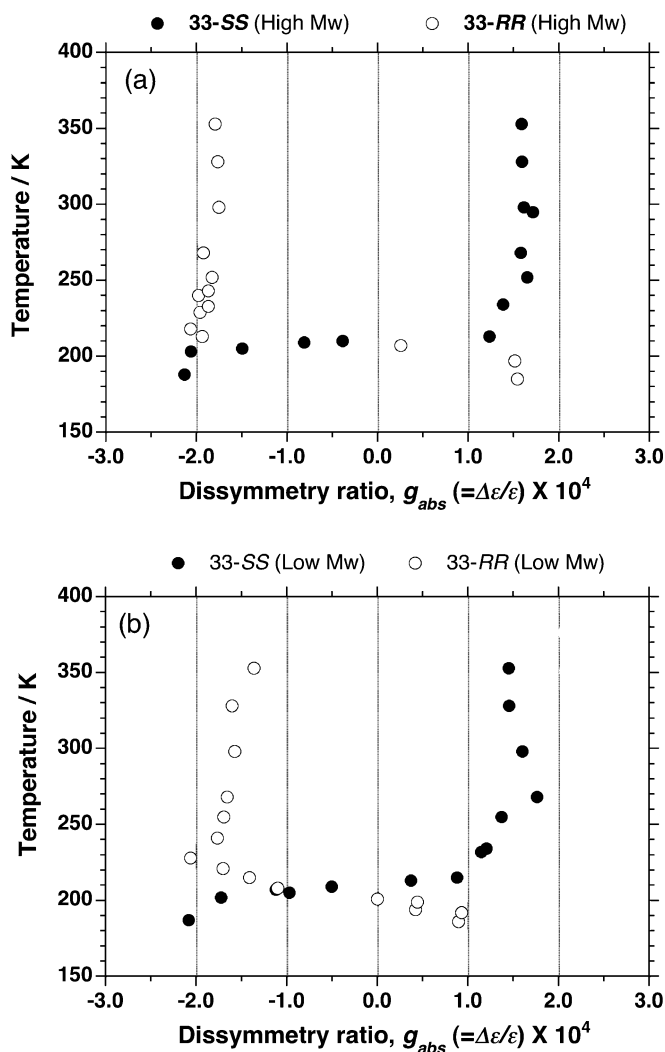


**Fig. 32** Comparisons of the apparent values of **a**  $g_{abs}$ , between 33-SS with  $M_w = 863\,000$  and  $M_n = 147\,000$  (filled circles) and 33-RR with  $M_w = 394\,000$  and  $M_n = 17\,400$  (open circles), **b**  $g_{abs}$ , between 33-SS with  $M_w = 31\,400$  and  $M_n = 85\,800$  (filled circles) and 33-RR with  $M_w = 30\,100$  and  $M_n = 20\,000$  (open circles) in isooctane as a function of temperature

solute  $g_{abs}$  magnitudes of 33-SS are always greater than those of 33-RR in the range from 190 to 353 K. The difference in the absolute  $g_{abs}$  magnitudes and PM-transition temperature between 33-SS and 33-RR tends to be pronounced in lower molecular weight samples with almost identical molecular weight (for 33-SSL,  $M_w = 31\,400$ ,  $M_n = 17\,400$ , and for 33-RRL,  $M_w = 30\,100$ ,  $M_n = 20\,000$ ) in isooctane as a function of temperature, as shown in Fig. 32b.

It is evident that the absolute magnitudes in the negative  $g_{\text{abs}}$  region are always greater than those in the positive  $g_{\text{abs}}$  region, regardless of the side chain chirality, temperature, and molecular weights. The difference in the observable  $g_{\text{abs}}$  should be connected to the  $2 \cdot g_{\text{PV}}$ , from the  $(g_{\text{PV}} - |g_{\text{PC}}|)$  term for the negative  $g_{\text{abs}}$  in polysilanes and  $(g_{\text{PV}} + |g_{\text{PC}}|)$  term for the positive  $g_{\text{abs}}$  in polysilanes. Therefore, the sign of  $g_{\text{PV}}$  is negative and the preferential screw-sense may be *M* rather than *P*, when a *P*-helix is assumed to give the positive-sign CD signal and vice versa, according to a previous molecular mechanics calculation [40, 41], as described in a previous section.

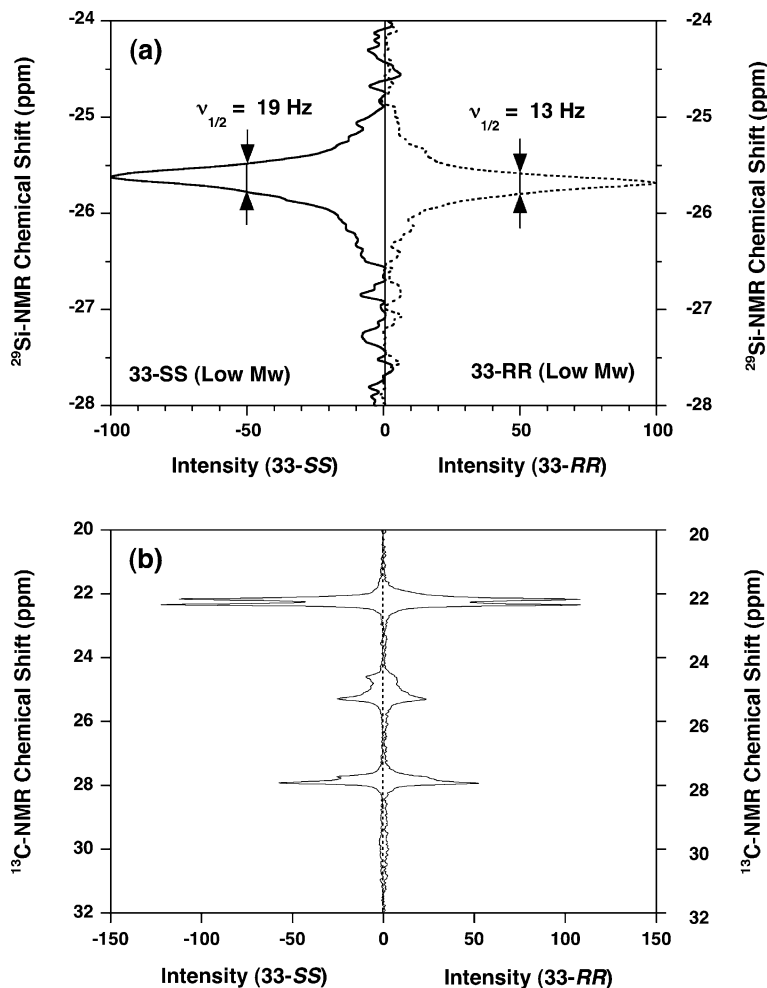


**Fig. 33** Comparisons of **a**  $^{29}\text{Si}$ -NMR spectra and **b**  $^{13}\text{C}$ -NMR spectra of 33-SS ( $M_w = 31\,400$ ,  $M_n = 17\,400$ ) and 33-RR ( $M_w = 30\,100$  and  $M_n = 20\,000$ ) in  $\text{CDCl}_3$  (50 mg in  $\text{CDCl}_3$  0.6 mL at  $40^\circ\text{C}$ )

As shown in Fig. 33a, detectable subtle differences were observed in the  $^{29}\text{Si}$ -NMR spectra between 33-SS and 33-RR with the almost identical low molecular weight samples. Although the apparent absolute  $g_{\text{abs}}$  value in chloroform at 30 °C is nearly identical for a pair of 33-SS ( $g_{\text{abs}} = 1.58 \times 10^{-4}$ ) and 33-RR ( $g_{\text{abs}} = -1.56 \times 10^{-4}$ ), the degrees of twisting mobility of the polysilane main chain in the ground states, which could be mediated by handed inner-shell electrons close to the nucleus, may be related to the difference

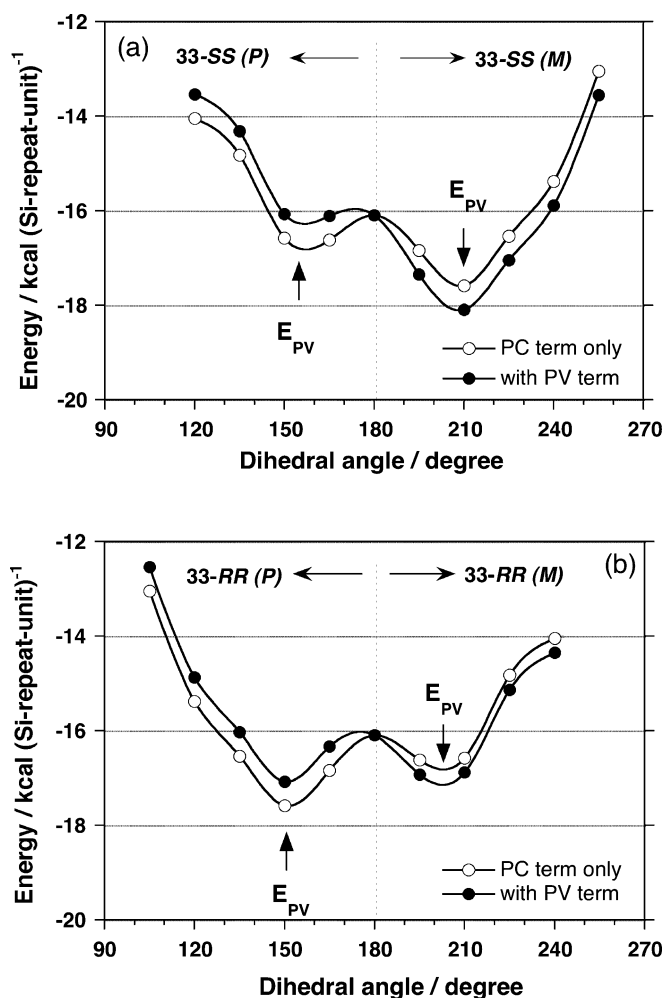


**Fig. 34** Comparisons of the potential energy curves between **a** 33-SS and **b** 33-RR model oligomers (50 silicon repeating units and hydrogen termini) with uncorrected and corrected PV terms. PV energy bias with 0.5 kcal per Si repeating unit was adopted hypothetically for demonstration purposes

in linewidth ( $\nu_{1/2}$ ), although a difference in chemical shift was predicted theoretically [114, 134]. For these **33-SS/33-RR** pairs, the main chain of **33-SS** appears to be less mobile than the corresponding **33-RR** because of its broader  $\nu_{1/2}$ : for **33-SS**,  $\Delta\nu_{1/2} = 19$  Hz at  $-25.62$  ppm, **33-RR**,  $\nu_{1/2} = 13$  Hz at  $-25.68$  ppm. Also, in the  $^{13}\text{C}$ -NMR spectra of these **33-SS** and **33-RR** pairs, detectable subtle differences in signal intensities at 22 ppm, 25 ppm, and 28 ppm due to side chains were also observed, as shown in Fig. 33b.

A possible explanation for these differences in absolute  $g_{\text{abs}}$  values between **33-SS** and **33-RR** is shown in a slight modification of potential energy curves of **33-SS** and **33-RR** model oligomers, as schematically shown in Fig. 34. For the purpose only of clarity and demonstration, the small positive PVED biases of  $+0.5$  kcal per Si atom for the *P*-motif and of  $-0.5$  kcal per Si atom for the *M*-motif were hypothetically added regardless of the side chain chirality, since the commercially available software (Molecular Simulation Inc., Discover 3, ver 400, San Diego, California, US) gives the energy curve based on the parity conserving term only. Before the PVED term addition, **33-SS** and **33-RR** are classified as conventional mirror-imaged polymers, since the preferential screw-sense in the asymmetric double-well potential energy is primarily determined by the choice of the side chain chirality. However, the pseudo-scalar PVED bias effectively allows the induction of inequality in the potential energy curves by 2PVED. Therefore, the PV term destabilizes for *P*-screw-sense and stabilizes for *M*-screw-sense regardless of the side chain chirality.

In recent years, it was reported that significant differences in specific heat, magnetization, and laser Raman spectroscopic properties between *d*- and *l*-alanine single crystals may be related to WNC and phase transition effects [136]. However, these results may originate from certain impurities incorporated in the crystals due to the lack of reproducibility which is carefully made by the other independent research groups [137].

The detectable macroscopic PV effects in chiroptical and achiral  $^{29}\text{Si}$ - and  $^{13}\text{C}$ -NMR spectral characteristics at helical polysilane level *in isotropic solution* could be the consequence of multiple great amplification mechanisms, providing a possible answer to the long-standing parity question at the molecular level. In the framework of the Charge-Parity-Time symmetry conservation theorem of fundamental physics law, a real enantiomer of polysilane bearing enantiopure side groups in the matter world may be an anti-polysilane with the opposite chirality side groups which are made of anti-atoms and anti-particles [119].

## 9

### Concluding Remarks

This chapter focused on several types of chiroptical amplification in optically active chromophoric polysilane helix systems, which exist in isotropic

homogeneous dilute solution, as aggregate forms dispersed in isotropic solution, in double layered films deposited onto a solid surface, and in the thermotropic cholesteric liquid crystal film state, by dictating invisible chiral weak and ultraweak intramolecular and intermolecular interactions at subatomic, and atomic, and molecular levels. The present knowledge on chiroptical generation, amplification, switching, and memory, including the *sergeants and soldiers experiment* and *majority rule* phenomena, might be the consequence of the uniqueness of chromophoric helical polymer systems which have a double-well potential with a small tunnelling barrier height.

**Acknowledgements** This research was supported by a Grant-in-Aid for Scientific Research in a priority area “Control of Super-Hierarchical Structures and Innovative Functions of Next-Generation Conjugated Polymers” (No. 446) from the Ministry of Education, Culture, Sports, Science and Technology, Japan. The author is acknowledged in part for grants from the Ministry of Education, Science, Sports, and Culture of Japan, for a Grant-in-Aid for Scientific Research, “Design, Synthesis, Novel Functionality of Nanocircle and Nanorod Conjugating Macromolecules (16205017)” and “Experimental Test of Parity Nonconservation at Helical Polymer Level (16655046)”.

## References

1. Frank P, Bonner WA, Zare RN (2001) In: Keinan E, Schechter I (ed) Chemistry for the 21st century, Chapt 11. Wiley-VCH, Weinheim, p 175
2. Mason SF (1984) Nature 311:19
3. Quack M (2002) Angew Chem Int Ed 41:4618
4. Shinitzky M, Haimovitz R (1993) J Am Chem Soc 115:12545
5. Lehn JM (1995) Supramolecular chemistry. VCH, Weinheim
6. Green MM, Nolte RJM, Meijer EW (eds) (2003) Materials chirality: Topics in stereochemistry. Wiley, New York
7. Itaya K (1998) Prog Surf Sci 58:121
8. Jandt KD (2001) Surf Sci 491:303
9. Samorì P, Surin M, Palermo V, Lazzaroni R, Leclère P (2006) Phys Chem Chem Phys 8:3927
10. Shinohara K, Yasuda S, Kato G, Fujita M, Shigekawa H (2001) J Am Chem Soc 123:3619
11. Sakurai S, Okoshi K, Kumaki J, Yashima E (2006) Angew Chem Int Ed 45:1245
12. Rai R, Saxena A, Ohira A, Fujiki M (2005) Langmuir 21:3957
13. Nishio M, Hirota M, Umezawa Y (1998) The CH/ $\pi$  interaction—evidence, nature, and consequences, Chapt 11. Wiley-VCH, New York, p 175
14. Desiraju GR, Steiner T (1999) The Weak hydrogen bond—in structural chemistry and biology, Chapt 5. Oxford Univ Press, New York, p 343
15. Akagi K, Piao G, Kaneko S, Sakamaki K, Shirakawa H, Kyotani M (1998) Science 282:1683
16. Cornelissen JJLM, Fischer M, Sommerdijk NAJM, Nolte RJM (1998) Science 280:1427
17. Green MM, Peterson NC, Sato T, Teramoto A, Cook R, Lifson S (1995) Science 268:1860
18. Green MM, Park JW, Sato T, Teramoto A, Lifson S, Selinger RLB, Selinger JV (1999) Angew Chem Int Ed 38:3138



19. Carlini C, Pino P, Ciardelli F (1968) *Makromol Chem* 119:244
20. Maeda K, Yashima E (2006) *Top Curr Chem* 265:47
21. Pino P, Ciardelli F, Montagnoli G, Pieroni O (1967) *J Polym Sci Polym Lett Ed* 5:307
22. Nolte RJM, van Beijnen AJM, Drenth W (1974) *J Am Chem Soc* 96:5932
23. Okamoto Y, Suzuki K, Ohta K, Hatada K, Yuki H (1979) *J Am Chem Soc* 101:4768
24. Goodman M, Chen SC (1971) *Macromolecules* 4:625
25. Green MM, Gross RA, Schilling FC, Zero K, Crosby CC III (1988) *Macromolecules* 21:1839
26. Deming TJ, Novak BM (1971) *J Am Chem Soc* 114:7926
27. Yashima E, Matsushima T, Okamoto Y (1995) *J Am Chem Soc* 117:11596
28. Lemaire M, Delabouglise D, Garreau R, Guy A, Roncali J (1988) *J Chem Soc Chem Commun*, p 658
29. Andersson M, Ekeblad PO, Hjertberg T, Wennerström O, Inganäs O (1991) *Polym Commun* 32:546
30. Bouman MM, Meijer EW (1995) *Adv Mater* 7:385
31. Salmon M, Bidan G (1985) *J Electrochem Soc* 132:1897
32. Majidi MR, Kane-Maguire LAP, Wallace GG (1994) *Polymer* 35:3113
33. Fiesel R, Scherf U (1998) *Acta Polym* 49:445
34. Oda M, Nothofer HG, Lieser G, Scherf U, Meskers SC, Neher D (2000) *Adv Mater* 12:362
35. Frey H, Möller M, Matyjaszewski K (1994) *Macromolecules* 27:1814
36. M Fujiki (1994) *J Am Chem Soc* 116:6017
37. Fujiki M (1994) *J Am Chem Soc* 116:11976
38. Fujiki M (1994) *Appl Phys Lett* 65:3251
39. Fujiki M (1996) *J Am Chem Soc* 118:7424
40. Fujiki M (2000) *J Am Chem Soc* 122:3336
41. Fujiki M, Koe JR, Nakashima H, Motonaga M, Terao K, Teramoto A (2001) *J Am Chem Soc* 123:6253
42. Saxena A, Guo GQ, Fujiki M, Yang YG, Okoshi K, Ohira A, Naito M (2004) *Macromolecules* 37:3081
43. Koe JR, Fujiki M, Nakashima H, Motonaga M (2001) In: Khan I (ed) *Synthetic macromolecules with higher structural order*, Chapt 6. Oxford, New York, p 67
44. Fujiki M, Koe JR (2000) In: Jones RG, Ando W, Chojnowski J (eds) *Silicon-containing polymers: the science and technology of their synthesis and applications*, Chapt 24. Kluwer, Dordrecht, p 643
45. Fujiki M (2001) *Macromol Rapid Commun* 22:539
46. Fujiki M, Koe JR, Terao K, Sato T, Teramoto A, Watanabe J (2003) *Polym J* 35:297
47. Fujiki M (2003) *J Organomet Chem* 685:15
48. Kipping FS (1921) *J Chem Soc* 19:830
49. Kipping FS (1924) *J Chem Soc* 125:2291
50. Fujino M, Isaka H (1989) *J Chem Soc Chem Commun*, p 466
51. Harada N, Nakanishi K (1983) *Circular dichroic spectroscopy: exciton coupling in organic chemistry*. University Science Books, Oxford
52. Michl J, West R (2000) *Acc Chem Res* 33:821
53. Koe JR, Powell DR, Buffy JJ, Hayase S, West R (1998) *Angew Chem Int Ed Engl* 37:1441
54. Miller RD, Michl J (1989) *Chem Rev* 89:1359
55. Fujiki M, Toyoda S, Yuan CH, Takigawa H (1998) *Chirality* 10:667
56. Sato T, Terao K, Teramoto A, Fujiki M (2003) *Polymer* 44:5477

57. Hansma HG, Vesenka J, Siegerist C, Kelderman G, Morrett H, Sinsheimer RL, Elings V, Bustamante C, Hansma PK (1992) *Science* 256:1180
58. Ebihara K, Koshihara S, Yoshimoto M, Maeda T, Ohnishi T, Koinuma H, Fujiki M (1997) *Jpn J Appl Phys* 36:L1211
59. Furukawa K, Ebata K, Fujiki M (2000) *Adv Mater* 12:1033
60. Shinohara K, Aoki T, Kaneko T, Oikawa E (1997) *Chem Lett* 361
61. Teramae H, Takeda K (1989) *J Am Chem Soc* 111:1281
62. Obata K, Kabuto C, Kira M (1997) *J Am Chem Soc* 119:11345
63. Fujiki M (1996) *Polym Prepr ACS Polym Sci Div* 37(2):454
64. Pohl FM, Jovin TM (1972) *J Mol Biol* 67:375
65. Bradbury EM, Carpenter BG, Goldman H (1968) *Biopolymers* 6:837
66. Mahadevan S, Palaniandavar M (1996) *Chem Commun*, p 2547
67. Okamoto Y, Nakano T, Ono E, Hatada K (1991) *Chem Lett* 525
68. Watanabe J, Okamoto S, Satoh K, Sakajiri K, Furuya H, Abe A (1996) *Macromolecules* 29:7084
69. Cheon KS, Selinger JV, Green MM (2000) *Angew Chem Int Ed* 39:1482
70. Yashima E, Maeda K, Sato O (2001) *J Am Chem Soc* 123:8159
71. Tabei J, Nomura R, Sanda F, Masuda T (2004) *Macromolecules* 37:1175
72. Koe JR, Fujiki M, Nakashima H (2000) *Chem Commun*, p 389
73. Teramoto A, Terao K, Terao Y, Nakamura N, Sato T, Fujiki M (2001) *J Am Chem Soc* 123:12303
74. Lloyd S (1995) *Sci Am* 273:140
75. Nakamura Y, Pashkin YA, Tsai JS (1999) *Nature* 398:786
76. Cina JA, Harris RA (1995) *Science* 267:832
77. Cina JA, Harris RA (1994) *J Chem Phys* 100:2531
78. Hund F (1927) *Physik* 43:805
79. Rouvray DH (1986) *Sci Am* 255:36
80. Nakashima H, Fujiki M, Koe JR, Motonaga M (2001) *J Am Chem Soc* 123:1963
81. Nakashima H, Koe JR, Torimitsu K, Fujiki M (2001) *J Am Chem Soc* 123:4877
82. Peng W, Motonaga M, Koe JR (2004) *J Am Chem Soc* 126:13822
83. Takeda K, Teramae H, Matsumoto N (1986) *J Am Chem Soc* 108:8186
84. Koe JR, Fujiki M, Nakashima H (1999) *J Am Chem Soc* 121:9734
85. Yue S, Berry GC, Green MM (1996) *Macromolecules* 29:6175
86. Bidan G, Guillerez S, Sorokin V (1996) *Adv Mater* 8:157
87. Gottarelli G, Spada GP (2000) In: Berova N, Nakanishi K, Woody RW (eds) *Circular dichroism: principles and applications*, Chapt 19, 2nd edn. Wiley-VCH, New York
88. Pirkle WH, Pochapsky TC (1989) *Chem Rev* 89:347
89. Okamoto Y, Honda S, Okamoto I, Yuki H, Murata S, Noyori R, Takaya H (1981) *J Am Chem Soc* 103:6971
90. Ramos E, Bosch J, Serrano JL, Sierra T, Veciana J (1996) *J Am Chem Soc* 118:4703
91. Lermo ER, Langeveld-Voss BMW, Janssen RAJ, Meijer EW (1999) *Chem Commun*, p 791
92. Saxena A, Guo GQ, Fujiki M, Yang YG, Okoshi K, Ohira A, Naito M (2004) *Macromolecules* 37:3081
93. Ichimura K (2000) *Chem Rev* 100:1847
94. Fukuda K, Seki T, Ichimura K (2002) *Macromolecules* 35:2177
95. Guo G, Naito M, Fujiki M, Saxena A, Okoshi K, Yang Y, Ishikawa M, Hagihara T (2004) *Chem Commun*, p 276
96. Watanabe J, Kamee H, Fujiki M (2001) *Polym J* 33:495

97. Watanabe J, Fukuda Y, Gehani R, Uematsu I (1984) *Macromolecules* 17:1004
98. Watanabe J, Ono H, Abe A, Uematsu I (1985) *Macromolecules* 18:2141
99. Natsume T, Wu L, Sato T, Terao K, Teramoto A, Fujiki M (2001) *Macromolecules* 34:7899
100. Cline DB (ed) (1996) *Physical origin of homochirality in life*. AIP Proc 378, New York
101. Pasteur L (1848) *Ann Chim Phys* 24:442
102. Kipping FS, Pope WJ (1898) *Nature* 73:606
103. Macdermott AJ (2002) In: Lough WJ, Wainer IW (eds) *Chirality in natural and applied science*, Chapt 2. Blackwell, Oxford, p 23
104. Barron LD (2002) In: Lough WJ, Wainer IW (eds) *Chirality in natural and applied science*, Chapt 3. Blackwell, Oxford, p 53
105. Lee TD, Yang CN (1956) *Phys Rev* 104:254
106. Wu CS, Ambler E, Hayward RW, Hoppes DD, Hudson RP (1957) *Phys Rev* 105:1413
107. Bouchiat MA, Pottier L (1986) *Science* 234:1203
108. Emmons TP, Reeves JM, Fortson EN (1983) *Phys Rev Lett* 51:2089
109. Hegstrom RA, Chamberlain JP, Seto K, Watson RG (1988) *Am J Phys* 56:1086
110. Rein D (1974) *J Mol Evol* 4:15111
111. Hegstrom RA, Rein DW, Sandars PGH (1980) *J Chem Phys* 73:2329112
112. Mason SF, Tranter GE (1985) *Proc R Soc Lond A* 397:45113
113. Yamagata Y (1966) *J Theoret Biol* 11:495114
114. Wiesenfeld L (1988) *Mol Phys* 64:739115
115. Harris RA, Stodolsky L (1978) *Phys Lett* 78B:313
116. Quack M (1989) *Angew Chem Int Ed Engl* 28:571
117. Kondepudi DK, Nelson GW (1985) *Nature* 314:438
118. Salam A (1991) *J Mol Evol* 33:105
119. Fujiki M (2001) *Macromol Rapid Commun* 22:669
120. Scolnik Y, Portnaya I, Cogan U, Tal S, Haimovitz R, Fridkin M, Elitzur AC, Deamer DW, Shinitzky M (2006) *Phys Chem Chem Phys* 8:333
121. Tikhonov VI, Volkov AA (2002) *Science* 296:236
122. Ulbricht TLV, Vester F (1962) *Tetrahedron* 18:629
123. Mahurin S, McGinnis M, Bogard JS, Hulett LD, Pagni RM, Compton RN (2001) *Chirality* 13:636
124. Akaboshi M, Noda M, Kawai K, Maki H, Kawamoto K (1979) *Orig Life* 2:181
125. Moradour A, Nicoud JF, Balavoine G, Kagan H, Tsoucaris G (1971) *J Am Chem Soc* 93:2353
126. Feringa BL, van Delden RA (1999) *Angew Chem Int Ed* 38:3405
127. Kawasaki T, Sato M, Ishiguro S, Saito T, Morishita Y, Sato I, Nishino H, Inoue Y, Soai K (2005) *J Am Chem Soc* 127:3274
128. Rikken GLJA, Raupach E (2000) *Nature* 405:932
129. Bailey J, Chrysostomou A, Hough JH, Gledhill TM, McCall A, Clark S, Ménard F, Tamura M (1998) *Science* 281:672
130. Engel MH, Macko SA (1997) *Nature* 389:265
131. Thiemann W, Darge W (1974) *Orig Life* 5:263
132. Ito O, Terajima M, Azumi T (1990) *J Am Chem Soc* 112:445
133. Stodolsky L (1981) *Nature* 290:735
134. Weijs V, Manninen P, Vaara J (2005) *J Chem Phys* 123:1
135. Fujiki M Unpublished data.
136. Wang W, Yi F, Ni Y, Zhao Z, Jin X, Tang Y (2000) *J Biol Phys* 26:51
137. Sullivan R, Pyda M, Pak J, Wunderlich B, Thompson JR, Pagni R, Pan H, Barnes C, Schwerdtfeger P, Compton R (2003) *J Phys Chem A* 107:6674

---

## Author Index Volumes 251–284

Author Index Vols. 26–50 see Vol. 50  
Author Index Vols. 51–100 see Vol. 100  
Author Index Vols. 101–150 see Vol. 150  
Author Index Vols. 151–200 see Vol. 200  
Author Index Vols. 201–250 see Vol. 250

*The volume numbers are printed in italics*

- Accorsi G, see Armaroli N (2007) 280: 69–115  
Afonin S, Dürr UHN, Wadhwani P, Salgado J, Ulrich AS (2008) Solid State NMR Structure Analysis of the Antimicrobial Peptide Gramicidin S in Lipid Membranes: Concentration-Dependent Re-alignment and Self-Assembly as a  $\beta$ -Barrel. 273: 139–154  
Ajayaghosh A, George SJ, Schenning APHJ (2005) Hydrogen-Bonded Assemblies of Dyes and Extended  $\pi$ -Conjugated Systems. 258: 83–118  
Akai S, Kita Y (2007) Recent Advances in Pummerer Reactions. 274: 35–76  
Albert M, Fensterbank L, Lacôte E, Malacria M (2006) Tandem Radical Reactions. 264: 1–62  
Alberto R (2005) New Organometallic Technetium Complexes for Radiopharmaceutical Imaging. 252: 1–44  
Alegret S, see Pividori MI (2005) 260: 1–36  
Alfaro JA, see Schuman B (2007) 272: 217–258  
Amabilino DB, Veciana J (2006) Supramolecular Chiral Functional Materials. 265: 253–302  
Anderson CJ, see Li WP (2005) 252: 179–192  
Anslyn EV, see Collins BE (2007) 277: 181–218  
Anslyn EV, see Houk RJT (2005) 255: 199–229  
Appukkuttan P, Van der Eycken E (2006) Microwave-Assisted Natural Product Chemistry. 266: 1–47  
Araki K, Yoshikawa I (2005) Nucleobase-Containing Gelators. 256: 133–165  
Arcamone F-M (2008) Sabarubicin. 283: 171–189  
Armaroli N, Accorsi G, Cardinali Fç, Listorti A (2007) Photochemistry and Photophysics of Coordination Compounds: Copper. 280: 69–115  
Armitage BA (2005) Cyanine Dye–DNA Interactions: Intercalation, Groove Binding and Aggregation. 253: 55–76  
Arseniev AS, see Bocharov EV (2008) 273: 155–181  
Arvinte T, see Bocharov EV (2008) 273: 155–181  
Arya DP (2005) Aminoglycoside–Nucleic Acid Interactions: The Case for Neomycin. 253: 149–178  
Asensio JL, Bastida A, Jiménez-Barbero J (2008) Studies on the Conformational Features of Neomycin-B and its Molecular Recognition by RNA and Bacterial Defense Proteins. 273: 117–138  
  
Bailly C, see Dias N (2005) 253: 89–108  
Balaban TS, Tamiaki H, Holzwarth AR (2005) Chlorins Programmed for Self-Assembly. 258: 1–38  
Baltzer L (2007) Polypeptide Conjugate Binders for Protein Recognition. 277: 89–106

- Balzani V, Bergamini G, Campagna S, Puntoriero F (2007) Photochemistry and Photophysics of Coordination Compounds: Overview and General Concepts. 280: 1–36
- Balzani V, Credi A, Ferrer B, Silvi S, Venturi M (2005) Artificial Molecular Motors and Machines: Design Principles and Prototype Systems. 262: 1–27
- Balzani V, see Campagna S (2007) 280: 117–214
- Barbieri CM, see Pilch DS (2005) 253: 179–204
- Barbieri A, see Flamigni L (2007) 281: 143–204
- Barchuk A, see Daasbjerg K (2006) 263: 39–70
- Bargon J, see Kuhn LT (2007) 276: 25–68
- Bargon J, see Kuhn LT (2007) 276: 125–154
- Barigelletti F, see Flamigni L (2007) 281: 143–204
- Barthel BL, see Koch TH (2008) 283: 141–170
- Bastida A, see Asensio JL (2008) 273: 117–138
- Bayly SR, see Beer PD (2005) 255: 125–162
- Beck-Sickinger AG, see Haack M (2007) 278: 243–288
- Beer PD, Bayly SR (2005) Anion Sensing by Metal-Based Receptors. 255: 125–162
- Beretta GL, Zunino F (2008) Molecular Mechanisms of Anthracycline Activity. 283: 1–19
- Bergamini G, see Balzani V (2007) 280: 1–36
- Bergamini G, see Campagna S (2007) 280: 117–214
- Bertini L, Bruschi M, de Gioia L, Fantucci P, Greco C, Zampella G (2007) Quantum Chemical Investigations of Reaction Paths of Metalloenzymes and Biomimetic Models – The Hydrogenase Example. 268: 1–46
- Bier FF, see Heise C (2005) 261: 1–25
- Blommers MJJ, see Bocharov EV (2008) 273: 155–181
- Blommers MJJ, Strauss A, Geiser M, Ramage P, Sparrer H, Jahnke W (2008) NMR-Based Strategies to Elucidate Bioactive Conformations of Weakly Binding Ligands. 273: 1–14
- Blum LJ, see Marquette CA (2005) 261: 113–129
- Bocharov EV, Pavlov KV, Blommers MJJ, Arvinte T, Arseniev AS (2008) Modulation of the Bioactive Conformation of Transforming Growth Factor  $\beta$ : Possible Implications of Cation Binding for Biological Function. 273: 155–181
- Boiteau L, see Pascal R (2005) 259: 69–122
- Bolhuis PG, see Dellago C (2007) 268: 291–317
- Borovkov VV, Inoue Y (2006) Supramolecular Chirogenesis in Host–Guest Systems Containing Porphyrinoids. 265: 89–146
- Boschi A, Duatti A, Uccelli L (2005) Development of Technetium-99m and Rhenium-188 Radiopharmaceuticals Containing a Terminal Metal–Nitrido Multiple Bond for Diagnosis and Therapy. 252: 85–115
- Braga D, D’Addario D, Giaffreda SL, Maini L, Polito M, Grepioni F (2005) Intra-Solid and Inter-Solid Reactions of Molecular Crystals: a Green Route to Crystal Engineering. 254: 71–94
- Bräse S, see Jung N (2007) 278: 1–88
- Braverman S, Cherkinsky M (2007) [2,3]Sigmatropic Rearrangements of Propargylic and Allenic Systems. 275: 67–101
- Brebion F, see Crich D (2006) 263: 1–38
- Breinbauer R, see Mentel M (2007) 278: 209–241
- Breit B (2007) Recent Advances in Alkene Hydroformylation. 279: 139–172
- Brizard A, Oda R, Huc I (2005) Chirality Effects in Self-assembled Fibrillar Networks. 256: 167–218
- Broene RD (2007) Reductive Coupling of Unactivated Alkenes and Alkynes. 279: 209–248
- Brogini M (2008) Nemorubicin. 283: 191–206

- Bromfield K, see Ljungdahl N (2007) 278: 89–134
- Brown JM, Gridnev I, Klankermayer J (2008) Asymmetric Autocatalysis with Organozinc Complexes; Elucidation of the Reaction Pathway. 284: 35–65
- Bruce IJ, see del Campo A (2005) 260: 77–111
- Bruschi M, see Bertini L (2007) 268: 1–46
- Buhse T, see Lavabre D (2008) 284: 67–96
- Bur SK (2007) 1,3-Sulfur Shifts: Mechanism and Synthetic Utility. 274: 125–171
- Burkhart DJ, see Koch TH (2008) 283: 141–170
- Campagna S, Puntoriero F, Nastasi F, Bergamini G, Balzani V (2007) Photochemistry and Photophysics of Coordination Compounds: Ruthenium. 280: 117–214
- Campagna S, see Balzani V (2007) 280: 1–36
- del Campo A, Bruce IJ (2005) Substrate Patterning and Activation Strategies for DNA Chip Fabrication. 260: 77–111
- Capobianco ML, Catapano CV (2008) Daunomycin-TFO Conjugates for Downregulation of Gene Expression. 283: 45–71
- Cardinali F, see Armaroli N (2007) 280: 69–115
- Carney CK, Harry SR, Sewell SL, Wright DW (2007) Detoxification Biomimetics. 270: 155–185
- Castagner B, Seeberger PH (2007) Automated Solid Phase Oligosaccharide Synthesis. 278: 289–309
- Catapano CV, see Capobianco ML (2008) 283: 45–71
- Chaires JB (2005) Structural Selectivity of Drug-Nucleic Acid Interactions Probed by Competition Dialysis. 253: 33–53
- Cheng EC-C, see Yam VW-W (2007) 281: 269–310
- Cherkinsky M, see Braverman S (2007) 275: 67–101
- Chiorboli C, Indelli MT, Scandola F (2005) Photoinduced Electron/Energy Transfer Across Molecular Bridges in Binuclear Metal Complexes. 257: 63–102
- Chiorboli C, see Indelli MT (2007) 280: 215–255
- Coleman AW, Perret F, Moussa A, Dupin M, Guo Y, Perron H (2007) Calix[n]arenes as Protein Sensors. 277: 31–88
- Cölfen H (2007) Bio-inspired Mineralization Using Hydrophilic Polymers. 271: 1–77
- Collin J-P, Heitz V, Sauvage J-P (2005) Transition-Metal-Complexed Catenanes and Rotaxanes in Motion: Towards Molecular Machines. 262: 29–62
- Collins BE, Wright AT, Anslyn EV (2007) Combining Molecular Recognition, Optical Detection, and Chemometric Analysis. 277: 181–218
- Collyer SD, see Davis F (2005) 255: 97–124
- Commeyras A, see Pascal R (2005) 259: 69–122
- Coquerel G (2007) Preferential Crystallization. 269: 1–51
- Correia JDG, see Santos I (2005) 252: 45–84
- Costanzo G, see Saladino R (2005) 259: 29–68
- Cotarca L, see Zonta C (2007) 275: 131–161
- Credi A, see Balzani V (2005) 262: 1–27
- Crestini C, see Saladino R (2005) 259: 29–68
- Crich D, Brebion F, Suk D-H (2006) Generation of Alkene Radical Cations by Heterolysis of  $\beta$ -Substituted Radicals: Mechanism, Stereochemistry, and Applications in Synthesis. 263: 1–38
- Cuerva JM, Justicia J, Oller-López JL, Oltra JE (2006)  $\text{Cp}_2\text{TiCl}$  in Natural Product Synthesis. 264: 63–92

- Daasbjerg K, Svith H, Grimme S, Gerenkamp M, Mück-Lichtenfeld C, Gansäuer A, Barchuk A (2006) The Mechanism of Epoxide Opening through Electron Transfer: Experiment and Theory in Concert. 263: 39–70
- D’Addario D, see Braga D (2005) 254: 71–94
- Danishefsky SJ, see Warren JD (2007) 267: 109–141
- Darmency V, Renaud P (2006) Tin-Free Radical Reactions Mediated by Organoboron Compounds. 263: 71–106
- Davis F, Collyer SD, Higson SPJ (2005) The Construction and Operation of Anion Sensors: Current Status and Future Perspectives. 255: 97–124
- Deamer DW, Dworkin JP (2005) Chemistry and Physics of Primitive Membranes. 259: 1–27
- Debaene F, see Winssinger N (2007) 278: 311–342
- Dellago C, Bolhuis PG (2007) Transition Path Sampling Simulations of Biological Systems. 268: 291–317
- Deng J-Y, see Zhang X-E (2005) 261: 169–190
- Dervan PB, Poulin-Kerstien AT, Fechter EJ, Edelson BS (2005) Regulation of Gene Expression by Synthetic DNA-Binding Ligands. 253: 1–31
- Dias N, Vezin H, Lansiaux A, Bailly C (2005) Topoisomerase Inhibitors of Marine Origin and Their Potential Use as Anticancer Agents. 253: 89–108
- DiMauro E, see Saladino R (2005) 259: 29–68
- Dittrich M, Yu J, Schulten K (2007) PcrA Helicase, a Molecular Motor Studied from the Electronic to the Functional Level. 268: 319–347
- Dobrawa R, see You C-C (2005) 258: 39–82
- Dötsch V (2008) Investigation of Proteins in Living Bacteria with In-Cell NMR Experiments. 273: 203–214
- Du Q, Larsson O, Swerdlow H, Liang Z (2005) DNA Immobilization: Silanized Nucleic Acids and Nanoprinting. 261: 45–61
- Duatti A, see Boschi A (2005) 252: 85–115
- Dupin M, see Coleman AW (2007) 277: 31–88
- Dürr UHN, see Afonin S (2008) 273: 139–154
- Dworkin JP, see Deamer DW (2005) 259: 1–27
- Edelson BS, see Dervan PB (2005) 253: 1–31
- Edwards DS, see Liu S (2005) 252: 193–216
- Ernst K-H (2006) Supramolecular Surface Chirality. 265: 209–252
- Ersmark K, see Wannberg J (2006) 266: 167–197
- Escudé C, Sun J-S (2005) DNA Major Groove Binders: Triple Helix-Forming Oligonucleotides, Triple Helix-Specific DNA Ligands and Cleaving Agents. 253: 109–148
- Evans SV, see Schuman B (2007) 272: 217–258
- Van der Eycken E, see Appukkuttan P (2006) 266: 1–47
- Fages F, Vögtle F, Žinić M (2005) Systematic Design of Amide- and Urea-Type Gelators with Tailored Properties. 256: 77–131
- Fages F, see Žinić M (2005) 256: 39–76
- Faigl F, Schindler J, Fogassy E (2007) Advantages of Structural Similarities of the Reactants in Optical Resolution Processes. 269: 133–157
- Fan C-A, see Gansäuer A (2007) 279: 25–52
- Fantucci P, see Bertini L (2007) 268: 1–46
- Fechter EJ, see Dervan PB (2005) 253: 1–31
- Fensterbank L, see Albert M (2006) 264: 1–62
- Fernández JM, see Moonen NNP (2005) 262: 99–132



- Fernando C, see Szathmáry E (2005) 259: 167–211
- Ferrer B, see Balzani V (2005) 262: 1–27
- De Feyter S, De Schryver F (2005) Two-Dimensional Dye Assemblies on Surfaces Studied by Scanning Tunneling Microscopy. 258: 205–255
- Fischer D, Geyer A (2007) NMR Analysis of Bioprotective Sugars: Sucrose and Oligomeric (1→2)- $\alpha$ -D-glucopyranosyl-(1→2)- $\beta$ -D-fructofuranosides. 272: 169–186
- Flamigni L, Barbieri A, Sabatini C, Ventura B, Barigelletti F (2007) Photochemistry and Photophysics of Coordination Compounds: Iridium. 281: 143–204
- Flood AH, see Moonen NNP (2005) 262: 99–132
- Florent J-C, Monneret C (2008) Doxorubicin Conjugates for Selective Delivery to Tumors. 283: 99–140
- Fogassy E, see Faigl F (2007) 269: 133–157
- Fricke M, Volkmer D (2007) Crystallization of Calcium Carbonate Beneath Insoluble Monolayers: Suitable Models of Mineral–Matrix Interactions in Biomineralization? 270: 1–41
- Fujiki M (2008) Helix Generation, Amplification, Switching, and Memory of Chromophoric Polymers. 284: 119–186
- Fujimoto D, see Tamura R (2007) 269: 53–82
- Fujiwara S-i, Kambe N (2005) Thio-, Seleno-, and Telluro-Carboxylic Acid Esters. 251: 87–140
- Geiser M, see Blommers MJJ (2008) 273: 1–14
- Gansäuer A, see Daasbjerg K (2006) 263: 39–70
- Garcia-Garibay MA, see Karlen SD (2005) 262: 179–227
- Gelinck GH, see Grozema FC (2005) 257: 135–164
- Geng X, see Warren JD (2007) 267: 109–141
- Gansäuer A, Justicia J, Fan C-A, Worgull D, Piester F (2007) Reductive C–C Bond Formation after Epoxide Opening via Electron Transfer. 279: 25–52
- George SJ, see Ajayaghosh A (2005) 258: 83–118
- Gerenkamp M, see Daasbjerg K (2006) 263: 39–70
- Gevorgyan V, see Sromek AW (2007) 274: 77–124
- Geyer A, see Fischer D (2007) 272: 169–186
- Giaffreda SL, see Braga D (2005) 254: 71–94
- Gianni L, see Menna P (2008) 283: 21–44
- Giernoth R (2007) Homogeneous Catalysis in Ionic Liquids. 276: 1–23
- de Gioia L, see Bertini L (2007) 268: 1–46
- Di Giusto DA, King GC (2005) Special-Purpose Modifications and Immobilized Functional Nucleic Acids for Biomolecular Interactions. 261: 131–168
- Greco C, see Bertini L (2007) 268: 1–46
- Greiner L, Laue S, Wöltinger J, Liese A (2007) Continuous Asymmetric Hydrogenation. 276: 111–124
- Grepioni F, see Braga D (2005) 254: 71–94
- Gridnev I, see Brown JM (2008) 284: 35–65
- Grimme S, see Daasbjerg K (2006) 263: 39–70
- Grozema FC, Siebbeles LDA, Gelinck GH, Warman JM (2005) The Opto-Electronic Properties of Isolated Phenylenevinylene Molecular Wires. 257: 135–164
- Guiseppi-Elie A, Lingerfelt L (2005) Impedimetric Detection of DNA Hybridization: Towards Near-Patient DNA Diagnostics. 260: 161–186
- Gunnlaugsson T, see Leonard JP (2007) 281: 1–44
- Guo Y, see Coleman AW (2007) 277: 31–88



- Haack M, Beck-Sickinger AG (2007) Multiple Peptide Synthesis to Identify Bioactive Hormone Structures. 278: 243–288
- Haase C, Seitz O (2007) Chemical Synthesis of Glycopeptides. 267: 1–36
- Hahn F, Schepers U (2007) Solid Phase Chemistry for the Directed Synthesis of Biologically Active Polyamine Analogs, Derivatives, and Conjugates. 278: 135–208
- Hansen SG, Skrydstrup T (2006) Modification of Amino Acids, Peptides, and Carbohydrates through Radical Chemistry. 264: 135–162
- Harmer NJ (2007) The Fibroblast Growth Factor (FGF) – FGF Receptor Complex: Progress Towards the Physiological State. 272: 83–116
- Harry SR, see Carney CK (2007) 270: 155–185
- Heise C, Bier FF (2005) Immobilization of DNA on Microarrays. 261: 1–25
- Heitz V, see Collin J-P (2005) 262: 29–62
- Herrmann C, Reiher M (2007) First-Principles Approach to Vibrational Spectroscopy of Biomolecules. 268: 85–132
- Higson SPJ, see Davis F (2005) 255: 97–124
- Hirao T (2007) Catalytic Reductive Coupling of Carbonyl Compounds – The Pinacol Coupling Reaction and Beyond. 279: 53–75
- Hirayama N, see Sakai K (2007) 269: 233–271
- Hirst AR, Smith DK (2005) Dendritic Gelators. 256: 237–273
- Holzwarth AR, see Balaban TS (2005) 258: 1–38
- Homans SW (2007) Dynamics and Thermodynamics of Ligand–Protein Interactions. 272: 51–82
- Houk RJT, Tobey SL, Anslyn EV (2005) Abiotic Guanidinium Receptors for Anion Molecular Recognition and Sensing. 255: 199–229
- Huc I, see Brizard A (2005) 256: 167–218
- Hyuga H, see Saito Y (2008) 284: 97–118
- Ihmels H, Otto D (2005) Intercalation of Organic Dye Molecules into Double-Stranded DNA – General Principles and Recent Developments. 258: 161–204
- Iida H, Krische MJ (2007) Catalytic Reductive Coupling of Alkenes and Alkynes to Carbonyl Compounds and Imines Mediated by Hydrogen. 279: 77–104
- Imai H (2007) Self-Organized Formation of Hierarchical Structures. 270: 43–72
- Indelli MT, Chiorboli C, Scandola F (2007) Photochemistry and Photophysics of Coordination Compounds: Rhodium. 280: 215–255
- Indelli MT, see Chiorboli C (2005) 257: 63–102
- Inoue Y, see Borovkov VV (2006) 265: 89–146
- Ishii A, Nakayama J (2005) Carbodithioic Acid Esters. 251: 181–225
- Ishii A, Nakayama J (2005) Carboselenothioic and Carbodiselenoic Acid Derivatives and Related Compounds. 251: 227–246
- Ishi-i T, Shinkai S (2005) Dye-Based Organogels: Stimuli-Responsive Soft Materials Based on One-Dimensional Self-Assembling Aromatic Dyes. 258: 119–160
- Islas JÚ R, see Lavabre D (2008) 284: 67–96
- Jahnke W, see Blommers MJJ (2008) 273: 1–14
- James DK, Tour JM (2005) Molecular Wires. 257: 33–62
- James TD (2007) Saccharide-Selective Boronic Acid Based Photoinduced Electron Transfer (PET) Fluorescent Sensors. 277: 107–152
- Jayalakshmi V, see Krishna NR (2008) 273: 15–54
- Jelinek R, Kolusheva S (2007) Biomolecular Sensing with Colorimetric Vesicles. 277: 155–180
- Jiménez-Barbero J, see Asensio JL (2008) 273: 117–138

- Johnson MA, Pinto BM (2008) Structural and Functional Studies of Peptide–Carbohydrate Mimicry. 273: 55–116
- Jones W, see Trask AV (2005) 254: 41–70
- Jung N, Wiehn M, Bräse S (2007) Multifunctional Linkers for Combinatorial Solid Phase Synthesis. 278: 1–88
- Justicia J, see Cuerva JM (2006) 264: 63–92
- Justicia J, see Gansäuer A (2007) 279: 25–52
- Kalet BT, see Koch TH (2008) 283: 141–170
- Kambe N, see Fujiwara S-i (2005) 251: 87–140
- Kane-Maguire NAP (2007) Photochemistry and Photophysics of Coordination Compounds: Chromium. 280: 37–67
- Kann N, see Ljungdahl N (2007) 278: 89–134
- Kano N, Kawashima T (2005) Dithiocarboxylic Acid Salts of Group 1–17 Elements (Except for Carbon). 251: 141–180
- Kappe CO, see Kremsner JM (2006) 266: 233–278
- Kaptein B, see Kellogg RM (2007) 269: 159–197
- Karlen SD, Garcia-Garibay MA (2005) Amphidynamic Crystals: Structural Blueprints for Molecular Machines. 262: 179–227
- Kato S, Niyomura O (2005) Group 1–17 Element (Except Carbon) Derivatives of Thio-, Seleno- and Telluro-Carboxylic Acids. 251: 19–85
- Kato S, see Niyomura O (2005) 251: 1–12
- Kato T, Mizoshita N, Moriyama M, Kitamura T (2005) Gelation of Liquid Crystals with Self-Assembled Fibers. 256: 219–236
- Kaul M, see Pilch DS (2005) 253: 179–204
- Kaupp G (2005) Organic Solid-State Reactions with 100% Yield. 254: 95–183
- Kawasaki T, see Okahata Y (2005) 260: 57–75
- Kawasaki T, see Soai K (2008) 284: 1–33
- Kawashima T, see Kano N (2005) 251: 141–180
- Kay ER, Leigh DA (2005) Hydrogen Bond-Assembled Synthetic Molecular Motors and Machines. 262: 133–177
- Kellogg RM, Kaptein B, Vries TR (2007) Dutch Resolution of Racemates and the Roles of Solid Solution Formation and Nucleation Inhibition. 269: 159–197
- Kessler H, see Weide T (2007) 272: 1–50
- Kimura M, Tamaru Y (2007) Nickel-Catalyzed Reductive Coupling of Dienes and Carbonyl Compounds. 279: 173–207
- King GC, see Di Giusto DA (2005) 261: 131–168
- Kirchner B, see Thar J (2007) 268: 133–171
- Kirgan RA, Sullivan BP, Rillema DP (2007) Photochemistry and Photophysics of Coordination Compounds: Rhenium. 281: 45–102
- Kita Y, see Akai S (2007) 274: 35–76
- Kitamura T, see Kato T (2005) 256: 219–236
- Klankermayer J, see Brown JM (2008) 284: 35–65
- Kniep R, Simon P (2007) Fluorapatite-Gelatine-Nanocomposites: Self-Organized Morphogenesis, Real Structure and Relations to Natural Hard Materials. 270: 73–125
- Koch TH, Barthel BL, Kalet BT, Rudnicki DL, Post GC, Burkhart DJ (2008) Anthracycline-Formaldehyde Conjugates and Their Targeted Prodrugs. 283: 141–170
- Koenig BW (2007) Residual Dipolar Couplings Report on the Active Conformation of Rhodopsin-Bound Protein Fragments. 272: 187–216
- Kolusheva S, see Jelinek R (2007) 277: 155–180

- Komatsu K (2005) The Mechanochemical Solid-State Reaction of Fullerenes. 254: 185–206
- Kratz F (2008) Acid-Sensitive Prodrugs of Doxorubicin. 283: 73–97
- Kremsner JM, Stadler A, Kappe CO (2006) The Scale-Up of Microwave-Assisted Organic Synthesis. 266: 233–278
- Kriegisch V, Lambert C (2005) Self-Assembled Monolayers of Chromophores on Gold Surfaces. 258: 257–313
- Krische MJ, see Iida H (2007) 279: 77–104
- Krishna NR, Jayalakshmi V (2008) Quantitative Analysis of STD-NMR Spectra of Reversibly Forming Ligand–Receptor Complexes. 273: 15–54
- Kuhn LT, Bargon J (2007) Transfer of Parahydrogen-Induced Hyperpolarization to Heteronuclei. 276: 25–68
- Kuhn LT, Bargon J (2007) Exploiting Nuclear Spin Polarization to Investigate Free Radical Reactions via in situ NMR. 276: 125–154
- Kumaresan D, Shankar K, Vaidya S, Schmehl RH (2007) Photochemistry and Photophysics of Coordination Compounds: Osmium. 281: 101–142
- Lacôte E, see Albert M (2006) 264: 1–62
- Lahav M, see Weissbuch I (2005) 259: 123–165
- Lambert C, see Kriegisch V (2005) 258: 257–313
- Lansiaux A, see Dias N (2005) 253: 89–108
- LaPlante SR (2007) Exploiting Ligand and Receptor Adaptability in Rational Drug Design Using Dynamics and Structure-Based Strategies. 272: 259–296
- Larhed M, see Nilsson P (2006) 266: 103–144
- Larhed M, see Wannberg J (2006) 266: 167–197
- Larsson O, see Du Q (2005) 261: 45–61
- Laue S, see Greiner L (2007) 276: 111–124
- Lavabre D, Micheau J-C, Islas JÚ R, Buhse T (2008) Kinetic Insight into Specific Features of the Autocatalytic Soai Reaction. 284: 67–96
- Leigh DA, Pérez EM (2006) Dynamic Chirality: Molecular Shuttles and Motors. 265: 185–208
- Leigh DA, see Kay ER (2005) 262: 133–177
- Leiserowitz L, see Weissbuch I (2005) 259: 123–165
- Leonard JP, Nolan CB, Stomeo F, Gunnlaugsson T (2007) Photochemistry and Photophysics of Coordination Compounds: Lanthanides. 281: 1–44
- Lhoták P (2005) Anion Receptors Based on Calixarenes. 255: 65–95
- Li WP, Meyer LA, Anderson CJ (2005) Radiopharmaceuticals for Positron Emission Tomography Imaging of Somatostatin Receptor Positive Tumors. 252: 179–192
- Liang Z, see Du Q (2005) 261: 45–61
- Liese A, see Greiner L (2007) 276: 111–124
- Lingerfelt L, see Guiseppi-Elie A (2005) 260: 161–186
- Listorti A, see Armaroli N (2007) 280: 69–115
- Litvinchuk S, see Matile S (2007) 277: 219–250
- Liu S (2005) 6-Hydrazinonicotinamide Derivatives as Bifunctional Coupling Agents for <sup>99m</sup>Tc-Labeling of Small Biomolecules. 252: 117–153
- Liu S, Robinson SP, Edwards DS (2005) Radiolabeled Integrin  $\alpha_v\beta_3$  Antagonists as Radiopharmaceuticals for Tumor Radiotherapy. 252: 193–216
- Liu XY (2005) Gelation with Small Molecules: from Formation Mechanism to Nanostructure Architecture. 256: 1–37
- Ljungdahl N, Bromfield K, Kann N (2007) Solid Phase Organometallic Chemistry. 278: 89–134
- De Lucchi O, see Zonta C (2007) 275: 131–161

- Luderer F, Walschus U (2005) Immobilization of Oligonucleotides for Biochemical Sensing by Self-Assembled Monolayers: Thiol-Organic Bonding on Gold and Silanization on Silica Surfaces. *260*: 37–56
- Maeda K, Yashima E (2006) Dynamic Helical Structures: Detection and Amplification of Chirality. *265*: 47–88
- Magnera TF, Michl J (2005) Altitudinal Surface-Mounted Molecular Rotors. *262*: 63–97
- Maini L, see Braga D (2005) *254*: 71–94
- Malacria M, see Albert M (2006) *264*: 1–62
- Marquette CA, Blum LJ (2005) Beads Arraying and Beads Used in DNA Chips. *261*: 113–129
- Mascini M, see Palchetti I (2005) *261*: 27–43
- Matile S, Tanaka H, Litvinchuk S (2007) Analyte Sensing Across Membranes with Artificial Pores. *277*: 219–250
- Matsumoto A (2005) Reactions of 1,3-Diene Compounds in the Crystalline State. *254*: 263–305
- McGhee AM, Procter DJ (2006) Radical Chemistry on Solid Support. *264*: 93–134
- Menna P, Salvatorelli E, Gianni L, Minotti G (2008) Anthracycline Cardiotoxicity. *283*: 21–44
- Mentel M, Breinbauer R (2007) Combinatorial Solid-Phase Natural Product Chemistry. *278*: 209–241
- Meyer B, Möller H (2007) Conformation of Glycopeptides and Glycoproteins. *267*: 187–251
- Meyer LA, see Li WP (2005) *252*: 179–192
- Micheau J-C, see Lavabre D (2008) *284*: 67–96
- Michl J, see Magnera TF (2005) *262*: 63–97
- Milea JS, see Smith CL (2005) *261*: 63–90
- Minotti G, see Menna P (2008) *283*: 21–44
- Mizoshita N, see Kato T (2005) *256*: 219–236
- Modlinger A, see Weide T (2007) *272*: 1–50
- Möller H, see Meyer B (2007) *267*: 187–251
- Monneret C, see Florent J-C (2008) *283*: 99–140
- Montgomery J, Sormunen GJ (2007) Nickel-Catalyzed Reductive Couplings of Aldehydes and Alkynes. *279*: 1–23
- Moonen NNP, Flood AH, Fernández JM, Stoddart JF (2005) Towards a Rational Design of Molecular Switches and Sensors from their Basic Building Blocks. *262*: 99–132
- Moriyama M, see Kato T (2005) *256*: 219–236
- Moussa A, see Coleman AW (2007) *277*: 31–88
- Murai T (2005) Thio-, Seleno-, Telluro-Amides. *251*: 247–272
- Murakami H (2007) From Racemates to Single Enantiomers – Chiral Synthetic Drugs over the last 20 Years. *269*: 273–299
- Mutule I, see Suna E (2006) *266*: 49–101
- Naka K (2007) Delayed Action of Synthetic Polymers for Controlled Mineralization of Calcium Carbonate. *271*: 119–154
- Nakayama J, see Ishii A (2005) *251*: 181–225
- Nakayama J, see Ishii A (2005) *251*: 227–246
- Narayanan S, see Reif B (2007) *272*: 117–168
- Nastasi F, see Campagna S (2007) *280*: 117–214
- Neese F, see Sinnecker S (2007) *268*: 47–83
- Nguyen GH, see Smith CL (2005) *261*: 63–90
- Nicolau DV, Sawant PD (2005) Scanning Probe Microscopy Studies of Surface-Immobilised DNA/Oligonucleotide Molecules. *260*: 113–160

- Niessen HG, Woelk K (2007) Investigations in Supercritical Fluids. 276: 69–110
- Nilsson P, Olofsson K, Larhed M (2006) Microwave-Assisted and Metal-Catalyzed Coupling Reactions. 266: 103–144
- Nishiyama H, Shiomi T (2007) Reductive Aldol, Michael, and Mannich Reactions. 279: 105–137
- Niyomura O, Kato S (2005) Chalcogenocarboxylic Acids. 251: 1–12
- Niyomura O, see Kato S (2005) 251: 19–85
- Nohira H, see Sakai K (2007) 269: 199–231
- Nolan CB, see Leonard JP (2007) 281: 1–44
- Oda R, see Brizard A (2005) 256: 167–218
- Okahata Y, Kawasaki T (2005) Preparation and Electron Conductivity of DNA-Aligned Cast and LB Films from DNA-Lipid Complexes. 260: 57–75
- Okamura T, see Ueyama N (2007) 271: 155–193
- Oller-López JL, see Cuerva JM (2006) 264: 63–92
- Olofsson K, see Nilsson P (2006) 266: 103–144
- Oltra JE, see Cuerva JM (2006) 264: 63–92
- Onoda A, see Ueyama N (2007) 271: 155–193
- Otto D, see Ihmels H (2005) 258: 161–204
- Otto S, Severin K (2007) Dynamic Combinatorial Libraries for the Development of Synthetic Receptors and Sensors. 277: 267–288
- Palchetti I, Mascini M (2005) Electrochemical Adsorption Technique for Immobilization of Single-Stranded Oligonucleotides onto Carbon Screen-Printed Electrodes. 261: 27–43
- Pascal R, Boiteau L, Commeyras A (2005) From the Prebiotic Synthesis of  $\alpha$ -Amino Acids Towards a Primitive Translation Apparatus for the Synthesis of Peptides. 259: 69–122
- Paulo A, see Santos I (2005) 252: 45–84
- Pavlov KV, see Bocharov EV (2008) 273: 155–181
- Pérez EM, see Leigh DA (2006) 265: 185–208
- Perret F, see Coleman AW (2007) 277: 31–88
- Perron H, see Coleman AW (2007) 277: 31–88
- Peters T, see Rademacher C (2008) 273: 183–202
- Pianowski Z, see Winssinger N (2007) 278: 311–342
- Piestert F, see Gansäuer A (2007) 279: 25–52
- Pilch DS, Kaul M, Barbieri CM (2005) Ribosomal RNA Recognition by Aminoglycoside Antibiotics. 253: 179–204
- Pinto BM, see Johnson MA (2008) 273: 55–116
- Pividori MI, Alegret S (2005) DNA Adsorption on Carbonaceous Materials. 260: 1–36
- Piwnica-Worms D, see Sharma V (2005) 252: 155–178
- Plesniak K, Zarecki A, Wicha J (2007) The Smiles Rearrangement and the Julia–Kocienski Olefination Reaction. 275: 163–250
- Polito M, see Braga D (2005) 254: 71–94
- Post GC, see Koch TH (2008) 283: 141–170
- Poulin-Kerstien AT, see Dervan PB (2005) 253: 1–31
- de la Pradilla RF, Tortosa M, Viso A (2007) Sulfur Participation in [3,3]-Sigmatropic Rearrangements. 275: 103–129
- Procter DJ, see McGhee AM (2006) 264: 93–134
- Puntoriero F, see Balzani V (2007) 280: 1–36
- Puntoriero F, see Campagna S (2007) 280: 117–214

- Quiclet-Sire B, Zard SZ (2006) The Degenerative Radical Transfer of Xanthates and Related Derivatives: An Unusually Powerful Tool for the Creation of Carbon–Carbon Bonds. 264: 201–236
- Rademacher C, Peters T (2008) Molecular Recognition of Ligands by Native Viruses and Virus-Like Particles as Studied by NMR Experiments. 273: 183–202
- Ramage P, see Blommers MJJ (2008) 273: 1–14
- Ratner MA, see Weiss EA (2005) 257: 103–133
- Raymond KN, see Seeber G (2006) 265: 147–184
- Rebek Jr J, see Scarso A (2006) 265: 1–46
- Reckien W, see Thar J (2007) 268: 133–171
- Reggelin M (2007) [2,3]-Sigmatropic Rearrangements of Allylic Sulfur Compounds. 275: 1–65
- Reif B, Narayanan S (2007) Characterization of Interactions Between Misfolding Proteins and Molecular Chaperones by NMR Spectroscopy. 272: 117–168
- Reiher M, see Herrmann C (2007) 268: 85–132
- Renaud P, see Darmency V (2006) 263: 71–106
- Revell JD, Wennemers H (2007) Identification of Catalysts in Combinatorial Libraries. 277: 251–266
- Rillema DP, see Kirgan RA (2007) 281: 45–102
- Robinson SP, see Liu S (2005) 252: 193–216
- Rudnicki DL, see Koch TH (2008) 283: 141–170
- Sabatini C, see Flamigni L (2007) 281: 143–204
- Saha-Möller CR, see You C-C (2005) 258: 39–82
- Saito Y, Hyuga H (2008) Rate Equation Approaches to Amplification of Enantiomeric Excess and Chiral Symmetry Breaking. 284: 97–118
- Sakai K, Sakurai R, Hirayama N (2007) Molecular Mechanisms of Dielectrically Controlled Resolution (DCR). 269: 233–271
- Sakai K, Sakurai R, Nohira H (2007) New Resolution Technologies Controlled by Chiral Discrimination Mechanisms. 269: 199–231
- Sakamoto M (2005) Photochemical Aspects of Thiocarbonyl Compounds in the Solid-State. 254: 207–232
- Sakurai R, see Sakai K (2007) 269: 199–231
- Sakurai R, see Sakai K (2007) 269: 233–271
- Saladino R, Crestini C, Costanzo G, DiMauro E (2005) On the Prebiotic Synthesis of Nucleobases, Nucleotides, Oligonucleotides, Pre-RNA and Pre-DNA Molecules. 259: 29–68
- Salgado J, see Afonin S (2008) 273: 139–154
- Salvatorelli E, see Menna P (2008) 283: 21–44
- Santos I, Paulo A, Correia JDG (2005) Rhenium and Technetium Complexes Anchored by Phosphines and Scorpionates for Radiopharmaceutical Applications. 252: 45–84
- Santos M, see Szathmáry E (2005) 259: 167–211
- Sato K (2007) Inorganic–Organic Interfacial Interactions in Hydroxyapatite Mineralization Processes. 270: 127–153
- Sauvage J-P, see Collin J-P (2005) 262: 29–62
- Sawant PD, see Nicolau DV (2005) 260: 113–160
- Scandola F, see Chiorboli C (2005) 257: 63–102
- Scarso A, Rebek Jr J (2006) Chiral Spaces in Supramolecular Assemblies. 265: 1–46
- Schaumann E (2007) Sulfur is More Than the Fat Brother of Oxygen. An Overview of Organosulfur Chemistry. 274: 1–34

- Scheffer JR, Xia W (2005) Asymmetric Induction in Organic Photochemistry via the Solid-State Ionic Chiral Auxiliary Approach. 254: 233–262
- Schenning APHJ, see Ajayaghosh A (2005) 258: 83–118
- Schepers U, see Hahn F (2007) 278: 135–208
- Schindler J, see Faigl F (2007) 269: 133–157
- Schmehl RH, see Kumaresan D (2007) 281: 101–142
- Schmidtchen FP (2005) Artificial Host Molecules for the Sensing of Anions. 255: 1–29 Author Index Volumes 251–255
- Scandola F, see Indelli MT (2007) 280: 215–255
- Schmuck C, Wich P (2007) The Development of Artificial Receptors for Small Peptides Using Combinatorial Approaches. 277: 3–30
- Schoof S, see Wolter F (2007) 267: 143–185
- De Schryver F, see De Feyter S (2005) 258: 205–255
- Schulten K, see Dittrich M (2007) 268: 319–347
- Schuman B, Alfaro JA, Evans SV (2007) Glycosyltransferase Structure and Function. 272: 217–258
- Seeber G, Tiedemann BEF, Raymond KN (2006) Supramolecular Chirality in Coordination Chemistry. 265: 147–184
- Seeberger PH, see Castagner B (2007) 278: 289–309
- Seitz O, see Haase C (2007) 267: 1–36
- Senn HM, Thiel W (2007) QM/MM Methods for Biological Systems. 268: 173–289
- Severin K, see Otto S (2007) 277: 267–288
- Sewell SL, see Carney CK (2007) 270: 155–185
- Shankar K, see Kumaresan D (2007) 281: 101–142
- Sharma V, Piwnica-Worms D (2005) Monitoring Multidrug Resistance P-Glycoprotein Drug Transport Activity with Single-Photon-Emission Computed Tomography and Positron Emission Tomography Radiopharmaceuticals. 252: 155–178
- Shinkai S, see Ishi-i T (2005) 258: 119–160
- Shiomi T, see Nishiyama H (2007) 279: 105–137
- Sibi MP, see Zimmerman J (2006) 263: 107–162
- Siebbeles LDA, see Grozema FC (2005) 257: 135–164
- Silvi S, see Balzani V (2005) 262: 1–27
- Simon P, see Kniep R (2007) 270: 73–125
- Sinnecker S, Neese F (2007) Theoretical Bioinorganic Spectroscopy. 268: 47–83
- Skrydstrup T, see Hansen SG (2006) 264: 135–162
- Smith CL, Milea JS, Nguyen GH (2005) Immobilization of Nucleic Acids Using Biotin-Strept(avidin) Systems. 261: 63–90
- Smith DK, see Hirst AR (2005) 256: 237–273
- Soai K, Kawasaki T (2008) Asymmetric Autocatalysis with Amplification of Chirality. 284: 1–33
- Sormunen GJ, see Montgomery J (2007) 279: 1–23
- Sparrer H, see Blommers MJJ (2008) 273: 1–14
- Specker D, Wittmann V (2007) Synthesis and Application of Glycopeptide and Glycoprotein Mimetics. 267: 65–107
- Sromek AW, Gevorgyan V (2007) 1,2-Sulfur Migrations. 274: 77–124
- Stadler A, see Kremsner JM (2006) 266: 233–278
- Stibor I, Zlatušková P (2005) Chiral Recognition of Anions. 255: 31–63
- Stoddart JF, see Moonen NNP (2005) 262: 99–132
- Stomeo F, see Leonard JP (2007) 281: 1–44
- Strauss A, see Blommers MJJ (2008) 273: 1–14



- Strauss CR, Varma RS (2006) *Microwaves in Green and Sustainable Chemistry*. 266: 199–231
- Suk D-H, see Crich D (2006) 263: 1–38
- Suksai C, Tuntulani T (2005) *Chromogenetic Anion Sensors*. 255: 163–198
- Sullivan BP, see Kirgan RA (2007) 281: 45–102
- Sun J-S, see Escudé C (2005) 253: 109–148
- Suna E, Mutule I (2006) *Microwave-assisted Heterocyclic Chemistry*. 266: 49–101
- Süssmuth RD, see Wolter F (2007) 267: 143–185
- Svith H, see Daasbjerg K (2006) 263: 39–70
- Swerdlow H, see Du Q (2005) 261: 45–61
- Szathmáry E, Santos M, Fernando C (2005) *Evolutionary Potential and Requirements for Minimal Protocells*. 259: 167–211
- Taira S, see Yokoyama K (2005) 261: 91–112
- Takahashi H, see Tamura R (2007) 269: 53–82
- Takahashi K, see Ueyama N (2007) 271: 155–193
- Tamiaki H, see Balaban TS (2005) 258: 1–38
- Tamaru Y, see Kimura M (2007) 279: 173–207
- Tamura R, Takahashi H, Fujimoto D, Ushio T (2007) *Mechanism and Scope of Preferential Enrichment, a Symmetry-Breaking Enantiomeric Resolution Phenomenon*. 269: 53–82
- Tanaka H, see Matile S (2007) 277: 219–250
- Thar J, Reckien W, Kirchner B (2007) *Car-Parrinello Molecular Dynamics Simulations and Biological Systems*. 268: 133–171
- Thayer DA, Wong C-H (2007) *Enzymatic Synthesis of Glycopeptides and Glycoproteins*. 267: 37–63
- Thiel W, see Senn HM (2007) 268: 173–289
- Tiedemann BEF, see Seeber G (2006) 265: 147–184
- Tobey SL, see Houk RJT (2005) 255: 199–229
- Toda F (2005) *Thermal and Photochemical Reactions in the Solid-State*. 254: 1–40
- Tortosa M, see de la Pradilla RF (2007) 275: 103–129
- Tour JM, see James DK (2005) 257: 33–62
- Trask AV, Jones W (2005) *Crystal Engineering of Organic Cocrystals by the Solid-State Grinding Approach*. 254: 41–70
- Tuntulani T, see Suksai C (2005) 255: 163–198
- Uccelli L, see Boschi A (2005) 252: 85–115
- Ueyama N, Takahashi K, Onoda A, Okamura T, Yamamoto H (2007) *Inorganic–Organic Calcium Carbonate Composite of Synthetic Polymer Ligands with an Intramolecular NH $\cdots$ O Hydrogen Bond*. 271: 155–193
- Ulrich AS, see Afonin S (2008) 273: 139–154
- Ushio T, see Tamura R (2007) 269: 53–82
- Vaidya S, see Kumaresan D (2007) 281: 101–142
- Varma RS, see Strauss CR (2006) 266: 199–231
- Veciana J, see Amabilino DB (2006) 265: 253–302
- Ventura B, see Flamigni L (2007) 281: 143–204
- Venturi M, see Balzani V (2005) 262: 1–27
- Vezin H, see Dias N (2005) 253: 89–108
- Viso A, see de la Pradilla RF (2007) 275: 103–129
- Vögtle F, see Fages F (2005) 256: 77–131
- Vögtle M, see Žinić M (2005) 256: 39–76



- Volkmer D, see Fricke M (2007) 270: 1–41  
Volpicelli R, see Zonta C (2007) 275: 131–161  
Vries TR, see Kellogg RM (2007) 269: 159–197
- Wadhwani P, see Afonin S (2008) 273: 139–154  
Walschus U, see Luderer F (2005) 260: 37–56  
Walton JC (2006) Unusual Radical Cyclisations. 264: 163–200  
Wannberg J, Ersmark K, Larhed M (2006) Microwave-Accelerated Synthesis of Protease Inhibitors. 266: 167–197  
Warman JM, see Grozema FC (2005) 257: 135–164  
Warren JD, Geng X, Danishefsky SJ (2007) Synthetic Glycopeptide-Based Vaccines. 267: 109–141  
Wasielewski MR, see Weiss EA (2005) 257: 103–133  
Weide T, Modlinger A, Kessler H (2007) Spatial Screening for the Identification of the Bioactive Conformation of Integrin Ligands. 272: 1–50  
Weiss EA, Wasielewski MR, Ratner MA (2005) Molecules as Wires: Molecule-Assisted Movement of Charge and Energy. 257: 103–133  
Weissbuch I, Leiserowitz L, Lahav M (2005) Stochastic “Mirror Symmetry Breaking” via Self-Assembly, Reactivity and Amplification of Chirality: Relevance to Abiotic Conditions. 259: 123–165  
Wennemers H, see Revell JD (2007) 277: 251–266  
Wich P, see Schmuck C (2007) 277: 3–30  
Wicha J, see Plesniak K (2007) 275: 163–250  
Wiehn M, see Jung N (2007) 278: 1–88  
Williams JAG (2007) Photochemistry and Photophysics of Coordination Compounds: Platinum. 281: 205–268  
Williams LD (2005) Between Objectivity and Whim: Nucleic Acid Structural Biology. 253: 77–88  
Winssinger N, Pianowski Z, Debaene F (2007) Probing Biology with Small Molecule Microarrays (SMM). 278: 311–342  
Wittmann V, see Specker D (2007) 267: 65–107  
Wright DW, see Carney CK (2007) 270: 155–185  
Woelk K, see Niessen HG (2007) 276: 69–110  
Wolter F, Schoof S, Süßmuth RD (2007) Synopsis of Structural, Biosynthetic, and Chemical Aspects of Glycopeptide Antibiotics. 267: 143–185  
Wöltinger J, see Greiner L (2007) 276: 111–124  
Wong C-H, see Thayer DA (2007) 267: 37–63  
Wong KM-C, see Yam VW-W (2005) 257: 1–32  
Worgull D, see Gansäuer A (2007) 279: 25–52  
Wright AT, see Collins BE (2007) 277: 181–218  
Würthner F, see You C-C (2005) 258: 39–82
- Xia W, see Scheffer JR (2005) 254: 233–262
- Yam VW-W, Cheng EC-C (2007) Photochemistry and Photophysics of Coordination Compounds: Gold. 281: 269–310  
Yam VW-W, Wong KM-C (2005) Luminescent Molecular Rods – Transition-Metal Alkynyl Complexes. 257: 1–32  
Yamamoto H, see Ueyama N (2007) 271: 155–193  
Yashima E, see Maeda K (2006) 265: 47–88

- Yokoyama K, Taira S (2005) Self-Assembly DNA-Conjugated Polymer for DNA Immobilization on Chip. 261: 91–112
- Yoshikawa I, see Araki K (2005) 256: 133–165
- Yoshioka R (2007) Racemization, Optical Resolution and Crystallization-Induced Asymmetric Transformation of Amino Acids and Pharmaceutical Intermediates. 269: 83–132
- You C-C, Dobrawa R, Saha-Möller CR, Würthner F (2005) Metallo-supramolecular Dye Assemblies. 258: 39–82
- Yu J, see Dittrich M (2007) 268: 319–347
- Yu S-H (2007) Bio-inspired Crystal Growth by Synthetic Templates. 271: 79–118
- Zampella G, see Bertini L (2007) 268: 1–46
- Zard SZ, see Quiclet-Sire B (2006) 264: 201–236
- Zarecki A, see Plesniak K (2007) 275: 163–250
- Zhang W (2006) Microwave-Enhanced High-Speed Fluorous Synthesis. 266: 145–166
- Zhang X-E, Deng J-Y (2005) Detection of Mutations in Rifampin-Resistant *Mycobacterium Tuberculosis* by Short Oligonucleotide Ligation Assay on DNA Chips (SOLAC). 261: 169–190
- Zimmerman J, Sibi MP (2006) Enantioselective Radical Reactions. 263: 107–162
- Žinić M, see Fages F (2005) 256: 77–131
- Žinić M, Vögtle F, Fages F (2005) Cholesterol-Based Gelators. 256: 39–76
- Zipse H (2006) Radical Stability—A Theoretical Perspective. 263: 163–190
- Zlatušková P, see Stibor I (2005) 255: 31–63
- Zonta C, De Lucchi O, Volpicelli R, Cotarca L (2007) Thione–Thiol Rearrangement: Miyazaki–Newman–Kwart Rearrangement and Others. 275: 131–161
- Zunino F, see Beretta GL (2008) 283: 1–19

---

# Subject Index

- Additive-additive interactions 89
- Additive-product interactions 90
- Additives, chiral 75
- AFM, single rod-like helical polymer molecule 134
- Aldehydes, asymmetric alkylation, dialkylzinc reagents 39
  - chiral amino alcohol catalyzed asymmetric dialkylzinc addition 3
  - structures 70
  - zinc alkyl addition 37
- 2-Alkynyl-5-pyrimidyl alkanol 71
- Alkynylpyrimidine 44
- 2-Alkynylpyrimidine-5-carbaldehyde 27
- Allenes 26
- Amino acids, chiral sensing 19
- Aminoalcohol 40
- Amplification 119
  - chirality 1
  - rate equation 97
- Anticatalyst 2
- Asymmetric synthesis, absolute 35
  - spontaneous 80
- Autocatalysis 53
  - asymmetric 1, 3, 4, 35
  - – amplification of chirality 3
  - – chiral organic compounds 11
  - – heterogeneous chiral substances 27
  - – isotopically chiral primary alcohols 26
  - linear 104
  - nonlinear 97
  - quadratic 106
- Automultiplication 1
- Binaphthyls 26
- 5-Carbamoyl-3-pyridyl alkanol 28
- Chiral additives 75
- Chiral crystals 17
- Chiral discrimination 24
- Chiral symmetry breaking 97, 110
  - crystallization 82
- Chirality transcription/memory 165
- Chromophoric polymers 119
  - main chain 123
- CPL 2, 12
- Cryptochirality, quaternary hydrocarbon 24
- DBAE 78
- DFT calculations 35
- Dialkylzinc 3, 39
  - binding, NMR 48
- Diisopropylzinc 4, 27, 35, 39, 45, 50–52, 74
- Discrete-state stochastic modeling 79
- DMNE 78
- DNA 98, 119, 134
- Enantiomeric excess (ee) 3–6, 9, 19, 37, 68, 79, 97, 99, 124
  - amplification 115
- Enantiomorphous inorganic crystals 15
- Enantioselectivity reversal 74, 89
- Ephedrine 27
- 5-Ethyl-5-propylundecane 24
- Extraterrestrial chirality, meteorites 21
- Flow trajectory 97
- Heavy metal atoms 175
- Helicenes 26, 75
- Helicity, quantized/superposed 153
- Helix generation 119
- Helix switching 144
  - copolymers 151
- Heterodimers, antagonistic, amplification 109
- Hexahelicene 13

- Hippuric acid 18  
 Homochirality 1, 97, 99, 122  
   – biological, asymmetric autocatalysis 12  
   – origin 1  
 Homodimer catalyst, amplification 107  
 Homopolymers, optically active 131  
 Hydrocarbons, cryptochiral quaternary,  
   chiral discrimination 25  
  
 Isocyano-L-alanine-L-alanine 120  
 Isopropylzinc alkoxides 69  
 Isopropylzinc-derived species 47, 58  
  
 Ketoolefin 14  
 Kinetics 39  
  
 Leucine 75  
  
*Majority rule* experiments 122, 159  
   – copolymers 143  
 Memory 119  
 Meteorites, extraterrestrial chirality 21  
 Methyl mandelate 11, 75  
 2-Methyl-1-(5-pyrimidyl)propan-1-ol 5  
 Methylzinc models 56  
 Microcalorimetric kinetics 35  
 Mirror-symmetry breaking 71, 86  
 Molecular chirality transcription/memory  
   165  
 Monomeric systems, amplification 100  
*M-screw sense*-selective photolysis 137  
  
 NMR 44  
   – analyses 35  
   – exchange spectroscopy 52  
   – autocatalysis 53  
   – spontaneous asymmetric synthesis 55  
   – thf-d<sub>8</sub> 45  
   – toluene-d<sub>8</sub> 48  
 Non-linear effects (NLE) 37  
  
 Olefins 26  
 Organic–inorganic hybrid 28  
 Organopolysilanes 125  
 Organozinc complexes 35  
 Orion constellation 12  
  
*P-screw sense* telomeres, Si–Cl termini  
   137  
 Paracyclophanes 26  
  
 Parity-violating energy difference (PVED)  
   2  
 Parity-violations (PV) 175  
 Phthalocyanine 120  
 Poly(alkylarylsilane)s 130  
 Poly[bis{(S)-3,7-dimethyloctyl}silylene]  
   176  
 Poly([bis{(S)-2-methylbutyl}silane]-*co*-  
   (di-*n*-pentylsilane)) 137  
 Poly(*t*-butyl isocyanides) 123  
 Poly(*n*-decyl-(S)-2-methylbutylsilane)  
   131  
 Poly(dialkylsilane)s 130  
 Poly(dichlorosilane) 127  
 Poly{*n*-hexyl-(S)-3-methylpentylsilane}  
   129  
 Poly{methyl-(S)-2-methylbutylsilane}  
   129  
 Poly(methyl-(–)-β-pinanylsilane) 135  
 Poly(phenylacetylene) 120  
 Poly(phenylenevinylene) 124, 128  
 Poly(*p*-phenylene) 124  
 Poly(triphenylmethyl methacrylate) 123,  
   128  
 Polyacetylene 124, 128, 137  
   – fiber 120  
 Polyanilines 124  
 Polycarbodiimides 124, 128  
 Polydiacetylenes 124  
 Polyfluorenes 124  
 Polyisocyanate 123, 128, 137  
   – helical 120  
 Poly-α-olefins 123  
 Polypyrroles 124  
 Polysilanes 124  
   – binary film, helix command surface  
     experiments 168  
   – chiroptical switching/memory 159  
   – helical, tunable cholesteric liquid  
     crystallinity 172  
   – – circular dichroism 126  
   – – optically active 124  
   – helix amplification 137  
   – helix switching 144  
 Polystyrene-*block*-  
   poly(methylmethacrylate)  
   134  
 Polythiophene 124, 128  
 Prebiotic world 99  
 PVED 2, 176

- 3-Pyridinecarbaldehyde 4  
Pyridyl alcohol, chiral, Asymmetric autocatalysis 4  
Pyrimidine-5-carbaldehyde 11  
Pyrimidinyl alcohol 41  
Pyrimidyl alkanols 1,6, 69, 74  
  
Quartz 77  
3-Quinoline carbaldehyde 70  
3-Quinolyl alkanol 28  
  
Recycling 97  
  
Screw sense, helical ordering 127  
– opposite 135  
– switching, preferential, homopolymers 144  
*Sergeants–soldiers* experiments 122, 159  
– copolymers 137  
– homopolymers 143  
Silsesquioxane 27  
  
Soai autocatalysis 35  
– amplifying, two-stage procedure 38  
Soai catalyst, solution structure 45  
Soai reaction 97  
– experimental features 70  
– kinetics 82  
Sodium chlorate 16  
STM 120, 134  
Switching 119  
  
Tetrahydrofuran- $d_8$  45  
Thermotropic cholesteric liquid crystalline (TChLC) 172  
  
Valine 75  
  
Weak natural current (WNC) 175  
  
Zinc alkoxide 51  
– dimer 70  
Zinc alkyl addition to aldehydes 37